Simulation of Oil Displacement from Oil-Wet Cores by Interfacial Tension Reduction and Wettability Alteration

By

Mohammad Hosein Kalaei

Submitted to the graduate degree program in Chemical and Petroleum Engineering and the Graduate Faculty of the University of Kansas School of Engineering in partial fulfillment of the requirements for the degree of Doctor of Philosophy

…….
Co-Chairperson: Dr. Don W. Green

…….
Co-Chairperson: Dr. G. Paul Willhite

……...
Dr. Shapour Vossoughi

……...
Dr. Carl D. McElwee

……...
Dr. Stan McCool

Date defended: …….

The Dissertation Committee for Mohammad Hosein Kalaei certifies
that this is the approved version of the following dissertation:

Simulation of Oil Displacement from Oil-Wet Cores by Interfacial Tension Reduction and Wettability Alteration

Committee:

…….
Co-Chairperson: Dr. Don W. Green

…….
Co-Chairperson: Dr. G. Paul Willhite

……...
Dr. Shapour Vossoughi

……...
Dr. Carl D. McElwee

……...
Dr. Stan McCool

Date approved: …….

Abstract

Waterflooding in oil-wet naturally fractured reservoirs is not successful because the ability of matrix blocks to imbibe the injected water and displace the oil into the fracture system is poor. Chemical enhanced oil recovery methods such as surfactant flooding are used in oil-wet naturally fractured reservoirs to enhance oil recovery. This method cannot be successfully implemented in the field unless all of the mechanisms involved in this process are fully understood. Surfactant can act in several ways to enhance the oil production in oil-wet systems. Lowering interfacial tension between oil trapped in small capillary pores and the water surrounding those pores may allow the oil to be mobilized via buoyancy forces. Altering the matrix wettability toward water-wet may increase spontaneous imbibition of water. This change in rock wettability leads to positive capillary pressure and results in higher brine counter-current imbibition and therefore a higher oil production rate.

A three-dimensional, two-phase numerical simulator was developed which models the process of surfactant and/or brine imbibition in different rock wettability states. The simulator incorporates all mechanisms involved in the surfactant/brine imbibition, changing interfacial tension between oil and water and also altering rock wettability. The simulator considers that alterations in IFT and wettability lead to changes in relative permeability of phases, capillary pressure and residual saturations.

The simulator was used to model pure brine imbibition into water-wet rocks. First, the results from the simulation showed consistency between the simulated results and those obtained from other modeling data in the literature. Second, the

results demonstrated that both gravity and capillary forces can be important when the IFT is moderately low, and that there is a transition from capillary-dominated flow to gravity dominated flow as the IFT is reduced. In the limit of very low values of interfacial tension, the flow is completely dominated by gravity. Next, the numerical results also showed an excellent agreement with experimental data reported in the literature in modeling cases with different boundary conditions, which demonstrates the capability of the simulator. Also, the core orientation, either vertical or horizontal, plays an important role for oil recovery.

A current available model in the literature (UTCHEM) for wettability alteration in oil-wet cores uses two extreme wetting conditions (water-wet and oil-wet) and interpolates between them to consider the wettability alteration mechanism in surfactant flooding of the reservoirs. We propose an alternative model with the capability to simulate oil recovery using chemicals to mechanistically alter wettability and lower interfacial tension. The proposed model of wettability alteration was tested against a number of experimental and simulation results. Excellent agreements between the simulation outcomes and experimental data from the literature were shown. The simulation of surfactant solution imbibition in laboratory scale cores showed that both interfacial tension reduction and wettability alteration play important roles in oil production from oil-wet systems. Even if the surfactants are not able to change the rock wettability toward a less oil-wet condition, gravity force can enhance oil production depending on the magnitude of the interfacial tension reduction between oil and water.

The contributions of the present work will provide better guidelines in designing and improving waterflooding performance in oil-wet naturally fractured reservoirs.

Acknowledgment

Many people have aided in the initiation, progress and achievement of this study, each in their own way. Without their help this work would not be possible. First of all, I would like to express my sincere appreciation to my advisors Dr. Don W. Green and Dr. G. Paul Willhite for their outstanding knowledge, supervision, encouragements, insight, and patience during my research at University of Kansas. I am grateful to them for giving me the opportunity to learn and grow under their guidance, and for always giving me enough independence to pursue my own thoughts.

My gratitude also extends to Dr. Hossein Kazemi from Colorado School of Mines for his excellent consultant and inspired discussions and the encouragement he has showed for my work.

I would like to thank my members of the supervising committee, Dr. Shapour Vossoughi, Dr. Carl D. McElwee, and Dr. Stan McCool for their time and comments.

I would like to express my appreciation to Dr. Mike Michnick for the discussion on surfactant chemistry and his suggestions.

I greatly appreciate Mr. Nate Oborny for providing me all computing equipment and software.

I would also like to thank my friends and fellow graduate students in Tertiary Oil Recovery Project (TORP), for their friendship and discussions during my years at University of Kansas, which made the research group an enjoyable and creative environment to work in. Help from Ms. Maxine Younes and Ms. Mayumi Crider are also appreciated. My gratitude also goes to the Iran Ministry of Science, Research and Technology, and the University of Tehran for providing me with a scholarship.

Finally, and most importantly, I have to express my deepest gratitude to my wife, Zahra, for her love, faith, understanding and support, without which this work would not have been accomplished. I am also grateful to have my son, Ali, whose smile always encourages me to advance.

Table of Content

List of Figures

List of Tables

Chapter 1 : Overview

1.1 Introduction

Naturally fractured reservoirs hold a great part of the world's oil reserves, many of which are found in carbonate rocks (Chilingar and Yen 1993). Oil recovery by conventional water-flooding is ineffective after the primary production period for fractured carbonate rocks because they are usually oil-wet in nature (Downs and Hoover 1989). Although the injected water flows through the shortest high permeability avenues of the fracture network to the producers, displacement from matrix is low because water is not imbibed into the oil-wet matrix to displace oil as it occurs in water-wet matrix. In the other words, the matrix blocks remain essentially unaffected by the normal secondary oil recovery method (waterflooding). In contrast, spontaneous imbibition of injected water into matrix blocks that are water-wet displaces oil into fractures and is the main recovery mechanism in waterflooding of water-wet fractured rocks.

Spontaneous imbibition is identified with the spontaneous uptake of wetting fluid into porous media by capillary forces, which results in the displacement of non-wetting fluid. The tendency of the matrix blocks to imbibe wetting fluid is generally explained by "wettability" of the matrix formation. The wettability of the reservoir rock controls the distribution of oil and water and affects their movement through pore spaces. Significant variations in wettability may be related to variation in pore-surface roughness and mineralogical composition. The presence of water or

previously adsorbed organic films, possibility from contact with crude oil or other organic materials, is an additional factor that influences wettability. The literature review reveals that only a fraction of crude-oil constituents are believed to be capable of reacting with the reservoir rock surface (Rosen 1963; 1989).

"Wettability alteration" is a term often used by researchers to address any change in the original rock wettability. Controlling the wettability to modify the behavior of reservoir rock presents a more complex problem. There are two major methods for altering the wettability of a rock from oil-wet to less oil-wet: elevation of temperature (thermal procedure) and the use of surface-active agents or surfactants (main scope of this research).

Surfactants are widely used and found in a large number of applications because of their ability to influence the properties of surfaces and interact with them (Pursley *et al.* 1973; Adams and Schievelbein 1987). Surfactants can act in several ways to enhance oil production:

- by reducing the interfacial tension (IFT) between oil trapped in small capillary pores and the water surrounding those pores, thus allowing the oil to be mobilized,
- by changing the wettability of the oil reservoirs,
- by forming emulsions of oil and water,
- by simply enhancing the mobility of oil.

In a fractured reservoir, the success of surfactant flooding depends on how effectively the surfactant residing in the fracture spaces can penetrate the matrix. The static

spontaneous imbibition helps the fluid in the fracture to invade the matrix and, thus, the fluids between the matrix and fracture network can be exchanged. Although experimental data on this procedure has been reported in the literature, it has yet to receive a comprehensive quantitative analysis and/or numerical study.

1.2 Statement of the Problem

Chemical enhanced oil recovery methods such as surfactant flooding are used in oil-wet naturally fractured reservoirs to improve oil recovery. Indeed, chemical stimulation with surfactant has the potential to enhance water imbibition to expel more oil from matrix to the fractures. Surfactant can act in several ways to enhance the oil production in oil-wet systems. Lowering interfacial tension between oil trapped in small capillary pores and the water surrounding those pores may allow the oil to be mobilized. Altering the matrix wettability toward water-wet may increase spontaneous imbibition of water.

Data reported in the literature for modeling the interfacial tension reduction and wettability alteration are very limited despite many experiments conducted to study these two mechanisms. A current available model for wettability alteration uses two extreme wetting conditions (water-wet and oil-wet) and interpolates between them to consider the wettability alteration mechanism in surfactant flooding of the reservoirs. Hence, the significance of altering was already assigned no matter what type or how much of the surfactant is used.

We propose an alternative model with the capability to simulate oil recovery using chemicals to mechanistically alter wettability and lower interfacial tension. As discussed

earlier, spontaneous imbibition of injected surfactant solution into matrix blocks is the main recovery mechanism that can expel oil from matrix blocks in the fracture. This procedure can be modeled in the laboratory by placing a core into a beaker of aqueous solution. Therefore, the present study focuses on modeling the static imbibition of surfactant solution into the oil-wet cores in the laboratories. Properly scaling the model from laboratory to field will help to predict the success of surfactant injection process by using an appropriate surfactant to reduce the interfacial tension and alter wettability.

1.3 Objectives

The objective of this work is to develop a modeling approach on the combined benefit of wettability alteration and interfacial tension reduction for static imbibition process of surfactant solution into the oil-wet cores in the laboratories. This dissertation is organized into five chapters. Chapter 2 provides background information on porous media fundamentals and the effect of wettability. Several experimental works performed on wettability alteration of oil-wet rocks to explore the fundamentals of wettability alteration in oil-wet reservoirs are reviewed. In Chapter 3, a discussion of the mathematical modeling involved in developing the numerical simulator is presented. The continuity equation is extended and a mechanistic wettability alteration model is also introduced. The results of simulation by matching the experimental data for water-wet state are shown at the beginning of Chapter 4. Different mechanisms involved in oil production are also discussed as are validity estimates of the proposed wettability alteration model. The results obtained from the simulator in different

wetting states are also discussed and analyzed. Chapter 5 concludes the thesis along with guidelines for future work.

Chapter 2: Background and Literature Review

In this chapter, a review of the literature related to the study of imbibition, surfactant systems, and wettability alteration is presented. First, a general introduction to porous media fundamentals is given, followed by a review of the imbibition process in reservoir systems. Surfactants and interfacial tension reduction are introduced in the next section. Finally, wettability alteration mechanism in different rock wettabilities is discussed in last section.

2.1 Porous Media Fundamentals

2.1.1 Porosity

The porosity of a porous rock is the ratio of the void space in a reservoir rock to the total volume and is generally expressed as either a percentage or a volume fraction. The total or absolute porosity includes pores that are not connected to other pores. Hence, the effective porosity is defined as the ratio of the volume of pores that are connected with respect to the bulk volume of rock (Cole 1969; Ahmed 2001) as follows:

$$\phi_{effective} = \frac{Volume\ of\ \ connected\ \ pores}{Bulk\ \ volume} \tag{2.1}$$

$$\phi_{absolute} = \frac{Bulk\ volume - Grain\ volume}{Bulk\ \ volume} \tag{2.2}$$

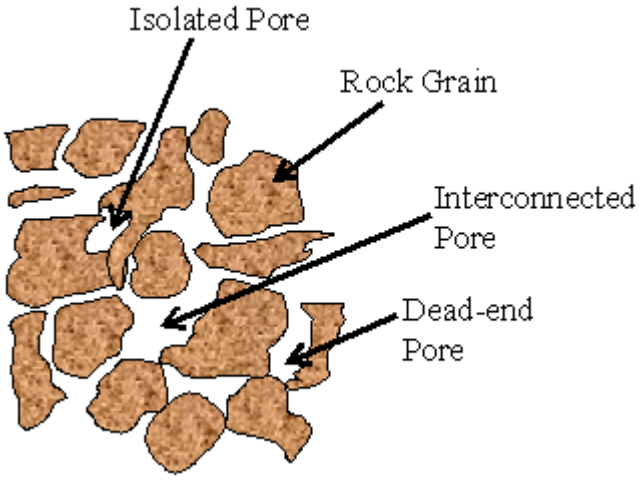

Figure 2-1: Conceptual representation of different type of pores (after Dandekar 2006)

Grain shape, grain size, compaction, sorting and cementation each has a different role on the porosity of reservoir rocks. The porosity of a rock sample is a very important factor in oil production as it is a measure of the fluid storing capacity of a rock. A number of experimental methods that can be used to measure porosity are listed as follows:

- Vacuum Saturation (imbibition method): a dry rock sample evacuated in a vacuum cell and saturated with a degassed liquid (wet fluid). The sample porosity is defined as the weight difference between the dry and wet core per bulk volume of the sample divided by wet fluid density. Also, the core can be flooded instead of immersing it in the wet fluid, and this is called the core flooding method in some studies.
- Gas Expansion (helium porosimeter): in a container of unknown volume and P_1 pressure (the sample chamber) connected to another evacuated container of

known volume V_2 and P_2 pressure (higher than P_1). A dry sample with a known bulk volume (V_B) is placed in a container with the known volume (V_2). The system is then brought to equilibrium by opening the valve between the containers to reach the equilibrium pressure P. Using the ideal gas law, the effective porosity of the sample is calculated by:

$$\phi = 1 - \frac{V_2}{V_B}\left(1 + \frac{P_2 - P}{P_1 - P}\right) \tag{2.3}$$

- Computerized Tomography (CT): this method is one of the non-conventional methods of porosity measurement that are increasingly being used. The objective of the X-ray computed tomography process (CT scanning) is to obtain descriptive images of density variations within an object. So, based on the density variations between air and brine, the computer can generate different numbers called CT numbers. Then, the porosity of the core sample is calculated from the CT number difference between brine-saturated and dry core (Honarpour *et al.* 1985; Hidajat *et al.* 2004):

$$\phi = \frac{CT_{wet} - CT_{dry}}{CT_{water} - CT_{air}} \tag{2.4}$$

The subscripts dry and wet refer to the CT numbers of air-filled and water-filled cores, respectively, whereas water and air indicate the CT numbers of pure water and air.

2.1.2 Absolute Permeability

Permeability of a porous medium is generally defined as how easily a fluid can flow through the porous medium. This property of the rock, k, is very important as it determines flow rate and direction. Moreover, thermodynamic and mechanical factors, rock type, and fluid type can also affect rock permeability. The French civil engineer, Henry Darcy, developed a fluid flow equation in 1856 known as Darcy's law that remains one of the standard mathematical tools in petroleum engineering today (Darcy 1856). The law defines rock permeability based on measurable quantities under sufficient slow, non-directional, and steady state flow as follows:

$$q = -A\frac{k}{\mu}\frac{dP}{dL} \tag{2.5}$$

Darcy's law is analogous to Fourier's law for flow of heat by conduction, Fick's law for flow of mass by diffusion, Poiseuille's law for flow of fluid in a tube, and Ohm's law for the flow of electrical current. The absolute permeability of a porous medium is usually expressed in Darcy units. The permeability of one Darcy (1 Darcy=9.87×10^{-13} m^2, which is a relatively high permeability as the permeabilities of most reservoir rocks are less than one Darcy) is defined when a single phase fluid (a gas or liquid) having a viscosity of one centipoise completely saturates the porous medium and flows through it at a rate of 1 cm^3/sec under a viscous flow regime and a pressure gradient of 1 atm/cm through a total cross-sectional area of 1 cm^2. The rock permeability is usually calculated based on the Darcy equation by measuring parameters such as: fluid properties, flow rate, pressure drop, and core dimensions.

No matter which fluid is used, gas or liquid, the absolute permeability is unique as long as there are not any interactions between the rock and the liquid.

2.1.3 Wettability

Interaction between the surface of the reservoir rock and the fluid phases confined in the pore space influences fluid distribution in rocks as well as flow properties (Willhite 1986). Wettability is the tendency of one fluid to spread onto or adhere to a solid surface in the presence of a second fluid (Green and Willhite 1998). When two immiscible phases are placed in contact with a solid surface, one of the phases is usually attracted to the surface more strongly than the other phase. This phase is identified as the wetting phase while the other phase is designated as the nonwetting phase. The wettability of reservoir rock controls the distribution of oil and water and affects their movement through pore space. In other words, fluid distributions in porous media are affected not only by the forces at fluid-fluid interfaces, but also by forces at fluid-solid interfaces.

In porous media, the wetting phase occupies the smallest pores and thus multiphase flow can be strongly affected by wettability. Homogeneous and heterogeneous are two common types of wettability. If the entire rock surface has a uniform molecular affinity for either water or oil, the rock is said to have a homogeneous wettability. A homogeneous wettability can be either strongly water/oil wet or intermediate wet while heterogeneous wettability refers to mixed wettability related to separate and distinct water wet and oil wet surfaces, which coexist in

porous media. Another type of heterogeneous wettability is spotted, fractional, dalmation or speckled wettability that relates to limited water/oil wet surfaces enclosing macroscopic regions of discontinuous oil-water wet surfaces (Cuiec 1991).

2.1.3.1 Water-wet, Oil-wet and Intermediate-wet Rock Systems

For a rock/oil/brine system, specific interactions of three phases change the wettability of the system from strongly water-wet to strongly oil-wet. A rock with no strong preference for either oil or water is said to be neutral or intermediate. Traditionally it was thought that most of the sandstone rocks were water-wet since they were originally deposited in aqueous environment. However, sandstone and carbonate reservoirs with mild to strong preference to oil were reported later (Chilingar and Yen 1993). Anderson (1986a) reported that wettability of the reservoir rock can change from its original water-wet state by adsorption of oil polar compounds or deposition of other organic matters in the crude oil.

2.1.3.2 Fractional and Mixed Wettability

Brown (1956) found cores with fractional wettability when different areas of the core have different wetting preferences. Salathiel (1973) introduced the term mixed wettability for a special type of fractional wettability as when oil invades an initially water-wet reservoir, displacing water from the large pores with the smaller pores remaining water-filled because of capillary forces. The oil deposits a layer of organic

material on the portion of the rock that is in direct contact with, thus changing the wettability. Melrose (1982) demonstrated that stability of the water film is defined by electrostatic forces arising from electric double layers and the oil/water, water/rock interfaces. He indicated that the water film formed on the rock surface thins as oil invades the rock until a critical thickness of water layer is reached where the water film in the large pores becomes unstable.

2.1.3.3 Wettability Measurement Methods

No method has been universally accepted as a unique measure of wettability (Willhite 1986); however, several procedures have been developed to measure rock wettability both qualitatively and quantitatively. Here, some of the quantitative methods are discussed in this section. Qualitative methods such as: imbibition rates, microscope examination, floatation, glass slide method, relative permeability curves, permeability/saturation relationships, capillary pressure curves, capillarimetric method, displacement capillary pressure, reservoir logs, nuclear magnetic resonance, and dye adsorption are discussed in the literature (Anderson 1986b).

Contact angle is the most universal measurement method for the wettability of flat and clean surfaces. Contact angle measurements involve two immiscible fluids placed on a smooth homogeneous solid surface. A fluid drop is typically dense fluid like water and surrounded fluid is lighter fluid like oil, as shown in Figure 2-2. The fluids are allowed to reach to equilibrium and then contact angle between the fluid drop and the solid surface is measured.

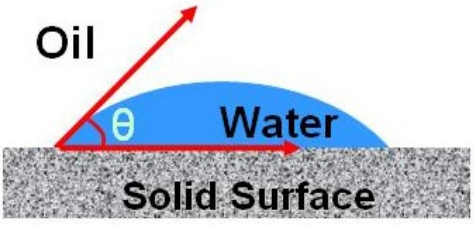

Figure 2-2: Contact angle measurement method

If the three phase (water/solid/oil) boundary is in actual motion the angles produced are called Dynamic Contact Angles and are referred to as *advancing* and *receding* angles. Advancing contact angle is higher than receding contact angle. Reader is referred to Willhite (1986) for more information about dynamic contact angle. A combination of crude oil characteristics and the mineralogy of the surface may produce different wettability conditions. Examples of water-wet and oil-wet systems are shown in Figure 2-3. Strongly water-wet systems are those with a contact angle near zero and strongly oil-wet systems have contact angles approaching 180°. The contact angle is measured in the denser phase. Systems with contact angles near 90° are referred to as having intermediate wettability.

Some authors use exact boundaries to separate the three types of homogeneous wettability. For instance, Chilingar *et al*. have chosen cut-off values of 80° for water-wet system and 100° for intermediate systems (1993); however, Treiber *et al*. arbitrarily used 75° and 105°, respectively (1972).

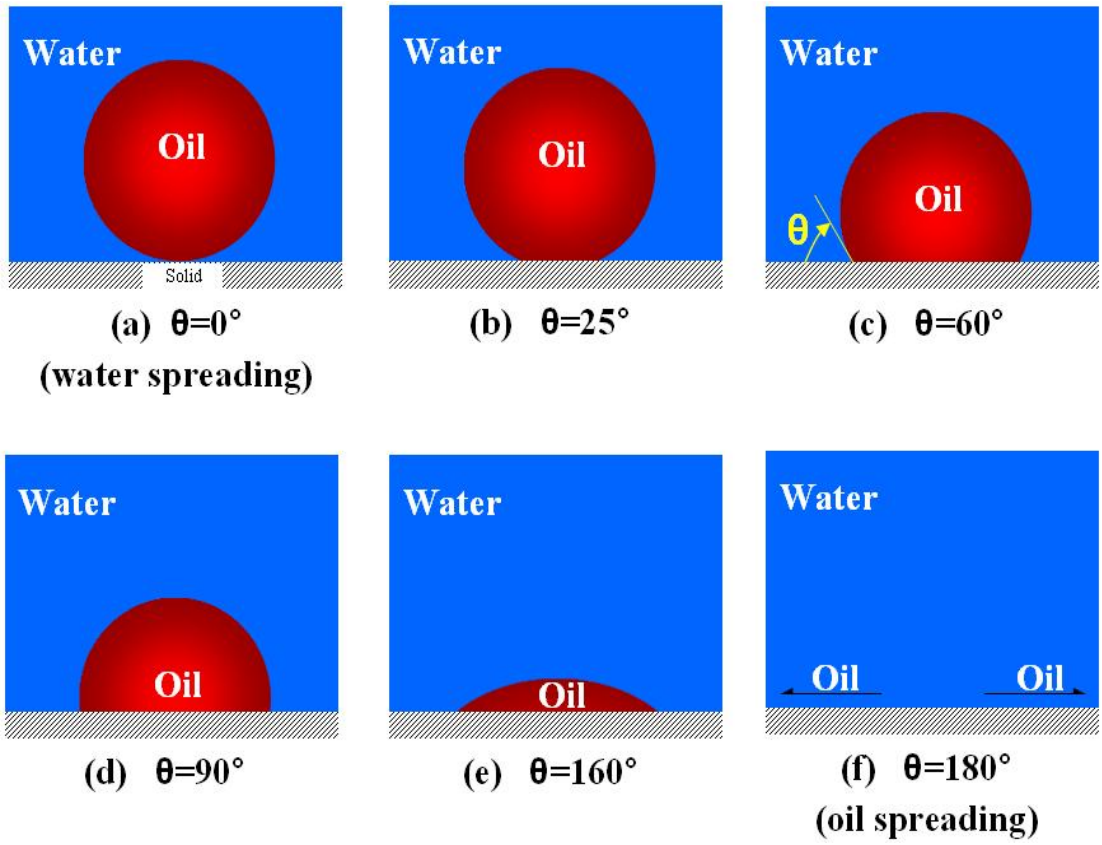

Figure 2-3: Idealized examples of contact angles and spreading (after Morrow 1990)

The Amott method was the first quantitative wettability measurement that was developed for rock cores (Amott 1959). The method involves four consecutive tests which utilize a sequence of imbibition and forced displacement tests in a porous rock saturated with oil at interstitial water saturation. These tests are as follows (Willhite 1986; Zhou *et al.* 2000):

1. Spontaneous imbibition of water to determine the volume of oil displaced,
2. Forced displacement of oil to residual oil saturation by water to determine additional volume of oil producing,

3. Spontaneous imbibition of oil to record the volume of water displaced,

4. Flooding the core with oil to reach residual water saturation.

Now, two wettability indexes (I_w and I_o) can be defined from the data and are presented as follows:

$$I_w = \frac{volume\ of\ water\ imbibed\ in\ step\ 1}{volume\ of\ water\ forced\ in\ step\ 2} \cong \frac{\Delta S_{w,im}}{\Delta S_{w,im} + \Delta S_{w,f}} \tag{2.6}$$

$$I_o = \frac{volume\ of\ oil\ imbibed\ in\ step\ 3}{volume\ of\ oil\ forced\ in\ step\ 4} \cong \frac{\Delta S_{o,im}}{\Delta S_{o,im} + \Delta S_{o,f}} \tag{2.7}$$

where:

$\Delta S_{w,im}$= water saturation alteration after spontaneous imbibition of water,

$\Delta S_{o,im}$= oil saturation change after spontaneous imbibition of oil,

$\Delta S_{w,f}$= water saturation alteration after forced imbibition of water,

$\Delta S_{o,f}$= oil saturation change after forced imbibition of oil.

Amott-Harvey method refers to a modification to the Amott method, which combines Amott indices together known as the Amott-Harvey wettability index as follows (Anderson 1986b):

$$I_{A-H} = I_w - I_o \tag{2.8}$$

where I_{A-H} varies between +1 (strongly water-wet) and -1 (strongly oil-wet).

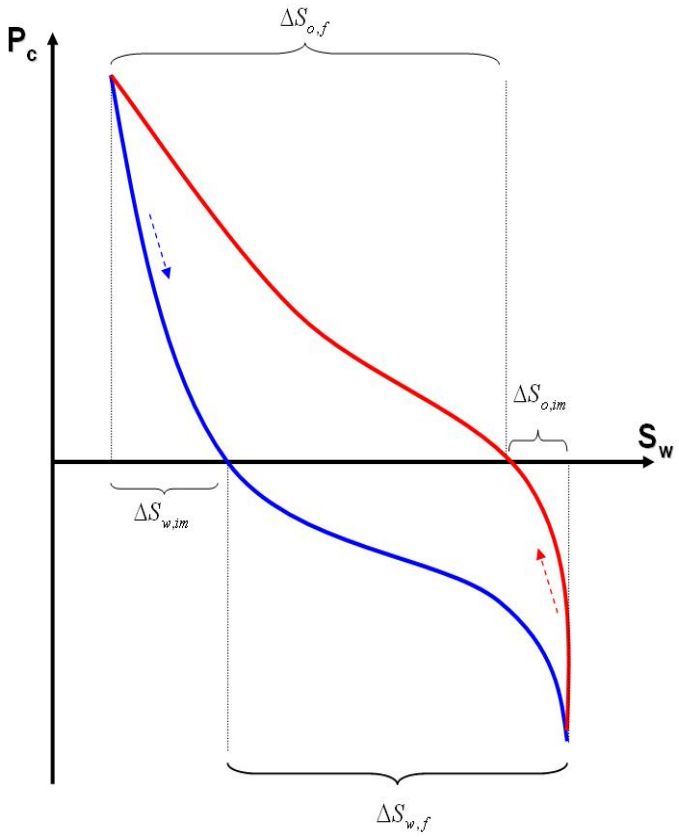

Figure 2-4: Capillary pressure curve illustrating Amott method steps

The third quantitative method is the USBM method where drainage and imbibition capillary pressures are measured using centrifuge tests. One benefit of the USBM method compared to the Amott method is that the USBM method is more sensitive near neutral wettability which the Amott method is not. This method is also less time consuming; however, it is restricted to the use of plug-size core samples. The methodology of the USBM method is that the work required for the wetting fluid to displace the nonwetting fluid is less than the work required for the opposite displacement. The required work is proportional to the area under the capillary

pressure curve as experimental data have showed (Anderson 1986b) and the wettability number is defined as (Donaldson *et al.* 1969):

$$N_W = \log\left(\frac{A_1}{A_2}\right) \tag{2.9}$$

where A_1 and A_2 are the areas under the water and oil derived capillary pressure curves, respectively.

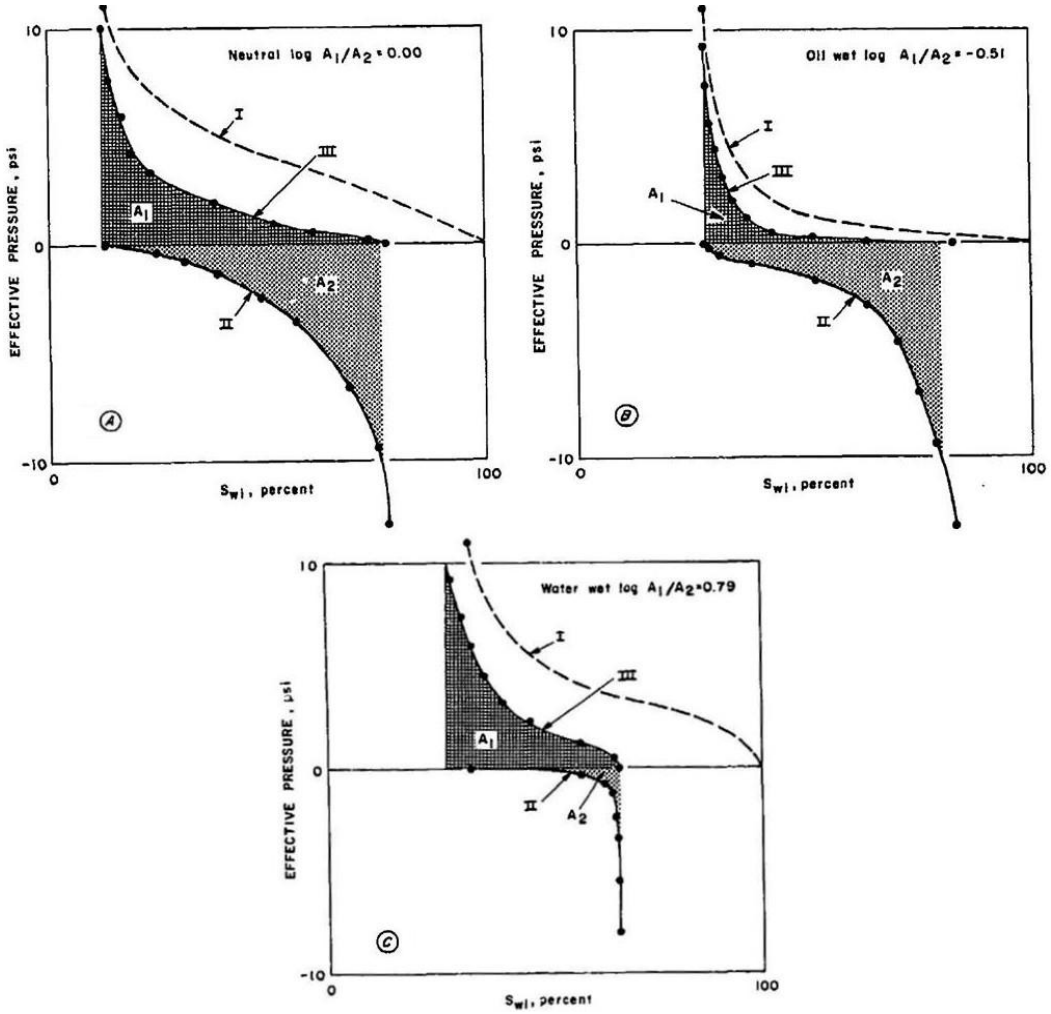

Figure 2-5: USBM method for wettability measurement (I = brine drive, II = oil drive); A: intermediate wet core, B: oil-wet core, C: oil-wet core (Donaldson *et al.* 1969)

As a comparison, the contact angle method only measures the wettability of a single solid surface (mineral crystal plate or rock surface), while the Amott and USBM methods measure the average wettability of a core sample. Table 2-1 shows criteria for each method based on the literature.

Table 2-1: Wettability measurement methods criteria (Anderson 1986b)

Methods	Water-wet	Naturally wet	Oil-wet
Contact angle (minimum)	0	60° to 75°	105° to 120°
Contact angle (maximum)	60° to 75°	105° to 120°	180°
Amott wettability index (displacement by water ratio)	Positive	0	0
Amott wettability index (displacement by oil ratio)	0	0	Positive
Amott-Harvey wettability index (Cuiec 1984)	0.3 to 1	-0.3 to 0.3	-1.0 to -0.3
USBM wettability index	~1	~0	~-1

2.1.4 Residual Saturation

Residual phase saturation, which is sometimes referred to as the irreducible saturation, is the saturation of a fluid in a porous medium that is trapped by capillary forces and is not displaced by an immiscible fluid flowing under a particular potential gradient; however, the residual phase saturation may decrease due to mass transfer effects or some other phenomena. The occurrence of the residual wetting phase saturation is consistent with capillary pressure phenomena. As the nonwetting phase is moved from the pore spaces, the wetting phase moves back into the void and is held immobile in the small pores and along the pore walls by capillary pressure. Since the viscous and/or buoyancy forces acting locally on the nonwetting phase cannot

overcome the large capillary forces at small pore throats within the rock that exist with high interfacial tension, the nonwetting phase becomes trapped as globules across several pores or blobs within a pore.

Experimental data have documented the change in residual oil saturation with changes in the Amott-Harvey wettability index. Figure 2-6 shows some of the experimental data for carbonate rocks and data for Berea sandstone is shown in Figure 2-7. By comparing these two figures, one can understand that the residual oil saturation in carbonate rocks is relatively higher than that in sandstone rocks. According to Figure 2-6 and Figure 2-7, the residual oil saturation is lowest when the wettability is nearest to neutral-wet or mixed-wet conditions corresponding to an index near zero. Also, Figure 2-7 reveals that the magnitude of the slope of the curve is approximately the same for both water-wet and oil-wet conditions. There have been few studies that determined the change of residual water saturation with changes in wettability. For instance, Jerauld *et al*. (1997) claimed that the residual water saturation also follows a similar trend to residual oil saturation.

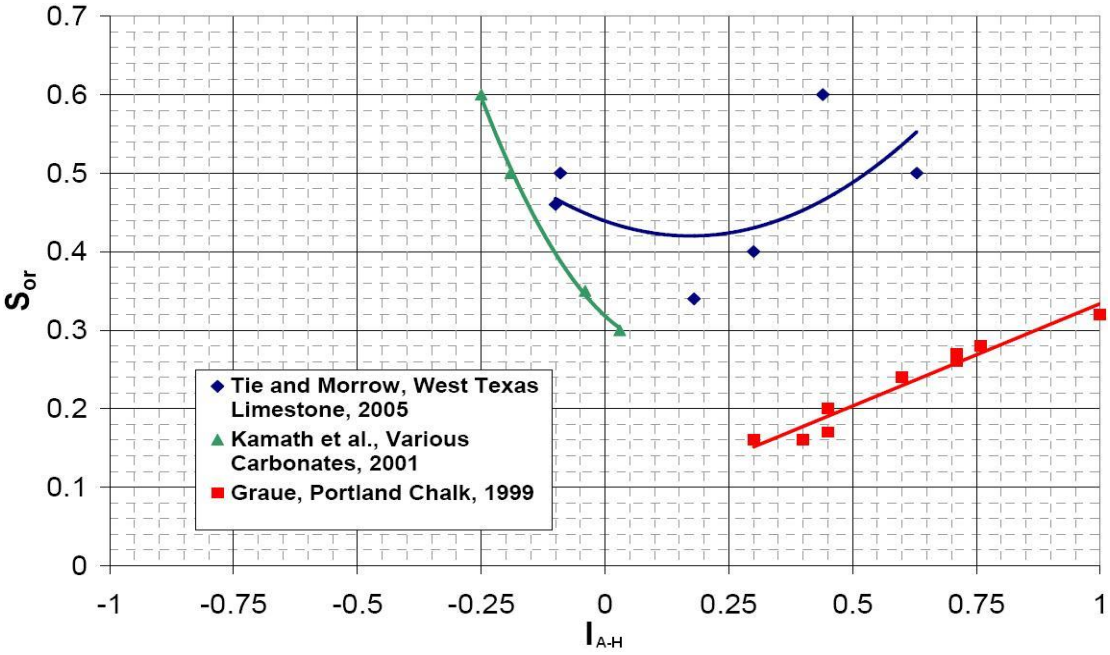

Figure 2-6: Effect of wettability on residual oil saturation for carbonate rocks (Anderson 2006)

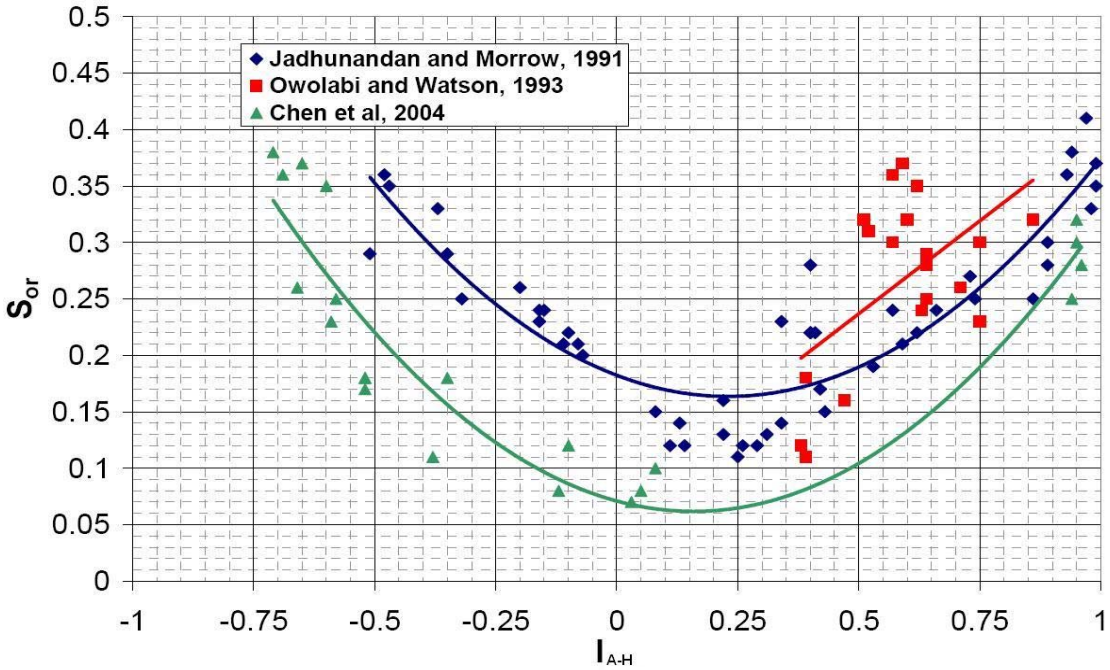

Figure 2-7: Effect of wettability on residual oil saturation for Berea sandstone (Hirasaki *et al.* 2005)

2.1.4.1 Capillary, Bond, and Trapping Number

One mechanism for enhancing the oil recovery from oil-wet reservoirs using surfactant is to mobilize trapped oil phase due to both interfacial tension reduction and wettability alteration of the rock. Buoyancy forces can also affect the mobilization of a trapped oil phase and can be expressed by the Bond number (or inverse of the Bond number). The Bond and capillary numbers for the trapping and mobilization of a nonwetting phase are usually treated as two separate dimensionless groups; one to represent gravity/capillary forces (Bond number) and the other to describe viscous/capillary forces (capillary number). In fluid dynamics, the capillary number represents the relative effect of viscous forces versus surface tension acting across an interface between a liquid and a gas, or between two immiscible liquids. This dimensionless number is defined as the following correlation (Green and Willhite 1998):

$$N_{Ca}^{*} = \frac{u\mu}{\sigma_{ow}} \tag{2.10}$$

Mobilization of trapped phase (oil) by alteration of viscous/capillary force ratio (capillary number) was discussed by Willhite (1986). Residual saturation data are correlated as a function of capillary number as shown in Figure 2-8.

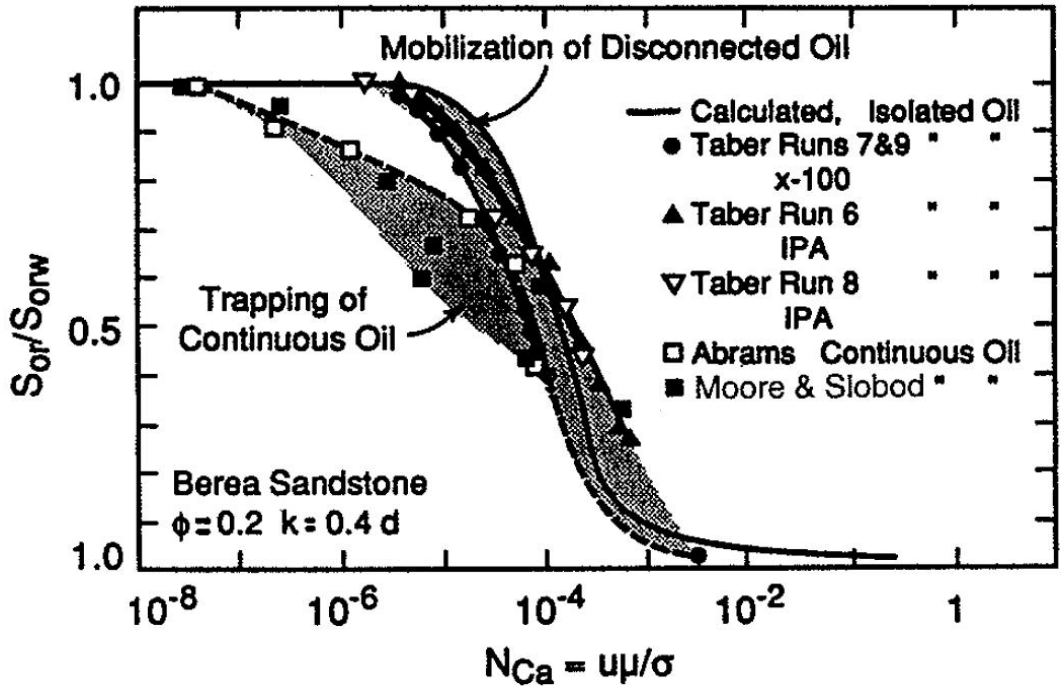

Figure 2-8: Correlation of residual oil saturation with capillary number at trapping and mobilization (Willhite 1986)

The ratio of capillary to gravity forces is given by the inverse Bond number. This number is defined as follows:

$$N_B^{-1} = C\frac{\sigma_{ow}}{\Delta\rho g H}\sqrt{\frac{\phi}{K}} \tag{2.11}$$

where C=0.4, and H is the height of medium. As this dimensionless number approaches to zero, gravity forces dominate the flow. Table 2-2 shows ranges of N_B^{-1} for which experiments were performed by some investigators, along with the method of reducing the number.

One of the uses of this number is to distinguish if the process is dominated by gravity force or capillary force. For instance, Schechter (1994) concluded that gas

injection process can be used to recover oil from fractured reservoirs by gravity drainage at low N_B^{-1}.

Table 2-2: Literature values of inverse Bond number during gravity drainage experiments (Schechter *et al.* 1994)

Mechanisms (Reference)	Fluids	Method of varying N_B^{-1}	Range of N_B^{-1}
Imbibition (Iffly et al.,1972)	Oil–water	Varying core height	23–1980
Imbibition (Du Prey, 1978)	Oil–water	Centrifuge	0.0456–16.5
Imbibition (Hamon and Vidal, 1986)	Oil–water	Varying core height	4.76–1441
Imbibition (Cuiec et al.,1990)	Oil–water–alcohol	Reduction of IFT	95.7–1193
Imbibition (Thiebot et al., 1990)	Oil–water–surfactant	Reduction of IFT	73–200
Drainage (Pavone et al., 1989)	Gas–oil	Reduction of IFT	0.03–0.07
Drainage (Jacquin et al.,1987)	Gas–oil	Reduction of IFT	0.3–1
Drainage (Stensen et al.,1990)	Brine–air, gas–oil	Reduction of IFT, long cores	0.773–1.37
Drainage (Suffridge and Renner, 1991)	Brine–air, gas–oil	Reduction of IFT, long cores	0.2–2
Drainage (Nectoux, 1987)	Gas–oil (nonequilibrium)	Reduction of IFT	?

Another use of the Bond number is in surfactant flood enhanced oil recovery. As mentioned earlier, surfactant solutions are able to improve oil recovery by altering wettability and lowering interfacial tension. According to the Equation 2.11, reducing the interfacial tension decreases the inverse Bond number (or increase the Bond number). Experimental data has documented that if interfacial tension can be reduced to very low values (like 10^{-3} mN/m); all oil may be ideally recovered and residual oil saturation decreases to a very low values (Ehrlich *et al.* 1974; Gupta and Trushenski 1979; Hirasaki *et al.* 2005). This concept has been well documented in the literature

and is shown in Figure 2-9. In this figure, all data presents residual saturation versus the capillary number except data from Hirasaki *et al*. (2005), which shows Bond number for different residual saturations.

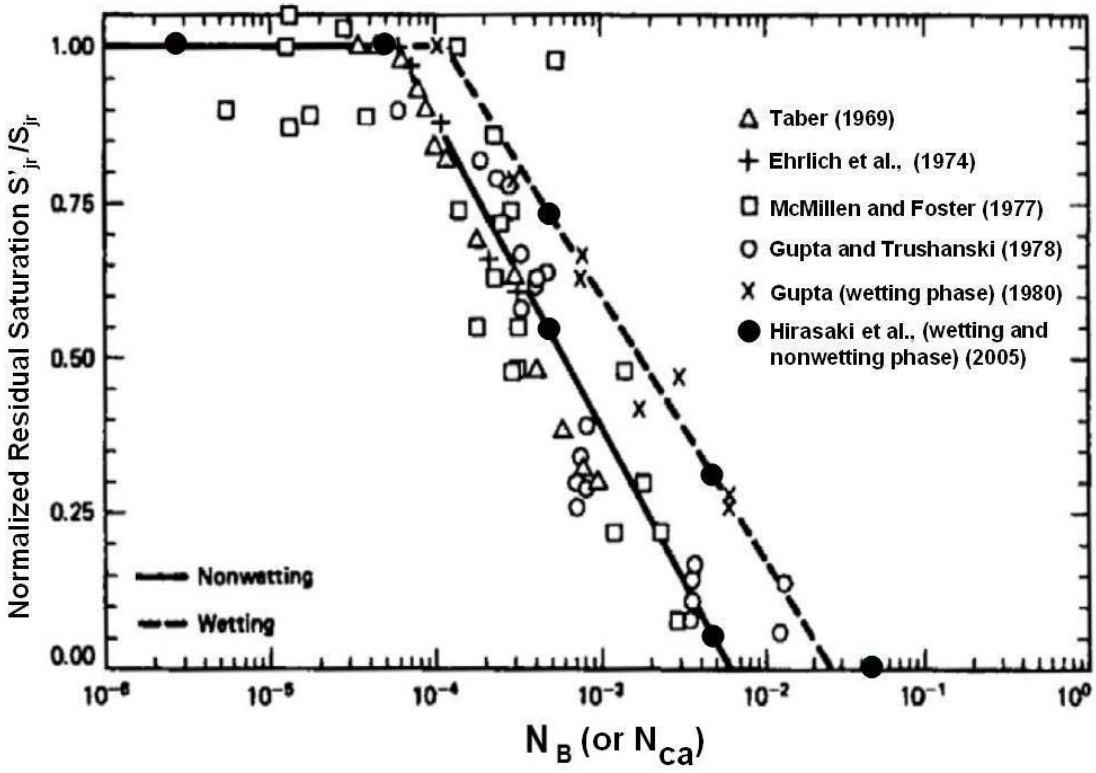

Figure 2-9: Correlation between Bond number and residual oil saturation (after Hirasaki *et al.* 2005)

Delshad *et al*. (1996) developed a new dimensionless number called trapping number, N_T, which includes both gravity and viscous forces. Trapping number is derived by applying a force balance on the trapped oil globule. The forces controlling the movement of the blob are the viscous force due to the hydraulic gradient, the trapping

force due to capillary pressure and the gravity force, which can act as either a driving or trapping force depending on the direction of the flow.

As mentioned, the trapping number is a combination of capillary number and Bond number and is defined as follows (e.g.: for oil phase):

$$N_T = \frac{\left|\vec{k}.\left(\nabla P_{oil} - \rho_w g \nabla D\right)\right|}{\sigma_{ow}} \tag{2.12}$$

The effect of wettability was not considered in the above equation; however, the effect can be considered on residual saturations instead as will be discussed later.

2.1.5 Capillary Pressure

The capillary forces in a petroleum reservoir are the result of the combined effect of the surface and interfacial tensions of the rock and two or more immiscible fluids, pore size, geometry, and wetting characteristics of a given system. Capillary pressure relates to pressure difference across a fluid-fluid interface when the immiscible fluids are contained within a capillary tube or rock pore. The pressure difference, called capillary pressure, can also be illustrated by fluid rise in a capillary tube (Green and Willhite 1998). As a consequence, to maintain a capillary tube (or porous medium) partially saturated with nonwetting fluid while the tube is exposed to wetting fluid, the pressure of the nonwetting fluid must be greater than that of the wetting fluid. This is the reason that a curvature develops between wetting and nonwetting phases in a capillary tube, as illustrated in Figure 2-10. The curvature of interface directed towards water, indicates a higher pressure in the oil phase. The radius of curvature at

the interface of nonwetting and wetting phases in reservoir rocks is dependent on various factors such as wettability, fluid saturation, pore walls mineralogy, pore geometry, and the saturation history of the system, which is dynamic with progress in oil production from the reservoir. These factors collectively cause the radii of curvature and contact angle of the fluids to vary from pore to pore within the media. The mathematical definition of capillary pressure based on the interface pressure of wetting and nonwetting phases is expressed as follows:

$$P_c = P_{nw} - P_w \tag{2.13}$$

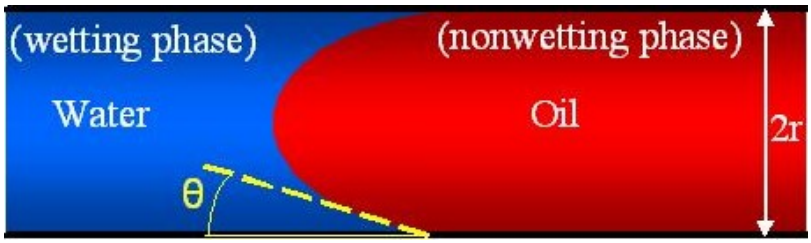

Figure 2-10: Illustration of water/oil interface

This is a general definition of the capillary pressure; however, researchers use the following version of the above equation because they usually use water-wet rock in their investigations:

$$P_c = P_{oil} - P_{water} \tag{2.14}$$

Washburn (1921) studied co-current imbibition in a capillary tube to find interactions between capillary driving forces and viscous resistance. The results of the study were used to develop capillary pressure correlations.

If a capillary tube with radius of "r" contains a perfectly wetting liquid with surface tension of σ, the capillary pressure P_c is given by:

$$P_c = \sigma\left(\frac{1}{r_1}+\frac{1}{r_2}\right) \tag{2.15}$$

where r_1 and r_2 are the principal radii of curvature of the interface between the two fluids in the capillary tube. For equal principal radii of curvature in the capillary rube, the above equation becomes:

$$P_c = \frac{2\sigma}{r} \tag{2.16}$$

For a non-perfectly wetting fluid, a contact angle exists between a droplet of the fluid and the media surface with which a contact is made (as discussed in 2.1.3.3). Therefore the above equation was modified for the contact angle phenomena and is known as Young-Laplace equation. The Young–Laplace equation is a nonlinear partial differential equation that describes the capillary pressure difference sustained across the interface between two static fluids, such as oil and water, due to the phenomenon of surface tension. According to Figure 2-10, the simplified form of the Young-Laplace equation can be written as follows:

$$P_c = \frac{2\sigma\cos\theta}{r} \tag{2.17}$$

where σ is interfacial tension between wetting and nonwetting phases. θ is the principal measure of wettability for a smooth homogeneous surface. All laboratory experimental tests are designed to reproduce the saturation history of the reservoir. The process of generating the capillary pressure curve by displacing the wetting phase

with the nonwetting phase is called the drainage process. Another principal flow process of interest involves reversing the drainage process by displacing the nonwetting phase with the wetting phase and the resulting curve from this process is called the imbibition capillary pressure. The process of saturating and desaturating a core with the nonwetting phase is called capillary hysteresis. In other words, capillary hysteresis is a phenomenon that the equilibrium positions of the oil/water interfaces in a system of pores are dependent on whether the system is increasing or decreasing in water content. For instance, the experimental data of imbibition/drainage capillary pressure in a water-wet dolomitic limestone rock sample obtained from an outcrop immediately north of Kingston, Ontario is shown in the following figure. Pressure is expressed as an equivalent height of water.

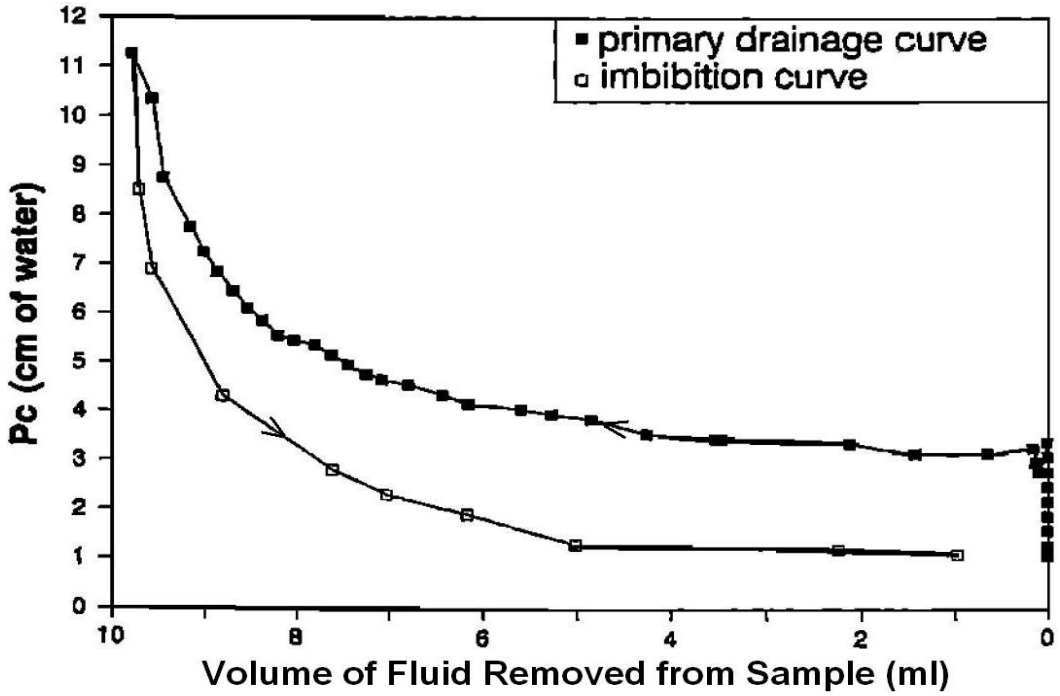

Figure 2-11: Capillary pressure curve of a water-wet rock sample (after Resitsma and Kueper 1994)

Webb *et al*. (2005) generated capillary pressure curves during their experimental investigation of methods for improving oil recovery from carbonate rocks. Figure 2-12 shows experimental data of measured capillary pressure curves for an oil-wet rock of North Sea carbonate (Valhall) using two different water injections: sea water (red, $S_{wi} \approx 0.25$) and brine (blue $S_{wi} \approx 0.21$). The capillary pressure values are negative for oil-wet cores (Equation 2.14).

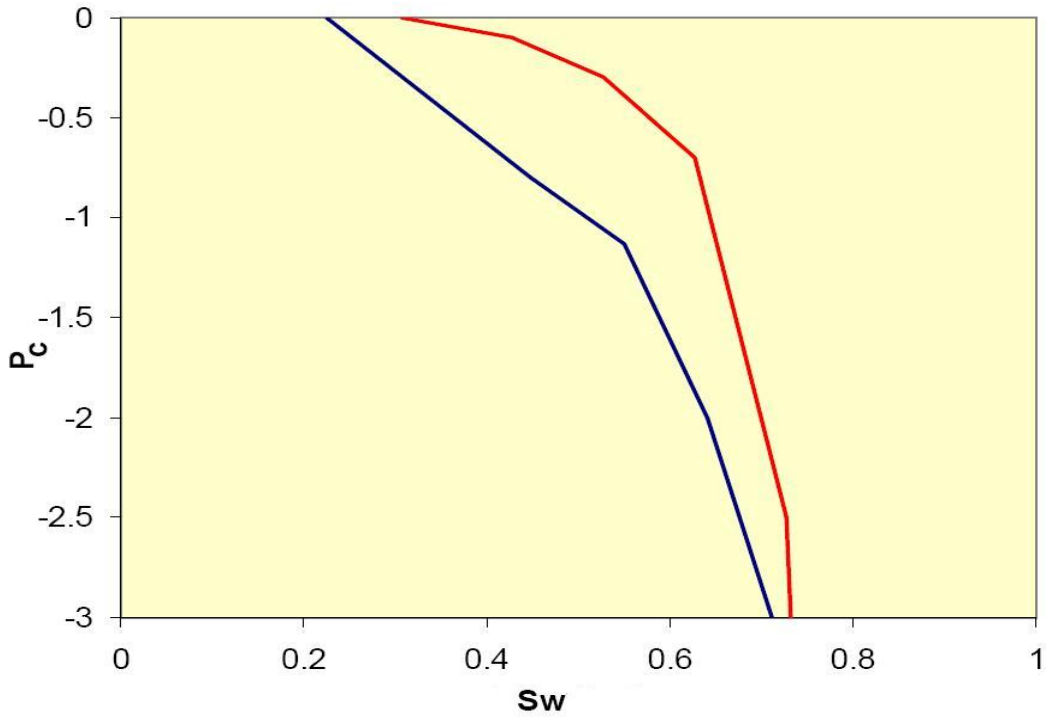

Figure 2-12: Imbibition capillary pressure for an oil-wet rock sample (Webb *et al.* 2005)

Figure 2-11 and Figure 2-12 are just two examples of capillary pressure curves based on different wettability conditions. So, the shape of the capillary pressure curve changes dramatically for imbibition when a rock is oil-wet compared to water-wet.

Also, an example capillary pressure curve for Berea sandstone that was treated to become oil-wet is shown in Figure 2-13. The difference in the primary drainage capillary pressure for various degrees of water-wetness was studied by Morrow (1976) and is shown in Figure 2-14. He used artificial cores of consolidated PTFE having porosities ranging from 16.5 to 47.5%. The cores were prepared by compacting PTFE powder in steel tubes. θ_{REC} and θ_{ADV} refer to the receiving and advancing contact angle which were described in 2.1.3.3.

Figure 2-14a shows the effect of wettability from moderately water-wet to strongly water-wet on the drainage capillary pressure curve is negligible while this effect is considerable for the imbibition curve (Figure 2-14b). The importance of this observation is based on the wettability of the rock and the fluid displacement process and oil entrapment mechanism.

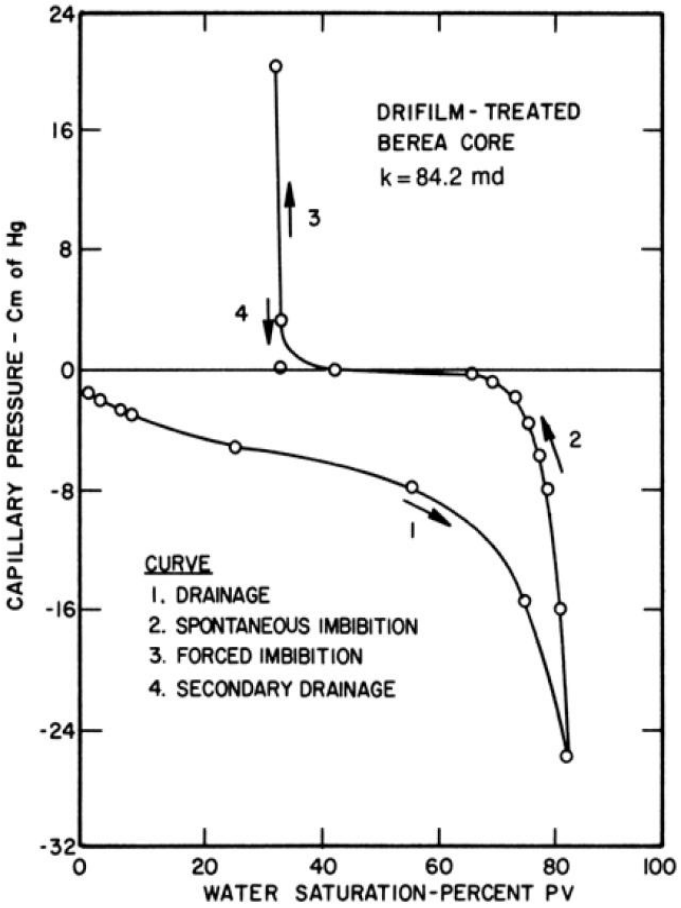

Figure 2-13: Capillary pressure curve for a treated Berea core to oil-wet state (Killins *et al.* 1953)

For the cases with uniform moderate to strong wettability, the rock is in contact with the wetting phase and the nonwetting phase flows through the center of the pore. This fluid displacement process causes little changes to the capillary pressure curve. On the other hand, during the imbibition process the wetting phase displaces the nonwetting phase and the nonwetting phase is trapped. During this displacement process, the nonwetting phase, which was in contact with the pore walls in the absence of the wetting phase, is removed and replaced with the wetting phase. This

phase replacement and nonwetting phase entrapment occurs at different rates for different wettabilities and has a significant effect on the capillary pressure.

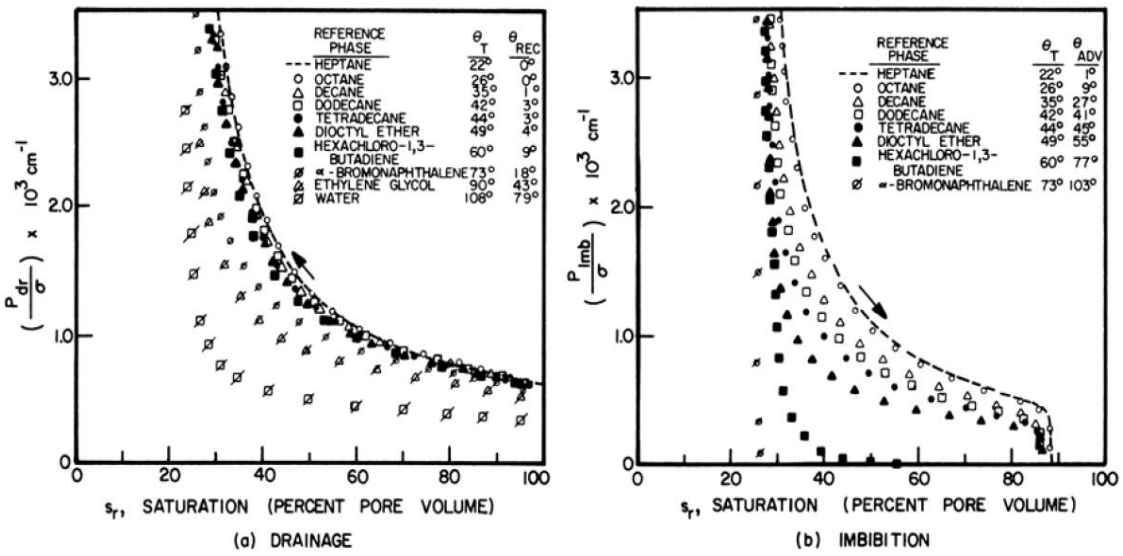

Figure 2-14: Drainage capillary pressure data for different wettability based on a water-wet state (Morrow 1976)

Techniques frequently used to measure capillary pressure are complicated and time-consuming. It is also difficult to measure the capillary pressure in low permeability rocks. It is valuable to find the capillary pressure from spontaneous imbibition test because such a test would be relatively simple, economical, and fast for water-wet systems.

Jia *et al*. (2006) conducted spontaneous imbibition tests in four different gas saturated rock samples and used a mathematical model developed by Li and Horne

(2002) to determine capillary pressure. The following table shows properties of rock samples along with capillary pressure results.

Table 2-3: Capillary pressure (and relative permeability) calculation (Jia *et al.* 2006)

	L (cm)	D (cm)	ϕ (%)	k (md)	S_{wf} (%)	P_c (psi) @S_{wf}	k_{rw} (psi) @S_{wf}
Glass beads	29.5	3.4	38.6	25700	89.1	0.143 (0.145*)	0.389
Fired Berea	43.5	5.06	24.5	1200	66.5	0.633	0.259 (0.261**)
Berea	9.962	4.982	21.2	804	61.5	0.277	0.614
Graywacke	3.521	8.250	4.73	0.60	86.9	0.106	0.833

2.1.6 Relative Permeability

In most reservoirs, there are two or three different phases of fluids flowing through reservoir rock; however, the discussion in 2.1.2 was limited to one phase. Therefore, the concept of absolute permeability must be modified to describe flow when more than one fluid is present in the reservoir. In this situation, the presence of each fluid partially affects the flow of the major fluid, and the absolute permeability of each fluid can be called effective permeability as applied in the Darcy equation. The effective permeability is a function of fluid saturation along with other properties such as pore geometry, capillary characteristics, surface forces, and wetting characteristics. Therefore, a fluid relative permeability is defined as the ratio of effective permeability of the fluid to the absolute permeability of the rock. A sample of relative permeability curves including hysteresis phenomenon is presented in the following figure.

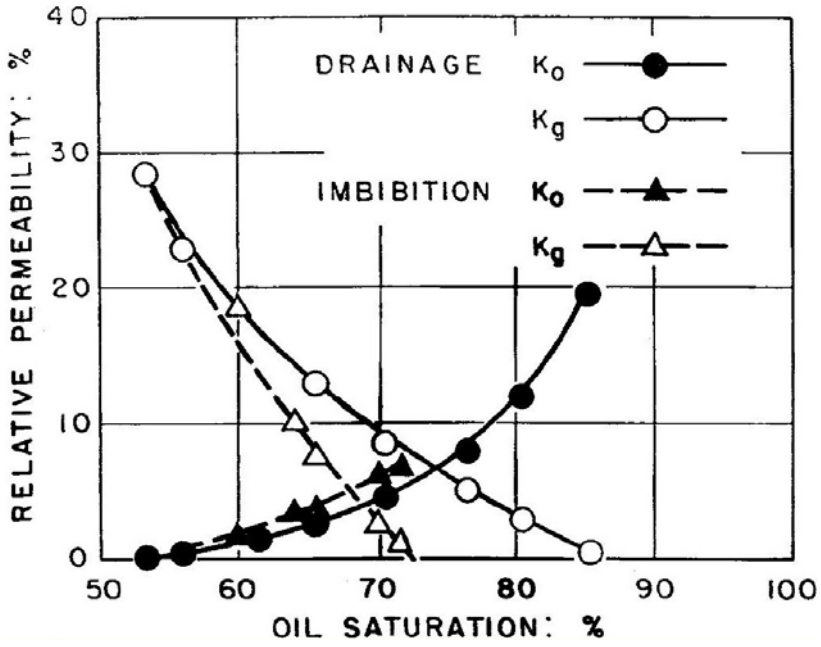

Figure 2-15: Relative permeability curves for a system of kerosene and helium (Osoba *et al.* 1951)

The laboratory methods used to determine relative permeability functions are grouped into centrifuge, steady state, unsteady state (JBN), and CT scanning. Although the centrifuge method has been improved (Hirasaki *et al.* 1992; 1995), it is not still of much interest because the flow mechanism assumed in this method is different from what observed in reservoirs (except those reservoirs undergoing the gravity drainage). In low permeable rock systems, capillary forces and capillary end effects are significant (Firoozabadi and Aziz 1986; Kamath *et al.* 1995). Also, most conventional unsteady state techniques cannot be applied because of inaccurate assessment of relative permeability in some cases with compressible fluids and viscous fingering phenomenon (Honarpour *et al.* 1986).

In the CT scanning method, X-ray CT scanner is used to measure saturation profiles along the length of the cores as a function of time. A similar imbibition cell can also be constructed for forced co-current imbibition processes. The saturation profile history allows direct computation of the relative permeability. In this method, capillary force is incorporated and there is no need to reach steady state conditions (Schembre and Kovscek 2003).

As mentioned, there are some variables such as temperature, pore size, rock type and fluid types that influence relative permeability curves. This has been documented in the literature since 1951 (Osoba *et al.* 1951; Craig 1971; Demond and Roberts 1987; Lake 1989; Green and Willhite 1998; Dandekar 2006); however, there has been greater interest in the effect of wettability and interfacial tension than that of those variables on displaced and displacing fluid relative permeabilities. For instance, McCaffery and Bennion (1974) studied the effect of wettability on relative permeability under three different wettability conditions. The following figure shows the resulting relative permeability curves. In Figure 2-16, "nonref" and "ref" refer to the nonwetting phase and the wetting phase, respectively.

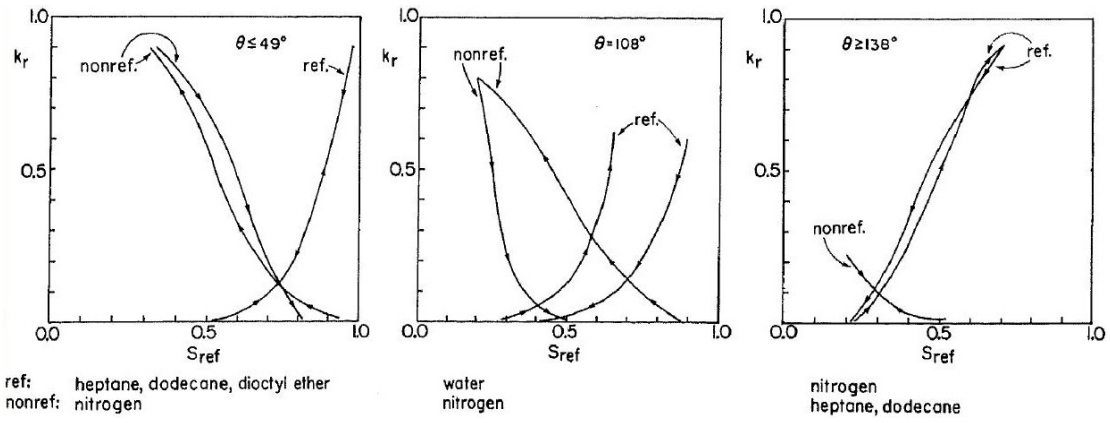

Figure 2-16: Relative permeability curves in different wet conditions (McCaffery and Bennion 1974)

Also, Dicarlo *et al*. (2000) studied three-phase flow in the wettability conditions of water-wet, oil-wet, and fractionally-wet in sand packs by using CT scanning techniques to measure indirectly the oil and water relative permeabilities for three-phase gravity drainage as well as gradients in the gas phase to determine the gas relative permeability. They found that the gas relative permeability is approximately half as much in an oil-wet medium than in a water-wet medium at the same gas saturation.

Bardon and Longeron (1980) showed that the oil and gas relative permeabilities determined from the displacement tests are strongly affected by interfacial tension, especially when it is lower than 10^{-2} mN/m. They used pure *n*-heptane as liquid phase and injection fluid was pure gaseous *n*-methane. The following figure shows how significant relative permeability depends on interfacial tension values in oil/gas systems. They claimed that the relative permeability curves are considered being straight lines as IFT is reduced (in the vicinity of critical point).

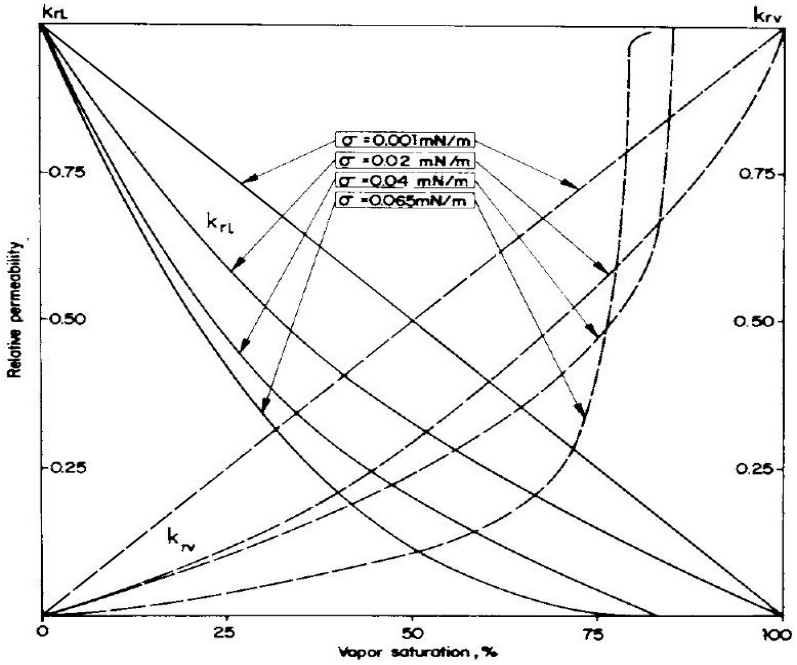

Figure 2-17: Vapor/liquid relative permeability curves for very low interfacial tension values (Bardon and Longeron 1980)

Furthermore, the same behavior was reported in high interfacial tension systems by the other studies (Torabzadey 1984; McDougall *et al.* 1997; Dicarlo *et al.* 2000; Shen *et al.* 2006; Cinar *et al.* 2007).

For example, Cinar *et al*. (2007) investigated the effect of interfacial tension (0.005 to 2 mN/m) on three-phase relative permeability in a system of C_{16}/*n*-butanol/H_2O. The obtained results indicated that as interfacial tension between the gas/oil pair of phases decreases, relative permeabilities for those phase increase at a given saturation as shown in the following figure.

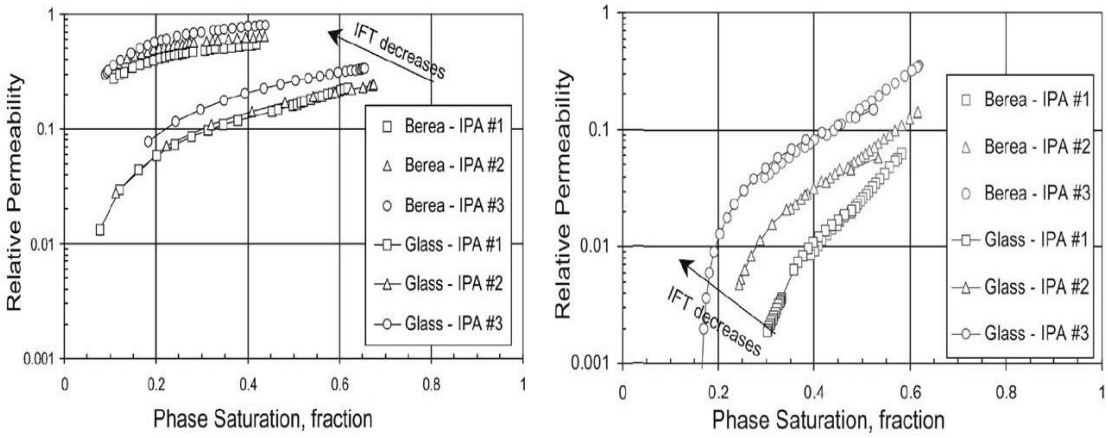

Figure 2-18: Relative permeability to oil (right) and gas (left) in oil-wet system (Cinar *et al.* 2007)

Among all physical parameters and correlations, water/oil relative permeability is perhaps the most important constitutive relation that characterizes two-phase flow and displacement processes in porous media. Since no general theoretical expression is available for the relative permeability function, two-phase relative permeabilities are modeled based on an empirical equation called modified Brooks-Corey (MBC), also known as the power law model (Lake 1989). Water and oil relative permeability equations are presented as follows (Pope and Nelson 1977):

$$k_{rw} = k_{rw}^{*}\left(\frac{S_w - S_{wr}}{1 - S_{wr} - S_{or}}\right)^{n_w} \tag{2.18}$$

$$k_{ro} = k_{ro}^{*}\left(1 - \frac{S_w - S_{wr}}{1 - S_{wr} - S_{or}}\right)^{n_o} \tag{2.19}$$

In the above equations, k_{ro} is the oil relative permeability (fraction), k_{ro}^{*} is the oil relative permeability endpoint (fraction), and n_o is an exponent for the oil relative permeability curve. Also, k_{rw} is the water relative permeability (fraction), k_{rw}^{*} is the

water relative permeability endpoint (fraction), and n_w is an exponent for the water relative permeability curve.

In a more abstract sense, this formulation is perhaps the most widely used and practical method describing laboratory-derived relative permeability relationships in terms of simple power functions. The powers and endpoint values are different in cases of water-wet and oil-wet and will be discussed later.

The valid relative permeability curve often yields a straight line on a log-log plot when the relative permeability data are plotted versus normalized saturations. The oil and water normalized saturations are defined by the following equations:

$$S_{wn} = \frac{S_w - S_{wr}}{1 - S_{or} - S_{wr}} \tag{2.20}$$

$$S_{on} = \frac{1 - S_w - S_{or}}{1 - S_{wr} - S_{or}} \tag{2.21}$$

Although the modified Brooks-Corey model has many useful features, it suffers from a number of shortcomings. These deficiencies may be summarized as follows:

- The model is a direct function of the endpoints, and as such, is biased towards endpoint data, being less influenced by the remaining data; as such the method is less suitable in actually validating a particular relative permeability data set.
- If one or both endpoints are unavailable, then the model fails to work properly.
- The model cannot predict a relative permeability relationship; rather it is intended to smooth and extend an existing relationship.

Parker et al. (1987) proposed extending the method of van Genuchten *et al*. (1985) to predict three-phase system relative permeability curves. They derived a parametric model for relationships between relative permeability saturation and pressure in porous media that contain up to three coexisting fluid phases. The following equations are for a system containing only oil and water phases:

$$k_{rw} = \sqrt{\overline{S}_w}\left[1-\left(1-\sqrt[m]{\overline{S}_w}\right)^m\right]^2 \tag{2.22}$$

$$k_{ro} = \sqrt{\left(\overline{S}_t - \overline{S}_w\right)}\left[\left(1-\sqrt[m]{\overline{S}_w}\right)^m - \left(1-\sqrt[m]{\overline{S}_t}\right)^m\right]^2 \tag{2.23}$$

where $\overline{S}_t$ is the total liquid saturation. This model has been barely used in simulations. They assumed that water relative permeability is a function of only water saturation while oil relative permeability is a function of both water and oil saturations.

Behrenbruch and Goda (2006) recently developed a semi-empirical model to predict relative permeability curves. In fact, the model can be considered as an extension of the Carman-Kozeny equation (Kozeny 1927; Carman 1937) and presented as follows:

$$k_{rw} = \frac{1014 m_w^2 \phi_e^3 S_w}{K}\left(\frac{S_w}{1-\phi_e S_w} - \frac{S_{wi}}{1-\phi_e S_{wi}}\right)^2 \tag{2.24}$$

$$k_{ro} = \frac{1014 m_o^2 \phi_e^3 \left(1-S_w\right)}{K}\left[\frac{1-S_w}{1-\phi_e\left(1-S_w\right)} - \frac{S_{or}}{1-\phi_e S_{or}}\right]^2 \tag{2.25}$$

where K is the absolute permeability in μm^2 and ϕ_e is the effective porosity (fraction). Also, m_w and m_o are the slope of linear relationships in the Carman-Kozeny equation, generally thought to be representative of wettability.

There are several other models to calculate oil/water relative permeability curves, such as the Purcell model (Purcell 1949), the Burdine model (Burdine 1953), the Corey model (Corey 1954), and the Brooks-Corey model (Brooks and Corey 1965). The above equations are not very useful when considering wettability alteration.

Rock wettability affects the nature of fluid saturation and the general relative permeability characteristics of a fluid/rock system. Considering the effect of wettability on fluid distributions, it is easy to rationalize that relative permeability curves are strongly functions of wettability (Willhite 1986). There are different proposed equations that relate the endpoint and exponent values of relative permeabilities to the wettability of the rock (Lake 1989; Adibhatla *et al.* 2005; Delshad *et al.* 2006). Because some methods use both phase residual saturations to calculate the new values of endpoint and exponent for the above equations, the results of some studies show that using conjugate phase residual saturation may not reasonably predict values. For instance, the following equations correlate the oil/water relative permeability with wettability alteration proposed by Adibhatla et al. (2005):

$$k^*_{(o/w)} = 1 + \left[k^{*,0}_{rw} + \frac{\cos\theta - \cos\theta^0}{\cos\left(\pi - \theta^0\right) - \cos\theta^0}\left(k^{*,0}_{ro} - k^{*,0}_{rw}\right) - 1 \right]\left(\frac{1 + T_{(w/o)}N^0_T}{1 + T_{(w/o)}N_T}\right) \tag{2.26}$$

$$n_{(o/w)} = 1 + \left[n_w^{*,0} + \frac{\cos\theta - \cos\theta^0}{\cos\left(\pi - \theta^0\right) - \cos\theta^0}\left(n_o^{*,0} - n_w^{*,0}\right) - 1 \right]\left(\frac{1 + T_{(w/o)}N_T^0}{1 + T_{(w/o)}N_T}\right) \quad (2.27)$$

All values with a superscript of "0" correspond to the initial condition. There are no experimental data to support these correlations. N_T is calculated by using Equation 2.12 while trapping value (T) can be found by curve fitting the experimental data of trapping number versus residual oil saturation (e.g.: Figure 3-13).

2.2 Imbibition

In the early 1950's, water injection became a commercial secondary recovery method, and the process of water imbibition became important to understand. Imbibition has been recognized as an important factor in recovering oil especially from water-wet fractured-matrix reservoirs subjected to water flood or water drive. Imbibition and drainage of wetting and nonwetting phases from the matrix blocks of fractured reservoirs depends on a combination of capillary forces, gravity forces, viscous forces, and wettability.

Imbibition is important in numerous daily activities, for example, using cloth or paper towels to dry dishes or clean up spilt liquid, or the transfer of ink or paint to a porous material such as paper (Morrow and Mason 2001). Many research papers have been also published to scale and/or model spontaneous water imbibition in both oil/water/rock and gas/liquid/rock systems (Mattax and Kyte 1962; Blair 1964; Kazemi and Merrill 1979; Schechter *et al.* 1991; Fischer and Morrow 2005; Li and

Horne 2006). But few have included the above mentioned forces along with the rock wettability, and ignoring them in the model might be the reason that the existing methods do not always function successfully. This is important because all the parameters may play important roles in many cases and should not be ignored.

The results of imbibition tests carried out in the laboratory are often scaled to reservoir conditions by scaling group. Mattax *et al*. (1962) extended an imbibition theory that indicated a relationship between the imbibition time and a fraction of oil recovered from a matrix block as shown in Figure 2-19. As a matter of fact, for a given rock type and oil-to-water viscosity ratio, by neglecting the gravity effect, oil recovery behavior can be scaled by the following proposed dimensionless time (t_d):

$$t_d = t\frac{\delta_{oil-water}}{\mu_{water}L^2}\sqrt{\frac{K}{\phi}} \tag{2.28}$$

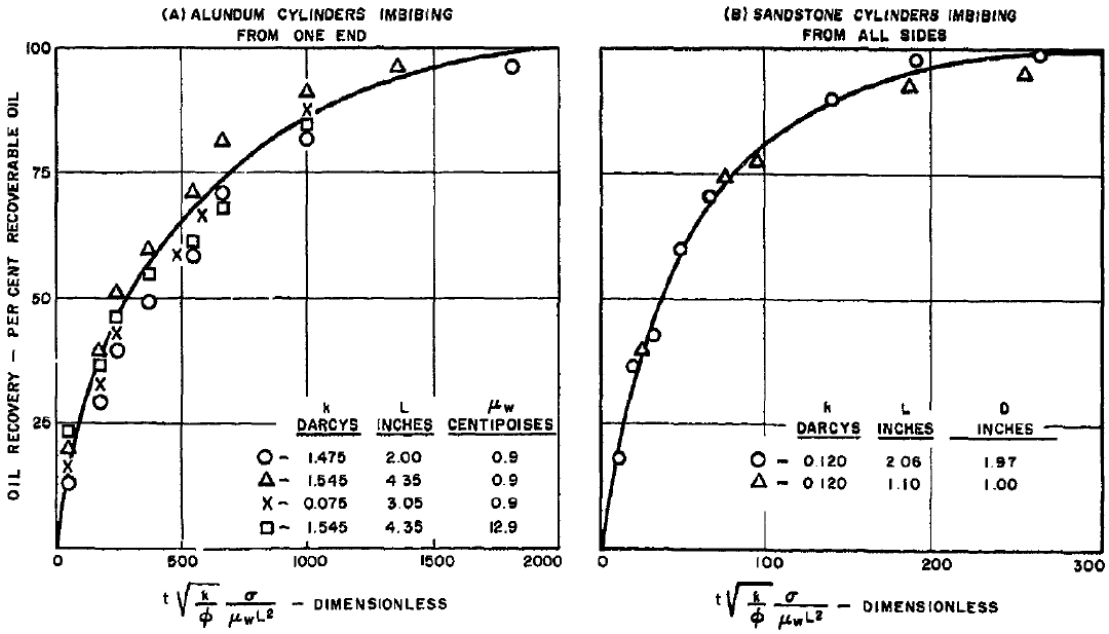

Figure 2-19: Experimental verification of imbibition scaling (Mattax and Kyte 1962)

In the above equation, "L" is characteristic dimension of matrix block or sample and "t" is the actual time of imbibition. The Mattax scaling model has been used and evaluated in many research studies (Schechter *et al.* 1991; Hognesen *et al.* 2004; Adibhatla *et al.* 2005; Fischer and Morrow 2005). This equation was later modified by changing water viscosity to oil viscosity by Cuiec *et al*. (1994). They found that lowering the interfacial tension between the imbibing brine phase and the oil phase in a chalk sample reduced the rate of oil recovery in accordance with the above equation. In 1995, Ma *et al*. suggested that a geometric mean of the viscosities of the two phases is better to use instead of a particular viscosity of any specific phase (Ma *et al.* 1995).

In the area of spontaneous imbibition, there are many publications proved that capillary force is not the only mechanism that drives the imbibition process. For instance, Schechter *et al*. (1991; 1994) showed that both gravity and capillary forces can be important depending on the interfacial tension between oil and water. They reported experimental results that show both gravity and capillary forces can be important when the IFT is moderately low, and that there is a transition from capillary-dominated flow to gravity dominated flow as the IFT is reduced in a ternary oil/water/alcohol system.

They produced three different systems (with three different IFT values) by adding different amount of isopropanol (IPA) to a mixture of isooctane and brine. Different combination of these equilibrated fluids can make various interfacial tension values (significantly different properties) as listed in Table 2-4.

Table 2-4: Phase properties for three different combinations of fluids (Schechter *et al.* 1991)

Test	$\Delta\rho\ (lb_m / ft^3)$	$\sigma_{ow}\ (mN/m)$	$\mu_w\ (cp)$	$\mu_o\ (cp)$
1	20.60	38.10	1.00	0.48
2	13.11	1.07	3.40	0.53
3	6.87	0.10	2.50	0.69

Cylindrical cores of 61 cm in length and 6.35 cm in diameter were mounted vertically in a plexiglass holder with an annular space of 8 mm. In a typical imbibition experiment, the core was saturated with the equilibrated oil, and then rapidly immersed in equilibrated water. Both drainage and imbibition were performed; therefore, cores were initially saturated with either oil or brine. They also used four different rocks with absolute permeabilities of 15, 100, 500, and 700 md. Figure 2-20 shows the recovery curves at different interfacial tension values for the core with permeability of 15 md.

They concluded that the higher total recovery in gravity driven co-current flow at low interfacial tension is due to suppression of entrapment mechanisms (gravity helps prevention of snap-off). Co-current flow occurs when two fluids like oil and water flow in the same direction while if the two moves in the opposite direction flow pattern is called counter-current.

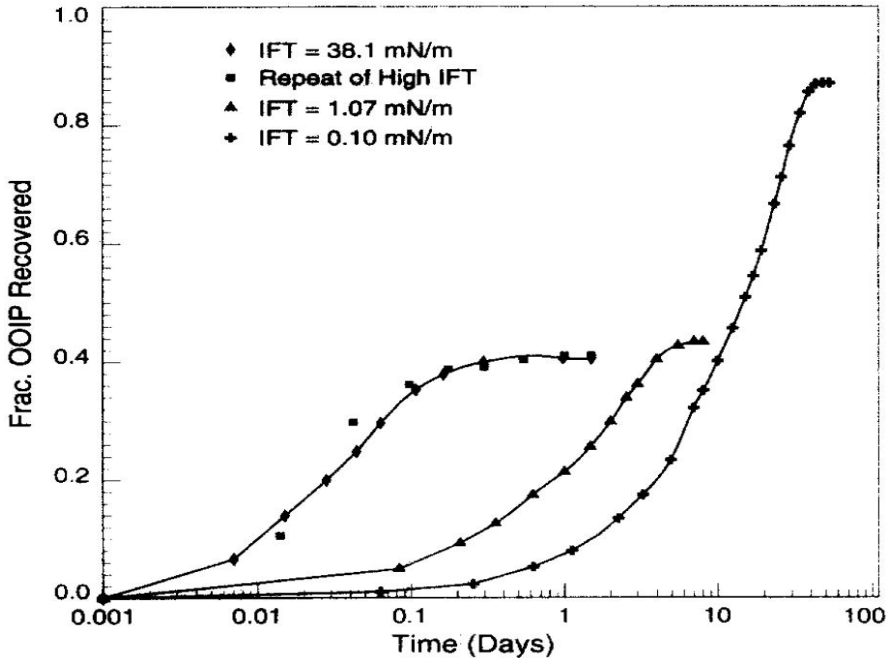

Figure 2-20: Recovery of equilibrated oil phase by capillary imbibition and gravity segregation from a 15 md Berea core (Schechter *et al.* 1991)

Therefore, scaling the experimental data of spontaneous imbibition without considering all mechanisms involved will not provide trustworthy data.

A group of researchers in Stanford University (Li and Horne 2002; 2005; 2006; 2006) developed another approach to scale the experimental data of spontaneous imbibition (Schechter *et al.* 1991) for systems of both counter-current and co-current cases. By assuming a constant gradient in the capillary pressure, which is $\frac{\partial P_c}{\partial x} = \frac{P_c}{x}$ or piston-like displacement, they derived a new relationship between recovery and imbibition time for linear spontaneous imbibition. The dimensionless time (t_d) is expressed as follows:

$$t_d = c^2 \frac{k_e^*}{\mu_e} \frac{P_c^*}{\phi} \frac{S_{w_f} - S_{w_i}}{L_a^2} t \tag{2.29}$$

where $\frac{k_e^*}{\mu_e}$ is the effective mobility ratio of the two phases, which can be calculated from the experimental data of spontaneous imbibition, P_c^* is the capillary pressure at S_{wf}, "*c*" is a parameter associated with the ratio of the gravity force to the capillary force. They used the experimental data of spontaneous water imbibition from Schechter *et al*. (1991) to validate the models in oil/water/rock systems in which gravity may not be negligible.

Figure 2-21 shows that all the experimental data performed at different interfacial tension values in rocks (diameter of 6.35 cm and length of 57-61 cm) with different permeabilities (15, 100, 500, and 700 md) were scaled satisfactorily with the proposed correlation. In this figure, normalized oil recovery is defined as multiplication of the recovery in the units of pore volume and parameter "*c*". Also, Jia *et al*. (2006) used the correlation in gas/liquid/rock systems to find the relative permeability of the liquid phase and the capillary pressure at S_{wf} (Table 2-3).

The general scaling model given by Equation 2.29 was tested for spontaneous imbibition of aqueous surfactant solution into preferential oil-wet carbonate rocks by Høgnesen *et al*. (2004). They commented that it was very surprising that the proposed imbibition model (Li and Horne 2002) seemed to fit their experimental data for a very complex surfactant-assisted spontaneous imbibition process, which had involved wettability alteration and interfacial tension gradients in the carbonate materials.

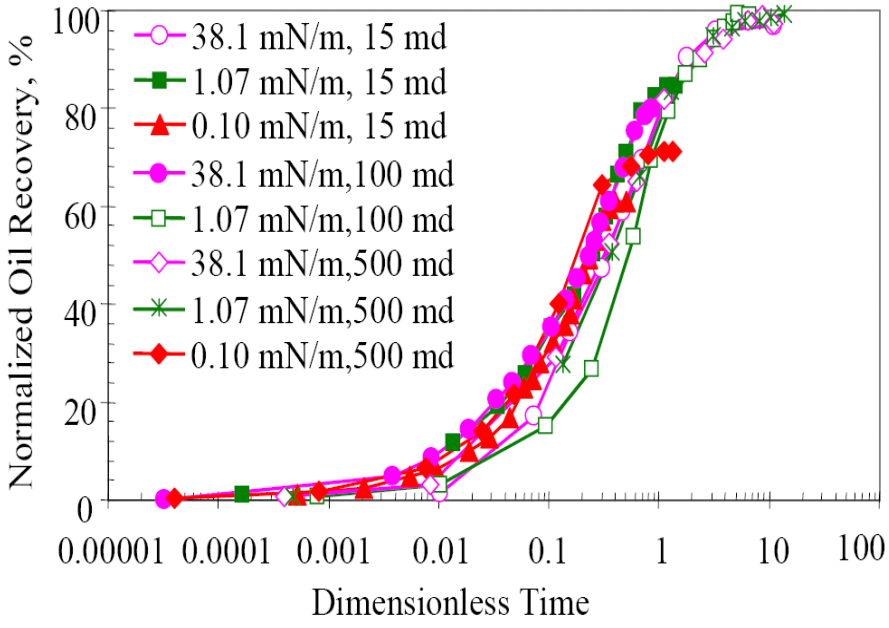

Figure 2-21: Scaling results using Equation 2.29 for different rocks at different values of IFT (Li and Horne 2002)

Blair (1964) developed a numerical solution for the equations describing imbibition in a water-wet core system. Figure 2-22 shows pressure and saturation profiles at 6.6 hours. Based on the simulation outcomes, he concluded that the time required to imbibe a fixed volume of water of a certain viscosity is approximately proportional to the square root of the viscosity of the reservoir oil whenever the oil viscosity is greater than the water viscosity. The effect of gravity was not considered in his calculations which was later included by some other researchers (Kazemi and Merrill 1979).

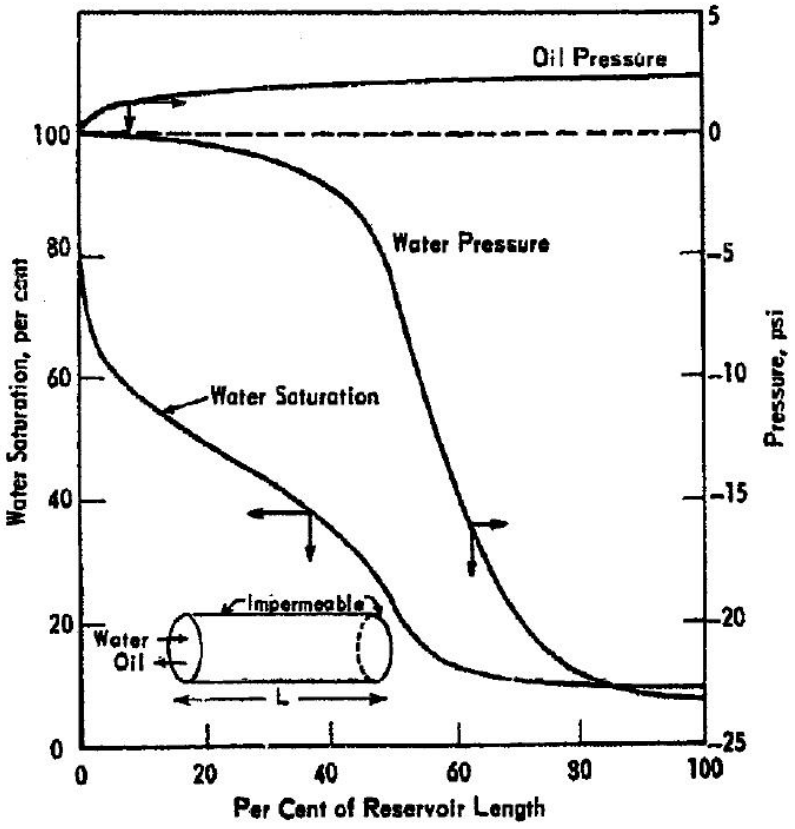

Figure 2-22: Water/Oil pressure and water saturation distributions (Blair 1964)

2.3 Surfactants

Surface-active agents, or surfactants, are chemical substances that adsorb onto or concentrate at a surface or fluid-fluid interface when present at low concentration in a system (Green and Willhite 1998). They contain both hydrophobic groups (head) and hydrophilic groups (tail). That is why they are typically soluble in both organic solvents (such as oil) and water. Many surfactants can also assemble in the bulk solution into aggregates. Examples of such aggregates are vesicles and micelles. The concentration at which surfactants begin to form micelles is known as the critical

micelle concentration (CMC). The size and shape of the micelle depends on the nature of the surfactant and its concentration. The head of an ionic surfactant carries a net charge so surfactants may be classified according to the ionic nature of the head group (charged groups in the head).

A *non-ionic* surfactant (e.g.: dodecylhexaoxyethylene glycol monoether, $C_{12}H_{25}[OCH_2CH_2]_6OH$) has no charge groups in its head. If the charge is negative, the surfactant is more specifically called *anionic* (e.g.: sodium dodecyl sulfate, $C_{12}H_{25}SO_4^-Na^+$); if the charge is positive, it is called *cationic* (e.g.: dodecyl trimethylammonium bromide, $C_{12}N\ [CH_3]_3Br$). If a surfactant contains a head with two oppositely charged groups, it is termed *zwitterionic* (e.g.: 3-dimethyldodecylamine propane sulfate, $C_{12}H_{25}Me_2N^+\ [CH_2]_3SO_3^-$).

2.3.1 Interfacial Tension

It is known that potential energy of molecules in the interior of a liquid is less than those of similar molecules at the surface of the liquid. The reason is that repulsive interactions of molecules at the surface, e.g. liquid and gas, where molecules in the gas phase are more widely spaced is greater than those in the interior of the liquid. At the interface between two condensed phases however, molecules that are dissimilar (either in structure or in the nature of their intermolecular forces) in opposed layers have potential energies different from those in their respective phases.

For example, consider an interface between two pure liquid phases α and β as shown in Figure 2-23. If the molecular interaction energy between α molecules at

the interface and similar molecules in the interior of the bulk phase is termed $\Psi_{\alpha\alpha}$ whereas $\Psi_{\alpha\beta}$ is used to symbolize the molecular interaction energy between α molecules at the interface and β molecules across the interface, then the increased potential energy of the α molecules at the interface over those inside that phase is $\Psi_{\alpha\alpha} - \Psi_{\alpha\beta}$. Therefore, the increased potential energy of all the molecules at the interface over those within the interior of the bulk phases, the interfacial free energy, is then $\left(\Psi_{\beta\beta} - \Psi_{\alpha\beta}\right) + \left(\Psi_{\alpha\alpha} - \Psi_{\alpha\beta}\right)$. This is the minimum work required to create the interface. The $\alpha - \beta$ interaction energy per unit area across the interface (interfacial free energy per unit area of interface), named ξ_I, is then given by the following expression:

$$\xi_I = \xi_\alpha + \xi_\beta - 2\xi_{\alpha\beta} \tag{2.30}$$

where ξ_α and ξ_β are the surface free energies per unit area of the pure liquids α and β, in the order designated.

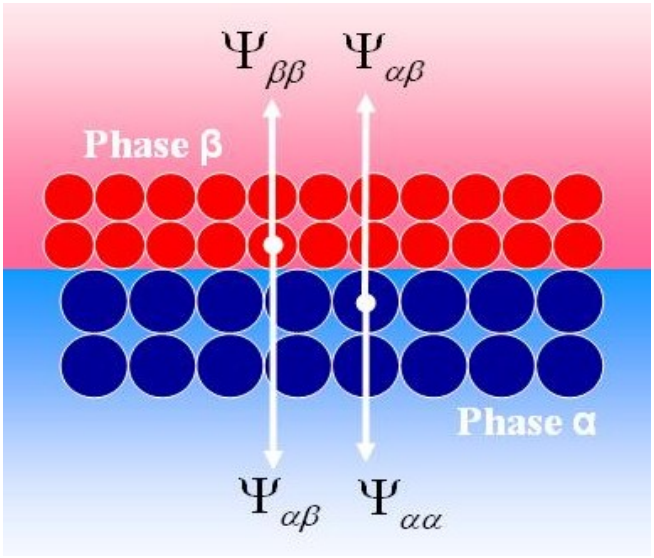

Figure 2-23: Simplified diagram of the interface between two immiscible phases

2.3.2 Interfacial Tension Reduction

If a surface active agent (called surfactant) is adsorbed at the interface between two immiscible phases like oil and water, surfactant will orient itself, mainly with the hydrophobic group toward the oil phase and the hydrophilic group toward the water phase. When surfactant molecules replace water and/or oil molecules at the original interface, one major interaction across the interface would be between the hydrophilic group of the surfactant and water molecules on one side of the interface and between the hydrophobic group of the surfactant and oil on the other side of the interface. Since these interactions would now be much stronger than the original interaction between the highly dissimilar oil and water molecules, the tension across the interface is reduced by the presence of the surfactant.

According to the above discussion, one can understand why interfacial tension reduction can happen in the presence of the surfactant molecule of both hydrophobic and hydrophilic portions. There are two roles for the hydrophilic portion of surfactants: first, to reduce spontaneous adsorption of the surfactant molecule at the interface and second, to increase interactions across the interface between the adsorbed surfactant molecules there and the molecules in the adjacent phase (Rosen 1989). Providing strong interactions between the surfactant molecules at the interface and the solvent molecules is the function of the hydrophobic group. If any of these functions is not performed, then the prominent reduction of interfacial tension that is characteristic of surfactants will probably not occur.

Therefore, we would not expect ionic surfactants containing hydrocarbon chains to reduce the surface tensions of hydrocarbon solvents, e.g. Benzene and Kerosene, despite the distortion of the solvent structure by the ionic groups in the surfactant molecules. This is because adsorption of such molecules at the air-hydrocarbon interface with the ionic groups oriented toward the predominantly nonpolar air molecules would result in decreased interactions across the interface.

2.4 Wettability Alteration by Crude Oil

Most oil reservoirs are located in sedimentary rocks consisting of either carbonate or sandstone. It is believed that all reservoirs were initially saturated with water before hydrocarbon accumulation so they were water-wet. However, after hydrocarbon invasion, precipitation of heavy oleic components and resin fractions of crude oil

made them less water-wet. It is broadly believed that asphaltenes and other high molecular weight polar constituents of crude oil are responsible for changing the wetting of reservoir rocks although alteration quantity can be affected by additional factors such as rock surface mineralogy, brine composition, crude oil composition (the most important), temperature, and pressure.

2.5 Wettability Alteration by Chemicals

Any changes in the original wettability of a rock either spontaneous or via enhanced oil recovery methods, is termed as *wettability alteration*. The following discussion emphasizes alteration from oil-wetness to water-wetness, which is a desirable event in producing oil from oil-wet fractured reservoirs. Wettability alteration has received more attention recently for carbonate formations compared to sandstones because carbonate formations are much more likely to be preferentially oil-wet (Treiber and Owens 1972). Also, carbonate formations are more likely to be fractured and depend on spontaneous imbibition or buoyancy for displacement of oil from the matrix to the fracture.

2.5.1 Effect of Surfactants: Experimental Studies

In this section, a review of the literature is presented to describe noteworthy experiments related to the main idea of the present research.

2.5.1.1 Water-wet Systems

A research group under the supervision of Dr. Tor Austad at the University of Stavanger (Norway) studied the effect of interfacial tension and core length on the imbibition of a surfactant solution into a 100% oil-saturated water-wet chalk material (Milter and Austad 1996a). The tests were performed with vertical short cores (5-6 cm long) and long composite chalk cores (21-27cm long).

They inferred that in the absence of surfactant, the imbibition mechanism is a counter-current flow governed by capillary forces, which has been documented in the literature properly (Mattax and Kyte 1962; Blair 1964; Kyte 1970; Willhite 1986; Schechter *et al.* 1991). In the presence of surfactant, at the beginning of the imbibition, capillary force is the dominant process because oil was produced from all over the core (counter-current flow); however, after a while, gravity force overcomes capillary force because the oil is mainly produced from the uppermost surface as was similarly reported by Babadagli *et al*. (2003).

Also, it was observed that the oil recovery in the case of low interfacial tension (0.02 mN/m) by using surfactant did not exceed oil recovery in the case of absence of surfactant in the system. Figure 2-24 shows imbibition profiles for the small-core experiments at both low interfacial tension and high interfacial tension (30 mN/m). Regardless of the experimental tests, this result is similar to Schechter's result (1991) shown in Figure 2-20. The upper curve shows that counter-current flow due to the capillary force domination derived the imbibition process. In the case of low interfacial tension, gravity force is the dominative force so the imbibition rate is low.

In the case of the long-core experiments, the trend of the profiles was the same as in Figure 2-24 except that the production plateau peaked around 55% at high interfacial tension.

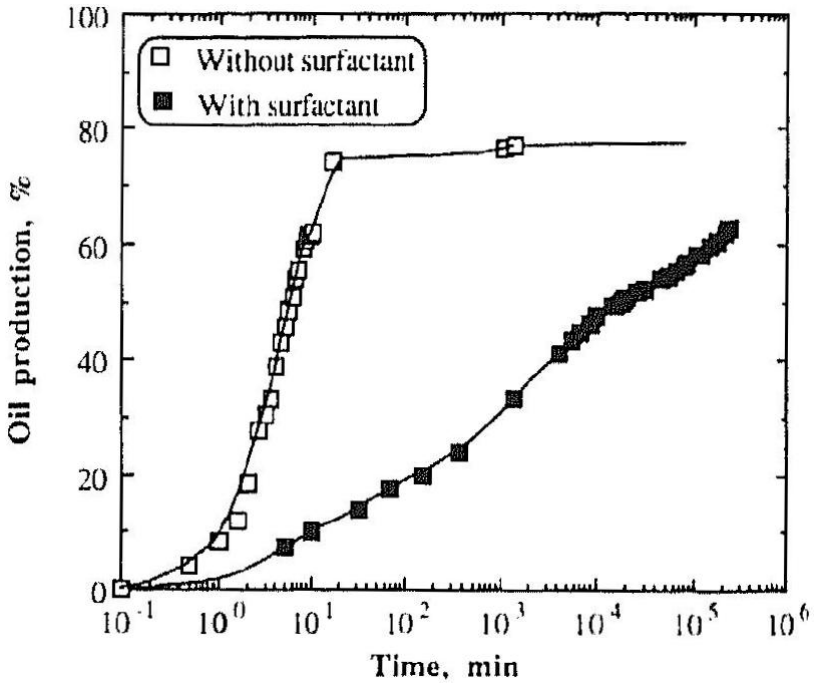

Figure 2-24: Imbibition profile for the small-core experiments (Milter and Austad 1996a)

If only the capillary force was active at the start of the oil expulsion, the imbibition profile (oil recovery vs. dimensionless time) should have been superimposed at low oil recoveries whether with or without surfactant. According to Figure 2-25, they claimed that the rate of oil production in the presence of surfactant is about 100 times faster than that in the absence of surfactant at the early time of imbibition. Therefore, gravity force is involved in oil production along with capillary force.

In the absence of surfactant, after reaching the oil production plateau, the brine was substituted with a mixture of brine and an anionic surfactant (1.0 wt. %). No significant extra oil was recovered. This evidence suggests that the capillary force alone, no longer remains the dominant mechanism in oil production when surfactant is added to the system (Austad and Milter 1997).

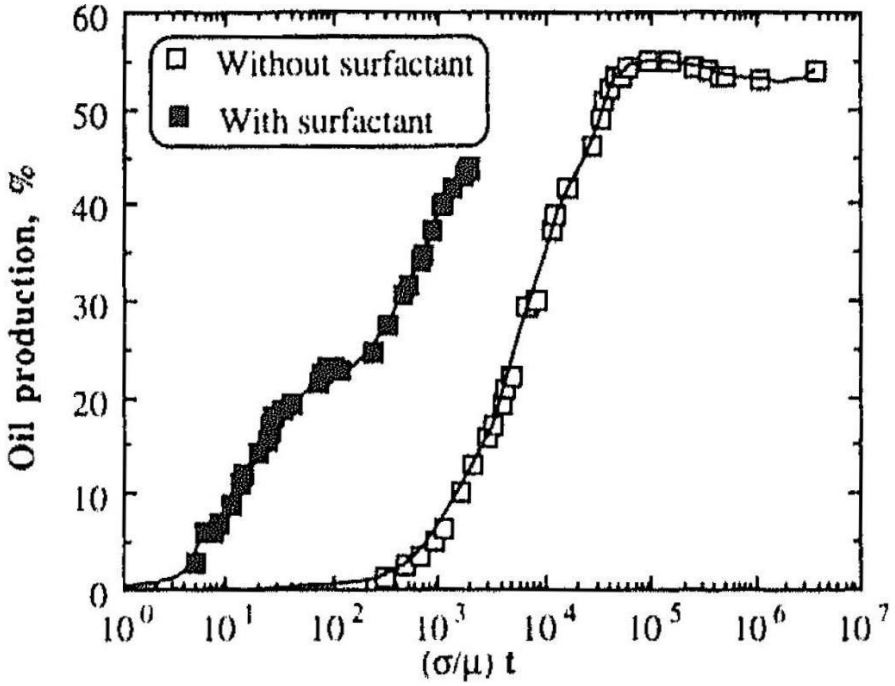

Figure 2-25: Oil production from the long water-wet core scaled according to the capillary forces (Milter and Austad 1996a)

Also, by using either cationic or anionic surfactants from the beginning of the imbibition process, a crossover from a counter-current flow to a co-current flow appears to be the flow mechanism. Oil recovery due to gravity forces (co-current

flow) did not exceed recovery via water imbibition even after 3500 hours (Austad *et al.* 1998).

2.5.1.2 Mixed-wet Systems

Milter and Austad (1996b) also studied the imbibition process for mixed-wet rocks (100% oil saturated). At the first step, they created mixed-wet cores by mixing different fractions of *n*-heptane with crude oil (e.g. Oil C contains 67% pure *n*-heptane and 33% crude oil of the Ekofisk field in the North Sea) and aging the chalk material in the oil mixture for 4 days at 50°C. They performed the imbibition tests in the presence and absence of surfactant in aqueous solution.

Recovery for the short core in the presence of surfactant was extremely slow, and appeared to stop after about 14 days. Only 5% of the oil was recovered; however, oil recovery in the long core (55cm) was almost twice as productive (10%) due to the use of gravity force.

Anionic surfactant (alkyl-propoxy-ethoxy-sulfate, 1.0 wt. % > CMC) was added in the brine used in the imbibition experiments of the long core. Recovery increased to 13% after 70 days. They believed that the extra oil is recovered by displacing oil from oil-wet areas inside the core due to alteration of the rock wettability towards water-wet (Austad and Milter 1997). In Figure 2-26 and Figure 2-27, those production profiles labeled as oil C belong to the mixed-wet cores (oil D is pure *n*-heptane). In fact, oil C was capable to turn a fresh core to a mixed-wet condition due to the presence of crude oil, while oil D was not able to do so because pure *n*-heptane

does not contain polar constituents which are responsible to change the initial rock wettability.

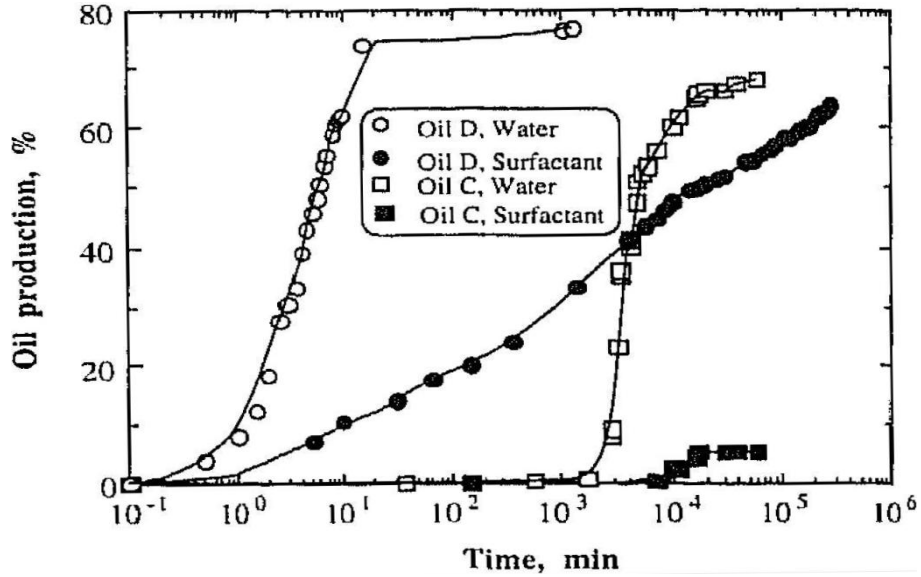

Figure 2-26: Imbibition profile for the short-core experiments (Milter and Austad 1996b)

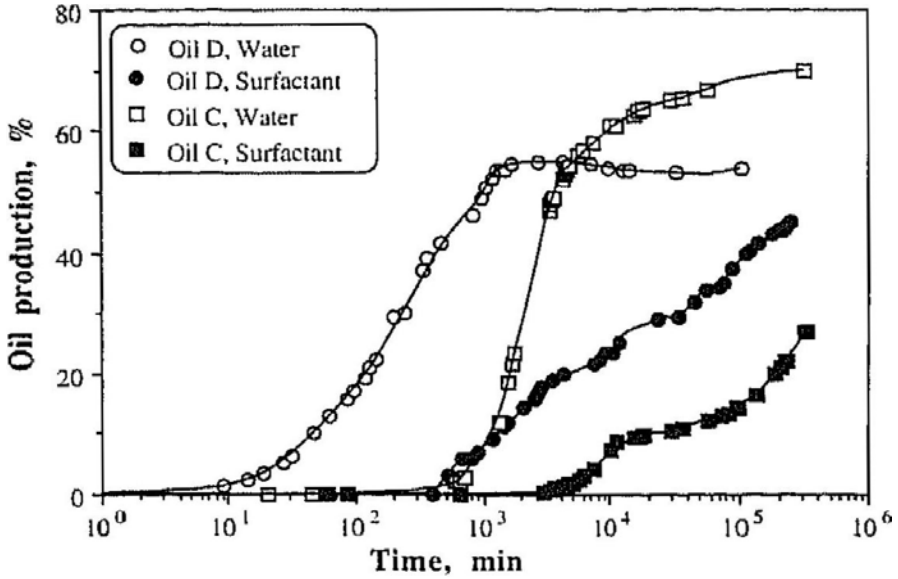

Figure 2-27: Imbibition profile for the long-core experiments (Milter and Austad 1996b)

2.5.1.3 Oil-wet Systems

The Austad group studied the effect of cationic and anionic surfactants on the oil production by imbibition. A series of spontaneous oil expulsion experiments were preformed with oil-wet cores at ambient conditions, with and without a cationic surfactant called dodecyltrimethylammonium bromide (C_{12}TAB). These tests showed that anionic surfactants have a negative effect on oil recovery for the tests (Austad *et al.* 1998).

To change the wettability of the cores toward oil-wet, dried cores were placed in a container completely filled with oil mixture (33 vol. % and 67 vol. % of the crude oil and *n*-heptane respectively). Cores imbibed the oil mixture and were saturated after approximately 12 hours. They aged the cores in the oil mixture for 22 days at 50°C in order to obtain nearly oil-wet chalk cores. They claimed that a homogeneous oil-wet core can be experimentally obtained by flooding the core with the oil in each direction and removing the outermost layer of the core after aging the core in the actual crude oil. The cores were finally characterized at initial water saturations of zero and 27%.

The imbibition tests were performed with and without surfactant present in aqueous solution. Without surfactant present, the rate of the oil expulsion was low as shown in Figure 2-28. After 95 days, the aqueous phase was exchanged with a 1 wt. % solution of the cationic surfactant. Oil production started immediately from all of the core surfaces, which indicates a counter-current flow mechanism governed mainly by capillary forces. If surfactant solution was present from the beginning, then the

final oil production plateau of 65% recovery was achieved within 90 days (Figure 2-28). With presence of surfactant in the water (1%, CMC=0.43 wt. %), the increase in capillary forces by making the surface water-wet must overcome the decrease in the capillary forces due to a decrease in interfacial tension. The cationic surfactant decreased initial interfacial tension (15.4 mN/m) by a factor of about 20, and the fact that the imbibition rate increases drastically even though the flow mode is counter-current points to a change in wettability towards a more water-wet system (Austad and Milter 1997). By cutting the core vertically, no segregation in the oil was observed, confirming that the displacement took place in a counter-current flow process (counter-current flow occurs when two fluids moves in the opposite directions).

The presence of counter-current flow was also reported by others (Chen *et al.* 2001; Adibhatla and Mohanty 2007; Salehi 2009). For example, Chen *et al*. (2001) suggested that capillary force and interfacial tension gradient expedited counter-current movement in the radial direction within a short period whereas vertical gravity segregation was responsible for the late stage ultimate recovery.

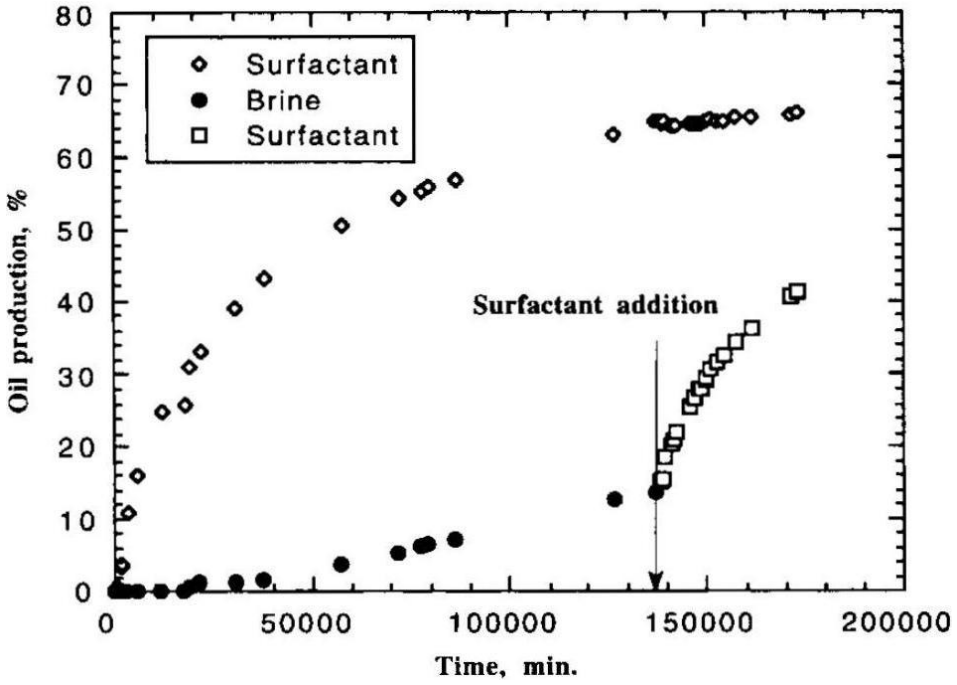

Figure 2-28: Imbibition profile with and without cationic surfactant (Austad *et al.* 1998)

They proposed a mechanism for changing the wettability in the oil-wet rock in the presence of the cationic surfactant, which is for nearly oil-wet samples, the water dissolved in surfactant micelles may act as powerful nucleophiles towards the chalk surface (the rather high HLB value for the cationic surfactant suggests that the reversed micelles are unstable). The water then adsorbs onto the chalk surface just across the oil-water interface in the pores and makes the surface more water-wet, which improves the imbibition of water. Here is a schematic of the proposed mechanism:

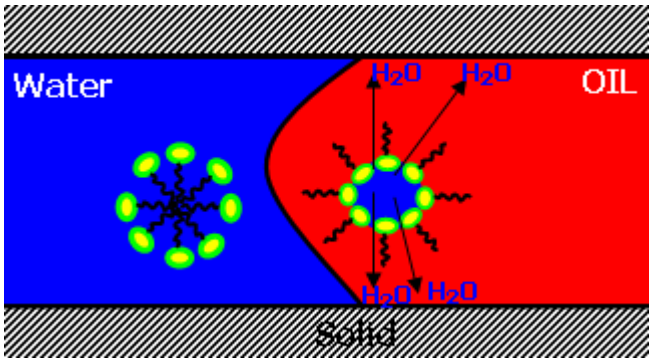

Figure 2-29: Schematic illustration of the proposed imbibition mechanism in the presence of surfactant (after Austad *et al.* 1998)

Standnes *et al*. (2000a) studied on the oil-wet cores with an initial water saturation of 23%. They believed that a clean core can be converted into an oil-wet core if the oil with high acid numbers is used in the preparation steps and that an acid number is the most important wetting parameter; however, aging temperature only plays a very minor role in determining wetting conditions (Standnes and Austad 2003; Zhang and Austad 2005a). For example, Figure 2-30 shows a brine imbibition of an oil-wet core at irreducible water saturation. Because of the low recovery shown in Figure 2-30, the wettability of a clean core was believed to be altered to the oil-wet condition.

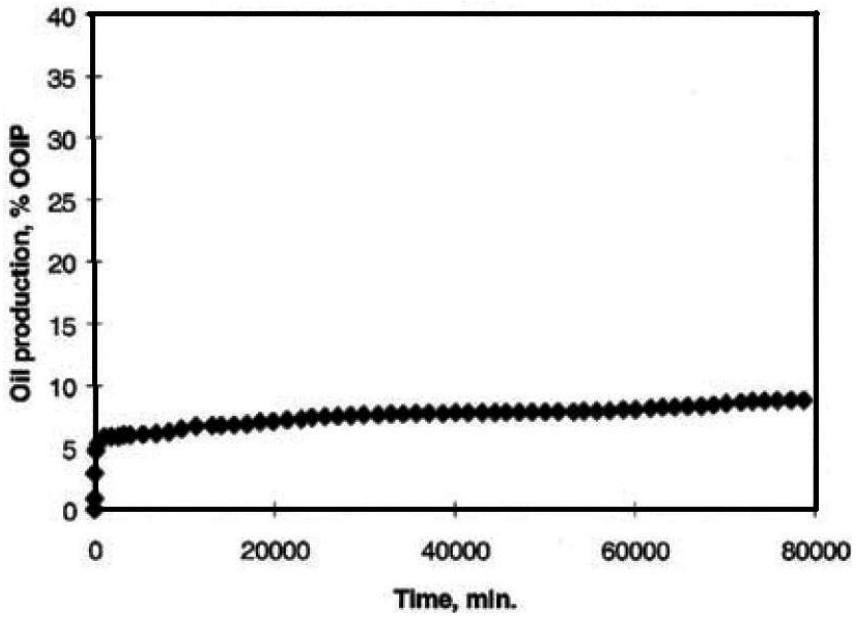

Figure 2-30: Spontaneous imbibition of brine into the claimed oil-wet chalk at irreducible brine saturation (Standnes and Austad 2000a)

Also, they used fourteen different surfactants (other than $C_{12}TAB$) for spontaneous imbibition into oil-wet chalk cores and discovered that cationic surfactants are able to make an irreversible ion-pair formation with adsorbed negatively charged carboxylates (Figure 2-31), which leads to less of an oil-wet core (Standnes and Austad 2000b; Standnes *et al.* 2002). This is the reason why they mostly used cationic surfactants in the oil-wet systems.

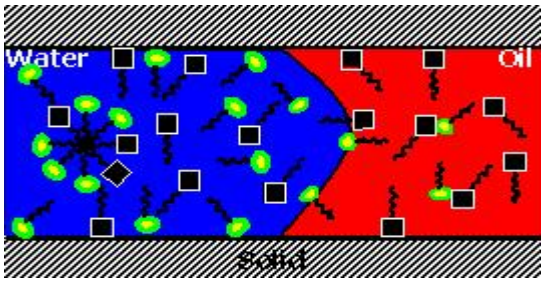

Figure 2-31: Schematic of wettability alteration mechanism proposed for oil-wet system (after Standnes and Austad 2000b)

However, this does not mean that the anionic surfactants are unable to change wettability. For instance, Seethepalli *et al*. (2004) examined several anionic surfactants and sodium carbonate against cationic surfactants. Most of the anionic surfactants were able to change the wettability of calcite surfaces equally well or better than the cationic surfactant, dodecyltrimethylammonium bromide (DTAB).

The same behavior was reported by Salehi *et al*. (2008). They aged two Berea sandstone cores (B04 and B05) with crude oil and flooded with Soltrol 130 (oil) to reach desirable water saturation. These two cores then were placed in 1% brine for two weeks and then one of them was placed in a cationic surfactant solution (C_{12}TAB) and the other in an anionic surfactant solution (STEOL CS-330). The anionic surfactant performed better compared with cationic surfactant, as shown in Figure 2-32. In fact, choosing the type of the surfactant (either anionic or cationic) depends on some factors such as rock type, crude oil properties.

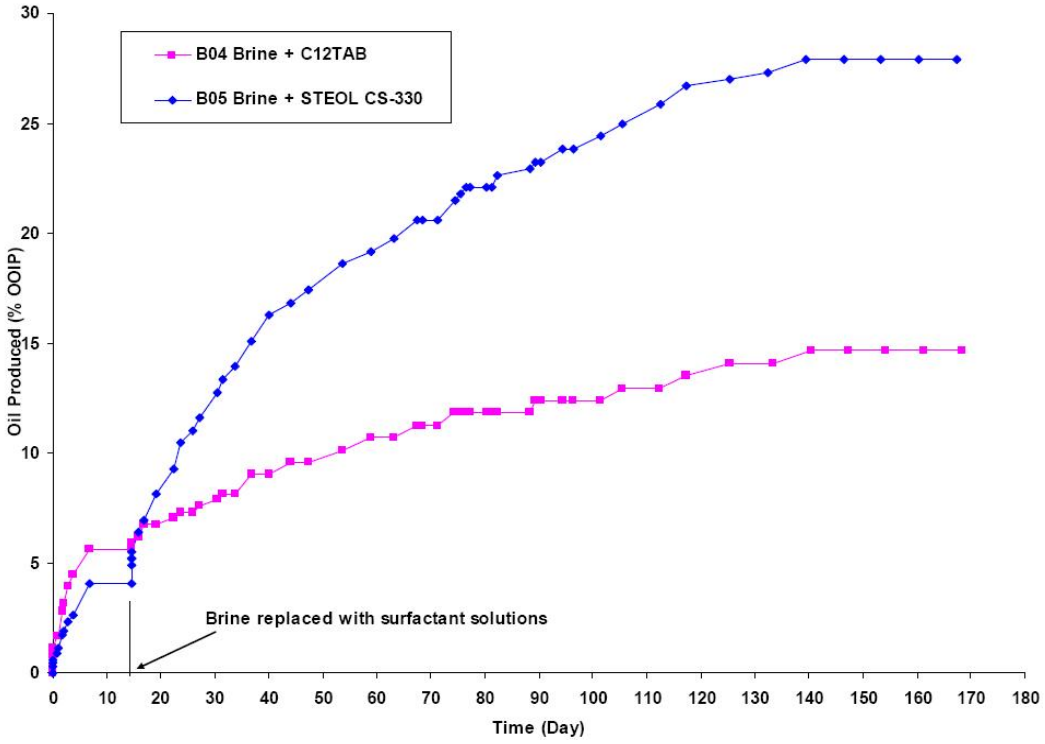

Figure 2-32: Sandstone cores B04 and B05 imbibition profiles in 1 % brine solution and in 1.0 mmol/L solution of cationic and anionic surfactant solutions (Salehi *et al.* 2008)

Standnes and Austad (2000b) claimed that the surfactant adsorbs via a hydrophobic interaction with the hydrocarbon layer adsorbed on the surface of the chalk as shown in Figure 2-31, leaving the water soluble head-group of the surfactant oriented toward the solution. This would result in the formation of a thin water zone and create weak capillary forces during the imbibition process. This hypotheses also recently verified by Salehi *et al*. (2008).

Figure 2-33 shows spontaneous imbibition curves for different concentrations of C_{12}TAB. The figure shows that spontaneous imbibition was strongly dependent on surfactant concentration (Høgnesen *et al.* 2006a). The presence of micelles seemed to

be of crucial importance for the spontaneous imbibition to proceed into oil-wet chalk material. Micelles were expected to enhance the desorption rate of organic material in two ways. First, they act as a supplier of surfactant monomer to ensure a high concentration of monomers at the oil-water-solid contact line. Second, micelles help in the solubilization of desorbed materials. Although Figure 2-33 at first seems to convey that maximum oil recovery decreases as the amount of surfactant increases at surfactant concentrations above CMC, in fact, as the surfactant concentration increases in the aqueous phase surrounding the core, more of the displaced oil is solubilized into micelles thereby decreasing the volume of excess oil during the experiment.

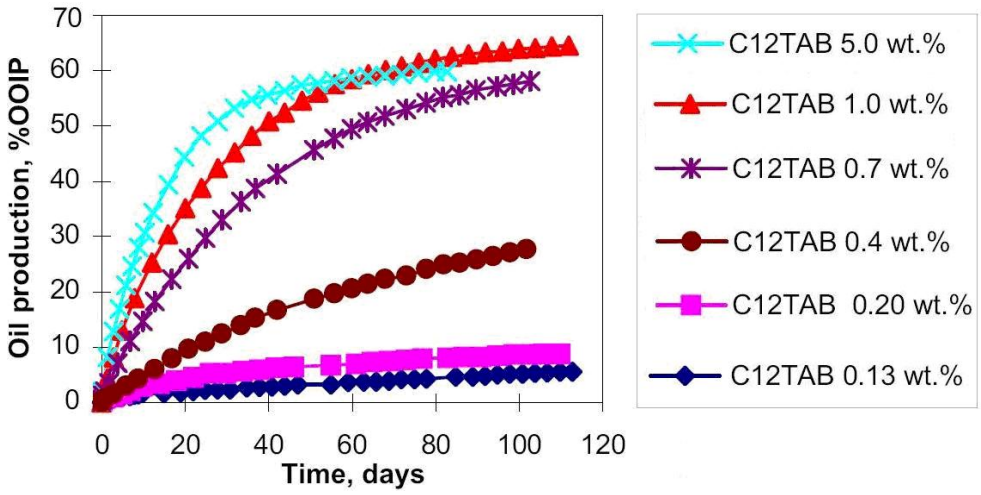

Figure 2-33: Spontaneous imbibition at various concentration of n-C_{12}TAB at 40°C and So_i=100% (after Standnes and Austad 2000b)

They also performed two imbibition tests at very low surfactant concentration, 0.1 wt. % (Figure 2-34), which is well below the CMC. For the two experiments, an average

of about 13% of the initial oil was produced, and the plateau was reached within 40 days. After 80 days, the cores were cleaved, and in this case a vertical segregation of the fluid inside the core was observed (Figure 2-35). In Figure 2-35 the area invaded with the aqueous solution is shown by drawing lines due to low quality of the original picture.

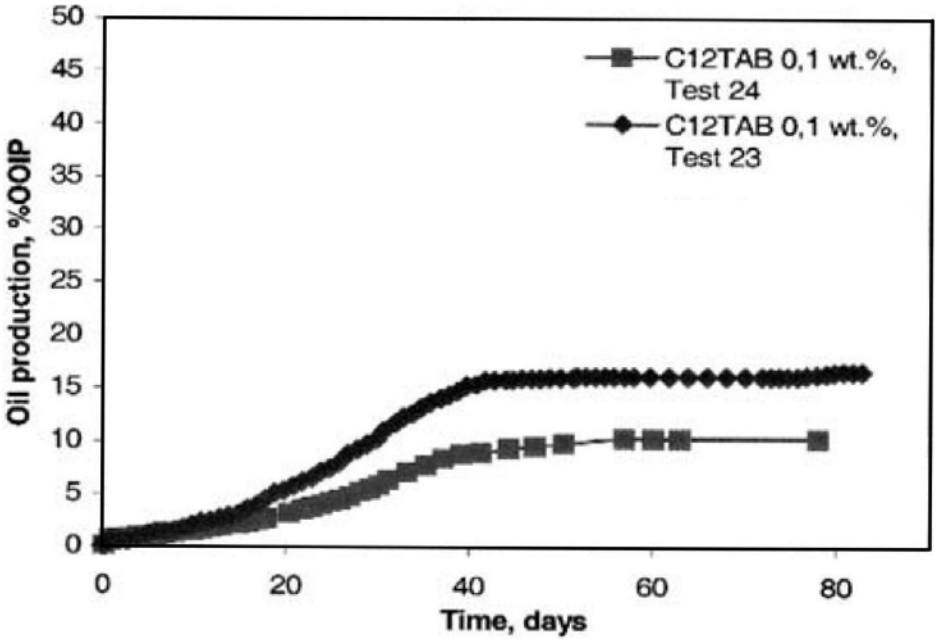

Figure 2-34: Spontaneous imbibition of n-C12TAB into oil-wet Core at initial surfactant concentration of 0.1wt % at 40°C and So_i=100% (Standnes and Austad 2000b)

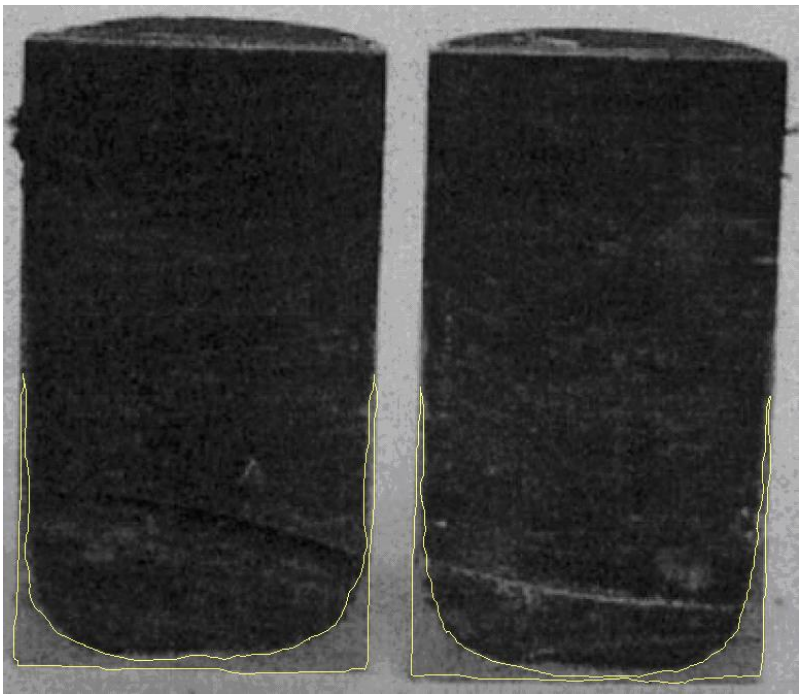

Figure 2-35: Fluid distribution inside the core at the end of the imbibition test using 0.1 wt% solution of n-C_{12}TAB (after Standnes and Austad 2000b)

Contrary to the 100% oil-saturated cores, the wettability alteration of the chalk core with initial water saturation of 23% must be somewhat heterogeneous and the outermost part of the core appears to be more water wet (Figure 2-36). They explained this due to end effects related to the saturation procedure used to establish residual water saturation. Although 2 mm of the core material were shaved off, this is probably insufficient to create a homogeneous oil-wet core (Standnes and Austad 2000b; a). However, they suggested that the imbibition behavior of cores with and without initial water saturation were quite similar and confirmed that the rate and extent of oil production were mainly determined by the surface-active materials initially present at the cores (Austad and Standnes 2003).

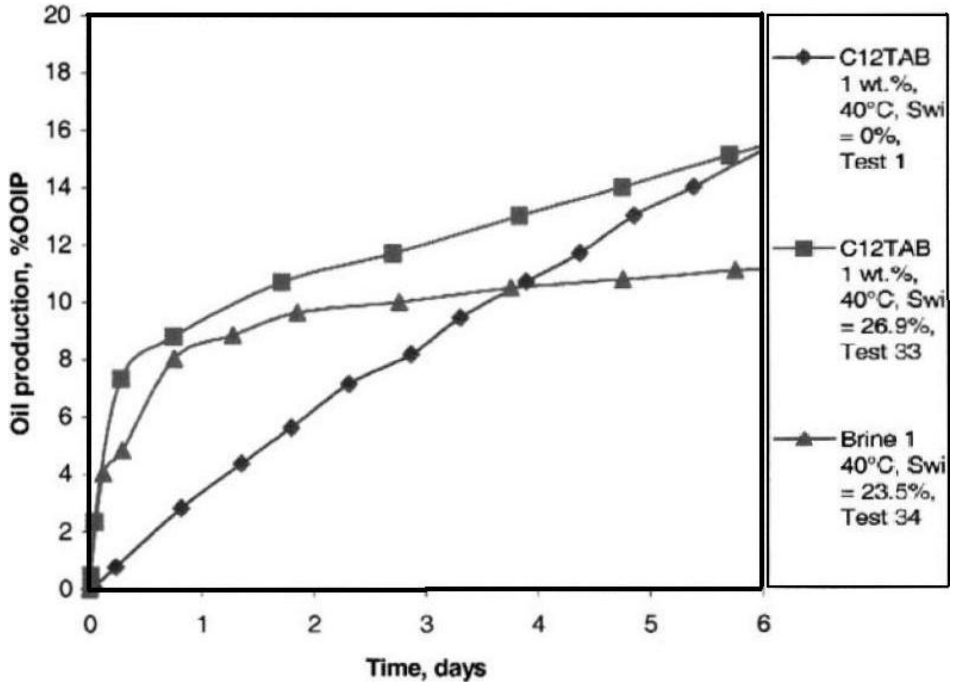

Figure 2-36: Spontaneous imbibition for cases with and without residual water saturation (Standnes and Austad 2000b)

At Rice University, Hirasaki *et al*. (2003; 2004; 2008) have studied characteristics of different surfactants (anionic, cationic, alkaline …) on oil-wet carbonate and sandstone cores through many experiments. The experiments consisted of dead crude oil, formation brine, and reservoir cores from the Yates oil reservoir in West Texas. Although several reservoir cores were used in different experiments under slightly different conditions, all were carbonates with low permeability and moderate porosity. The core samples were flooded by crude oil to residual water saturation and some were aged for 24 hours at 80°C. The formation brine used in the experiment contained mostly NaCl and small concentrations of $CaCl_2$ and $MgCl_2$. The crude oil

used in their studies had a viscosity of 19.1 cp and an API gravity of 30°. They found that the spontaneous imbibition in carbonate formations often does not occur or is slow compared to sandstone formations as reported in the literature (Treiber and Owens 1972; Schneider 1976; Anderson 1986a). If the formation is preferentially oil-wet, the matrix will retain oil by capillary, and high oil saturation transition zones will exist where the upward oil film flow path is interrupted by fractures. This is illustrated in Figure 2-37, which shows the oil retained by oil-wet capillaries of different radii. They concluded that interfacial tension reduction and wettability alteration are two responsible mechanisms for producing oil from oil-wet rocks (Figure 2-38).

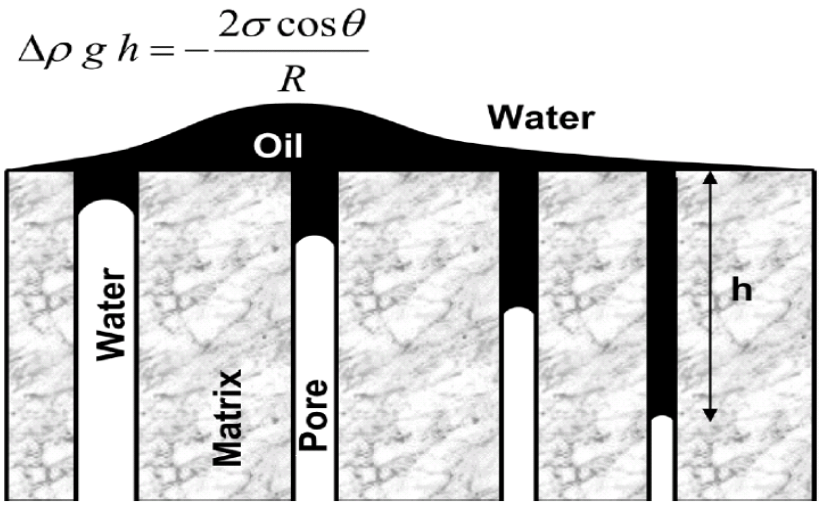

Figure 2-37: The height of the retained oil in oil-wet matrix pores as a function of the radius, interfacial tension, and contact angle followed Equation 2.17 (Hirasaki and Zhang 2004)

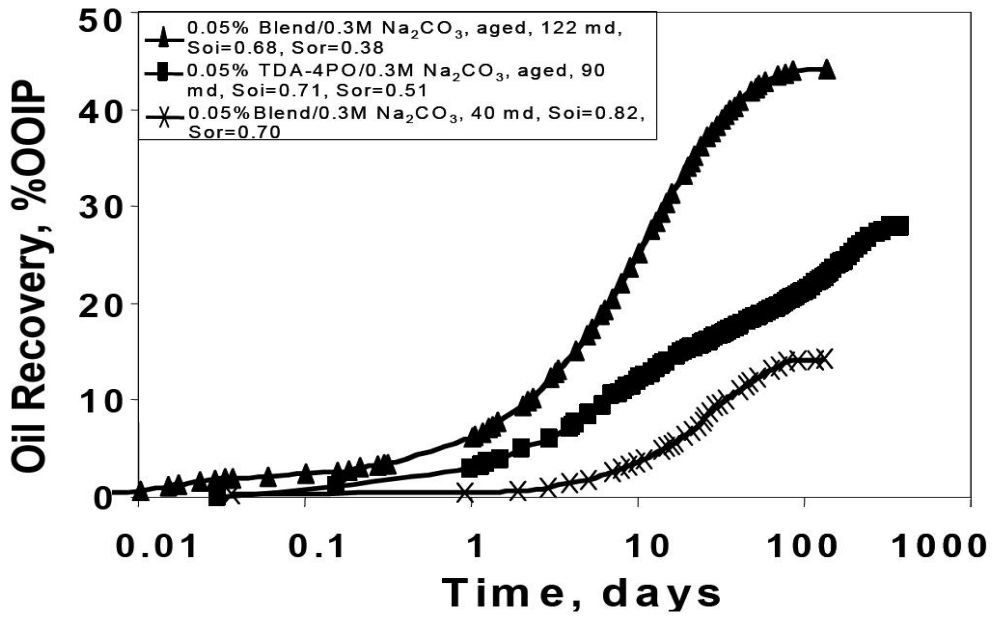

Figure 2-38: Oil recoveries from spontaneous imbibition of surfactant solutions for different conditions (Hirasaki *et al.* 2004)

2.5.2 Effect of Surfactants: Numerical Studies-Critique of Available Wettability Alteration Models

In a broad sense, reservoir simulation has been developed since the beginning of petroleum engineering in the 1930's. CO_2 injection, chemical (surfactants/polymer) flooding, miscible flooding and steam or hot water flooding began to feature in commercial reservoir simulator due to the sharp rise in oil prices during the 1970's (Coats 1982). Since then, reservoir simulation science for many reservoir types has progressed; however, oil-wet reservoirs have not been paid enough attention due to difficulties in understanding and characterizing the phenomena occurring in these types of the reservoirs. On the other hand, the dimensionless time formula, scaling

groups, and one-dimensional analytical solution do not apply practically to imbibition processes with changing the rock wettability and interfacial tension.

Numerical simulators have been developed for chemical flooding where interfacial tension changes with time; however, wettability alteration has been numerically considered in a few studies. Delshad *et al*. (2006) adapted the chemical flooding simulator, UTCHEM, to model an improved oil recovery process that involves wettability alteration using surfactants. This model is based on the effect of surfactant on capillary pressure, relative permeability, and residual saturation of each phase. Two extreme wetting conditions are assumed, original and final wetting conditions and, for example, relative permeability of each phase, which is computed using Corey-type exponential functions (Equations of 2.18 and 2.19), is calculated for both extreme cases in any gridblock (Najafabadi *et al.* 2008). The relative permeability used for each gridblock, which is referred to as actual relative permeability, at each timestep is then obtained by interpolation between these two extreme values.

A scaling factor for wettability alteration is then defined as the following equation (Delshad *et al.* 2006; 2009):

$$\omega = \frac{\hat{C}_{surf}}{\hat{C}_{surf} + C_{surf}} \tag{2.31}$$

where $\hat{C}_{surf}$ and C_{surf} represent the adsorbed and total concentration of surfactant, respectively. This factor can be also set as a constant value regardless of surfactant adsorption.

The same strategy is used for capillary pressure values as used for relative permeability. The capillary pressure as a function of wettability is also modeled using linear interpolation between the capillary pressure of the initial wetting state and the final condition as follows;

$$P_c = \omega P_c^{final} + (1-\omega) P_c^{initial} \tag{2.32}$$

and for relative permeability curves;

$$k_{r(w/o)} = \omega k_{r(w/o)} + (1-\omega) k_{r(w/o)} \tag{2.33}$$

The following figure shows a result of their model.

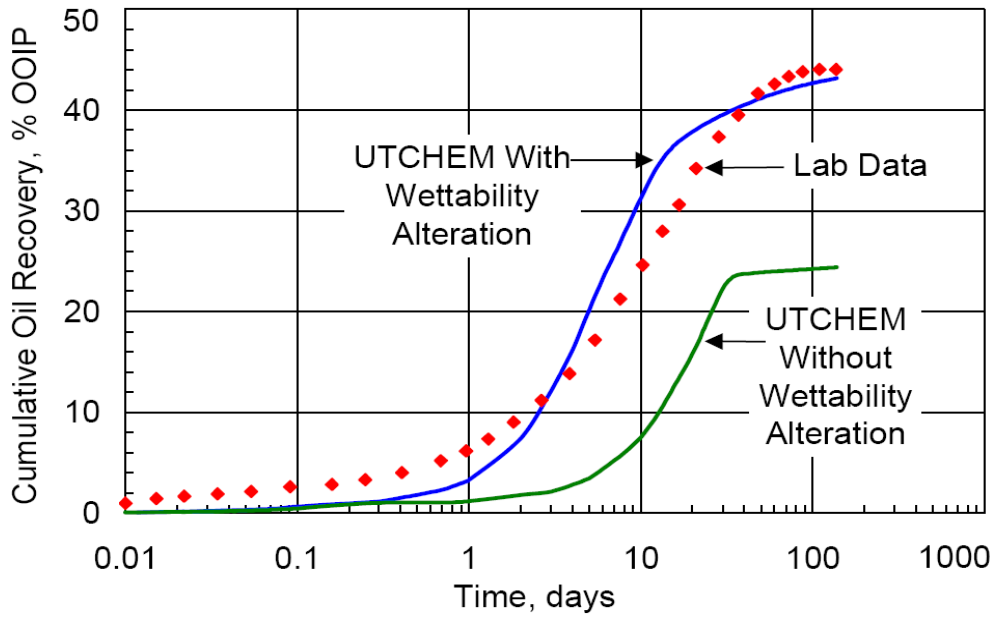

Figure 2-39: Comparison of simulated and laboratory imbibition oil recovery (Delshad *et al.* 2006)

To get the above match, a value of 0.5 was used for the scaling factor (ω) since the surfactant adsorption was assumed to be zero.

As mentioned earlier, two set of parameters for residual phase saturations, relative permeability endpoints, relative permeability exponents, capillary pressure endpoints, capillary pressure exponents, and oil and water trapping parameters are required to run the model. Getting all these information through the experimental tests is either impossible or expensive as a matter of both economy and time. And if there are no such data, one should play with these values to get a proper match with experimental data, which is not a proper method to handle it. According to the literature (Delshad *et al.* 2006; Najafabadi *et al.* 2008; Delshad *et al.* 2009), the scaling factor, ω, was selected as a constant value to obtain a good match with laboratory data.

Høgnesen *et al*. (2006) simulated a high temperature imbibition process into preferential oil-wet chalk by using the commercial simulator ECLIPSE 100. They believe that a very good fit to the experimental production was obtained by tuning the capillary pressure function using experimentally determined relative permeabilities.

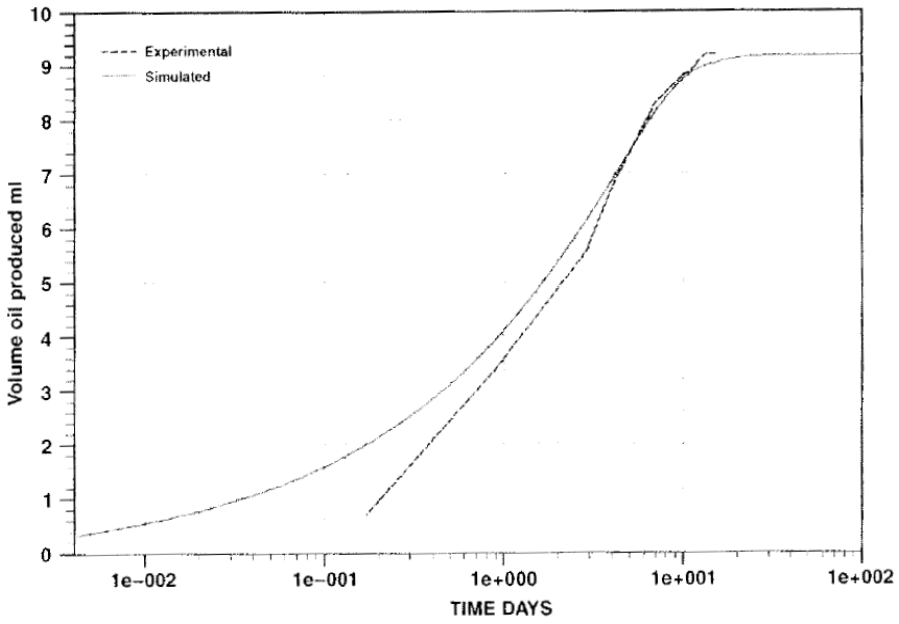

Figure 2-40: History matching oil recovery vs. time by numerical simulation to the production curve obtained experimentally (Høgnesen *et al.* 2006b)

Since the spontaneous imbibition has taken place at elevated temperature, they interpreted it as a wettability modification process. The oil and water relative permeability was measured using the steady-state method after re-saturating the core with crude oil. Core was close to neutral wettability due to the high end-point relative permeability of water, which was 0.761. Then, they utilized the measured relative permeability curves to generate a capillary pressure curve by history matching oil production versus time to the oil production measured experimentally using ECLIPSE 100. Therefore, there was no wettability alteration model applied in the numerical study. This type of history matching for wettability alteration was also reported using UTCHEM in the literature (Hirasaki *et al.* 2006).

Adibhatla *et al*. developed a three-dimensional numerical simulator to model wettability alteration (Adibhatla *et al.* 2005; Adibhatla and Mohanty 2007). The simulator takes into consideration the capillary pressure between oil and brine phase, the relative permeabilities and the residual saturation of both phases as functions of interfacial tension and wettability by using a trapping number and a contact angle. Wettability, measured through contact angle, depends on the surfactant and salt concentration. In their model, this dependence is modeled (for simplicity) similar to IFT behavior, a constant initial contact angle for low surfactant concentrations (<0.01 wt. %), a constant final contact angle for high surfactant concentrations (>0.035 wt. %) and a linear variation of contact angle from the initial value to the final value between the two surfactant concentrations. Therefore the same idea as presented in UTCHEM model, which is interpolation between two extremes, was somehow applied here. Also, they reported only one set of data which has been experimentally simulated by their model as presented in Figure 2-41. Estimates of oil in the aqueous phase emulsion are shown as vertical bars in this figure. They claimed that if this emulsion oil is included to the calculation, then the simulation results match the experimental data closely although the relative permeability curves in the numerical model were even adjusted to get this match (Adibhatla and Mohanty 2008).

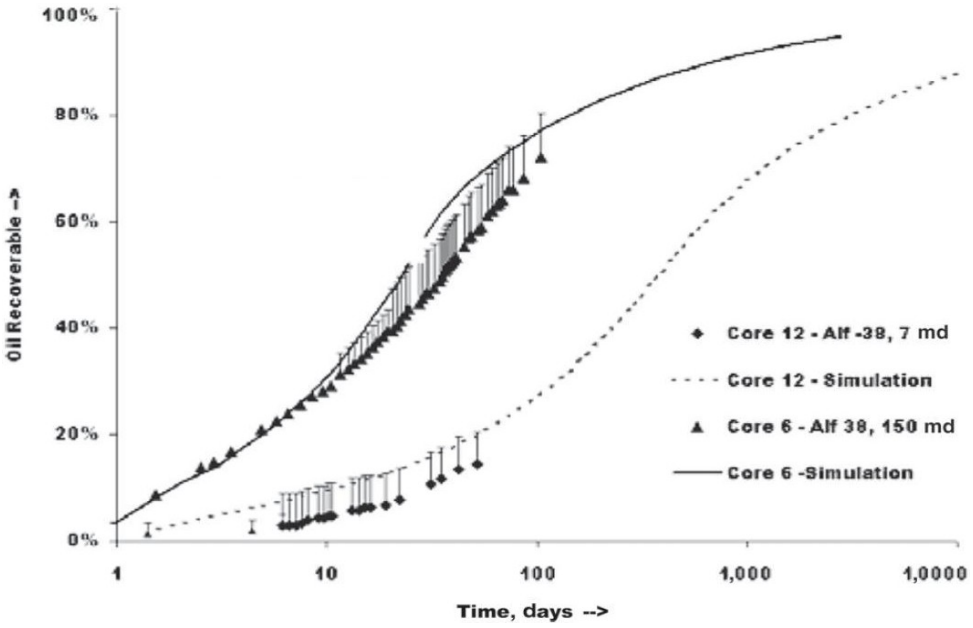

Figure 2-41: Comparison of experimental results with theoretically predicted curve for 0.05 wt. % Alf38 systems for two different cores (Adibhatla *et al.* 2005)

2.5.3 Effect of Temperature and Brine Composition

Høgnesen *et al*. (2005) studied the effect of brine composition and temperature on oil recovery from preferential oil-wet cores. They found that oil recovery increased beyond the recovery at completely water-wet conditions in chalk samples when the concentration of sulfate was increased three times relative to seawater at 130°C. The activity of sulfate as a wettability modifier also appeared to increase as the temperature is increased. The idea of sulfate as a wettability modifier has been reported by others (Webb *et al.* 2005; Zhang and Austad 2005a; Tweheyo *et al.* 2006) Also, Hamouda *et al*. (2006) observed that increasing the temperature alters calcite to a more water-wet condition. The degree of wetting change is a complicated function

of surface charge and fluid-fluid and fluid-rock interactions where the combined effect of those functions determines the degree of wettability alteration.

The Austad group has also proposed that seawater is able to improve the water wetness of oil-wet carbonate cores, especially chalk, leading to increase oil recovery (Strand *et al.* 2006; Zhang *et al.* 2007; Austad *et al.* 2008). In fact, the composition of the injected water can change wetting properties of the reservoir during a water-flood in a favorable way to improve oil recovery at elevated temperature (Doust *et al.* 2009). Therefore, injection of "Smart Water" with a correct composition and salinity can act as a tertiary recovery method as shown in Figure 2-42.

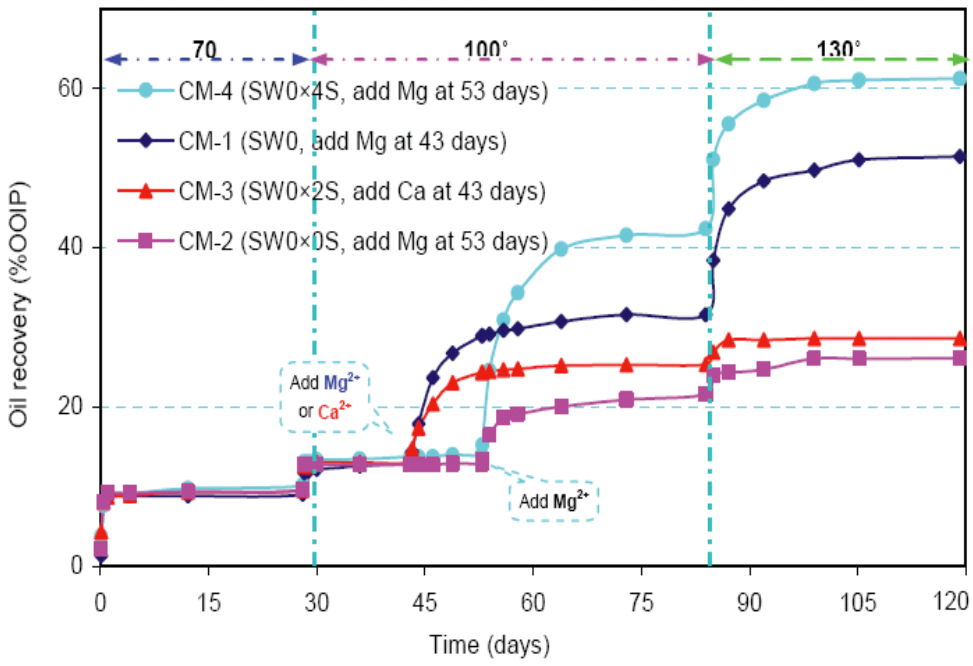

Figure 2-42: The Effect of temperature and ions of injected brine in oil recovery from oil-wet chalk core (Zhang *et al.* 2007)

Chapter 3: Mathematical Modeling and Formulation of Model

3.1 Introduction

Chemical enhanced oil recovery methods such as surfactant flooding are used in oil-wet naturally fractured reservoirs to improve oil recovery. Indeed, chemical stimulation with surfactant has the potential to enhance water imbibition to expel more oil from matrix to the fractures. As mentioned earlier, surfactant can act in several ways to enhance the oil production in oil-wet system. Lowering interfacial tension between oil trapped in small capillary pores and the water surrounding those pores, thus allowing the oil to be mobilized, and altering the matrix wettability toward water-wet, thus increasing the countercurrent flow rate in spontaneous imbibition of water, are the two most efficient and complicated mechanisms which have not been numerically modeled properly.

Data reported in the literature for modeling the interfacial tension reduction and wettability alteration are very limited despite much experimental research conducted to study these two mechanisms, which were discussed in Chapter 2. A current available model for wettability alteration uses two extreme wetting conditions (water-wet and oil-wet) and interpolates between the extremes to consider the wettability alteration mechanism in surfactant flooding of the reservoirs. Hence, the significance of altering was already assigned no matter what type of the surfactant is used.

Here, we present a model with the capability to simulate oil recovery using chemicals to mechanistically alter wettability and lower interfacial tension. As

discussed earlier, spontaneous imbibition of surfactant solution into matrix blocks is the main recovery mechanism that can expel oil from matrix blocks. This procedure can be modeled in the lab by placing a core into a beaker of aqueous solution. Therefore, the present study focuses on modeling the static imbibition of surfactant solution into the oil-wet cores in the laboratories.

In this chapter, in order to provide a comprehensive overview of the oil recovery process in oil-wet fractured rock systems using surfactants, a mathematical model is developed and presented. The model consists of three partial differential equations of water, oil, and surfactant. The governing equations used in the simulator for two-phase flow and three components (oil/water/surfactant) in porous media are described. The finite difference formulation of the component conservation equations is also given along with the physical modeling of the fluid-fluid and fluid-rock interactions. At the end, a flow chart of numerical solution sequence is presented.

3.2 Oil-Water Material Balance Equations

To investigate imbibition mechanisms in porous media (either water-wet or oil-wet), a Cartesian element of a core (saturated by oil and water) with sizes of Δx, Δy, and Δz is assumed.

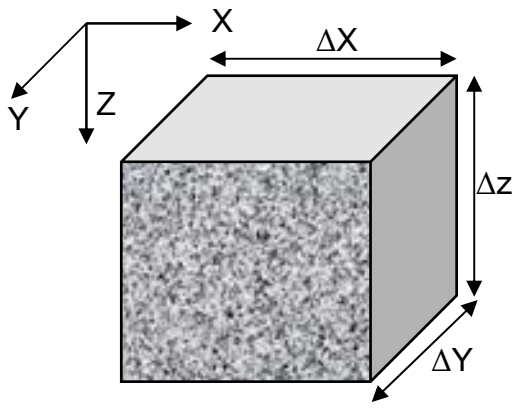

Figure 3-1: Rectangular volume element of a core

According to the experimental observations outlined above (Austad and Standnes 2003; Seethepalli *et al.* 2004; Adibhatla and Mohanty 2007), the following are the basic assumptions made in the development of this mathematical model of the oil/water flow equations:

- Darcy's law describes the multiphase flow of fluids through the porous media,
- Instantaneous local thermodynamic equilibrium is considered between phases,
- Diffusion of oil into the water phase and water into the oleic phase are neglected,
- There is no consumption for oil and water in the rock,
- Porous media is immobile and has a constant temperature,
- The amount of salt in aqueous phase is sufficiently low to be neglected.

The detailed derivation of oil and water conservation equations is given in Appendix A. The final mass-conservation equations for water and oil are as follows:

$$\frac{\partial}{\partial x}\left(\beta K_x \frac{k_{rw}}{\mu_w B_w}\left(\frac{\partial P_w}{\partial x} - \gamma_w \frac{\partial D}{\partial x}\right)\right) + \frac{\partial}{\partial y}\left(\beta K_y \frac{k_{rw}}{\mu_w B_w}\left(\frac{\partial P_w}{\partial y} - \gamma_w \frac{\partial D}{\partial y}\right)\right) + \frac{\partial}{\partial z}\left(\beta K_z \frac{k_{rw}}{\mu_w B_w}\left(\frac{\partial P_w}{\partial z} - \gamma_w \frac{\partial D}{\partial z}\right)\right) = \frac{1}{\alpha}\frac{\partial}{\partial t}\left(S_w \frac{\phi}{B_w}\right) \tag{3.1}$$

$$\frac{\partial}{\partial x}\left(\beta K_x \frac{k_{ro}}{\mu_o B_o}\left(\frac{\partial P_o}{\partial x} - \gamma_o \frac{\partial D}{\partial x}\right)\right) + \frac{\partial}{\partial y}\left(\beta K_y \frac{k_{ro}}{\mu_o B_o}\left(\frac{\partial P_o}{\partial y} - \gamma_o \frac{\partial D}{\partial y}\right)\right) + \frac{\partial}{\partial z}\left(\beta K_z \frac{k_{ro}}{\mu_o B_o}\left(\frac{\partial P_o}{\partial z} - \gamma_o \frac{\partial D}{\partial z}\right)\right) = \frac{1}{\alpha}\frac{\partial}{\partial t}\left(S_o \frac{\phi}{B_o}\right) \tag{3.2}$$

3.3 Surfactant Equation

To develop a mathematical equation for surfactant flow in porous media, there are some additional assumptions to those assumed for the water/oil flow equation:

- Surfactant can exist in an aqueous phase and an oil phase, and it can also be adsorbed onto a solid surface,
- Molecular diffusion of surfactant occurs into oil and water phases according to Fick's law,
- Ideal mixing holds true (i.e. volume alterations of mixing are zero),
- Surfactant density is constant.

The mass-conservation equation for surfactant is detailed in Appendix B; however, the general form of the surfactant flow equation is as follows:

$$
\begin{aligned}
&-\frac{\partial}{\partial x}\left(\begin{array}{l}\left(C_{sw}\left[\beta K_x \frac{k_{rw}}{\mu_w}\left(\frac{\partial P_w}{\partial x}-\gamma_w \frac{\partial D}{\partial x}\right)\right]-\phi S_w D_{sw}^0\left(\frac{\partial C_{sw}}{\partial x}\right)\right)\\ +\left(C_{so}\left[\beta K_x \frac{k_{ro}}{\mu_o}\left(\frac{\partial P_o}{\partial x}-\gamma_o \frac{\partial D}{\partial x}\right)\right]-\phi S_o D_{so}^0\left(\frac{\partial C_{so}}{\partial x}\right)\right)\end{array}\right)\\
&\quad -\frac{\partial}{\partial y}\left(\begin{array}{l}\left(C_{sw}\left[\beta K_y \frac{k_{rw}}{\mu_w}\left(\frac{\partial P_w}{\partial y}-\gamma_w \frac{\partial D}{\partial y}\right)\right]-\phi S_w D_{sw}^0\left(\frac{\partial C_{sw}}{\partial y}\right)\right)\\ +\left(C_{so}\left[\beta K_y \frac{k_{ro}}{\mu_o}\left(\frac{\partial P_o}{\partial y}-\gamma_o \frac{\partial D}{\partial y}\right)\right]-\phi S_o D_{so}^0\left(\frac{\partial C_{so}}{\partial y}\right)\right)\end{array}\right)\\
&\quad\quad -\frac{\partial}{\partial z}\left(\begin{array}{l}\left(C_{sw}\left[\beta K_z \frac{k_{rw}}{\mu_w}\left(\frac{\partial P_w}{\partial z}-\gamma_w \frac{\partial D}{\partial z}\right)\right]-\phi S_w D_{sw}^0\left(\frac{\partial C_{sw}}{\partial z}\right)\right)\\ +\left(C_{so}\left[\beta K_z \frac{k_{ro}}{\mu_o}\left(\frac{\partial P_o}{\partial z}-\gamma_o \frac{\partial D}{\partial z}\right)\right]-\phi S_o D_{so}^0\left(\frac{\partial C_{so}}{\partial z}\right)\right)\end{array}\right)\\
&=\frac{1}{\alpha}\frac{\partial}{\partial t}\left(\phi\left(S_w C_{sw}+S_o C_{so}\right)+\left(1-\phi\right)C_{sg}\right) \qquad (3.3)
\end{aligned}
$$

In the above equation, C_{sw} and C_{so} are the surfactant concentration in the water and oil phases, respectively. Also, C_{sg} represents the amount of the surfactant adsorbed on the rock.

3.4 Typical Initial and Boundary Conditions

3.4.1 Boundary Conditions

The model developed in this study is used to simulate a single matrix block with constant pressure support at any of its boundaries; naturally these boundaries are open to fluid flow from the fracture (or beaker). The boundary transmissibility terms are used in calculating the transfer of both aqueous (surfactant and water) and oil phases

between the matrix and surrounding fracture, therefore there is no need for a rate term and hence the no-flow boundary conditions are imposed by setting the oil and water transmissibilities equal to zero.

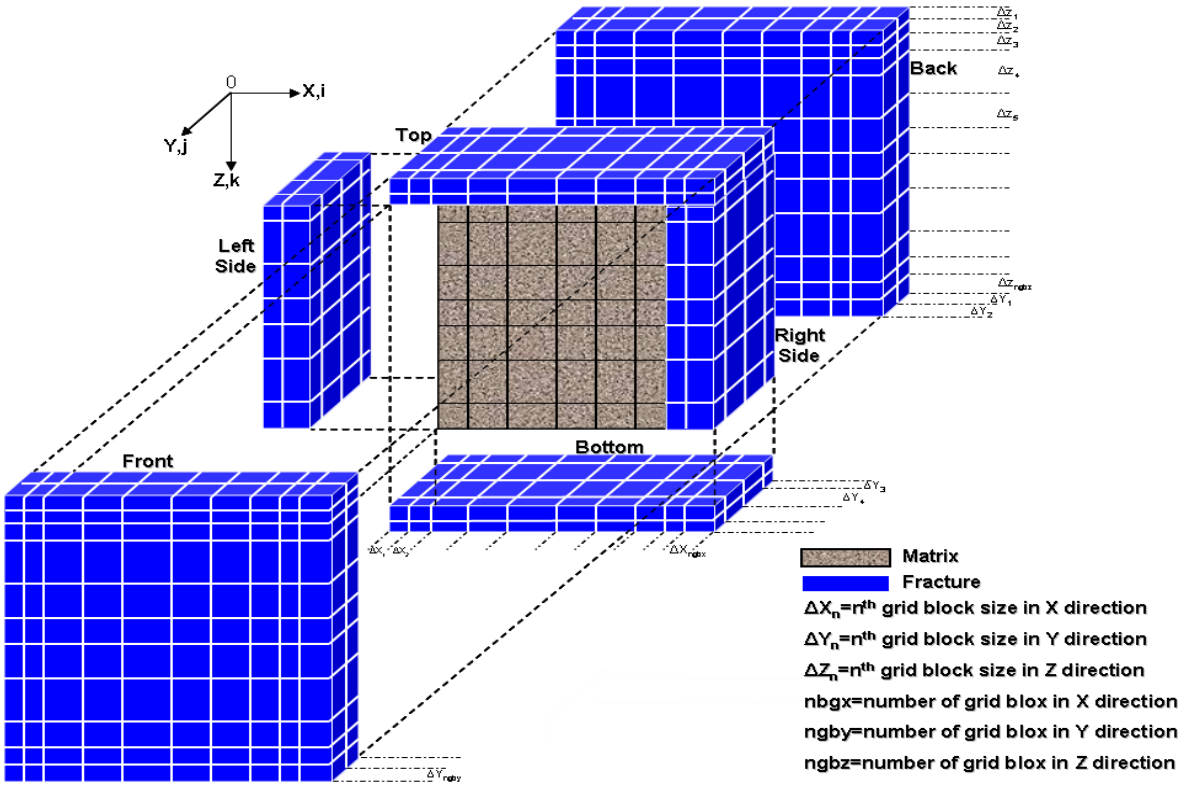

Figure 3-2: meshing method for matrix and fracture system

3.4.2 System Initialization

The matrix block is assumed to be initially above the transition zone and hence water saturation in the matrix block is at the irreducible or residual level. Capillary pressure in the fracture is set equal to zero. The pressure at the datum is specified, which is the

position just above the top of the matrix block. The datum pressure and specified fluid gradients are used to calculate phase pressures at any other points in the matrix block and there are no pressure gradients in the horizontal plane in the matrix block, therefore:

$$\frac{\partial P_{oil}}{\partial X} = \frac{\partial P_{oil}}{\partial Y} = 0 \qquad \forall x, y, z \ \& \ t = 0 \tag{3.4}$$

$$\frac{\partial P_{oil}}{\partial Z} = \gamma_{oil} \qquad \forall x, y, z \ \& \ t = 0 \tag{3.5}$$

$$\Rightarrow P_{oil} = P_{datum} + \gamma_{oil}\left(Z - Z_{datum}\right) \qquad \forall x, y, z \ \& \ t = 0 \tag{3.6}$$

Afterwards, the water pressure in the matrix block at any point is calculated using the oil pressure and the specified capillary pressure at that point using the Brooks and Corey capillary pressure-saturation relationship (Equation 3.8 which will be discussed in section 3.5.2). The difference between the water pressures inside and outside the matrix block is the driving force for water to move inside the matrix. This is because inside the matrix block, the water phase is initially immobile and dependent on the mobile oil phase and the capillary pressure. The water pressure in fractures can be calculated based on the hydrostatic length of the water (aqueous) phase.

Also, surfactant concentration is initially assumed to be zero inside a core while it is defined for fracture (beaker) according to the initial amount of the surfactant available in aqueous solution.

3.5 Auxiliary Equations: Rock and Fluid Properties

3.5.1 Wettability Alteration Model

Wettability modification of solid rocks by using surfactants is an important process that is used in practical applications such as oil recovery from porous media. When wettability is altered, the capillary pressure and relative permeability relationships change at each location in the porous rock contacted by surfactant. Although there are numerical studies to simulate the effect of wettability alteration on oil recovery from oil-wet rock systems (Høgnesen *et al.* 2004; Delshad *et al.* 2006; Adibhatla and Mohanty 2008; Gupta and Mohanty 2008; Najafabadi *et al.* 2008) , the wettability models are empirical and do not permit alteration of the rock wettability with time. The wettability models used in each of these studies assumed the final condition of wettability (contact angle) and calculates values such as capillary pressure, oil and water relative permeability, and interfacial tension either by direct equations or use of an interpolation-scaling factor as discussed in section 2.5.2.

In this dissertation, a wettability alteration model is proposed in which the contact angle is correlated to the surfactant concentration through an empirical correlation developed from experimental data:

$$\frac{\theta^f - \theta^0}{\theta(t) - \theta^0} = 1 + \left(\frac{C(t)}{CMC} \right)^{0.434/d} \tag{3.7}$$

This equation was developed based on history matching of experimental data from two papers (Fletcher and Nicholls 2000; Szymczyk *et al.* 2006). In Equation 3.7, $C(t)$ is the concentration of surfactant in the aqueous phase that changes with time while θ^0 and θ^f are the initial and desired final contact angle that are based on surfactant type used and initial wetness of the surface and the composition of the surface. The parameter "*d*" is determined by history match of the experimental data and ranges between -0.2 to -3 according to our history matching of the available experimental data.

Figure 3-3 shows the match of the data of Fletcher *et al*. (2000) data. They measured contact angles for a range of pure oils of different cohesive energy density and surfactant solutions (like $C_{12}B$; dodecylbenzene, $CMC \cong 6.9 \times 10^{-3}$) on polyethylene (PE) and polytetrafluoroethylene (PTFE) solid surfaces. The values of "*d*" were -0.5 and -0.4 for the contact angles measured on PE and PTFE, respectively.

Figure 3-4 also shows the match of the experimental data of Szymczyk *et al*. (2006) was matched by using Equation 3.7. Contact angles were measured out for aqueous solutions of cetyltrimethylammonium (CTAB, $CMC \cong (4.8 \pm 0.4) \times 10^{-4}$) and cetylpyridinium bromide (CPyB, $CMC \cong 3.5 \times 10^{-4}$) on PTFE and PMMA (polymethyl methacrylate). The values of "*d*" were -0.5 and -0.2 to match the experimental data.

Similar trend to these two figures were also reported by other researchers (Adamson and Gast 1997; Adibhatla *et al.* 2005).

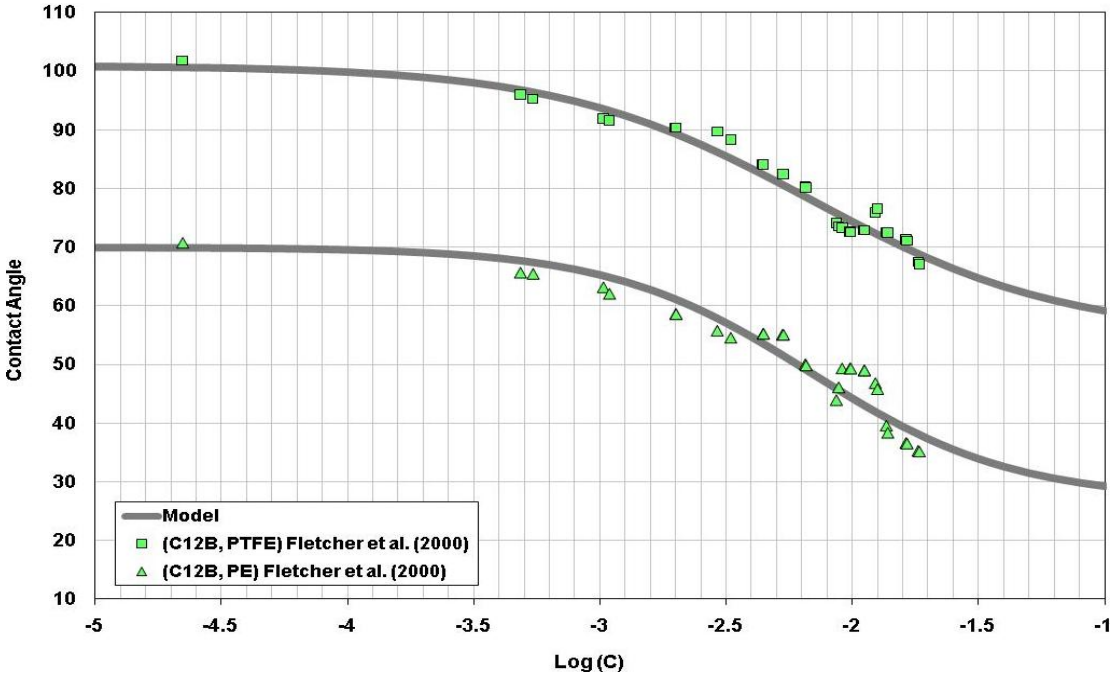

Figure 3-3: Prediction of literature data using the proposed wettability alteration model in Equation 3.7

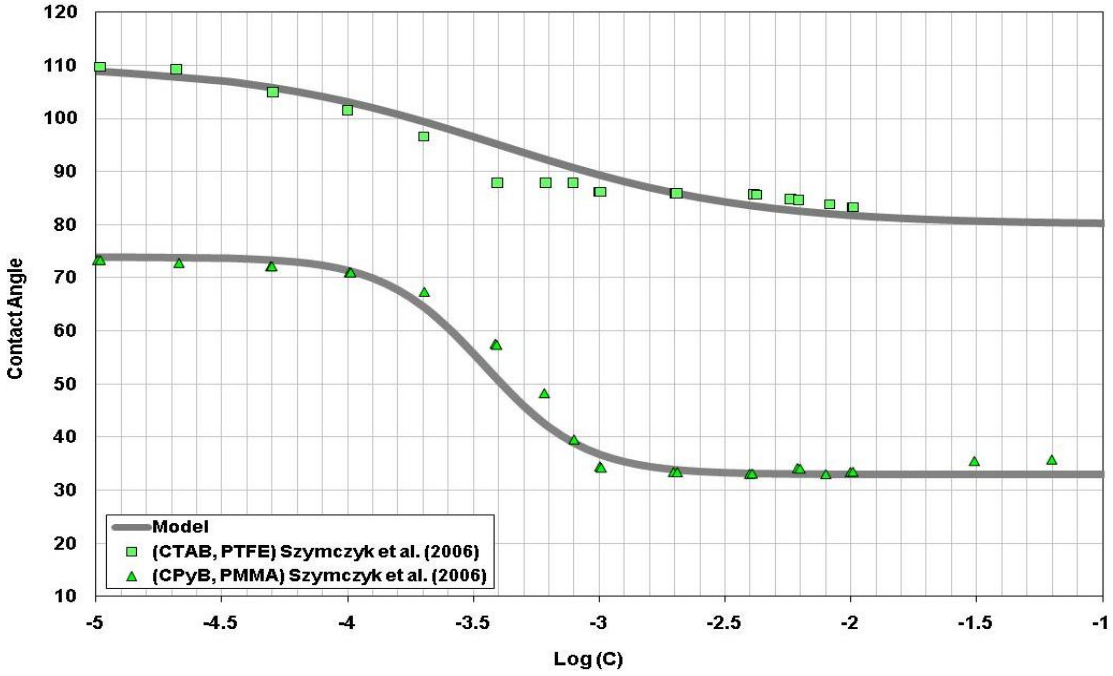

Figure 3-4: Prediction of experimental data using the proposed wettability alteration model in Equation 3.7

3.5.2 Capillary Pressure Model

Capillary pressure in the Brooks and Corey capillary pressure-saturation relationship is scaled for interfacial tension, permeability, and porosity (Corey *et al.* 1956; Brooks and Corey 1965). So, the capillary pressure between two phases of oleic and aqueous is calculated as follows:

$$P_c = C_p \frac{\sigma_{oil-aqueous}}{\sigma_{oil-water}} \sqrt{\frac{\phi}{k}} \left(1 - \frac{S_w - S_{wr}}{1 - S_{wr} - S_{or}}\right)^{n_p} \tag{3.8}$$

Parameters of C_p and n_p are input parameters whereas $\sigma_{oil-aqueous}$ is calculated based on the surfactant concentration and will be discussed later in this chapter. Figure 3-5 shows how good capillary pressure data can be predicted by the above correlation.

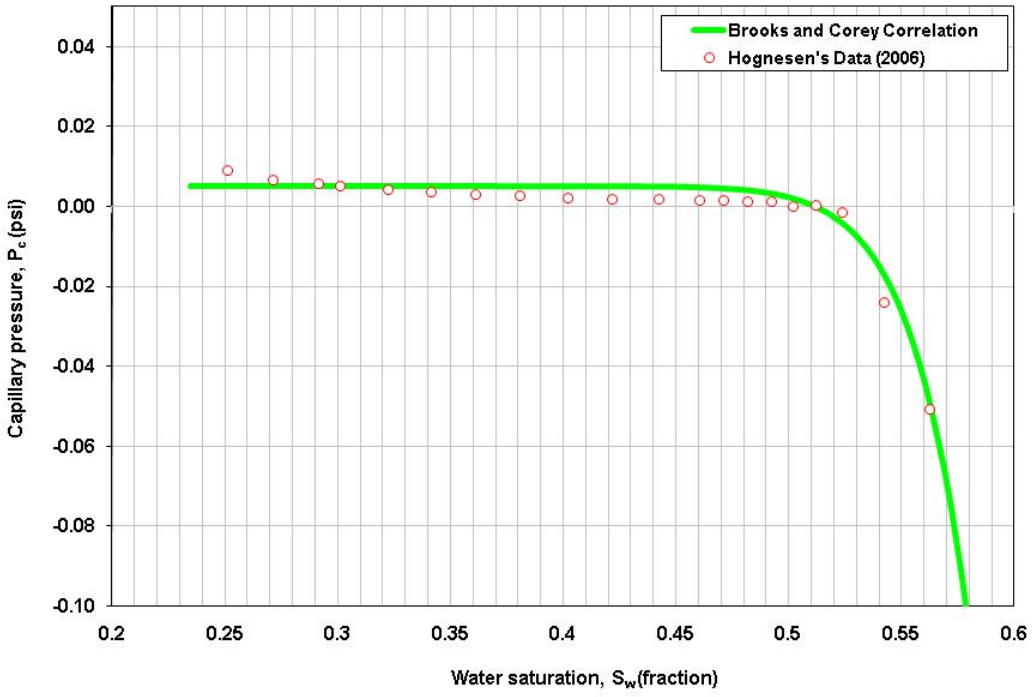

Figure 3-5: Prediction of capillary pressure data with Brooks and Corey correlation

The whole capillary pressure curve can be shifted up or down by adding or subtracting a constant value. For example, in Figure 3-5, 0.007 was added to the equation to get a match with Hogonsen's data while C_p and n_p are chosen to be -0.11 and 13, respectively. The effect of wettability alteration on capillary pressure can be described with the following equation according to the Leverett J-function:

$$P_c = P_c^0 \frac{\cos\theta}{\cos\theta^0} \tag{3.9}$$

In calculations, P_c^0 is obtained from Equation 3.8. An example of the capillary pressure curve alteration from oil-wet to water-wet state is shown in Figure 3-6.

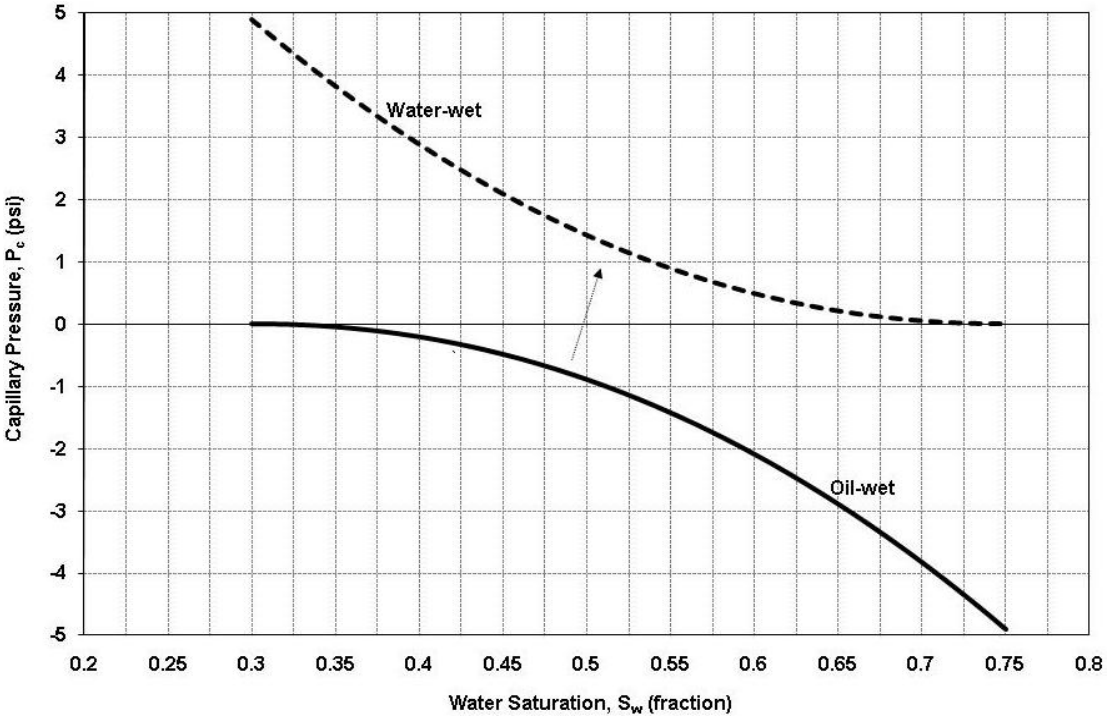

Figure 3-6: Calculated capillary pressure curves for oil- and water-wet states

3.5.3 Relative Permeability Model

Among all physical parameters and correlations, water/oil relative permeability is perhaps the most important constitutive relation that characterizes two-phase flow and displacement processes in porous media. Since no general theoretical expression is available for the relative permeability function, two-phase relative permeabilities are modeled based on an empirical modified Brooks-Corey (MBC), also known as the power law model (Lake 1989), functions as follows (Pope and Nelson 1977):

$$k_{rw} = k_{rw}^{*}\left(\frac{S_w - S_{wr}}{1 - S_{wr} - S_{or}}\right)^{n_w} \tag{3.10}$$

$$k_{ro} = k_{ro}^{*}\left(1 - \frac{S_w - S_{wr}}{1 - S_{wr} - S_{or}}\right)^{n_o} \tag{3.11}$$

In the above equations, k_{ro} is the oil relative permeability (fraction), k_{ro}^{*} is the oil relative permeability endpoint (fraction), and n_o is an exponent for the oil relative permeability curve. Also, k_{rw} is the water relative permeability (fraction), k_{rw}^{*} is the water relative permeability endpoint (fraction), and n_w is an exponent for the water relative permeability curve. In a more abstract sense, this formulation is perhaps the most widely used, practical method describing laboratory-derived relative permeability relationships in terms of simple power functions. The powers and endpoint values are different in cases of water-wet and oil-wet.

The valid relative permeability curve often yields a straight line on a log-log plot when the relative permeability data are plotted versus normalized saturations. The oil and water normalized saturations are defined by the following equations:

$$S_{wn} = \frac{S_w - S_{wr}}{1 - S_{or} - S_{wr}} \tag{3.12}$$

$$S_{on} = \frac{1 - S_w - S_{or}}{1 - S_{wr} - S_{or}} \tag{3.13}$$

Prediction of relative permeability curves using Equations of 3.10 and 3.11 is shown in Figure 3-7. Also, values for the parameters used in Equations 3.10 and 3.11 to generate the figure are shown in the following table.

Table 3-1: Parameters used to predict the curves in Figure 3-7

Property	Value
k_{rw}^*	0.751
k_{ro}^*	1.00
n_w	2.5
n_o	2.0

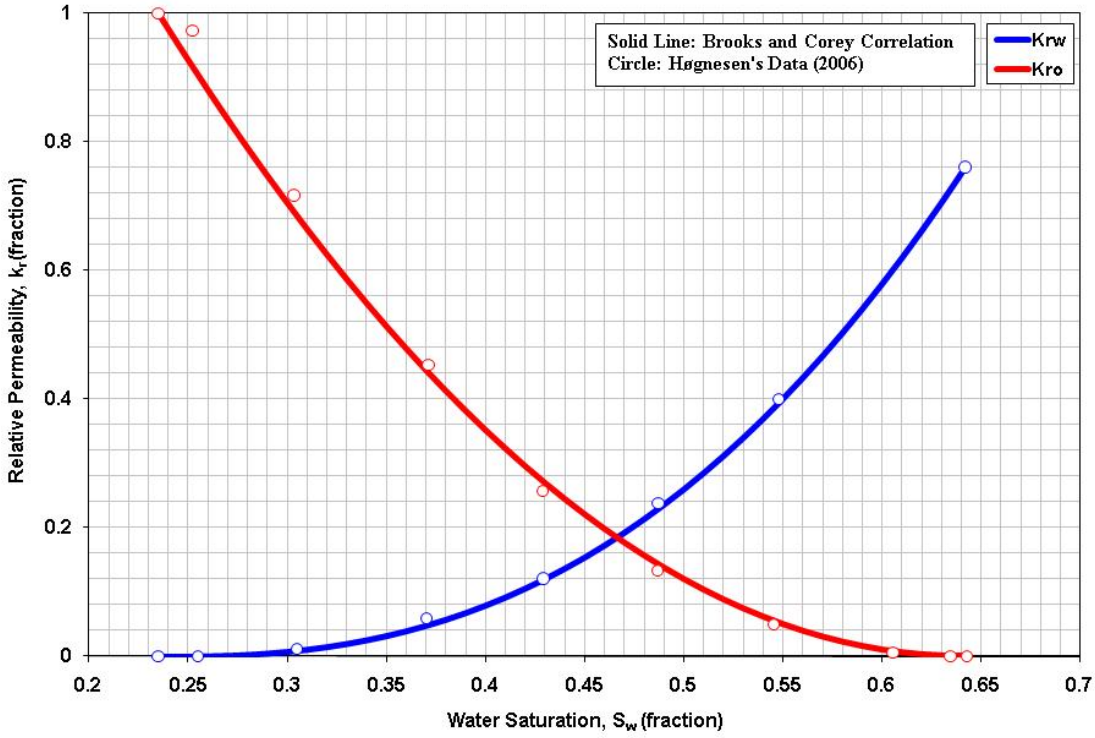

Figure 3-7: Prediction of relative permeability data with Brooks and Corey correlations

The above equations are not very useful when considering wettability alteration. On the other hand, rock wettability affects the nature of fluid saturation and the general relative permeability characteristics of a fluid/rock system. Considering the effect of wettability on fluid distributions (Willhite 1986), it is easy to rationalize that relative permeability curves are strongly functions of wettability. There are different proposed equations that relate the endpoint and exponent values of relative permeabilities to the wettability of the rock (Lake 1989; Adibhatla *et al.* 2005; Delshad *et al.* 2006). Because some methods use conjugate phase residual saturation to calculate the new values of endpoint and exponent for the above equations, the results of some studies show that using conjugate phase residual saturation may not reasonably predict

values. The following equations correlate the water relative permeability with wettability alteration as used in the present research:

$$k^{*}_{(o/w)} = 1 + \left[k^{*,0}_{rw} + \frac{\cos\theta - \cos\theta^{0}}{\cos\left(\pi - \theta^{0}\right) - \cos\theta^{0}} \left(k^{*,0}_{ro} - k^{*,0}_{rw} \right) - 1 \right] \left(\frac{1 + T_{(w/o)} N^{0}_{T}}{1 + T_{(w/o)} N_{T}} \right) \tag{3.14}$$

$$n_{(o/w)} = 1 + \left[n^{*,0}_{w} + \frac{\cos\theta - \cos\theta^{0}}{\cos\left(\pi - \theta^{0}\right) - \cos\theta^{0}} \left(n^{*,0}_{o} - n^{*,0}_{w} \right) - 1 \right] \left(\frac{1 + T_{(w/o)} N^{0}_{T}}{1 + T_{(w/o)} N_{T}} \right) \tag{3.15}$$

All values with a superscript of "0" correspond to the initial condition. For generating the oil relative permeability curve $(\pi - \theta)$ should be substituted instead of θ. The values of the parentheses in above equations are normally close to one for imbibition process. The reason will be discussed in section 3.5.7. As mentioned earlier, N_T is calculated by using Equation 2.12 while trapping value (T) can be found by curve fitting the experimental data of trapping number versus residual oil saturation (e.g.: Figure 3-13). An example of the relative permeability curves alteration from oil-wet to water-wet state is displayed in Figure 3-8.

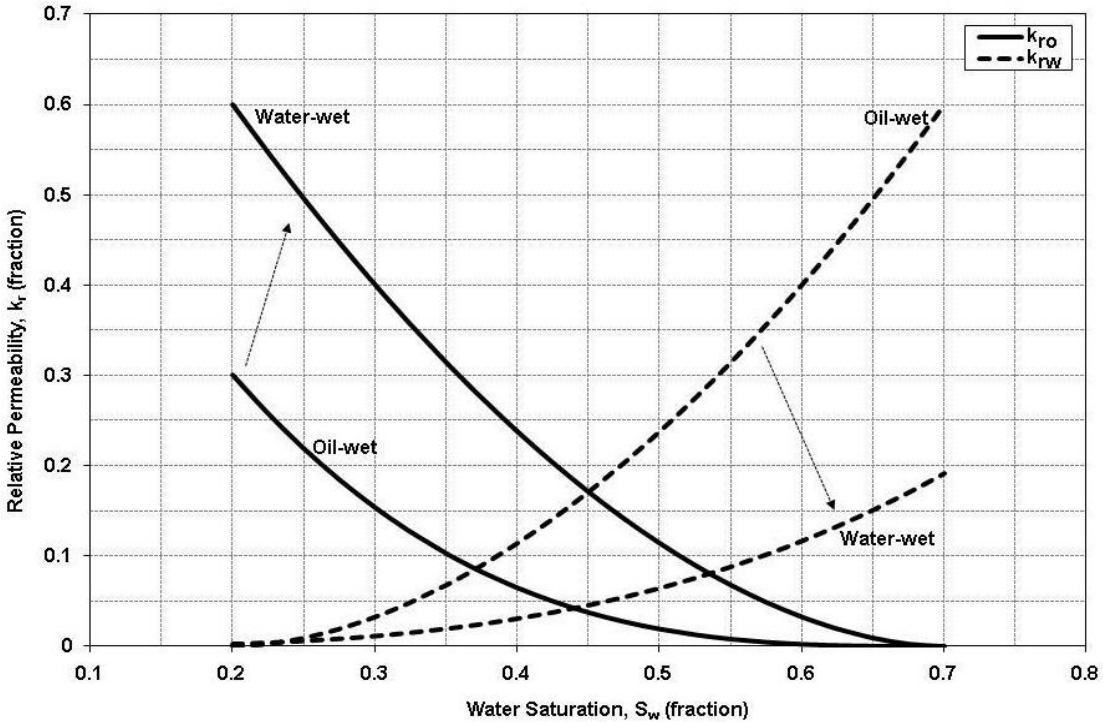

Figure 3-8: Calculated oil/water relative permeability curves for two different wettabilities

3.5.4 Interfacial Tension Reduction Model

The interfacial tension between aqueous and oleic phases as a function of surfactant concentration is necessary for taking into account the effect of surfactant on interfacial tension reduction. This function could be either an input function or experimental data. For example, the following graph shows the interfacial tension alterations between oil (Soltrol 130) and aqueous phase at varying surfactant concentrations for different surfactants.

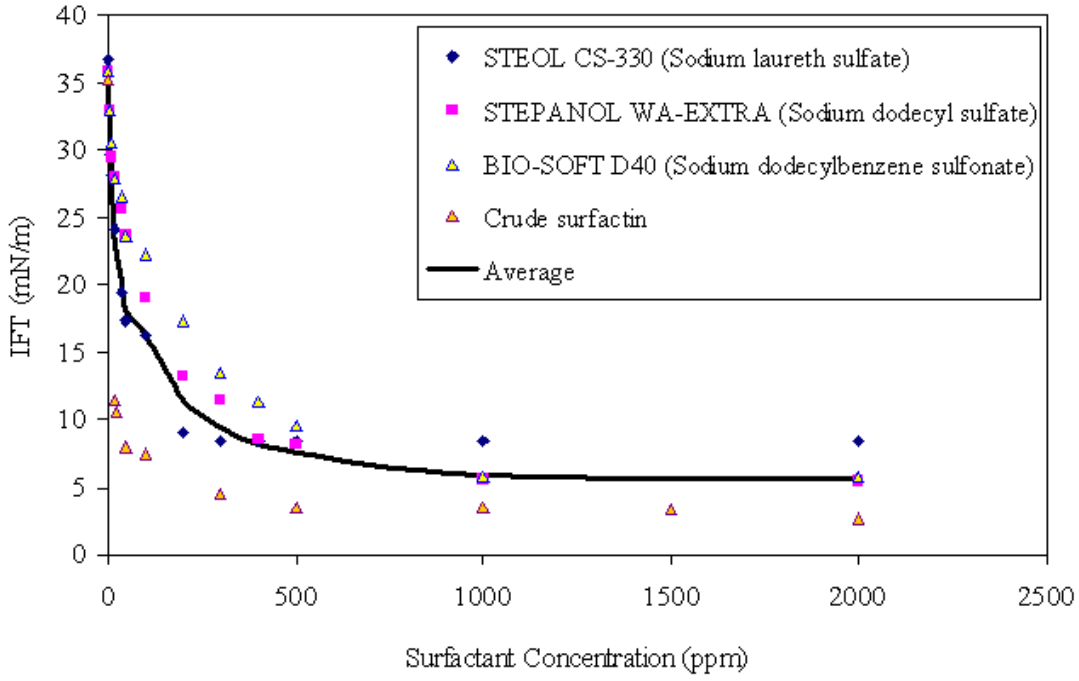

Figure 3-9: Interfacial tension between oil and aqueous phase (after Johnson *et al.* 2007)

Note that the interfacial tension does not significantly change when the surfactant concentration is below to the critical micelle concentration (CMC). The following equation so-called modified Chun-Huh, for instance, can be included to the calculation of the interfacial tension (Hirasaki 1981):

$$\sigma_{oil-aqueous} = \sigma_{oil-water} e^{-\varepsilon a} + \frac{\eta b}{a^2}\left(1 - e^{-\varepsilon a^3}\right) \tag{3.16}$$

where "*a*" is the oil solubilization ratio and "*b*" is the correction factor that ensures the interfacial tension at the plait point is zero. Two parameters of ε and η can be found by matching experimental data; however, in some studies, they were typically taken equal to 10 and 0.3, respectively (Han *et al.* 2007). For more information about Equation 3.16, reader is referred to Lake (1989) and Delshad *et al*. (1996).

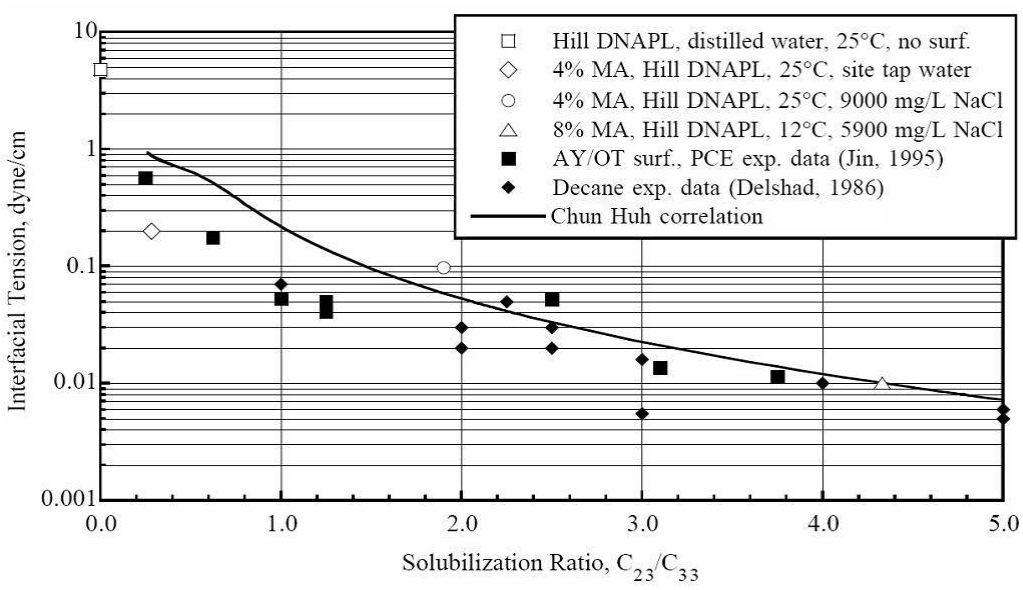

Figure 3-10: Prediction of interfacial tension reduction data by Equation 3.16

3.5.5 Adsorption Model

Surfactant adsorption may be an important mechanism for EOR processes since it causes retardation and consumption of surfactant, which reduces performance of EOR processes. For more quantitative work, surfactant adsorption is presented by a Langmuir-type isotherm as follows (Knaebel 2006; Han *et al.* 2007):

$$C_{sg} = \frac{aC_s}{1+bC_s} \tag{3.17}$$

Hence, C_s is the equilibrium surfactant concentration in aqueous phase and the amount of surfactant retained by the rock is presented by C_{sg}. Laboratory surfactant adsorption data can help identify the values of "*a*" and "*b*" in the Equation 3.17. Parameter "*a*" depends on salinity whereas parameter *b* controls the curvature of the

isotherm curve. The maximum amount of monolayer adsorbed surfactant can be presented by *a/b*. This model is able to describe many adsorption data both for the gas/solid and liquid/solid interfaces. Its two adjustable parameters "*a*" and "*b*" give the model flexibility to be matched to many sets of data. It is worth mentioning that this model has been used in several different fashions and units according to the area of application. For example, the adsorption of hydrolyzed polycrylamide (polymer) on Berea core material was investigated by Shah (1978), which is modeled by Langmuir-type isotherm model as shown in Figure 3-11. To generate this figure *a* and *b* were chosen 0.66 and 0.02, respectively.

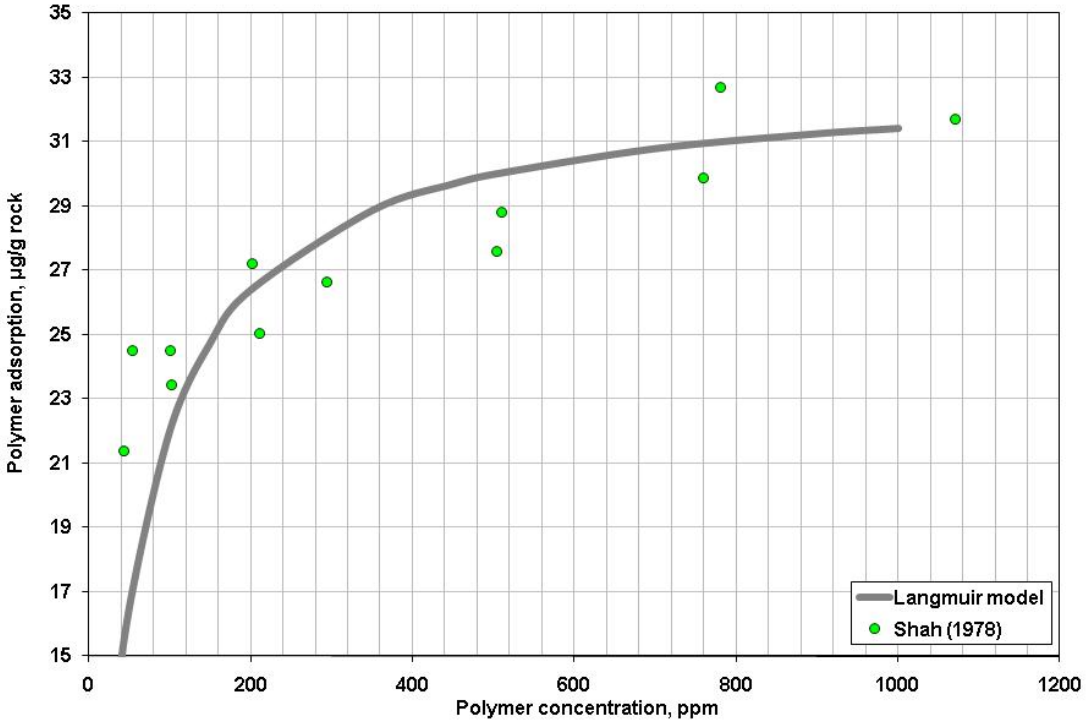

Figure 3-11: Prediction of experimental data by using Langmuir-type isotherm model

3.5.6 Phase Density and Viscosity

Because the goal of this research is to use a low surfactant concentration in systems, density and viscosity values do not change significantly. So, the phase density and viscosity are assumed to be constant.

3.5.7 Residual Saturations

Pope *et al*. (2000) proposed the following equation to correlate residual saturation with the trapping number:

$$S_{(o/w)r} = \min\left(S_{(o/w)}, S^{high}_{(o/w)r} + \frac{S^{low}_{(o/w)r} - S^{high}_{(o/w)r}}{1 + T_{(o/w)}\left(N_{T_{(o/w)}}\right)^{\tau_{(o/w)}}} \right) \tag{3.18}$$

The superscript "low" and "high" refers to the residual saturations at low and high trapping number, respectively, which is discussed in the next section. The values of $S^{low}_{(o/w)r}$ and $T_{(o/w)}$ can be obtained by matching experimental data. Typically, $\tau_{(o/w)}$ is designated 1.0 and $S^{high}_{(o/w)r}$ is zero. Changes in trapping number can occur for various reasons such as interfacial tension reductions, pressure gradient changes, and changes in displacing fluid density (constant in the cases presented here) (Coats 1980). Changing the wettability affects both $S^{low}_{(o/w)r}$ and $T_{(o/w)}$. The following equation correlates these two parameters with contact angle (Adibhatla *et al.* 2005):

$$\frac{S^{low}_{(o/w)r} - S^{low,0}_{wr}}{S^{low,0}_{or} - S^{low,0}_{wr}} = \frac{Ln\left(T_{(o/w)}\right) - Ln\left(T^0_w\right)}{Ln\left(T^0_o\right) - Ln\left(T^0_w\right)} = \frac{\cos\theta - \cos\theta^0}{\cos\left(\pi - \theta^0\right) - \cos\theta^0} \tag{3.19}$$

In the above equation, T^0 and $S_r^{low,0}$ correspond to the trapping value and residual saturation at θ^0 (initial condition). In order to calculate the new values of T_o and S_{or}^{low} the contact angle of θ must be substituted by $(\pi - \theta)$. S_{or}^{low} is used to find $S_{(o/w)r}$ in Equation 3.18.

As shown in Figure 3-12, there is a very large difference between the nonwetting and wetting phase data. A much larger trapping number is required to decrease the residual saturation for the wetting phase than for the nonwetting phase. The relationship between trapping number and residual phase saturation can be shown graphically as a capillary desaturation curve (CDC) which has been also reported in the literature as shown in Figure 3-13.

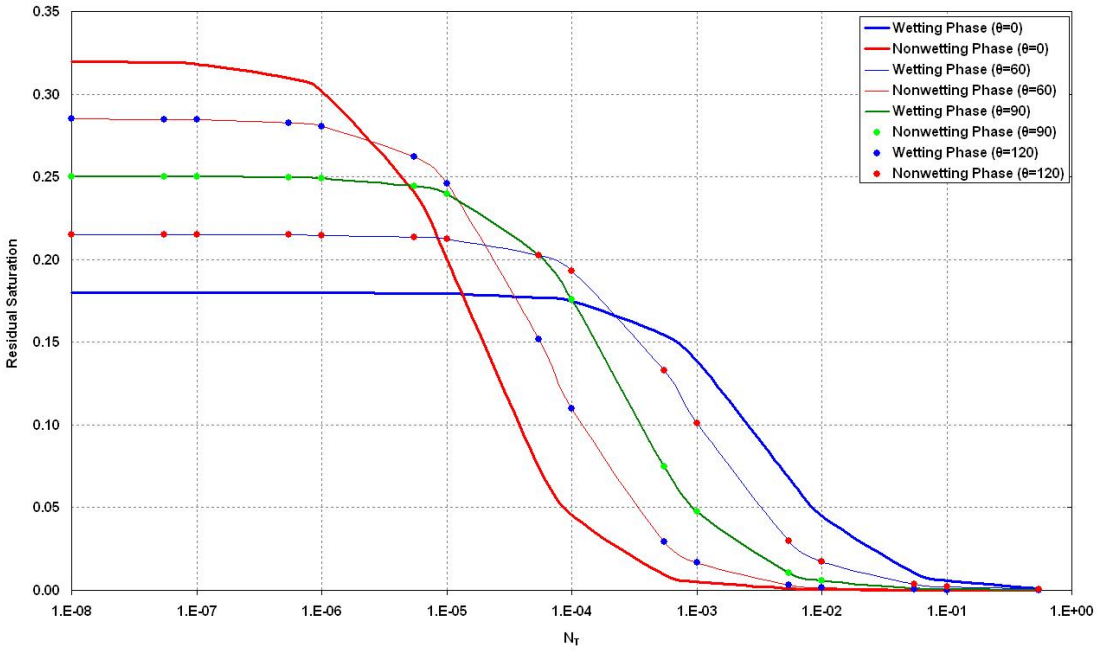

Figure 3-12: Correlation of residual saturations with wettability

In the surfactant solution imbibition process, residual fluid saturations generally change very little since alteration of the trapping number during the process is not significant (Equation 2.12), i.e. the trapping number remains very small. Therefore, the multiplication of trapping values (N_T) by trapping numbers (T) means the third term in the right side of equations of 3.14 and 3.15 is close to one.

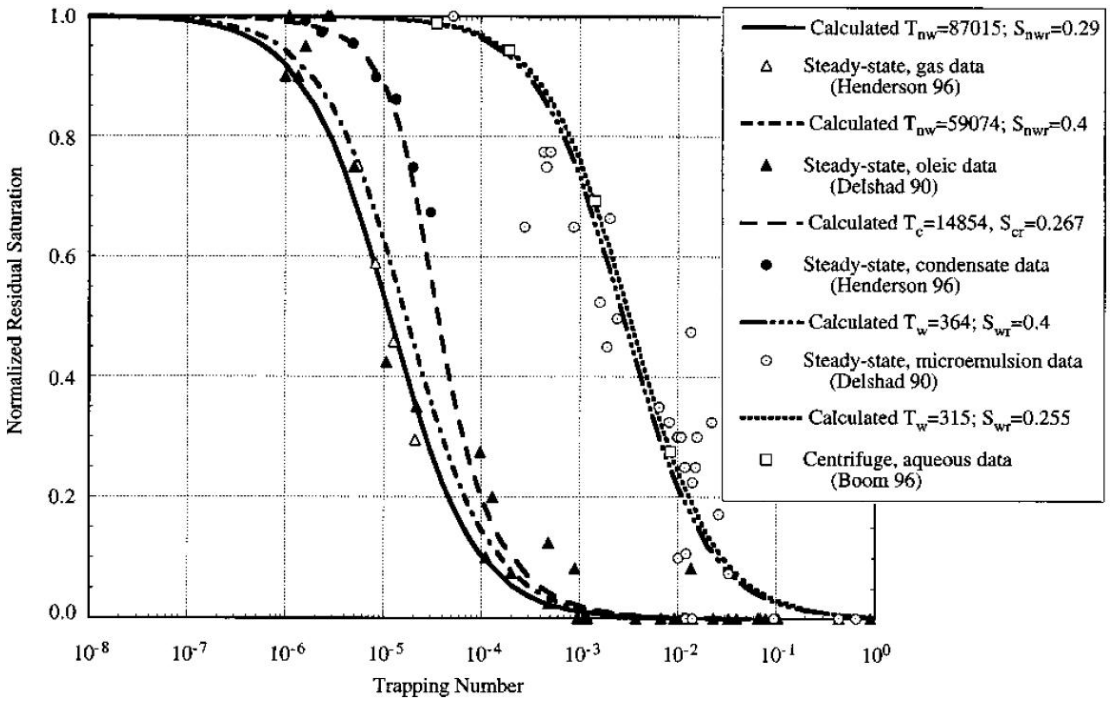

Figure 3-13: Effect of wettability on the desaturation curves for Berea sandstone (Pope *et al.* 2000)

3.6 Numerical Solution

In general, fluid-flow equations cannot be solved analytically due to their nonlinear nature (Equations of 3.1, 3.2, and 3.3). So, fluid flow in reservoirs can typically be modeled numerically by applying the traditional finite-difference expansion of

continuity equations. A three-dimensional Implicit Pressure Explicit Concentration and Saturation (IMPECS) model is used in this research. The model takes into account capillary, viscous and gravity forces for the modeling of incompressible fluids. Convective flow, molecular diffusion, and adsorption are also considered. Molecular diffusion and adsorption do not contribute significantly to fluid flow; however, they do affect surfactant behavior within a system.

3.6.1 Oil and Water Finite-Difference Equation

The water pressure in the matrix block, either oil-wet or water-wet, at any point is calculated using the oil pressure and the specified capillary pressure at that point using the following equation:

$$P_{water} = P_{oil} - P_c = f\left(S_w, IFT, wettability\right) \tag{3.20}$$

So, by applying the capillary pressure equation into the water phase mass-conservation equation and combining with the oil phase one, Equations of 3.1 and 3.2 can be summarized as the following equation:

$$\begin{aligned}
&\frac{\partial}{\partial x}\left(\beta K_x\left(\frac{k_{rw}}{\mu_w}+\frac{k_{ro}}{\mu_o}\right)\left(\frac{\partial P_o}{\partial x}\right)-\beta K_x\left(\frac{k_{rw}}{\mu_w}\gamma_w+\frac{k_{ro}}{\mu_o}\gamma_o\right)\left(\frac{\partial D}{\partial x}\right)-\beta K_x\left(\frac{k_{rw}}{\mu_w}\right)\left(\frac{\partial P_c}{\partial x}\right)\right)+\\
&\frac{\partial}{\partial y}\left(\beta K_y\left(\frac{k_{rw}}{\mu_w}+\frac{k_{ro}}{\mu_o}\right)\left(\frac{\partial P_o}{\partial y}\right)-\beta K_y\left(\frac{k_{rw}}{\mu_w}\gamma_w+\frac{k_{ro}}{\mu_o}\gamma_o\right)\left(\frac{\partial D}{\partial y}\right)-\beta K_y\left(\frac{k_{rw}}{\mu_w}\right)\left(\frac{\partial P_c}{\partial y}\right)\right)+\\
&\frac{\partial}{\partial z}\left(\beta K_z\left(\frac{k_{rw}}{\mu_w}+\frac{k_{ro}}{\mu_o}\right)\left(\frac{\partial P_o}{\partial z}\right)-\beta K_z\left(\frac{k_{rw}}{\mu_w}\gamma_w+\frac{k_{ro}}{\mu_o}\gamma_o\right)\left(\frac{\partial D}{\partial z}\right)-\beta K_z\left(\frac{k_{rw}}{\mu_w}\right)\left(\frac{\partial P_c}{\partial z}\right)\right)=\frac{1}{\alpha}\left(\phi^0 c_\phi\right)\frac{\partial P_o}{\partial t}
\end{aligned} \tag{3.21}$$

For more details on parameters used in the above equations, one is referred to Appendix A and nomenclatures.

Equation 3.21 is necessarily non-linear and should be linearized by approximation-finite-difference formulas. The following equation, so-called pressure equation, is a finite difference expansion of the above equation:

$$
\begin{Bmatrix}
\left(T_w+T_o\right)_{i+\frac{1}{2},j,k}\left(P_{o_{i+1}}^{n+1}-P_{o_i}^{n+1}\right)_{j,k}+\left(T_w+T_o\right)_{i-\frac{1}{2},j,k}\left(P_{o_{i-1}}^{n+1}-P_{o_i}^{n+1}\right)_{j,k}+\\
\left(T_w+T_o\right)_{i,j+\frac{1}{2},k}\left(P_{o_{j+1}}^{n+1}-P_{o_j}^{n+1}\right)_{i,k}+\left(T_w+T_o\right)_{i,j-\frac{1}{2},k}\left(P_{o_{j-1}}^{n+1}-P_{o_j}^{n+1}\right)_{i,k}+\\
\left(T_w+T_o\right)_{i,j,k+\frac{1}{2}}\left(P_{o_{k+1}}^{n+1}-P_{o_k}^{n+1}\right)_{i,j}+\left(T_w+T_o\right)_{i,j,k-\frac{1}{2}}\left(P_{o_{k-1}}^{n+1}-P_{o_k}^{n+1}\right)_{i,j}+
\end{Bmatrix}-
$$

$$
\begin{Bmatrix}
\left(T_w\gamma_w+T_o\gamma_o\right)_{i+\frac{1}{2},j,k}\left(D_{i+1}-D_i\right)_{j,k}+\left(T_w\gamma_w+T_o\gamma_o\right)_{i-\frac{1}{2},j,k}\left(D_{i-1}-D_i\right)_{j,k}+\\
\left(T_w\gamma_w+T_o\gamma_o\right)_{i,j+\frac{1}{2},k}\left(D_{j+1}-D_j\right)_{i,k}+\left(T_w\gamma_w+T_o\gamma_o\right)_{i,j-\frac{1}{2},k}\left(D_{j-1}-D_j\right)_{i,k}+\\
\left(T_w\gamma_w+T_o\gamma_o\right)_{i,j,k+\frac{1}{2}}\left(D_{k+1}-D_k\right)_{i,j}+\left(T_w\gamma_w+T_o\gamma_o\right)_{i,j,k-\frac{1}{2}}\left(D_{k-1}-D_k\right)_{i,j}+
\end{Bmatrix}-
$$

$$
\begin{Bmatrix}
\left(T_w\right)_{i+\frac{1}{2},j,k}\left(P_{c_{i+1}}^{n}-P_{c_i}^{n}\right)_{j,k}+\left(T_w\right)_{i-\frac{1}{2},j,k}\left(P_{c_{i-1}}^{n}-P_{c_i}^{n}\right)_{j,k}+\\
\left(T_w\right)_{i,j+\frac{1}{2},k}\left(P_{c_{j+1}}^{n}-P_{c_j}^{n}\right)_{i,k}+\left(T_w\right)_{i,j-\frac{1}{2},k}\left(P_{c_{j-1}}^{n}-P_{c_j}^{n}\right)_{i,k}+\\
\left(T_w\right)_{i,j,k+\frac{1}{2}}\left(P_{c_{k+1}}^{n}-P_{c_k}^{n}\right)_{i,j}+\left(T_w\right)_{i,j,k-\frac{1}{2}}\left(P_{c_{k-1}}^{n}-P_{c_k}^{n}\right)_{i,j}+
\end{Bmatrix}=\frac{V_{b_{i,j,k}}}{\alpha\Delta t}\left(\phi^0 c_\phi\right)^n{}_{i,j,k}\left(P_o^{n+1}-P_o^n\right)_{i,j,k}
\tag{3.22}
$$

All "T"s are transmissibility terms and evaluated at the previous time step (n). To find the pressure distribution at each time step the above equation should be considered for each grid nodes and a set of pressure equations needs to be solved.

3.6.1 Saturation Finite-Difference Equation

As mentioned earlier, the IMPECS method is used to solve the pressure, saturation, and concentration equations. In this method, the oil pressure distribution of the entire system is implicitly calculated first. Then, oil and water saturations are calculated in the second steps. In the second steps, the water saturation at new time step ($n+1$) is calculated by using the latest oil pressure for individual grid blocks (P_o^{n+1}) and substituting it into the water equation (Equation 3.1) as presented in the following equation in the finite-difference form:

$$S_{w_{i,j,k}}^{n+1} = S_{w_{i,j,k}}^{n}\left[1-\left(c_w+c_\phi\right)\left(P_o^{n+1}-P_o^{n}\right)\right]_{i,j,k} + \left(\frac{\Delta t}{V_b\phi}\right)^{n}_{i,j,k}\left[\begin{array}{l} T_{wx}^{n}\left(\Delta_x P_o^{n+1}-\Delta_x P_c^{n}-\overline{\gamma}_w^{n}\Delta_x D\right)+ \\ T_{wy}^{n}\left(\Delta_y P_o^{n+1}-\Delta_y P_c^{n}-\overline{\gamma}_w^{n}\Delta_y D\right)+ \\ T_{wz}^{n}\left(\Delta_z P_o^{n+1}-\Delta_z P_c^{n}-\overline{\gamma}_w^{n}\Delta_z D\right) \end{array}\right]_{i,j,k} \quad (3.23)$$

3.6.1 Surfactant Finite-Difference Equation

As presented in Equation 3.3, surfactant equation consists of more terms than water/oil equation. Hence, its finite-difference equation is not presented here and one is referred to Appendix B.

3.7 Solution Sequence

Figure 3-14 shows the sequence of events in executing the wettability alteration simulator.

After initializing the system and calculating fluid properties, the direction of flow is determined using single point upstream weighting. The pressure equation (Equation 3.6) is then solved using a linear equation solver, which employs the process of Gaussian elimination and back substitution after which the phase pressure arrays are updated to the new time level.

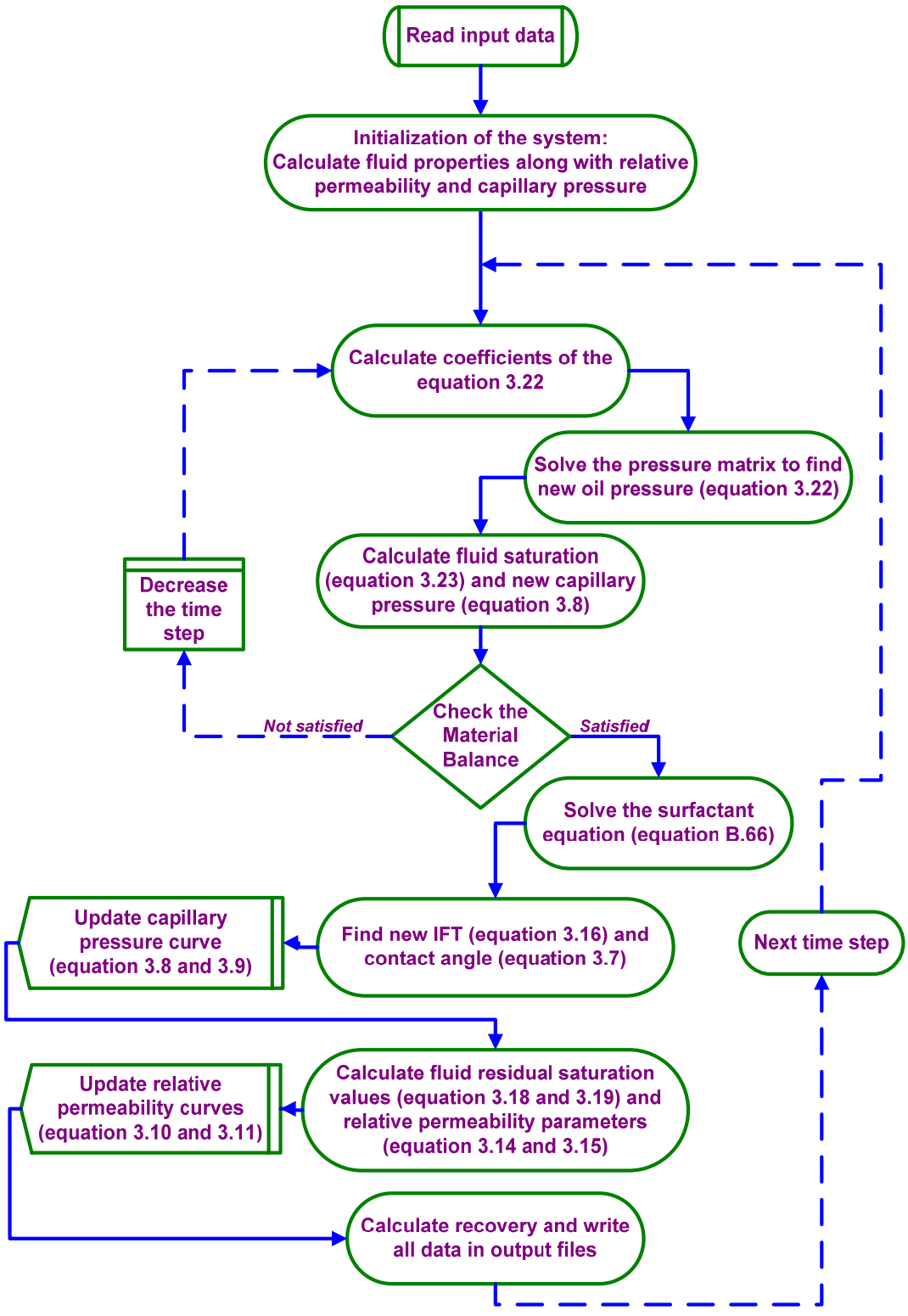

Figure 3-14: Flowchart showing the sequence of events in the execution of the simulator

The new pressures are then used to calculate the velocity vector field for the oil and water phases. These velocities are used in calculating the water saturation and oil production rate, after which the oil recovery can be calculated. Next, material balance is checked by comparing the water saturation changes of the core with that of the fracture.

The surfactant concentration equation is solved as described in Appendix B. New values for surfactant concentration lead to the calculation of interfacial tension and contact angle values according to Equation 3.21 and 3.22, respectively. At this time capillary pressure values for each cell are updated after finding the new values for residual fluid saturations. At the end, new relative permeability values for each phase are calculated. The whole process is repeated as shown in the flowchart (Figure 3-14) for the next time level.

Chapter 4: Numerical Simulation and Discussion of the Results

4.1 Introduction

In this chapter, the model is validated for two different rock wettabilities; water-wet and oil-wet systems using experimental data in the literature. In the section dedicated to water-wet systems, results obtained from the numerical simulation are presented for comparison to the experimental profile. This allows a detailed discussion of the influence of boundary conditions, core orientations, capillary force, gravity force, and interfacial tension on the production history.

The oil-wet studies include mathematical modeling of several experimental studies regarding the wettability alteration, as well as some parametric studies. The unifying theme behind these studies is to improve the understanding of the wettability alteration in oil-wet rock systems using surfactants.

The most challenging part of developing the simulation model is that laboratory experiments are performed by immersing an oil-saturated cylindrical core inside an imbibition cell at ambient conditions rather than in a more conventional arrangement where the core is confined to a core holder or sleeve. In some cases, the sides or ends of the core are sealed to prevent fluid flow. The simulation model was developed to simulate both the core and surrounding fluid in the imbibition cell. Therefore, the grid consists of fluid gridblocks surrounding the porous media and rock gridblocks. The purpose of the fluid grid is to simulate fluid flowing from the open imbibition cell into the rock and expelling oil from all sides that are open to fluid flow to the top.

Since the simulator is written in Cartesian coordinates, the cross-sectional area is not circular; however, both length and pore volume are kept the same as the experimental core.

The fluid gridblocks of this model are located at the top, bottom and on the sides of the grid. Each fluid gridblock is given a set of petrophysical properties with the intent of simulating flow through the open imbibition cell.

In this chapter, the modeling of ten laboratory studies of surfactant/brine imbibition process is presented. The first four studies are the modeling of brine imbibition in water-wet cores. The imbibition process of brine and/or surfactant in oil-wet cores is investigated in the rest of the studies. Generally, parameters used in the model were those reported by the persons conducting experiments or were taken from the literature. Where data as parameters were not available, they were estimated and used as history matching parameters. These are identified in the description of the different cases. In the modeling of the experimental data for wettability change, the parameter "*d*" in Equation 3.7 was used (the last four cases).

All parameters used in modeling of the following case studies were listed in Appendix C.

4.2 Water-wet Systems

4.2.1 Case Study 1: Numerical Solution of Co-current/Counter-current Imbibition

The imbibition process is of practical importance in recovering oil from formations and has been studied for a long time. The efficiency of a water-injection process for fractured reservoirs cannot be accurately predicted because of poor knowledge of the different fracture networks and the individual production behavior of the matrix blocks in contact with water. Each block produces its oil more or less independently from its adjacent blocks under the combined effects of gravity and capillary forces. The mechanisms controlling the imbibition are analyzed in this study.

Spontaneous imbibition involves both co-current and counter-current flows of oil and aqueous phases in proportions that depend on the ratio of gravity to capillary forces (Equation 2.11). It is necessary to have a useful prototype that can model and predict the experimental data taken to understand the process of imbibition.

As discussed in Chapter 2, a variety of scale-up or dimensionless groups have been developed, which require numerous rules to be followed for any specific conditions (different rock types, various boundary conditions, heterogeneity, fluid properties). The numerical method is an excellent alternative for solving this problem because many conditions can easily be considered, which can strongly influence the results.

Blair (1964) presented the first numerical solutions of the equations describing the imbibition of water and the counter-current flow of oil in porous rocks. He studied the effect of varying capillary pressure, oil/water relative permeability, oil viscosity,

and initial water saturation on imbibition rate for water-wet rocks. He showed that capillary pressure curve and relative permeability have an important impact on the oil recovery rate, with capillary pressures probably having a stronger effect than relative permeability.

In this study, an accurate numerical description of the spontaneous co-current and counter-current flow mechanisms occurring in a single block of water-wet porous medium subjected to two different capillary pressures is presented. One set of oil/water relative permeability curves and capillary pressure used in Blair's original calculations was chosen to compare the present simulator outcomes with his results. This calculation involves counter-current imbibition of water into a porous medium containing a high oil (and low water) saturation. The petrophysical and fluid properties used in this study are shown in Table 4-1.

Table 4-1: Fluid and rock properties (Blair 1964)

Property	**Value**
Length (cm)	50
Diameter (cm)	3.175
Porosity (%)	32.1
Permeability (mD)	200
Oil Viscosity (cp)	5
Water Viscosity (cp)	1
Oil Density (lb/ft^3)	55
Water Density (lb/ft^3)	62.35
Initial Water Saturation (%)	9.2

Figure 4-1 shows the oil and water relative permeability curves using Equation 3.10 and 3.11. The capillary pressure curve used in the calculation is presented in Figure 4-2.

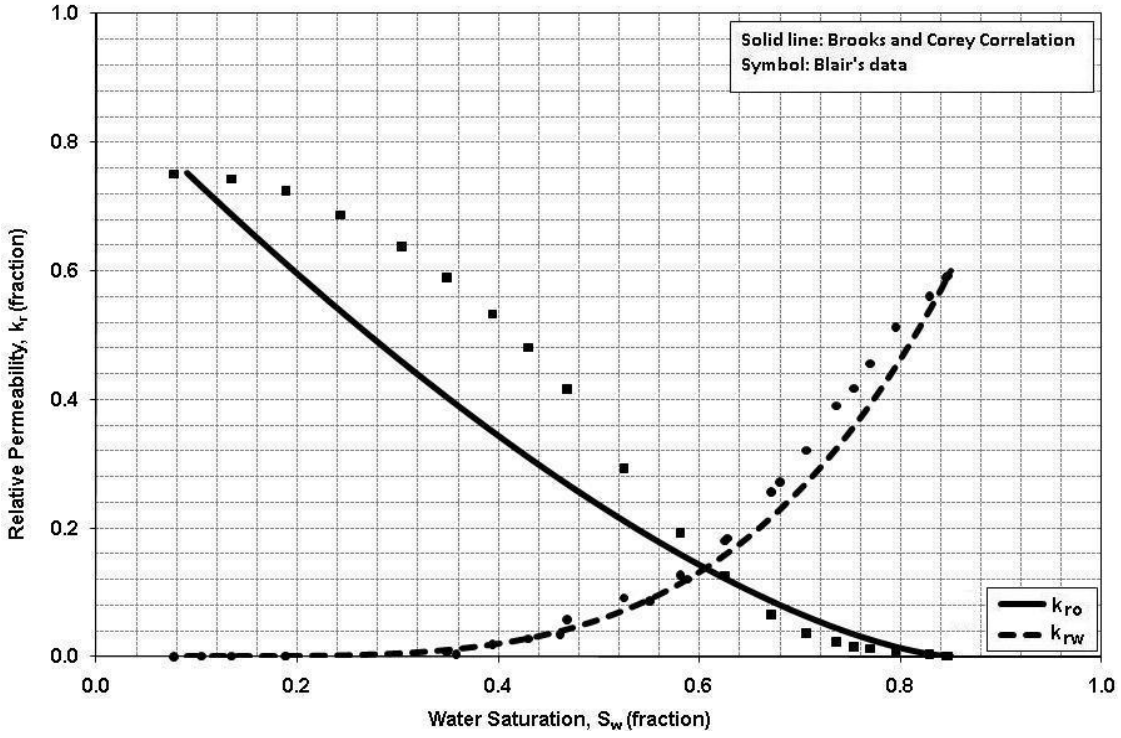

Figure 4-1: Relative permeability-saturation relations

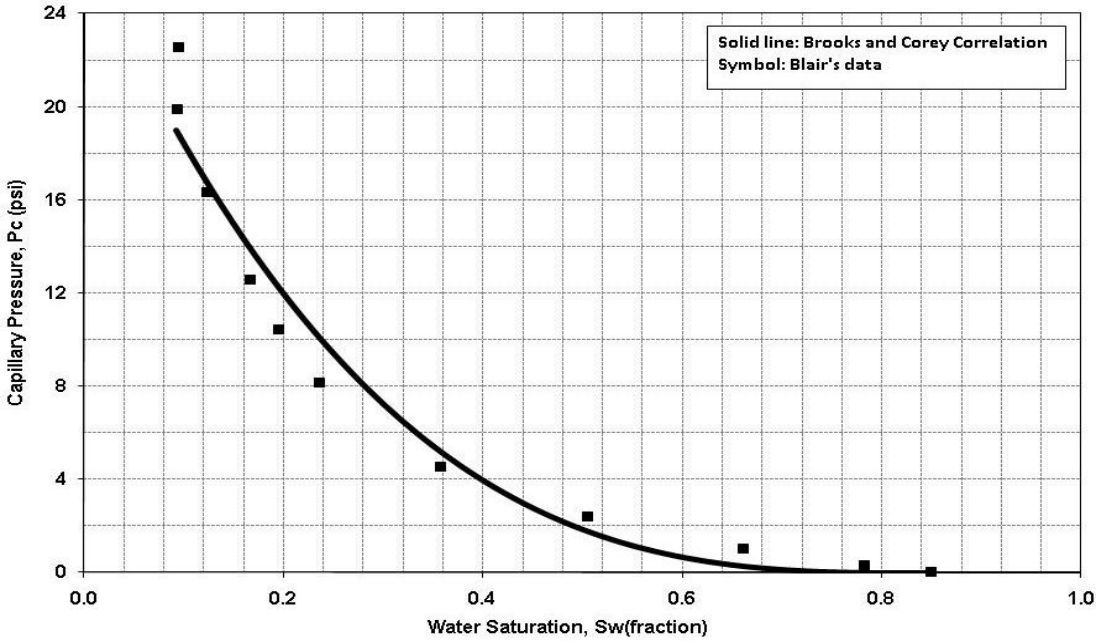

Figure 4-2: Capillary pressure-saturation relation

Table 4-2 shows a summary of some input data for simulation of Blair's model. The actual time of Blair run was 20 hours; however, the model was run for one day (24 hours) for further investigation.

Table 4-2: Input parameters in the simulation of case study 1

Parameter	Value
Grid Block Sizes Δx, Δy, Δz (mm)	10.2, 7.03, 7.03
Number of Grid Blocks in X, Y, Z Direction	49, 4, 4
Time Interval (sec)	1.73
Number of Days Simulated (days)	1

The core is placed horizontally. The sides and one of the ends are closed as shown in Figure 4-3. Water is admitted to the open end and enters the core by imbibition. The

physical boundary condition is that there is no flow of either phase at the closed sides of the core. This may be mathematically described that there was no pressure gradient in either phase at those boundaries. The core was assumed to be homogeneous with uniform water saturation so that the initial capillary pressure was constant along its length. When a lower capillary pressure was imposed at the open end, water was imbibed into the open end of the core and oil was expelled in a counter-current fashion. Therefore, capillary pressure was set equal to zero at the outflow boundary according to some experimental evidence (Perkins 1957; Kyte *et al.* 1958; Willhite 1986).

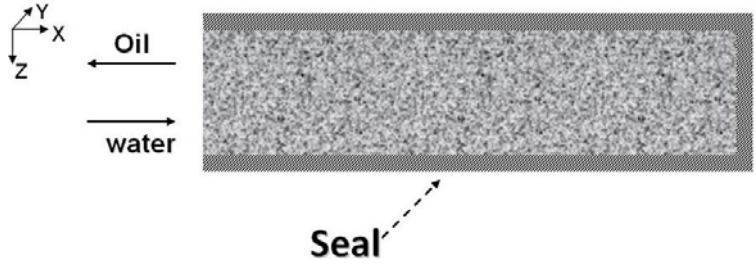

Figure 4-3: Schematic of the core modeled in Blair's simulation

Figure 4-4 is a comparison between Blair's data and results from the present simulator. This figure shows the pressure and saturation profiles for the imbibition time of 6.6 hours where the water front has advanced approximately half the length of the core. The lower curve in the figure is the water-saturation profile. Near the open end, the water saturation is high and abruptly decreases. The middle curve in Figure 4-4 is the water-pressure profile, and the upper one is the oil-pressure profile.

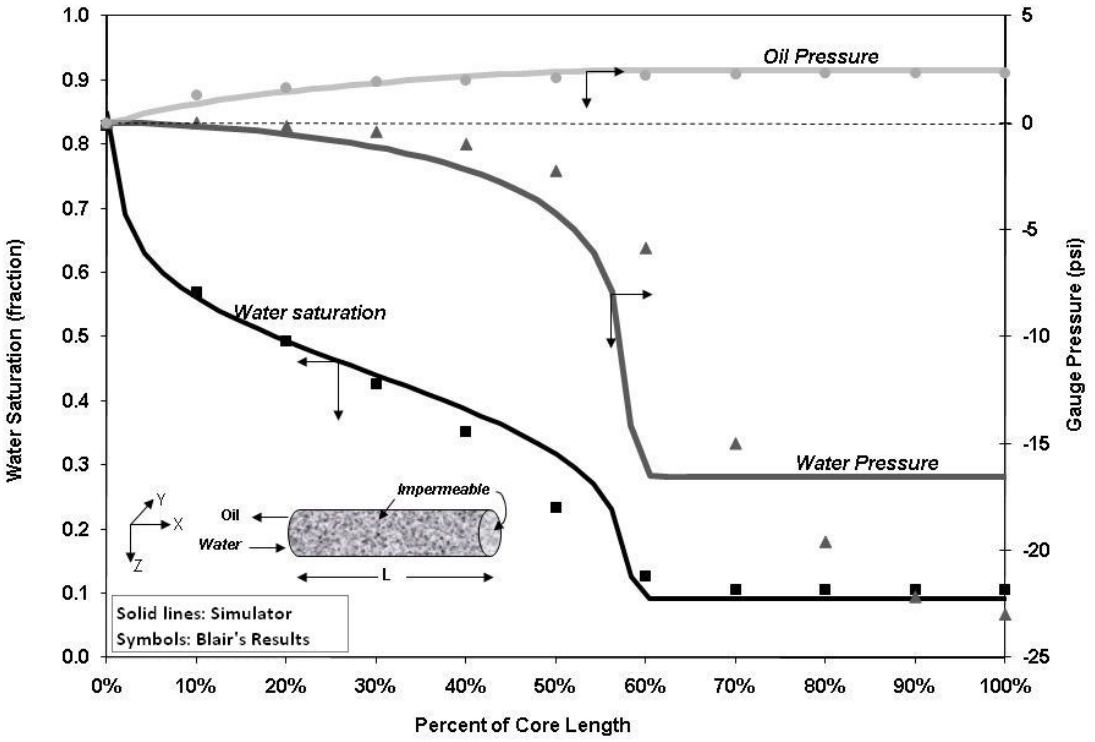

Figure 4-4: Pressure and saturation profiles at 6.6 hours

Figure 4-4 shows that there is a difference between simulator outcome and Blair's results in water pressure profile near the water front.

It is important to note that the capillary pressure curve and relative permeability curves used in the simulator are not exactly the same as those curves that Blair used, so some differences are obviously expected. In addition, reservoir simulation techniques such as one-point upstream, two-point upstream, total-variation-diminishing (TVD) to control the solution oscillations associated with high order differencing schemes have recently progressed to make reservoir simulation results

more precise. So, his result of water pressure is not as good agreement with the simulator outcome as it is in water saturation.

The successive water-saturation profiles given in Figure 4-5 show that water/oil front moved regularly from the open end to the closed end of the core. As the water front moves further into the block, the water saturation profile is stretched. The water front reaches the center of the core at t=4.8 hours.

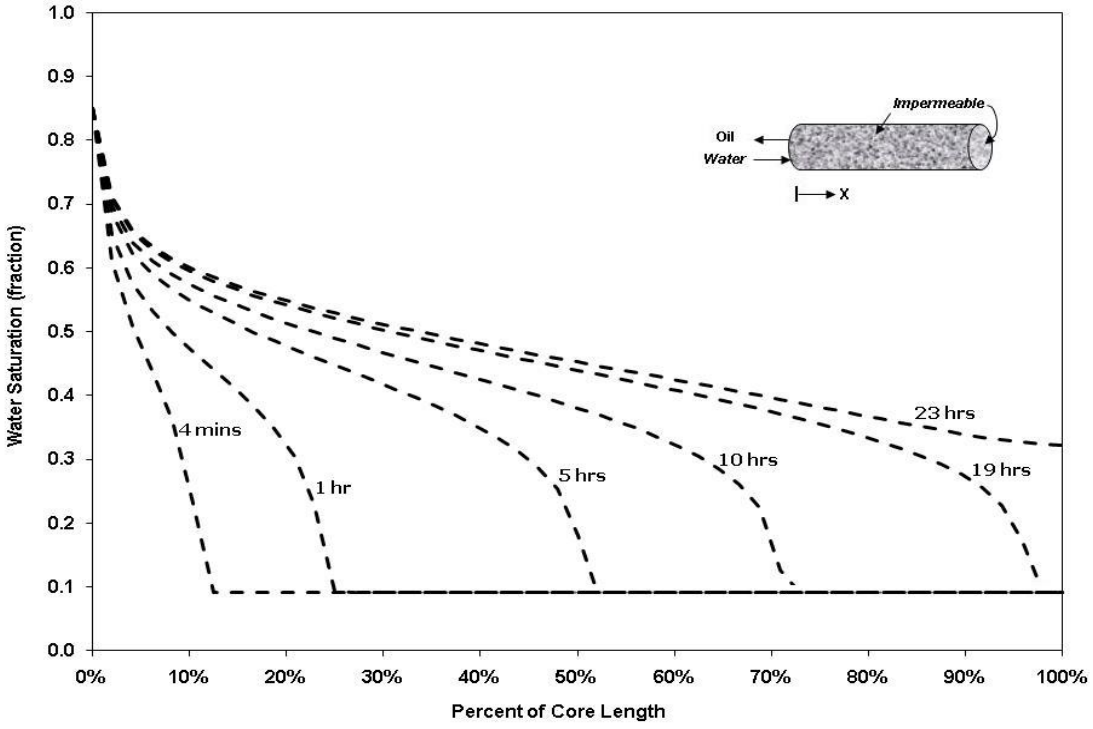

Figure 4-5: Water saturation distributions along the core length at various times of imbibition

Figure 4-6 shows saturation and pressure profiles after 22.8 hours from beginning of the imbibition process. This figure shows that the water front already reached the

impermeable core end (water reaches the closed end approximately at 19.8 hours: Figure 4-5).

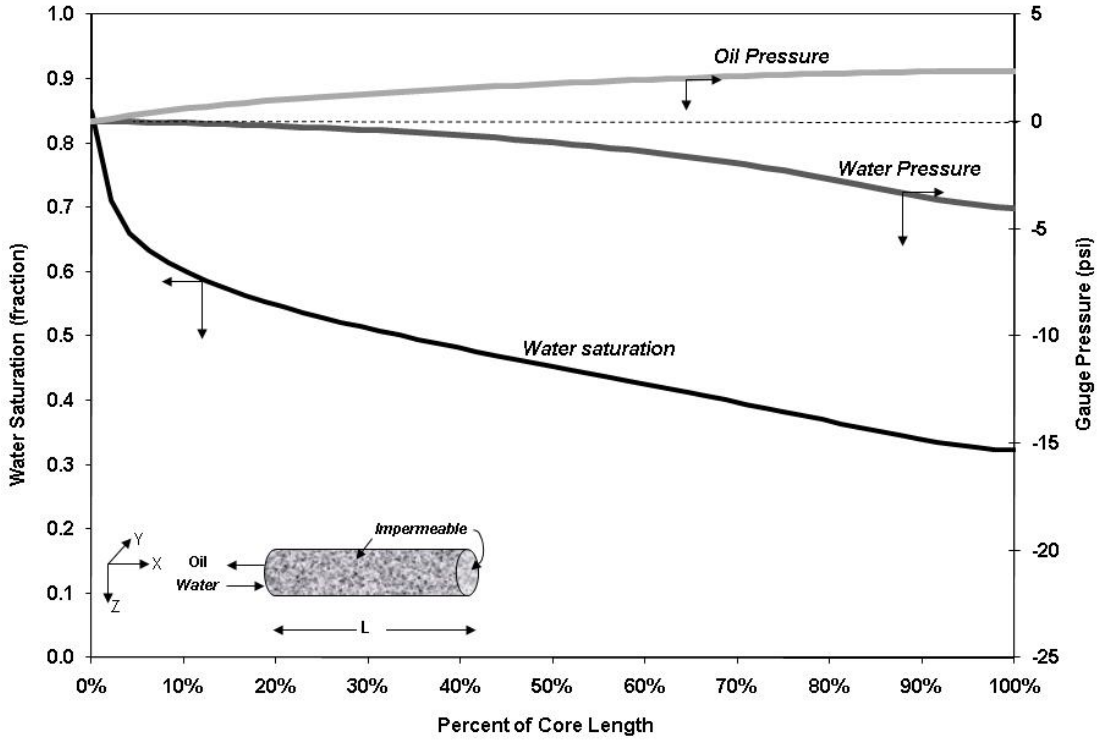

Figure 4-6: Pressure and saturation profile at 22.8 hours

To study fluid flow, the cross section of the core was divided into cells across its length. The water saturation in the lower part of the cross sectional area was higher than the top part, confirming that the process was counter-current. This is shown in the following figure. The saturation difference from top to the bottom is insignificant because capillary force dominates the imbibition process comparing to the gravity force. As mentioned earlier, to model cylindrical cores with the present three-

dimensional simulator model, the same cross-sectional area but square and the same length were chosen. For this reason, the cross-sectional area in Figure 4-7 is not circular. The X-axis shows the distance in X direction and Y-axis presents the distance in Y direction from the coordinate center.

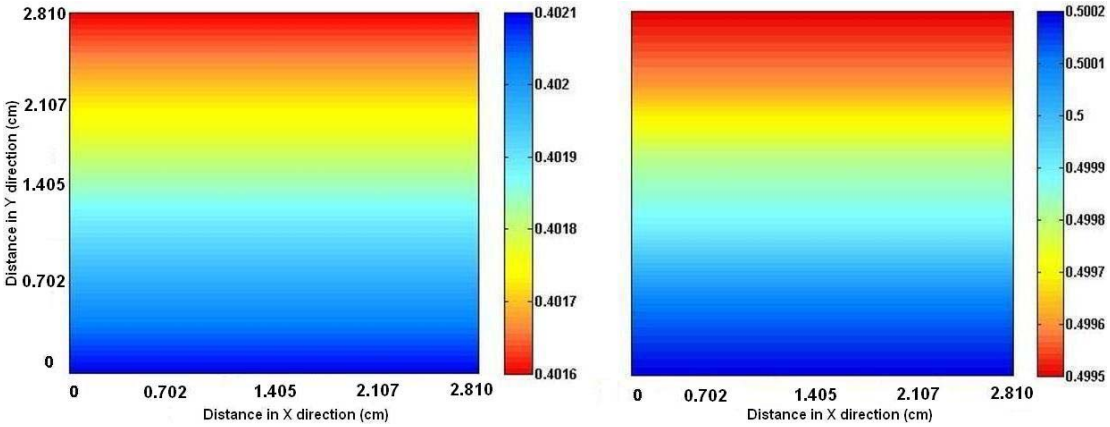

Figure 4-7: Cross-sectional view of water saturation distributions: left) after 6.6 hrs and right) after 23 hrs

Since early in the history of the oil industry, the importance of gravity has been recognized as one of the three important natural forces (alongside capillary and viscous force) for expelling oil from reservoir rock. Further study of this force is needed to round out our knowledge of reservoir behaviors and to gain a balanced viewpoint of the interplay of forces that occur in reservoirs. It is obvious that gravity force plays a particularly important role when capillary force is negligible, which results in a co-current flow in spontaneous imbibition process. To distinguish between these two forces in a water-wet core, the capillary pressure curve used in Blair's model was lowered such that the highest capillary pressure value was reduced to

0.0128 psi, as shown in Figure 4-8. The same relative permeability curves as shown in Figure 4-1 are used. Also, other parameters are kept constant as presented before in Table 4-1and Table 4-2.

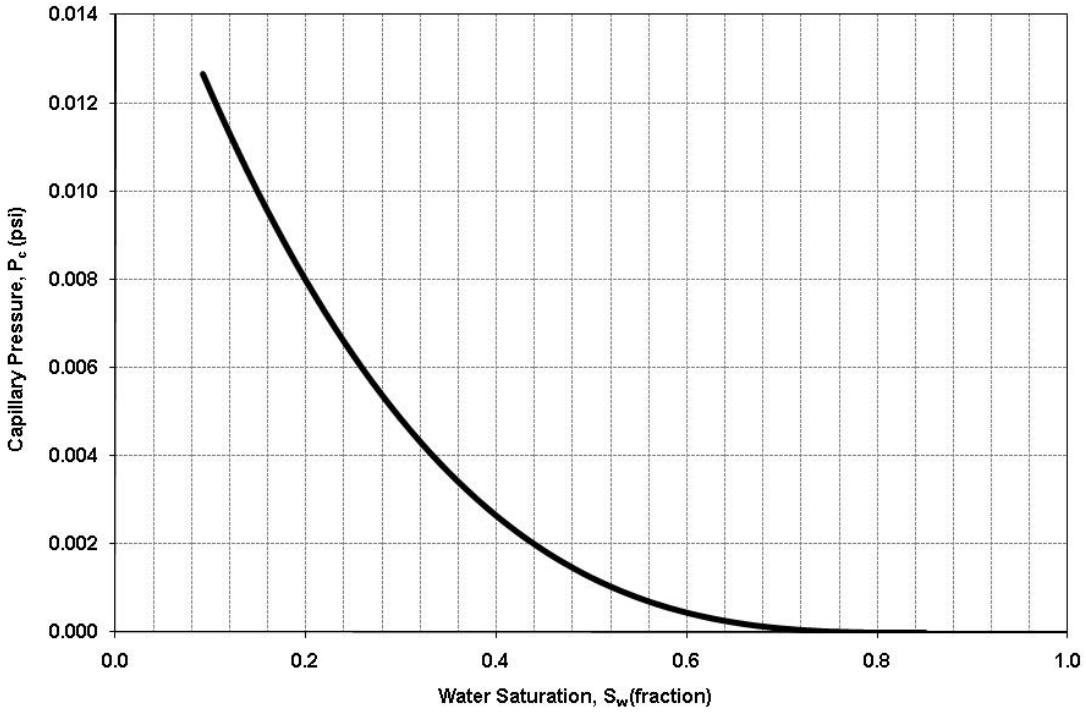

Figure 4-8: Low capillary pressure curve

To assure that gravity is dominated, N_B^{-1} must be calculated (see Equation 2.11). According to Equation 2.11, capillary pressure can be lowered by reducing the interfacial tension. So, if we assume that the capillary pressure curve presented in Figure 4-8 happens because of having different oil/water with low interfacial tension (e.g. 0.026 mN/m), the inverse bond number will be 2.3×10^{-2}, which proves that the

gravity is dominative force . Figure 4-9 shows oil production versus time for Blair's core with the new capillary pressure curve from Figure 4-8. Also, this figure compares the production between the two recent cases: capillary force dominant and gravity force dominant.

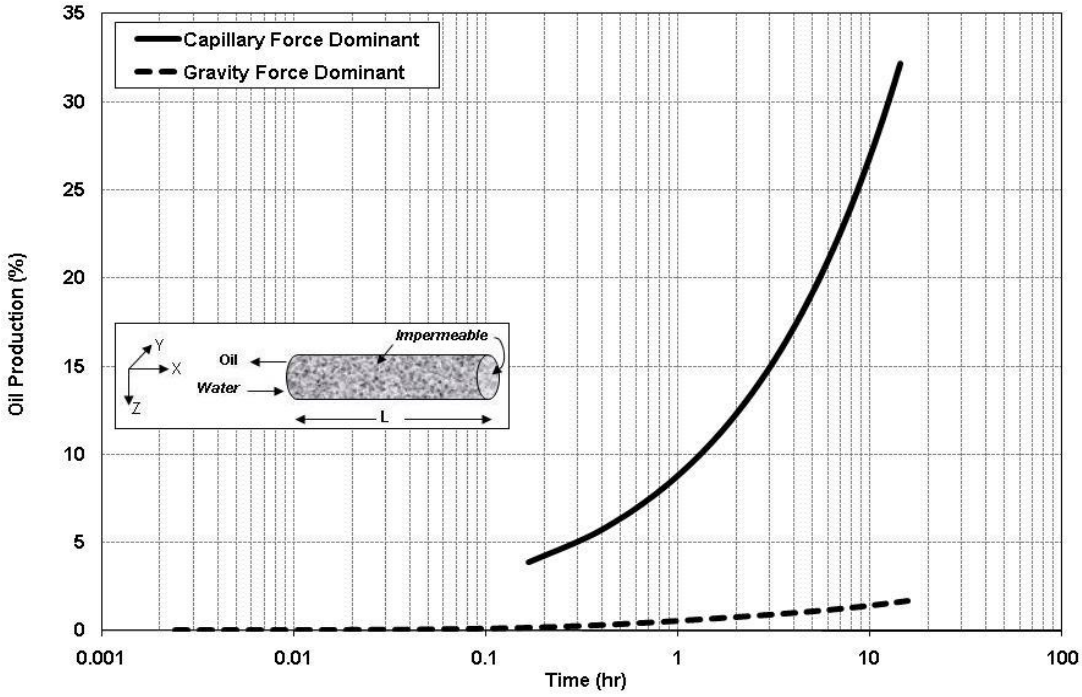

Figure 4-9: Oil productions for the horizontal core with one end open when either gravity force or capillary force is dominant

The effects of gravity were investigated by simulating the oil displacement in a horizontal core that was open on all sides. Two cases were simulated using the capillary pressure curves presented in Figure 4-2 and Figure 4-8, respectively. Oil recovery is shown in Figure 4-10. When capillary force is a dominant mechanism in imbibition of water into a non-coated horizontal core, the brine rapidly imbibed into

the core and the completion of imbibition occurs around two days. In the case of low capillary force, complete imbibition occurs after eight days. Figure 4-10 shows that oil is produced at a much faster rate in the case of capillary force domination as compared to the other case. This phenomenon has been experimentally observed in the literature (Hamon and Vidal 1986; Bourbiaux and Kalaydjian 1990; Cuiec *et al.* 1994; Schechter *et al.* 1994; Milter and Austad 1996a).

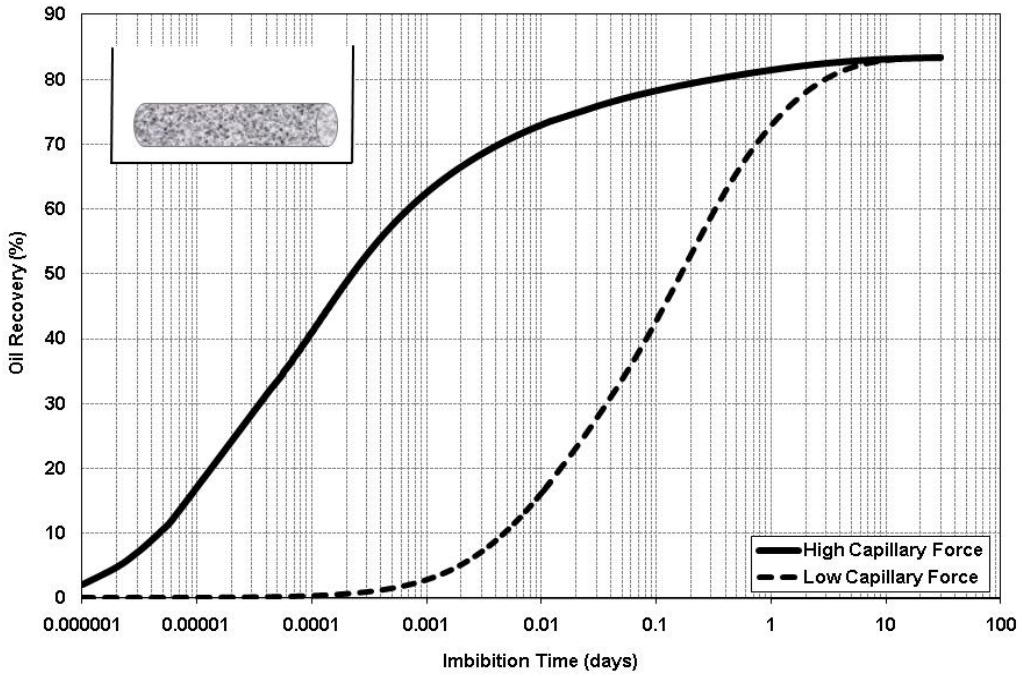

Figure 4-10: Oil production comparison for cases of either capillary force or gravity force domination in the imbibition process of a non-coated horizontal core

4.2.2 Case Study 2: Vertical versus Horizontal Core Orientations

The effect of core orientation on oil saturation distribution and recovery was studied for the case where capillary force was low. Therefore, the capillary pressure curve presented in Figure 4-8 is used here, and the relative permeability curve was the same as presented in Figure 4-1. All other properties are identical to the Blair data presented in Table 4-1. The uncoated core was placed in a beaker of pure water; once vertical and then horizontal. Figure 4-11 shows the oil production from the core at two orientations of horizontal and vertical.

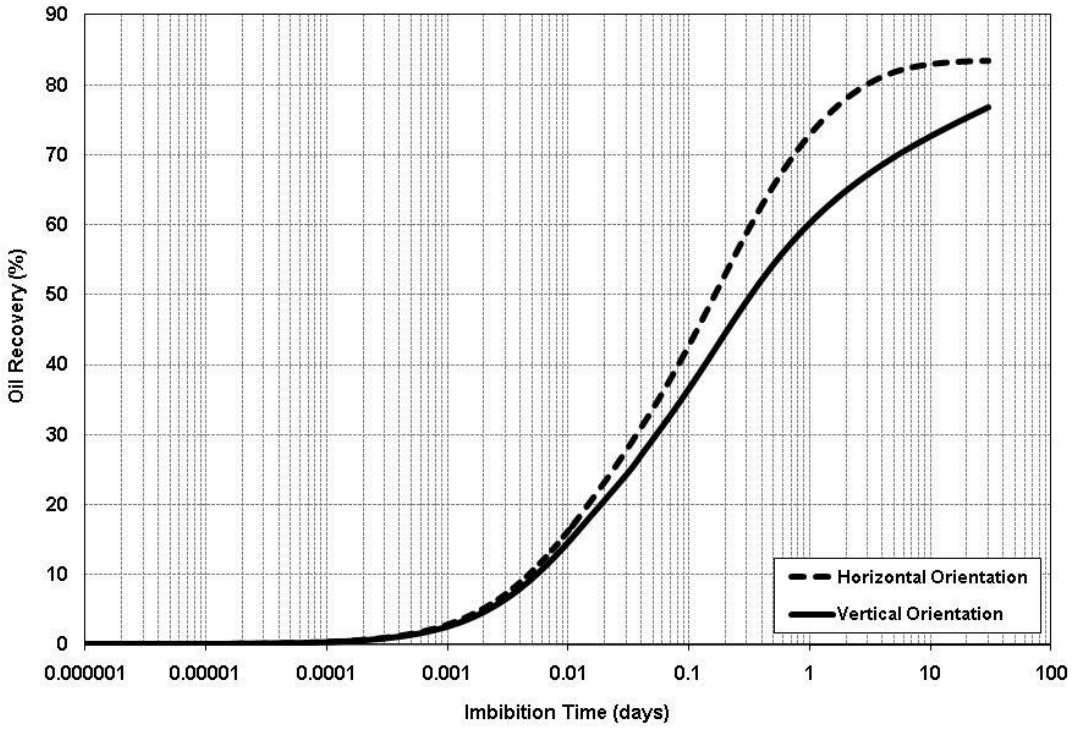

Figure 4-11: Oil production comparison for two different orientations-low capillary forces

At the beginning of imbibition, the oil rates for both horizontal and vertical orientations are identical. After a while, oil rate of the horizontal core increases. The reason is that the capillary forces are very small (see Figure 4-8) and the process is mainly running via gravity force. This can be observed by looking at oil phase velocity profiles in the core shown in Figure 4-12 for the half core. It can be seen from this figure that the flow is mostly co-current and oil produces from the top of the core from the beginning of the imbibition process until the late time of the process. Therefore, oil has bigger area to produce in the horizontal orientation as compared to the vertical orientation, which leads to a higher rate of oil production.

Distribution of oil saturation through the horizontal and vertical orientations after producing about 50% of recoverable oil is displayed in Figure 4-13 as longitudinal view. As shown in this figure, water enters to the horizontal core from the lower part of the core while oil is produced from the top (higher oil saturation). In the vertical orientation, water barely enters from top of the core since the imbibition process is mainly gravity dominant. Needless to say, the ultimate oil recovery will be the same in both orientations.

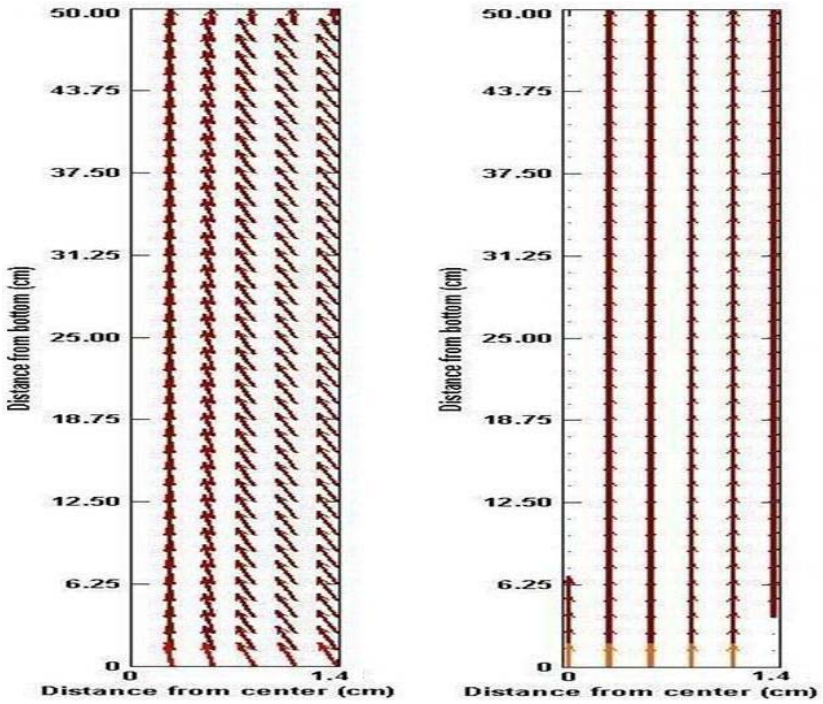

Figure 4-12: Oil phase velocity streamlines for imbibition of water in a vertical water-wet core: left) after 15 mins and right) after 25 days

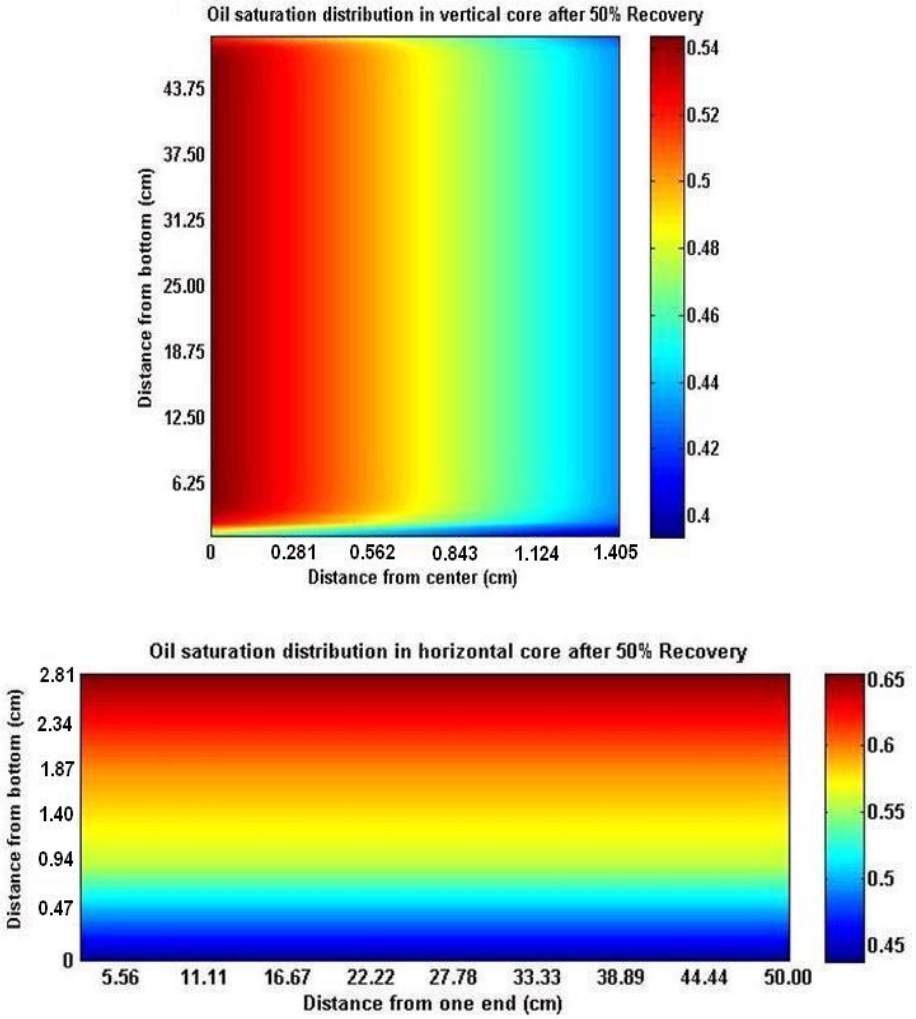

Figure 4-13: Oil saturation distribution after about 50% oil recoveries from: top) vertical core and bottom) horizontal core

Figure 4-14 shows in-situ oil saturation profiles at different imbibition times for the vertical orientation case. The X-axis shows the distance from the center of the core and the Y-axis reveals the distance from the bottom of the core.

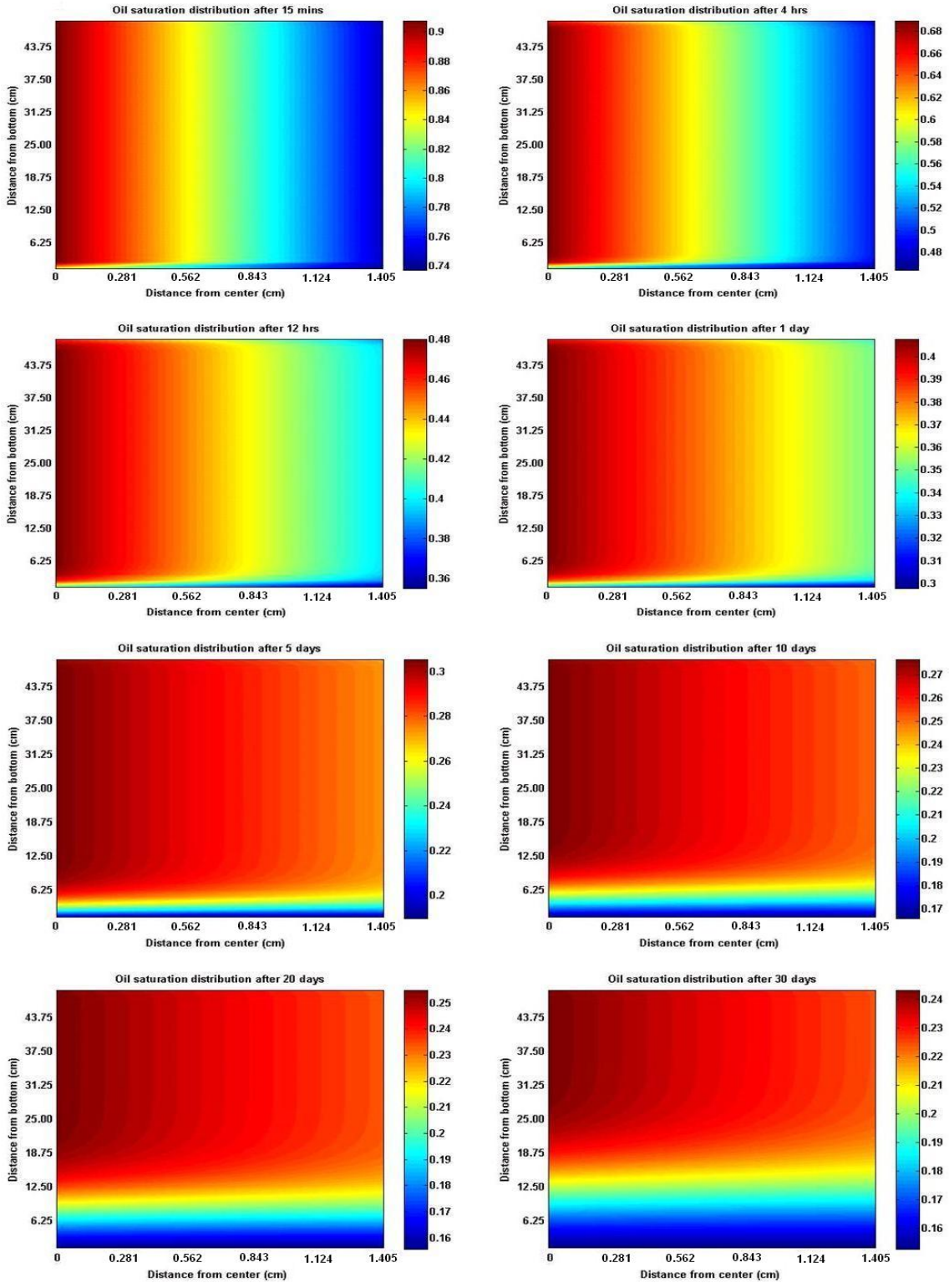

Figure 4-14: Oil saturation profiles within the vertical core at different times

4.2.3 Case Study 3: The Effect of Interfacial Tension between Oil and Water on Imbibition

The effects of interfacial tensions on the oil recovery by spontaneous imbibition and gravity segregation in water-wet cores have been reported in the literature. Schechter *et al*. (1991) conducted several experiments to investigate the effect of interfacial tension on spontaneous imbibition of vertically oriented cores. The purpose of the current study is to model their experimental data and validate the simulator. A ternary fluid system consisting of isooctane, brine, and isopropanol was used in their study (equilibrated oil and water). Different mixtures of these fluids produce significantly different interfacial tension values (different properties) as shown in Table 4-3.

Cylindrical water-wet cores of 61 cm in length and 6.35 cm in diameter were mounted vertically in a plexiglass holder with an annular space of 8 mm. In a typical imbibition experiment, the core was saturated with equilibrated oil and then rapidly immersed in equilibrated water. Both drainage and imbibition were performed; therefore, cores were initially saturated with either oil or brine.

Table 4-3: Phase properties for three different mixtures of fluids (Schechter *et al.* 1991)

Test	$\Delta\rho\ (lb_m/ft^3)$	$\sigma_{ow}\ (mN/m)$	$\mu_w\ (cp)$	$\mu_o\ (cp)$	S_{or}
1	20.60	38.10	1.00	0.48	0.56
2	13.11	1.07	3.40	0.53	0.55
3	6.87	0.10	2.50	0.69	0.10

They also used four different rocks with absolute permeabilities of 15, 100, 500, and 700 md. In the present study, limestone with permeability of 15md was chosen to be modeled (ϕ=15.8%, PV= 305 cm). Relative permeability data and the capillary pressure curve for the first test are presented in Figure 4-15 and Figure 4-16, respectively. Capillary pressure curves for other tests can be found based on Equation 3.8 and corresponding interfacial tension values.

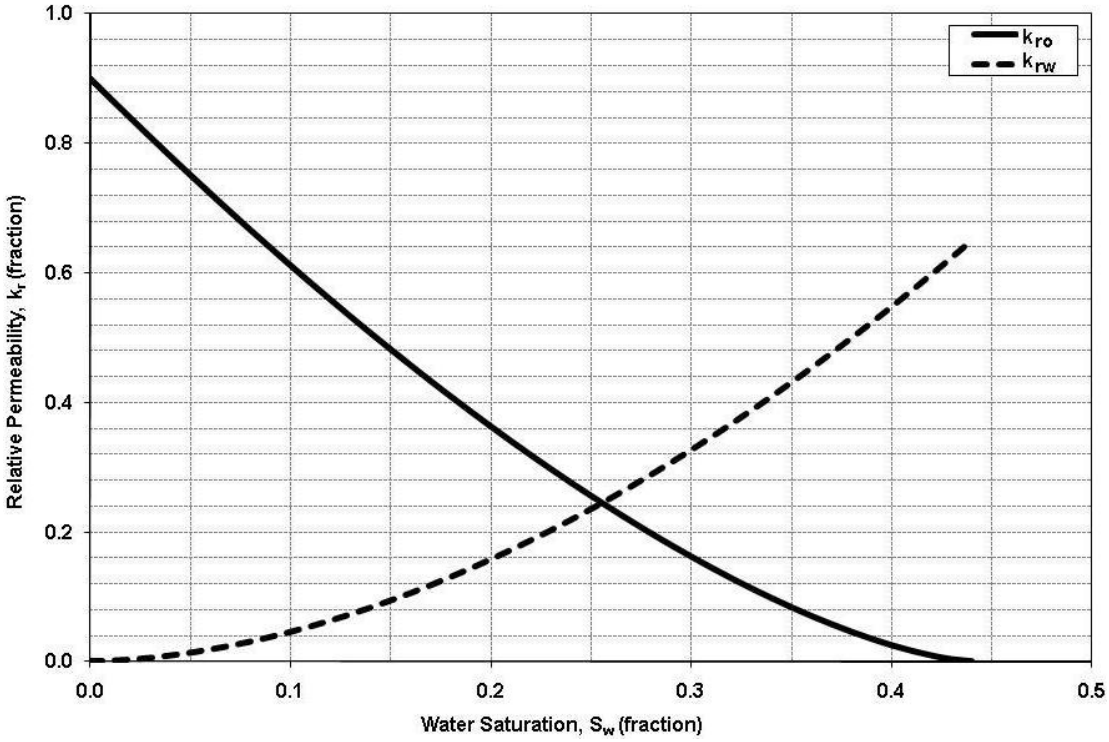

Figure 4-15: Relative permeability-saturation relations

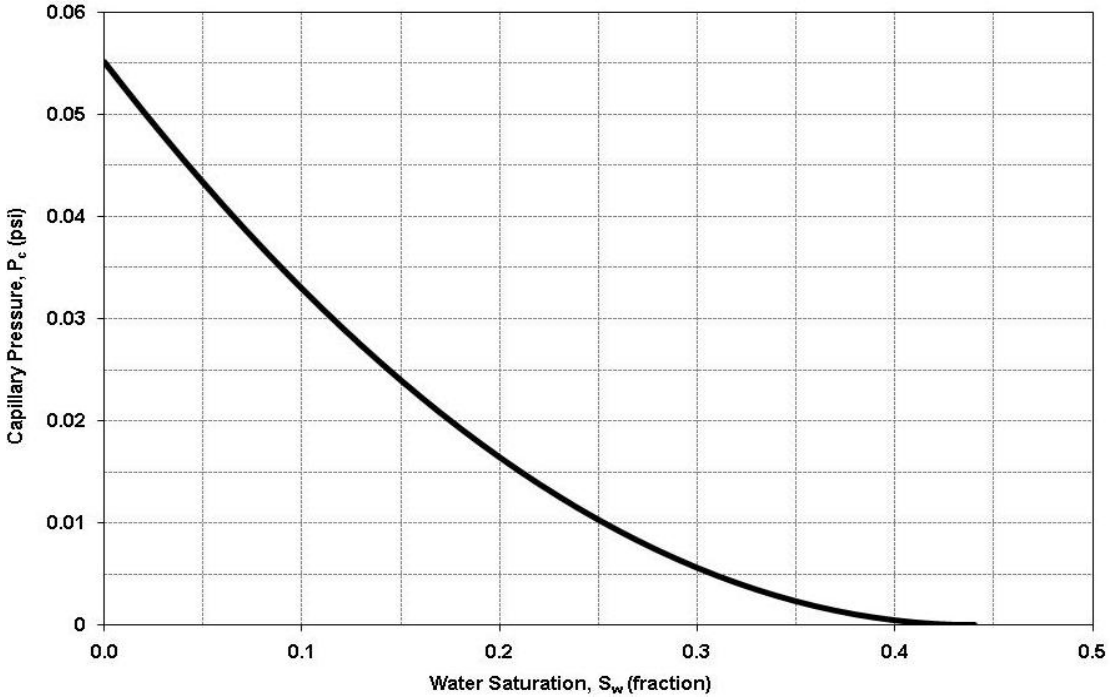

Figure 4-16: Capillary pressure-saturation relation

Table 4-4 shows a summary of input data for simulation of the experimental data. The maximum running time varies at each simulation.

Table 4-4: Input parameters in the simulation of all tests

Parameter	**Value**
Grid Block Sizes Δx, Δy, Δz (cm)	0.7, 0.7, 3.39
Number of Grid Blocks in X, Y, Z Direction	8, 8, 18
Time Interval (sec)	10
Number of Days Simulated (days)	60 (test #3)

The oil saturation distribution after one day imbibition of water into the core for these three different tests is shown in Figure 4-17. Also, Figure 4-18 shows the oil

distribution after 40% production of the original oil in place of the core for the three tests.

Low interfacial tension makes gravity forces more important as the values of N_B^{-1} indicate. In the limit of very low values of interfacial tension, the flow is completely segregated by gravity as can be seen in Figure 4-19. For the test of low interfacial tension, the resistance to flow is lower than the other tests, but there is no significant capillary force to drive imbibition. So, the initial rate is set by the density difference and imbibition is dominated by vertical flow driven by gravity forces. This can be observed by examining the oil phase velocity profiles in the core as shown in Figure 4-19.

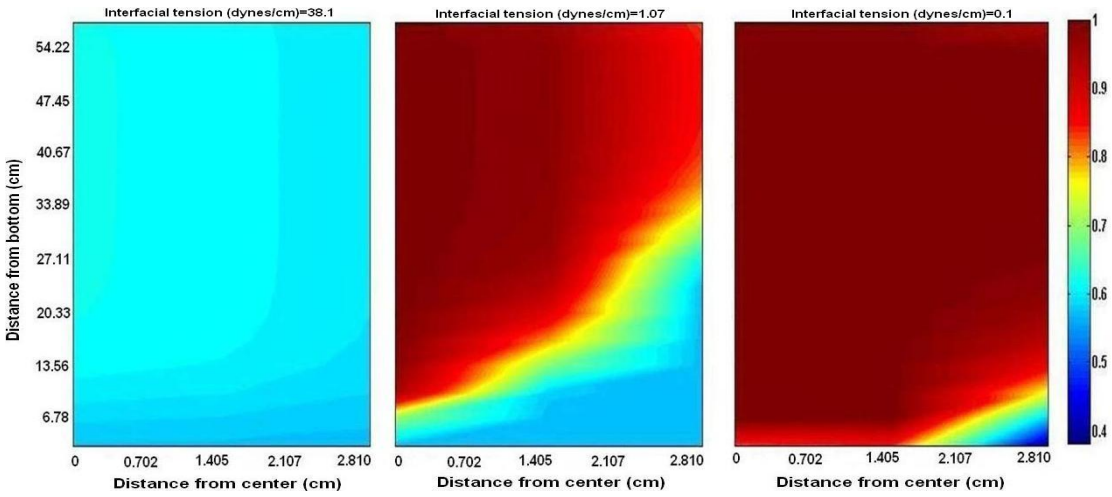

Figure 4-17: Oil saturation distribution for all three tests after 1 day

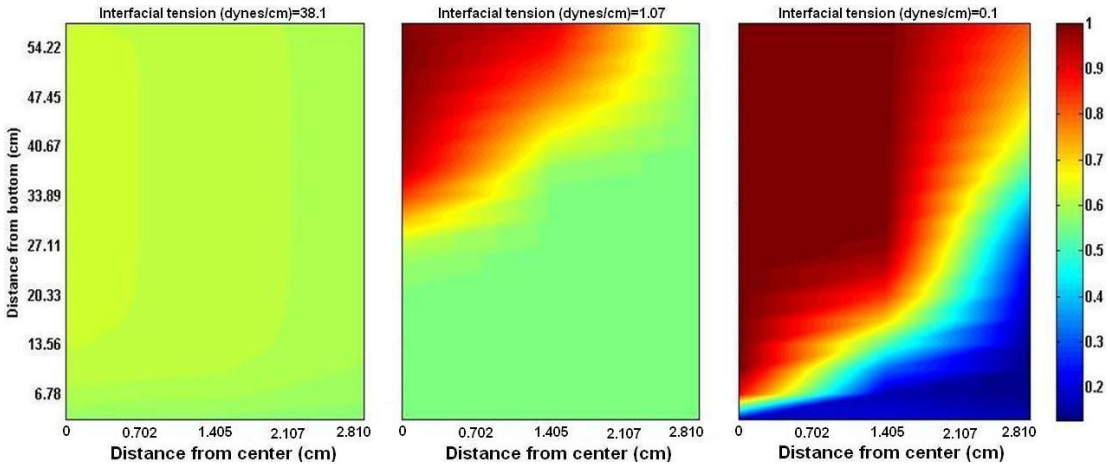

Figure 4-18: Oil saturation distribution for all three tests after 40% recovery

Based on Equation 2.11, the inverse Bond number (N_B^{-1}) for these three tests are 25.66, 1.13, and 0.202, respectively. As discussed in Chapter 2, the inverse of Bond number indicates the effect of gravity on the reduction of residual saturation. At high values of N_B^{-1}, imbibition is dominated by capillary forces, and hence counter-current flow occurs at all the faces of the core. Since the flow is counter-current, relative permeabilities of both phases are low. Therefore, the initial rate of imbibition represents a balance between the relatively large capillary force that is driving imbibition and the flow resistance created by the two phases flowing behind each other.

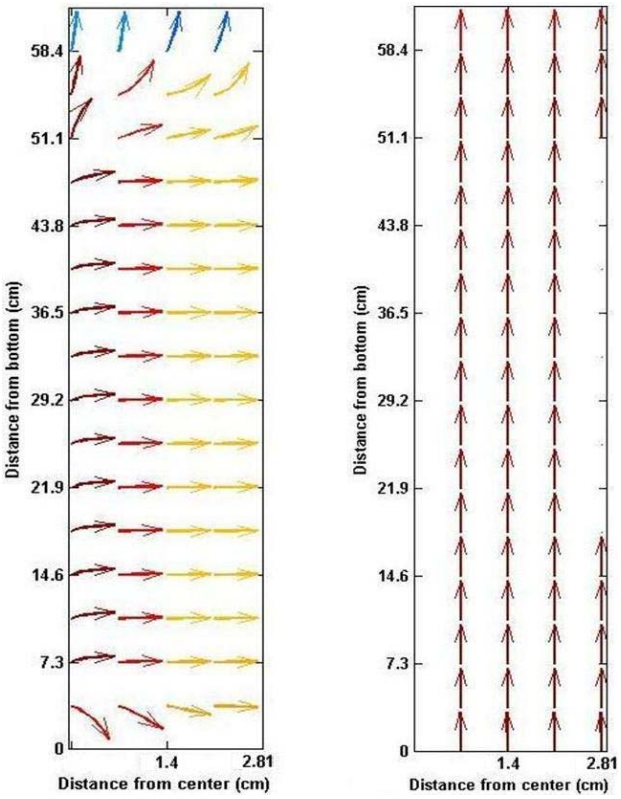

Figure 4-19: Oil phase velocity streamlines for imbibition of water in a vertical core water-wet core after 30% oil recovery: left) IFT=38.1 mN/m and right) IFT=0.1 mN/m

Oil saturation distribution for the test with low interfacial tension is shown in Figure 4-20 for various imbibition times.

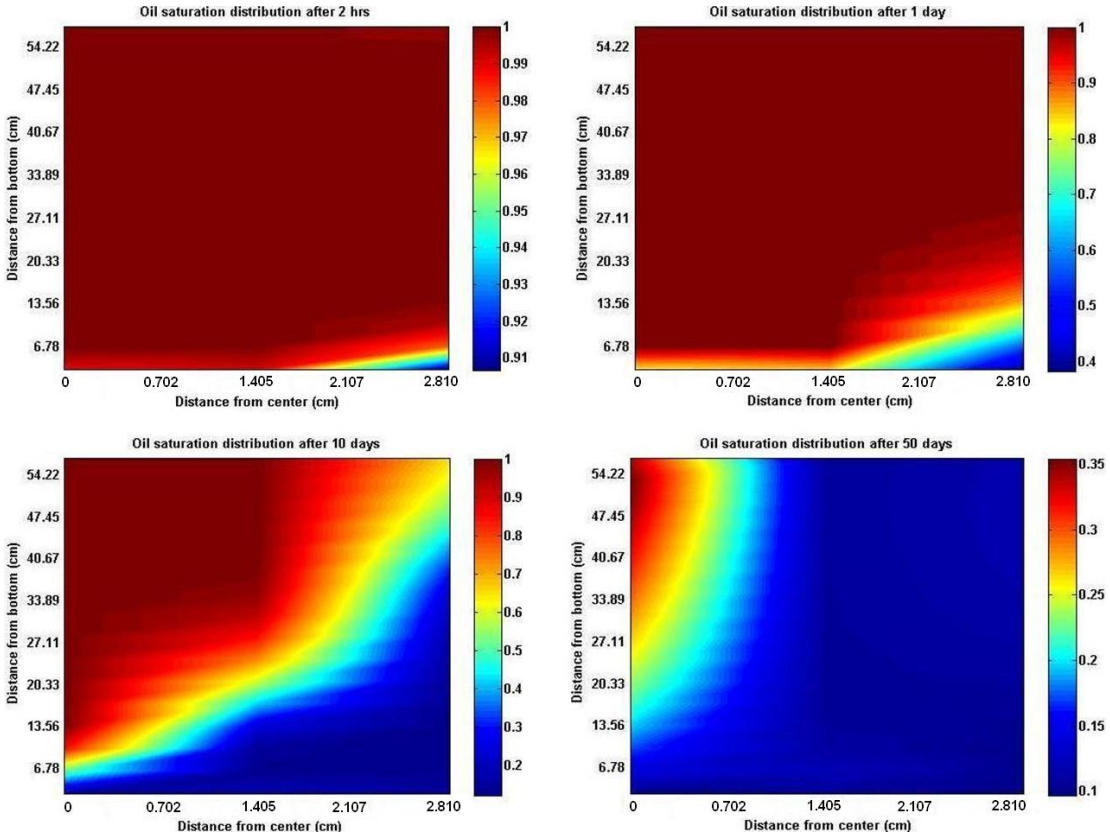

Figure 4-20: Longitudinal view of oil saturation distribution at different water imbibition times for half core when IFT=0.1 mN/m

Figure 4-21 demonstrates that the experimental data for the limestone core (K=15md) was satisfactorily modeled. As discussed, this shows as interfacial tension is reduced, the rate of imbibition slows in this core. The same behavior was also reported by Cuiec et al. (1994). In the case of high interfacial tension, the brine rapidly imbibed into the core, with completion of imbibition occurring after seven hours for 40% recovery (Figure 4-18).

In the low IFT system, the relative permeabilities of both phases are high (e.g.: $k_{rw}^{*} = 0.980$) due to co-current flow and segregated flow; which is in line with

experimental data presented by Bourbiaux and Kalaydjian (1990) who showed that co-current relative permeabilities are higher than counter-current values.

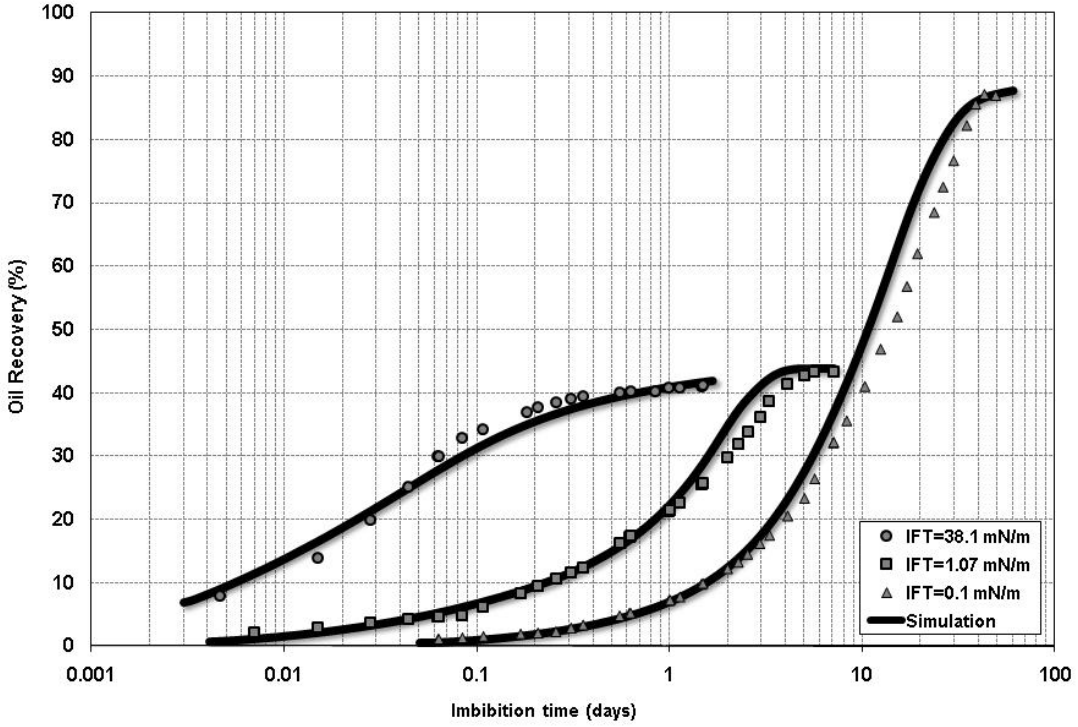

Figure 4-21: History matching the effects of IFT on recovery of the nonwetting phase during spontaneous imbibition into a 15md limestone core

In gravity driven co-current flow at low interfacial tension, total recoveries are high due to suppression of entrapment mechanisms. Two mechanisms are identified for entrapment of oil in water-wet system, i.e. a snap-off process where the wetting phase flows towards the pore throat and forms a collar that grows and breaks the non-wetting phase, and a bypass process caused by competition of flow between pores. At the microscopic level, the hydrostatic pressure due to gravitational forces would

supplement imbibition pressures and prevent snap-off and entrapment of a blob (Morrow and Songkran 1981). Therefore, a blob that would have been trapped in the capillary dominated case can continue to flow as the ratio of gravity to capillary forces is increased. In other words, in a system with low interfacial tension between oil and water, residual saturation of nonwetting phase may reduce according to Figure 2-8.

4.2.4 Case Study 4: The Effect of Boundary Conditions on Imbibition

System boundary conditions can affect the oil recovery from a matrix block. Fischer and Morrow (2005) studied oil recovery from cylindrical Berea sandstone cores at three different boundary conditions of AFO (all faces open), OEO (one end open), and TEC (two ends closed) through spontaneous imbibition at very strongly water-wet conditions for viscosity ratios of unity. They used combinations of mineral oils and aqueous solutions of glycerol to obtain matched viscosities. Oil production as a function of imbibition time was measured in standard glass imbibition cells at ambient temperature. Table 4-5 shows fluid and rock properties.

Table 4-5: General fluid and rock properties (Fischer and Morrow 2005)

Property	Value
Length (cm)	6.35
Diameter (cm)	3.8
Porosity (%)	16-18
Permeability (mD)	59-83
Oil Viscosity (cp)	3.9-173
Oil Density (lb/ft3)	48-55
Initial Water Saturation (%)	0
Residual Oil Saturation (%)	47.5

Also, Table 4-6 shows the specification of the three different tests which are chosen for the present study.

Table 4-6: Specifications of the tests (Fischer and Morrow 2005)

Test	$\mu_w\ (cp)$	$\mu_o\ (cp)$	μ_o/μ_w	$\sigma_{ow}\ (mN/m)$	$K\ (md)$	$\phi\ (\%)$
AFO, C1-24	13.6	13.6	1.00	36.8	59.7	17.4
TEC, C5-15	13.7	13.2	0.96	35.3	67.0	17.6
OEO, C1-24	14.3	14.0	0.98	36.2	58.7	15.9

Core boundary conditions are defined by the parts of the external surface of the core that are open to water imbibition, as illustrated in Figure 4-22 for this study.

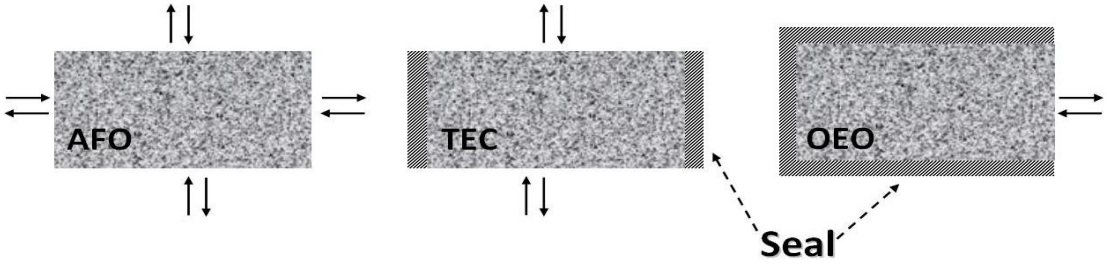

Figure 4-22: Boundary condition for the three tests

Table 4-7 contains properties used to define the properties of the rock grid blocks for the AFO test. In modeling the other tests, minor adjustments in the properties presented in this table were applied.

Table 4-7: Rock gridblock properties for the spontaneous imbibition simulation of AFO

Property	Value
Oil Relative Permeability Endpoint	0.85
Water Relative Permeability Endpoint	0.381
Oil Relative Permeability Exponent	1.3
Water Relative Permeability Exponent	1.5
Capillary Pressure Endpoint	0.097
Capillary Pressure Exponent	1.2

Table 4-8 shows a summary of some input data for simulation of their experimental data in the boundary condition of all sides open.

Table 4-8: Input parameters in the simulation of test AFO

Parameter	Value
Grid Block Sizes Δx, Δy, Δz (mm)	5.77, 4.2, 4.2
Number of Grid Blocks in X, Y, Z Direction	11, 8, 8
Time Interval (sec)	10
Number of Days Simulated (days)	30

Oil saturation distributions after half a day production due to the water imbibition are shown in Figure 4-23 for tests of AFO, TEC, and OEO. All distributions show that the process is counter-current.

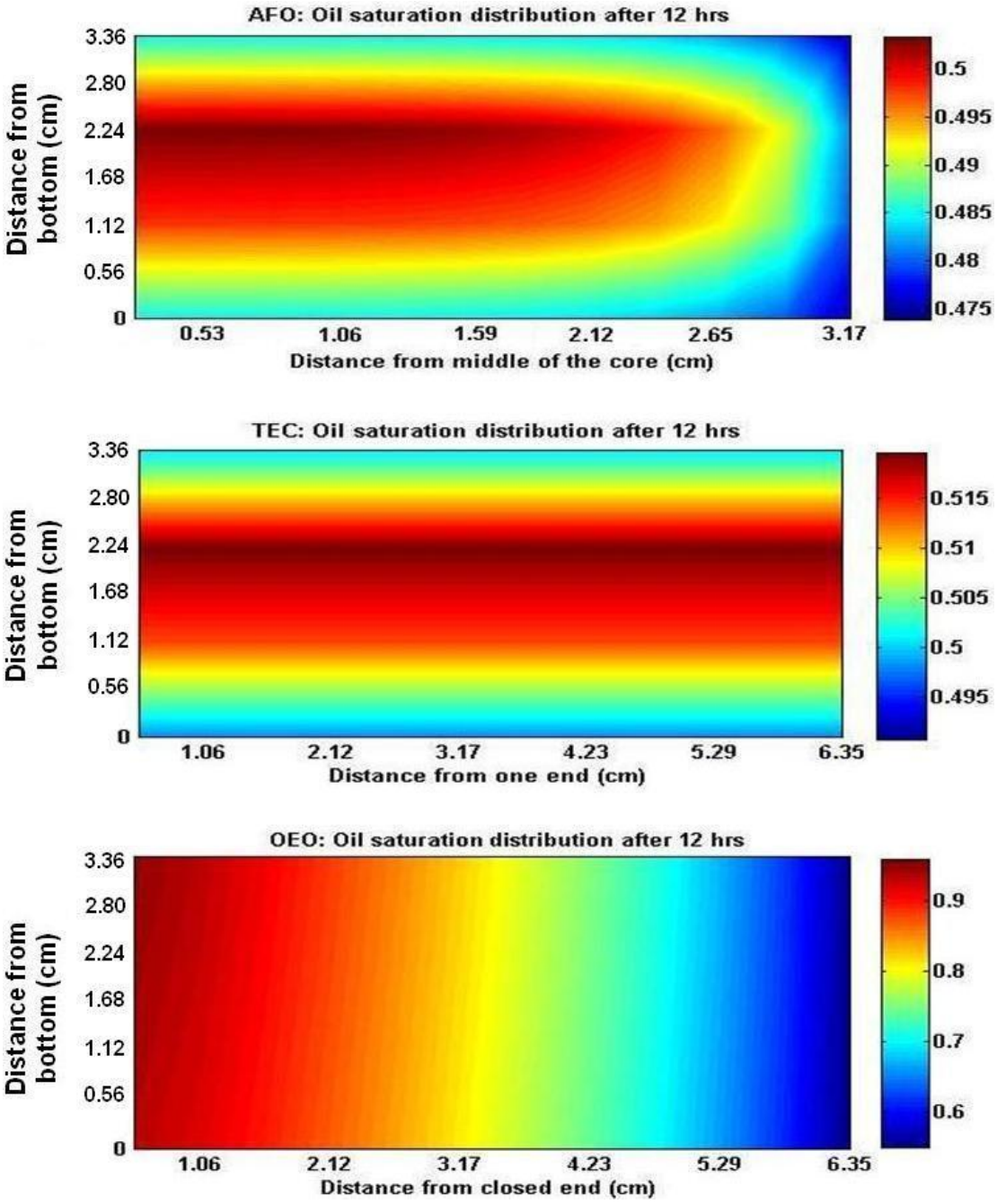

Figure 4-23: Oil saturation distribution after 12 hours of water imbibition for all three tests

Comparison of the imbibition curves for equal matched viscosity and the three different boundary conditions are displayed in Figure 4-24. The numerical results also

show an excellent agreement with experimental data, which proves the capability of the present simulator in modeling different boundary conditions.

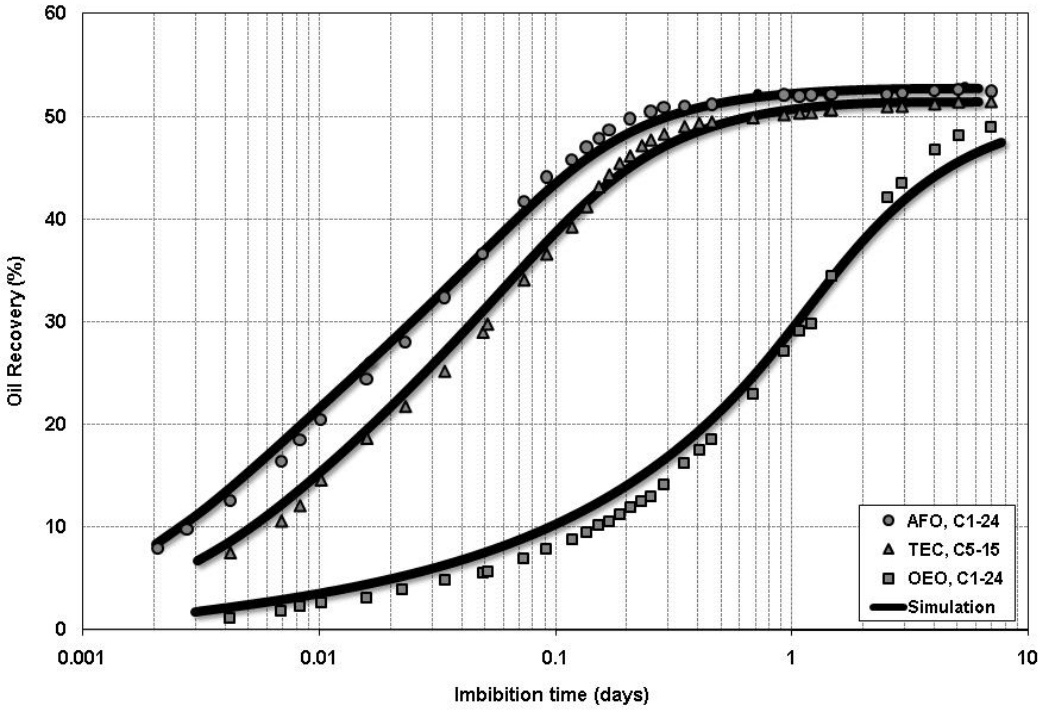

Figure 4-24: History matching the experimental imbibition data for different boundary conditions and matched viscosity

The numerical outcomes for different boundary conditions follow the expected systematic trend with the AFO boundary condition yielding the fastest imbibition, followed closely by the TEC boundary condition; imbibition for OEO is always more than an order of magnitude slower. From inspection of Figure 4-24, it is clear that the numerical imbibition outcomes obtained for OEO is distinctly more S-shaped than for other boundary conditions.

One of the interesting cases investigated by Fischer and Morrow (2005) was to study the effect of increasing oil viscosity, while maintaining the oil/water viscosity ratio as unity, on oil production. The simulation results were generated by changing the oil viscosity of AFO presented in Figure 4-24 to the values of 44.1, 80.1, and 173 cp. For each experiment, the fluid viscosities were matched to give viscosity ratios very close to unity. No other adjustments to simulation parameters were made. Satisfactory matches of experimental data to the simulation results were obtained for the entire viscosity range as shown in Figure 4-25.

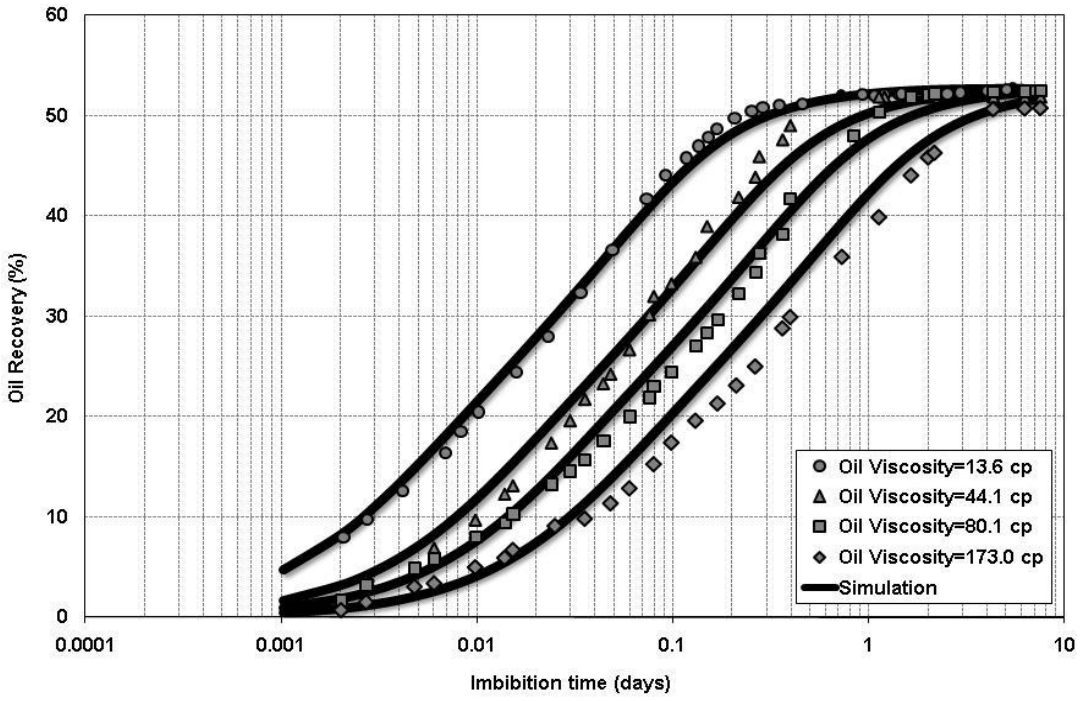

Figure 4-25: Oil recovery alterations by increasing the oil viscosity through spontaneous imbibition for AFO case

The results show that the oil production time increased systematically with increase in viscosity; however, the oil rate pattern or shape of the production curve remained the same.

4.3 Oil-wet Systems

Previously, spontaneous imbibition in water-wet systems was discussed. There were two driving forces contributed to oil displacement in water-wet systems: capillary forces and gravity forces. While capillary force mainly drives brine into rock media in most cases, the story is different when dealing with oil-wet rock systems. In oil-wet rocks the capillary pressure is negative which prevents spontaneous imbibition of brine. Imbibition may occur when gravity force causes water to be displaced into the core. For this to happen, the gravity head must be larger than the capillary force in the porous matrix.

Assume an uncoated oil-wet core saturated with oil and water is immersed in aqueous solution containing pure brine (or surfactant solution). Figure 4-26 shows oil and water (if any) pressure gradients in the core (matrix) and aqueous phase in a beaker (fracture) used in initializing the system when the core is completely immersed in aqueous phase. The force that drives aqueous phase into the core (matrix) is the difference between the aqueous phase pressure outside the matrix block and water pressure inside the matrix block. In the fracture, a fixed value of water pressure is specified at the core (matrix) top to initialize the system.

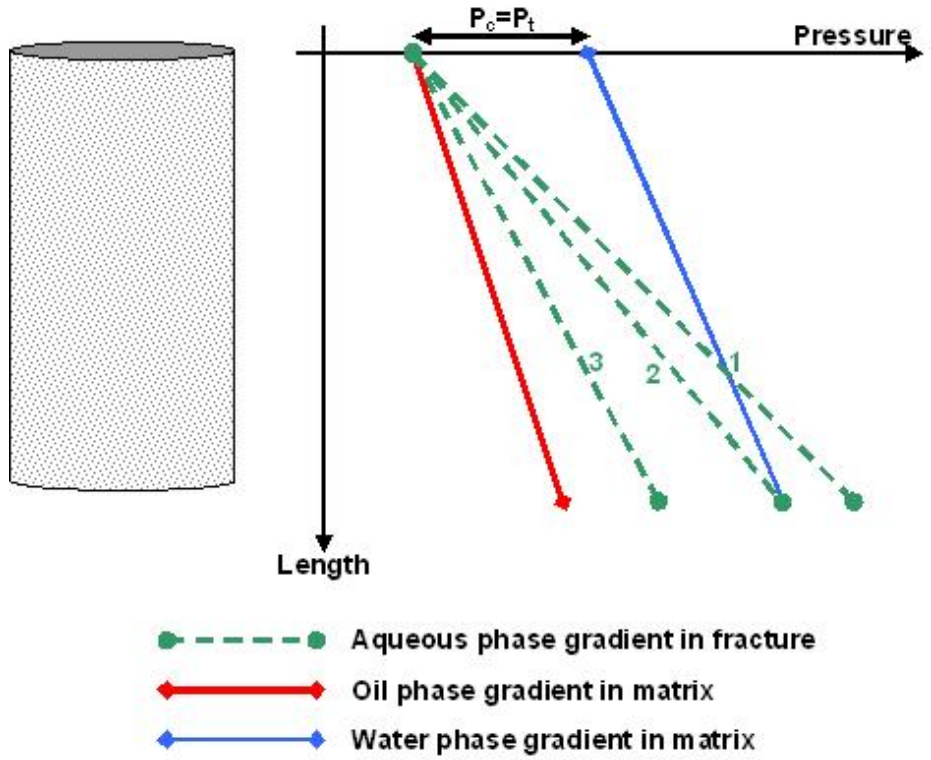

Figure 4-26: Schematic of oil-aqueous phases gravity/capillary force balance for an oil-wet core which has a uniform oil distribution at immobile water saturation

The pressure difference between aqueous phase in the fracture (beaker) and water phase (immobile water saturation) in the matrix is a driving force to push the aqueous phase inside the matrix. This is because of the unique approach used in defining the boundary conditions where the influx/ efflux of fluids take place. The aqueous phase can enter the core where the pressure difference can overcome the matrix's entry pressure. Three possible aqueous phase pressures in the fracture, depending on the core length and/or the initial capillary pressure of the core, are also shown in Figure 4-26. For example, for the cases of 2 and 3, the aqueous phase pressure cannot overcome the entry pressure and there would be no oil displacement while the

difference pressure would be the driving force from the depth that the aqueous phase gradient line (in fracture) crosses the water phase gradient line (in matrix) in the case of 1.

When surfactants are involved, however, the story is different. Surfactants are able to reduce the interfacial tension between oil and water, and may change the wettability of the core to less oil wet. If the surfactant reduces the interfacial tension, gravity force can act more efficiently and capillary pressure of an oil-wet rock will increase (become less negative). As surfactant concentration increases inside the core leading to interfacial tension reduction, the capillary pressure curve moves toward zero, even if wettability is not changed. Since capillary pressure is initially negative (and thus causes the oil to be held in the matrix), increasing the capillary pressure is advantageous to the release of oil. Therefore, gravity force can be the effective mechanism in the oil production.

In the case of wettability alteration, as the aqueous phase invades a core, surfactant enters the core and alters the core wettability, depending on the surfactant concentration, surfactant types and the core. Thus, the driving force is increased and gets stronger over time due to changing the wettability toward water-wet. This causes the oil production to increase.

Wettability alteration and interfacial tension reduction are the two most important mechanisms that can enhance oil production from oil-wet rock systems (especially in natural fractured systems). The following section will discuss this in detail.

4.3.1 Case Study 5: Effect of Interfacial Tension Values on Imbibition

If water imbibes spontaneously into an oil saturated core, the core is considered water-wet to some extent. Chen et al. (2001) evaluated the imbibition of water into oil-wet carbonate reservoir cores by using a CT scan technique. The cores in their study were obtained from a massive naturally fractured carbonate reservoir located at the southern tip of the Central Basin Platform in the Permian Basin of West Texas. Using the rock and fluid properties as presented in Table 4-9, what is presented here is a parametric study that demonstrates the effect of interfacial tension on oil production in oil-wet rock systems.

Table 4-9: Rock and fluid properties

Property	Value
Length (cm)	5.52
Diameter (cm)	3.83
Porosity (%)	15
Permeability (mD)	100
Oil Viscosity (cp)	12.8
Water Viscosity (cp)	1
Oil Density (lb/ft^3)	54.56
Water Density (lb/ft^3)	64.36
Initial Water Saturation (%)	30
Initial Interfacial Tension (mN/m)	50

Figure 4-27 shows a synthetic capillary pressure curve for the matrix. It is assumed that the capillary pressure is zero outside of the core. Figure 4-28 shows water (aqueous) and oil relative permeability curves.

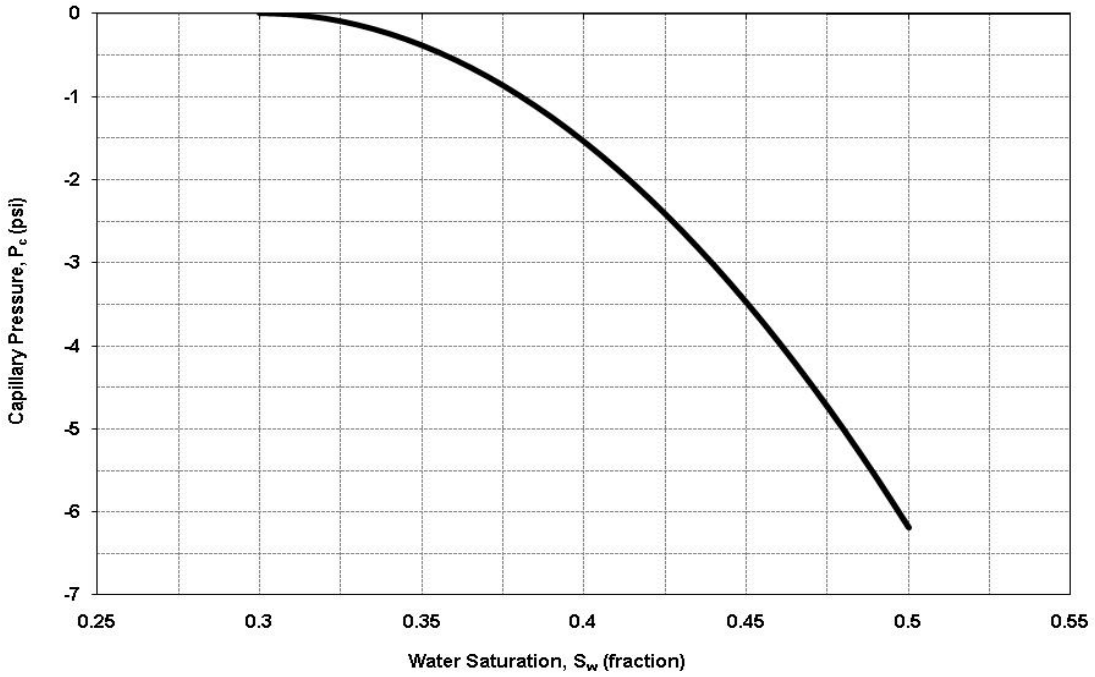

Figure 4-27: Capillary pressure-saturation relation

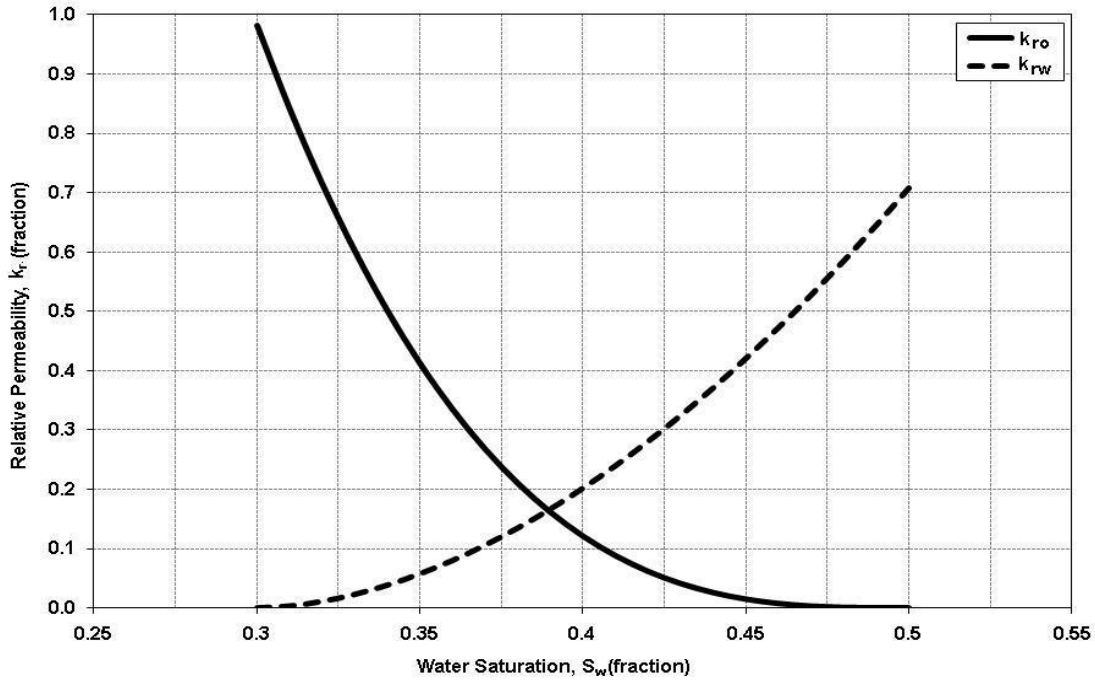

Figure 4-28: Relative permeability-saturation relations

Table 4-8 shows a summary of some input data for simulation of their experimental data when the boundary condition was all sides open.

Table 4-10: Input parameters in the simulation of case study 5

Parameter	Value
Grid Block Sizes Δx, Δy, Δz (mm)	3.4, 3.4, 6.9
Number of Grid Blocks in X, Y, Z Direction	10, 10, 8
Time Interval (sec)	10
Number of Days Simulated (days)	20

Figure 4-29 shows the oil production versus imbibition time when the oil saturated core was immersed in brine with the axis of the core positioned vertically. Water is able to displace less than one percent of the original oil in place of the core after 20 days. Calculations show that this much production is less than a drop (0.06 cm^3) which cannot be observed. This reveals that the characterizations assumed for the core, including capillary pressure curve and oil/water relative permeability curves, were correctly selected. Figure 4-30 shows that little change in oil saturation distribution ($S_{oi} = 70\%$) happened after one day of brine imbibition.

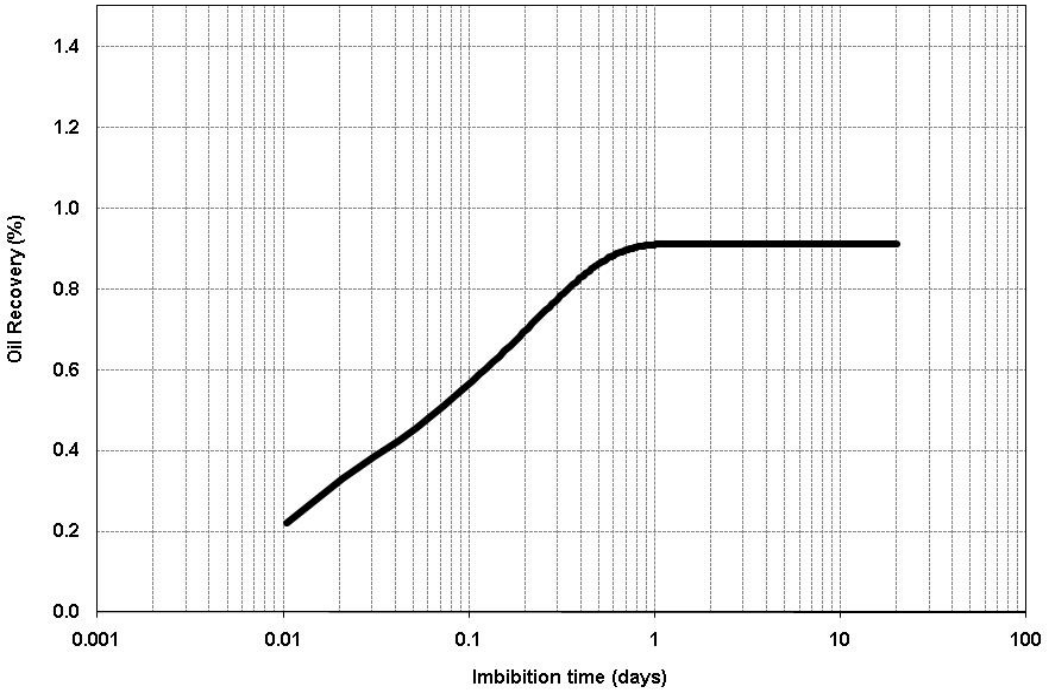

Figure 4-29: Oil production history using data of Table 4-9 and Figure 4-27 & Figure 4-28

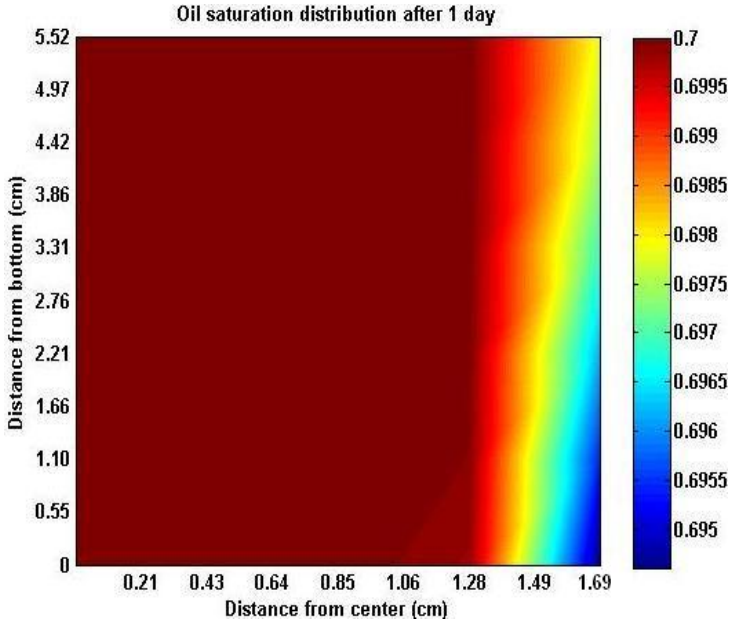

Figure 4-30: Oil saturation distribution in an assumed oil-wet core through pure water imbibition

Capillary forces exist because an interfacial tension is present at the interface between two immiscible fluids, which resists externally applied viscous forces and causes the injected and backed-up connate waters to bypass oil. If the IFT becomes zero, the capillary pressure becomes zero and the two fluids become miscible. The IFT reduction then affects the imbibition and oil mobilization in two ways. A reduction in the IFT can shift the capillary pressure to values close to zero depending on the magnitude of the IFT reduction. Another effect of IFT reduction is oil mobilization. By reducing the residual oil saturation, more oil is allowed to be mobilized and can result in higher oil recovery.

The effect of various interfacial tensions on oil production from oil-wet cores can be investigated by generating capillary pressure curves using Equation 3.8 which describes a strong relationship between capillary pressure and interfacial tension. In oil-wet rocks, capillary pressure is negative, holding the oil in the porous media. By reducing interfacial tension, capillary pressure can be increased to zero in some cases.

Figure 4-31 shows four capillary pressure curves corresponding to different values of interfacial tension. The capillary pressure curve for the highest value of interfacial tension (50 mN/m) is the same as presented in Figure 4-27. These curves are generated using Equation 3.8.

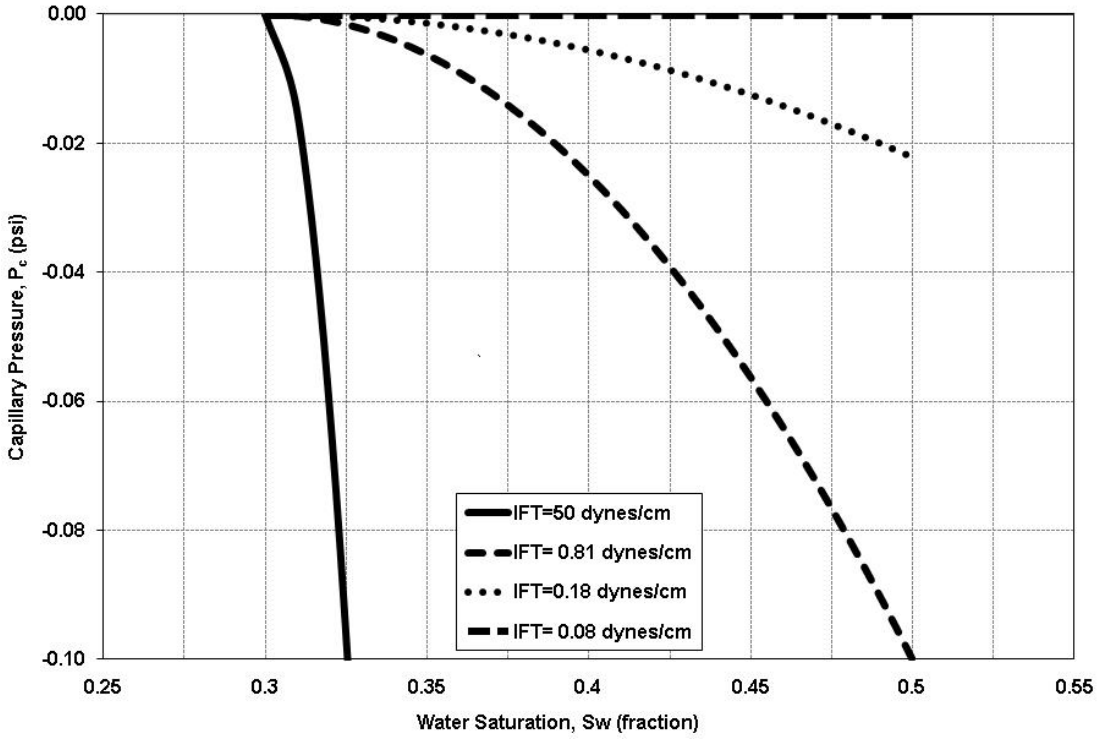

Figure 4-31: Different capillary pressure curves generated with different interfacial tension

According to this figure, if interfacial tension between oil and water in the porous media can be reduced to low values such as: 0.81, 0.18, and 0.08 dynes/cm, the strength of the capillary force to hold the oil in pores will reduce. Gravity force may be able to overcome the capillary force and help expel the oil from a porous medium.

This finding should be very beneficial to the study of the influence of capillary pressure curves on oil production. Figure 4-32 shows oil production based on use of the different capillary pressure curves exhibited in Figure 4-31 (four different simulation runs). Rock and fluid properties are the same as listed at Table 4-9. Each capillary pressure curve represents a specific oil/water interfacial tension value.

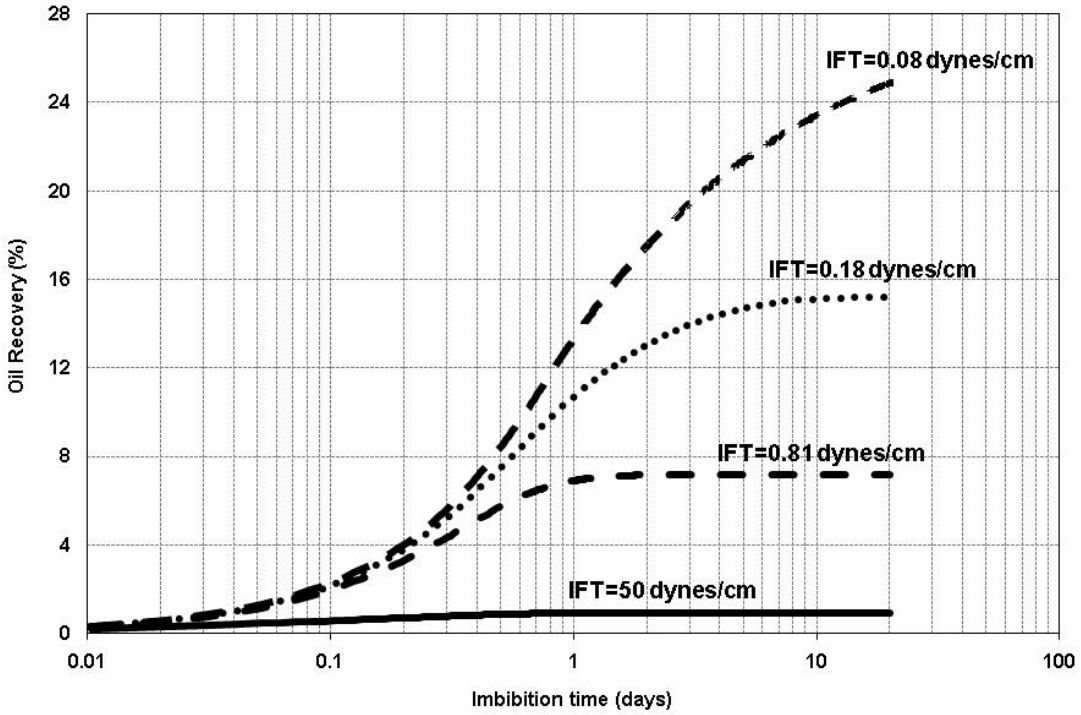

Figure 4-32: Oil production at different capillary pressure curves shown in Figure 4-31

In this test, there is no interfacial tension reduction involved throughout each runs (this case will be discussed in the next study). It means that interfacial tension between oil and water is same throughout the core and throughout the imbibition time at each runs. This means that the oil-wet core is vertically placed in a beaker of pure water and there is no surfactant in the system (core and beaker). Practically, this can happen by changing the fluid properties to reach a certain IFT value and then characterizing the core with this fluid, as Schecter *et al*. (1994) performed in their experiments.

Hypothetically, one can interpret it such that if the interfacial tension between oil and water in the entire core (not just the boundaries) can be lowered by using

surfactant to those values, the ultimate recoveries shown in Figure 4-32 can be reached. Oil saturation distributions after a full day of water imbibition for tests corresponding to the different IFT values are shown in Figure 4-33.

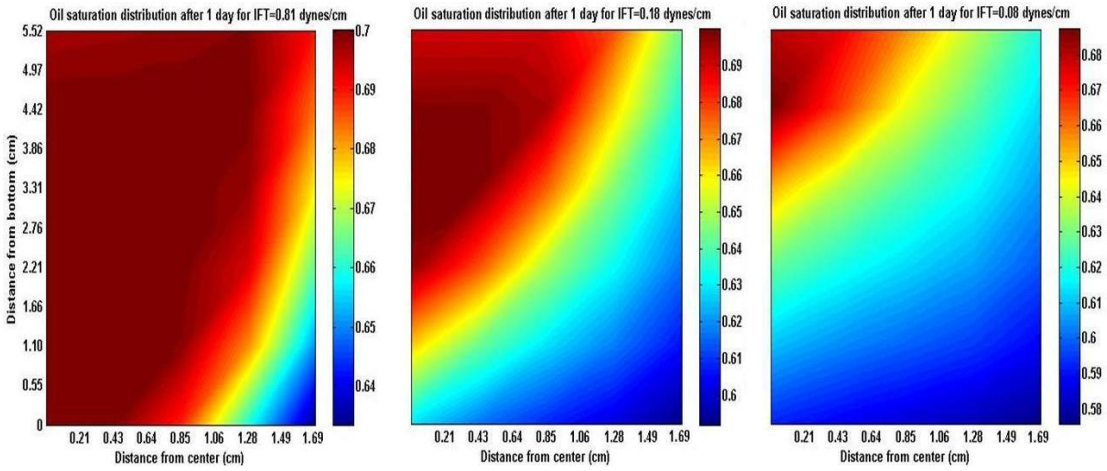

Figure 4-33: Longitudinal view of oil saturation distributions for half core at three different capillary pressures presented in Figure 4-31

4.3.2 Case Study 6: Effect of Interfacial Tension Reduction on Imbibition

In case study 5, the effect of various interfacial tensions on the oil recovery from oil-wet cores was illustrated. The interfacial tension was assumed to be uniform throughout the core and throughout the imbibition time. It is also noteworthy to study the effect of interfacial tension reduction, due to the presence of surfactant in the aqueous solution surrounding the core, on oil production in oil-wet cores.

Oil-wet fractured porous media usually demonstrate poor waterflooding performance because the injected water flows in the fractures, making spontaneous imbibition into the matrix nearly insignificant. Using surfactants in the injected water is one possible method to increase the oil recovery via mechanisms of interfacial tension reduction and wettability alteration. In this case study, attention is paid to the interfacial tension reduction and it is assumed that surfactants are not able to change the rock wettability.

Interfacial tension between oil and water in the core will be lowered as surfactant solution invades the core. The current case study is the first place that the three equations of water, oil, and surfactant are solved together (Equations 3.1, 3.2 and 3.3).

It is assumed that the core is vertically immersed in a beaker of surfactant solution with surfactant concentration of 1% (with critical micelle concentration of 800 ppm). This amount of the surfactant can reduce the interfacial tension between oil and water to a low value of 0.016 dynes/cm in the current system. The surfactant is considered to be able to lower only the interfacial tension between oil and water (no

wettability alteration is involved). The assumption made here is that relative permeability of water and oil do not change much with variation in IFT, which is not entirely true. At ultra low IFT ($IFT < 1 \times 10^{-3}\, dynes/cm$), the relative permeability of both phases become linear and enhance the rate of recovery (Hirasaki *et al.* 2005). However, in the range of IFT's considered in this study, interfacial tension variation does not lead to large alteration in phase relative permeabilities.

Petrophysical properties are presented in Table 4-9, Figure 4-27 and Figure 4-28. Figure 4-34 exhibits the oil production history in the process of surfactant solution imbibition.

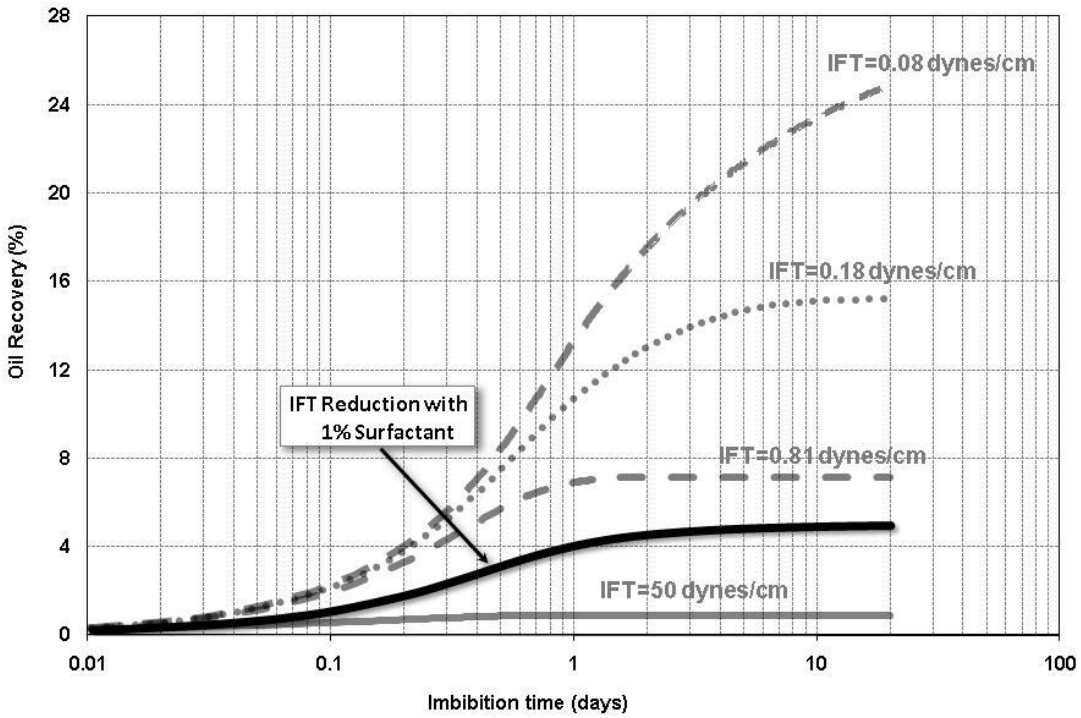

Figure 4-34: Oil recovery due to the interfacial tension reduction using surfactant

As expected, a decrease in interfacial tension leads to increase in the rates of recovery, because decreasing the IFT shifts the capillary pressure for oil-wet cores from negative values to zero and thus enhances the driving force for oil recovery. Figure 4-35 shows the oil saturation distribution after a full day of surfactant solution imbibition. As shown in this figure, aqueous phase enters from the side and oil is produced from the top of the core. After a day of oil production, there were no changes in oil saturation distribution, explaining reaching a plateau in the production history graph (Figure 4-34).

Surfactant is distributed throughout the core, reducing the original interfacial tension between oil and water. Both surfactant concentration and interfacial tension distribution are displayed for various times of surfactant solution imbibition in Figure 4-36 and Figure 4-37, respectively.

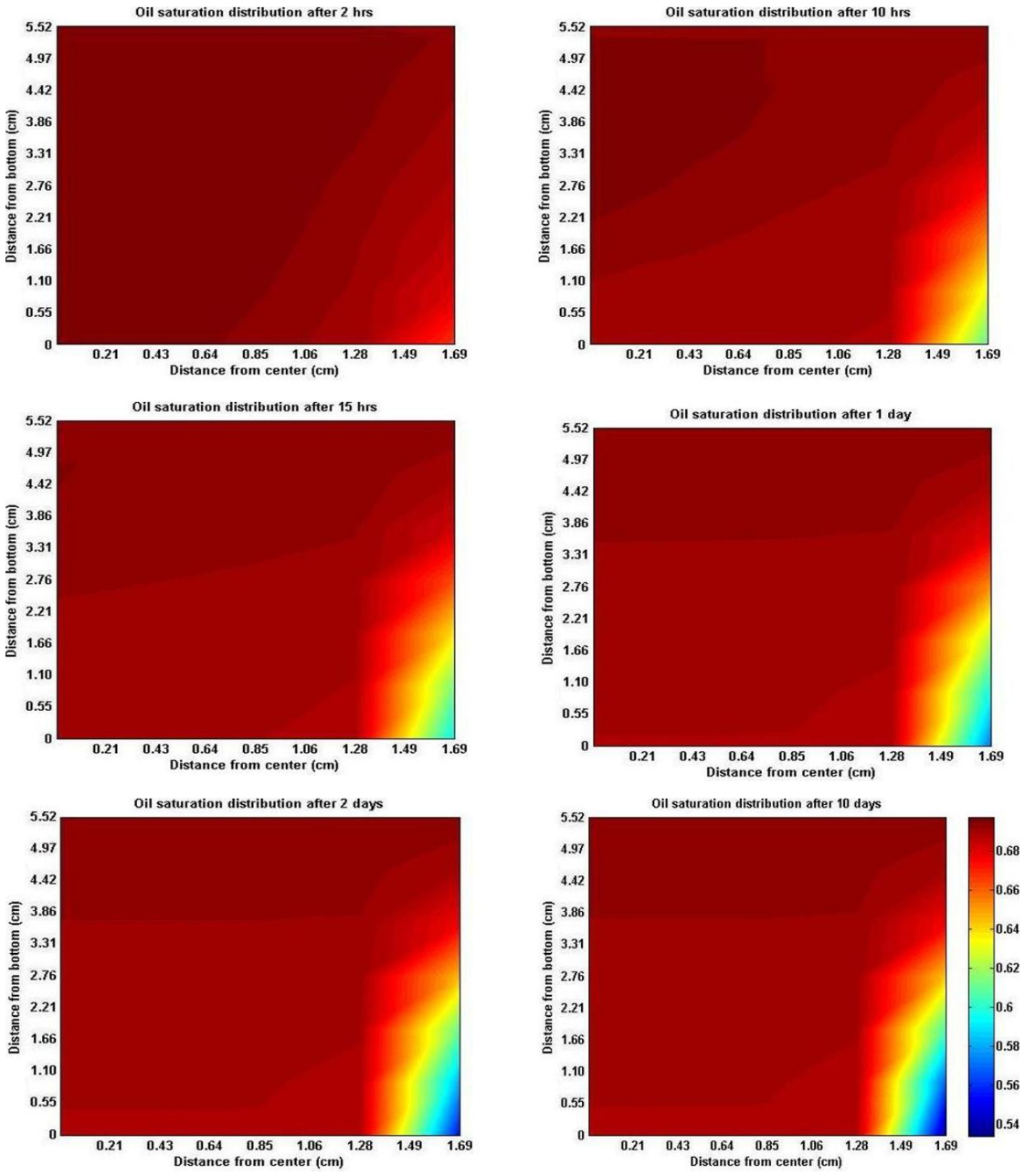

Figure 4-35: Longitudinal view of oil saturation distributions for half core in interfacial tension reduction test through surfactant solution imbibition

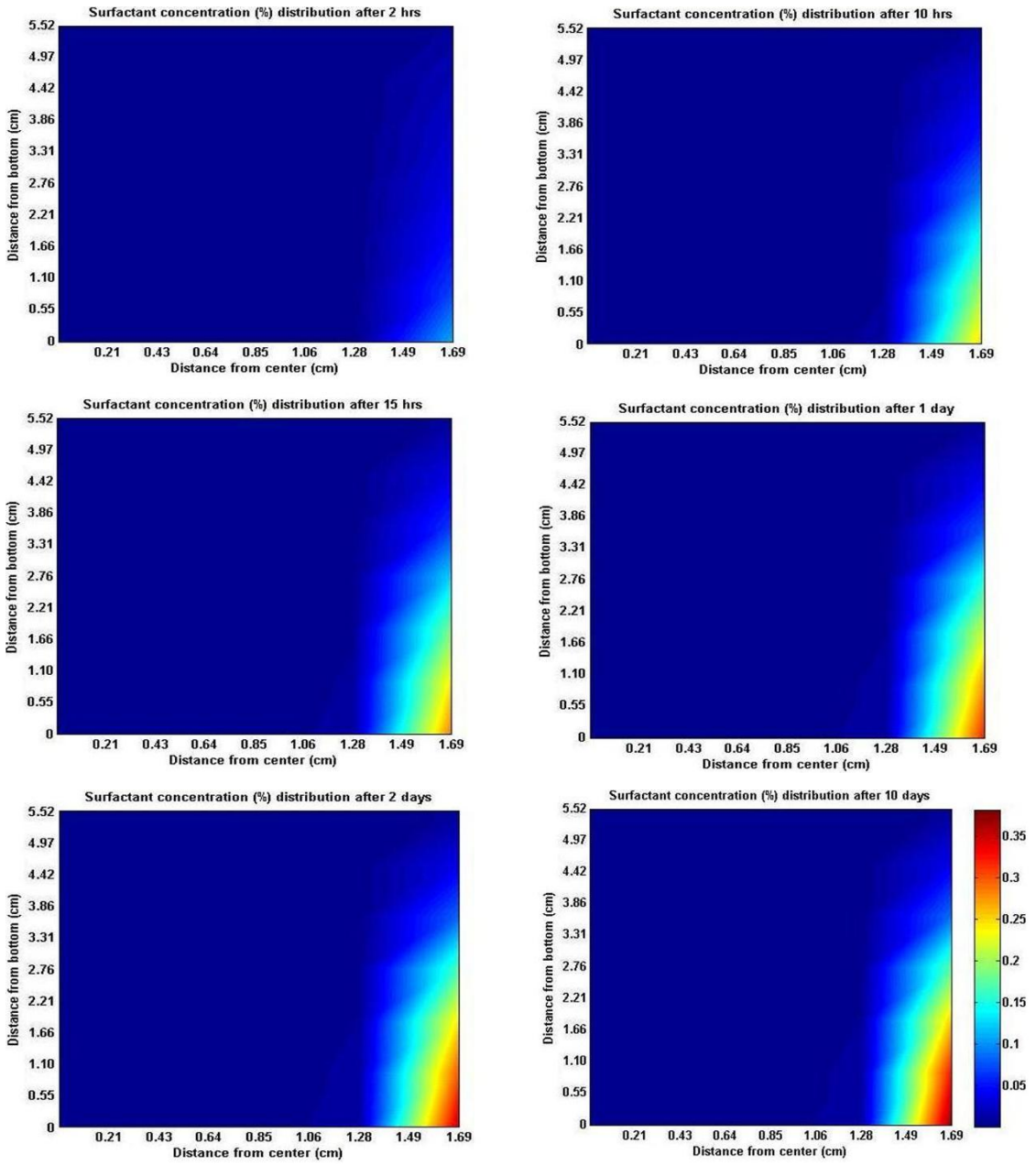

Figure 4-36: Longitudinal view of surfactant concentration distributions in aqueous phase for half core at various times in case study 6

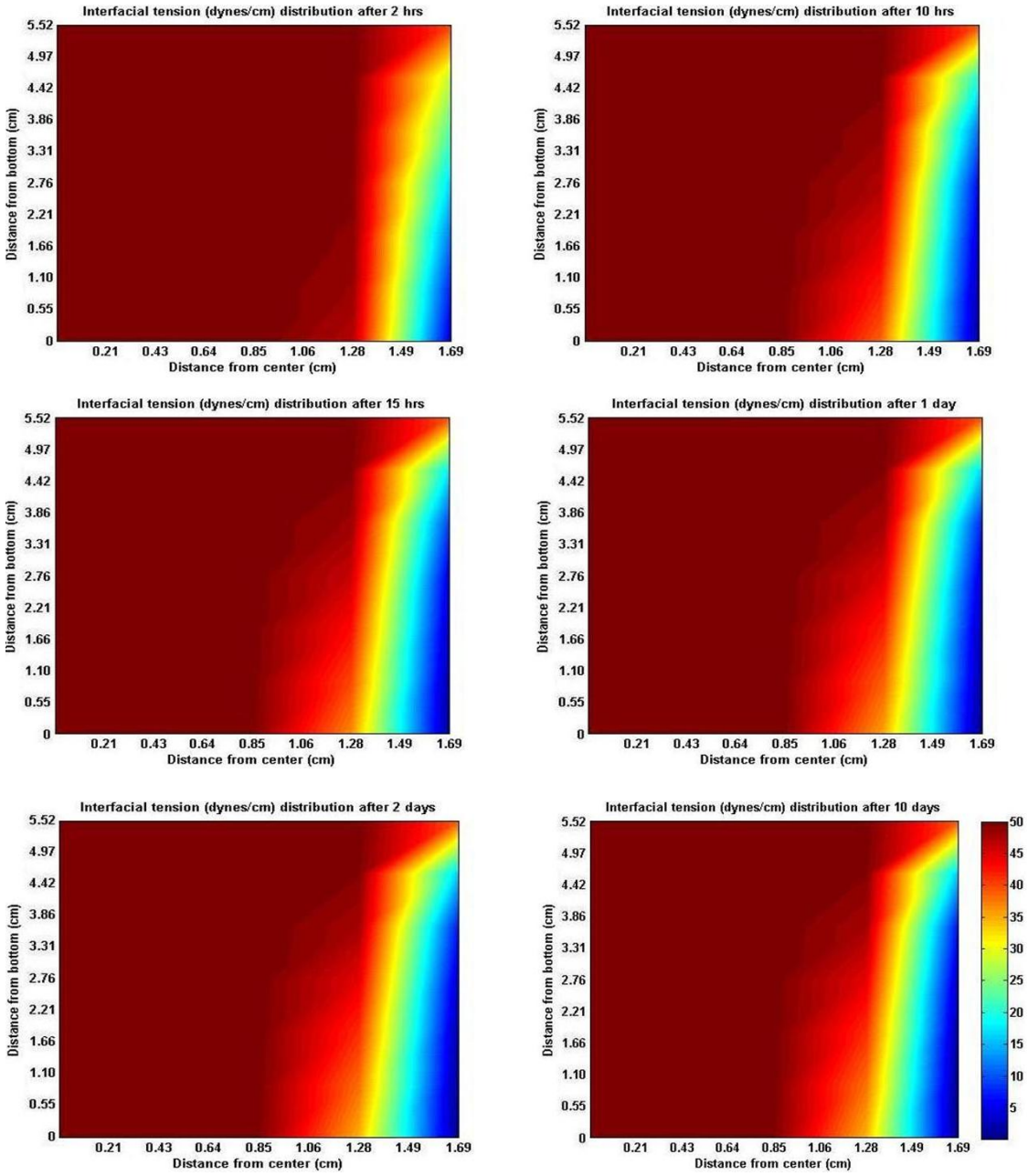

Figure 4-37: Longitudinal view of interfacial tension reduction for half core

A comparison between Figure 4-30 and the fourth snap shot of Figure 4-35 (a day after imbibition) shows how effective interfacial tension reduction can be in oil recovery from oil-wet cores.

In addition, Figure 4-38 shows a comparison between two different tests. The left snap-shots reveal capillary pressure distribution at various times when imbibition of the surfactant solution occurs. Capillary pressure distribution at the same times as left snap-shots for the situation where pure brine was used as the aqueous solution to be imbibed into the core is presented as right snap-shots.

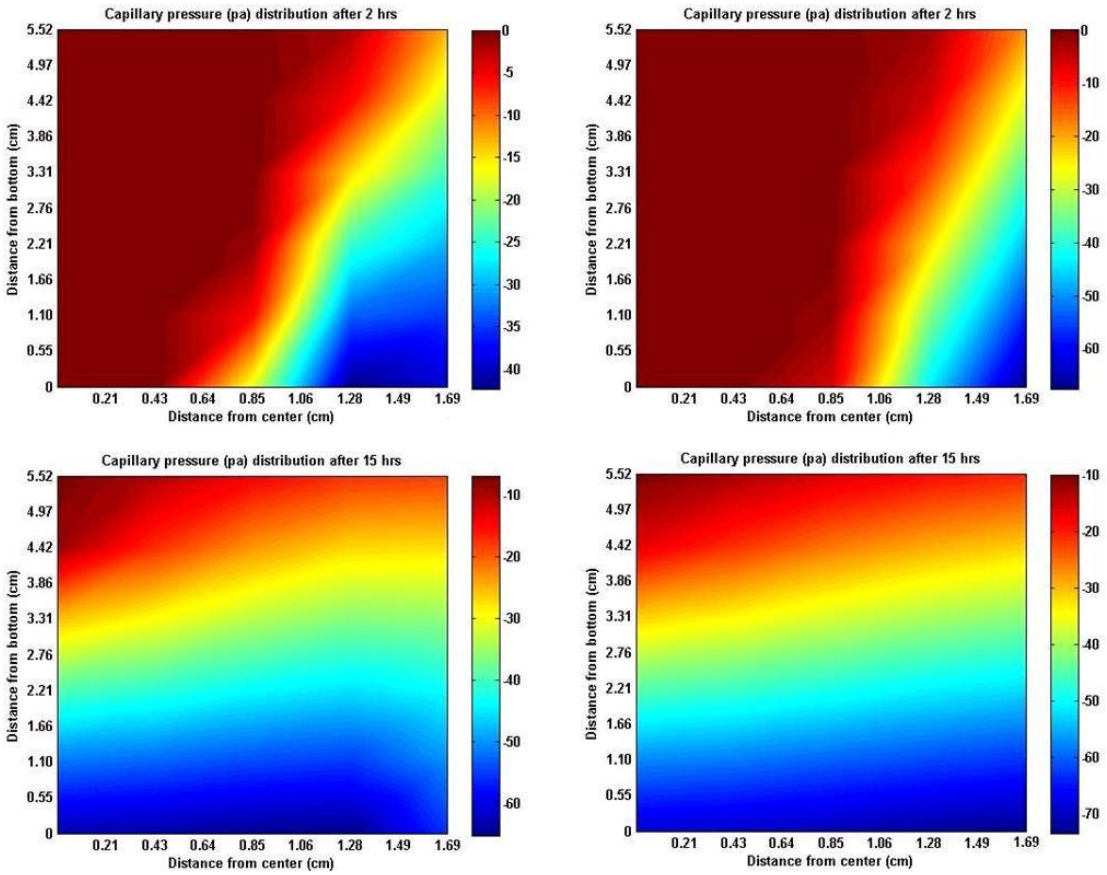

Figure 4-38: Capillary pressure distribution for half core: left) with interfacial tension reduction right) without interfacial tension reduction (no surfactant)

4.3.3 Case Study 7: Effect of Wettability Alteration on Imbibition: Standnes and Austad (2000b): Test 33

As discussed in Chapter 2, oil-wet fractured porous media usually demonstrate poor waterflooding performance because the injected water flows in the fractures, making spontaneous imbibition into the matrix nearly insignificant. Surfactants have potential to be used for increasing the oil recovery by increasing the imbibition of water into a matrix rock. The mechanisms for oil recovery are combined effects of reduced interfacial tension, reduced mobility ratio, and wettability alteration.

Austad and his colleagues (1997; 2000b; 2002; 2003; 2005b; 2007) conducted many imbibition experiments in low-permeable chalk material (2-7 md) saturated with oil, both with and without surfactant presence in the aqueous solution. The Ekofisk oil from the Norwegian sector of the North Sea was mixed with *n*-heptane to get a volume ratio of 67/33 and used as the oil for experiments. The cores were aged in a closed container filled with oil for 30 days at 90°C. The volume ratio between the core and the oil was about 2 during the aging process. The outermost layer (2-3 mm) of the core was removed by shaving off the core in a lathe before the imbibition test. They characterized some cores with and others without initial water saturation to investigate the effect of initial water saturation on wettability alteration.

Tests 33 and 34 were chosen to be numerically modeled in this study. These two tests look nearly identical, with the exception that no surfactant was used in test 34 and brine was the only fluid in the imbibition cell. The reason for modeling this test is to find the capillary pressure and the relative permeability curves to use in test 33

(alteration in wettability and interfacial tension). Rock and fluid properties of this test are presented in Table 4-11. Table 4-12 shows a summary of some input data for simulation of test 33.

Table 4-11: Fluids and rock properties of test 34 (Standnes and Austad 2000b)

Property	Value
Length (cm)	6.22
Diameter (cm)	3.84
Porosity (%)	45.2
Permeability (md)	6
Oil Viscosity (cp)	2.6
Water Viscosity (cp)	0.8
Oil Density (lb/ft^3)	50.94
Water Density (lb/ft^3)	64.36
Initial Water Saturation (%)	23.5
Interfacial Tension (dynes/cm)	15.4

Table 4-12: Input parameters in the simulation of case study 5

Parameter	Value
Grid Block Sizes Δx, Δy, Δz (mm)	3.4, 3.4, 6.2
Number of Grid Blocks in X, Y, Z Direction	10, 10, 10
Time Interval (sec)	10
Number of Days Simulated (days)	7

They observed that contrary to the 100% oil saturated cores (which will be discussed in the next study), the core containing initial water saturation spontaneously imbibed a small amount of brine, i.e. about 11% of initial oil was displaced. Therefore, the core appeared to be mixed-wet (or slightly water-wet) in the presence of brine.

Based on the above conclusion and also another publication of theirs (Høgnesen *et al.* 2006b), Figure 4-39 and Figure 4-40 were chosen for modeling test 33 (similar to Figure 3-5 and Figure 3-7). A small picture of the positive part in the capillary pressure is displayed in Figure 4-39.

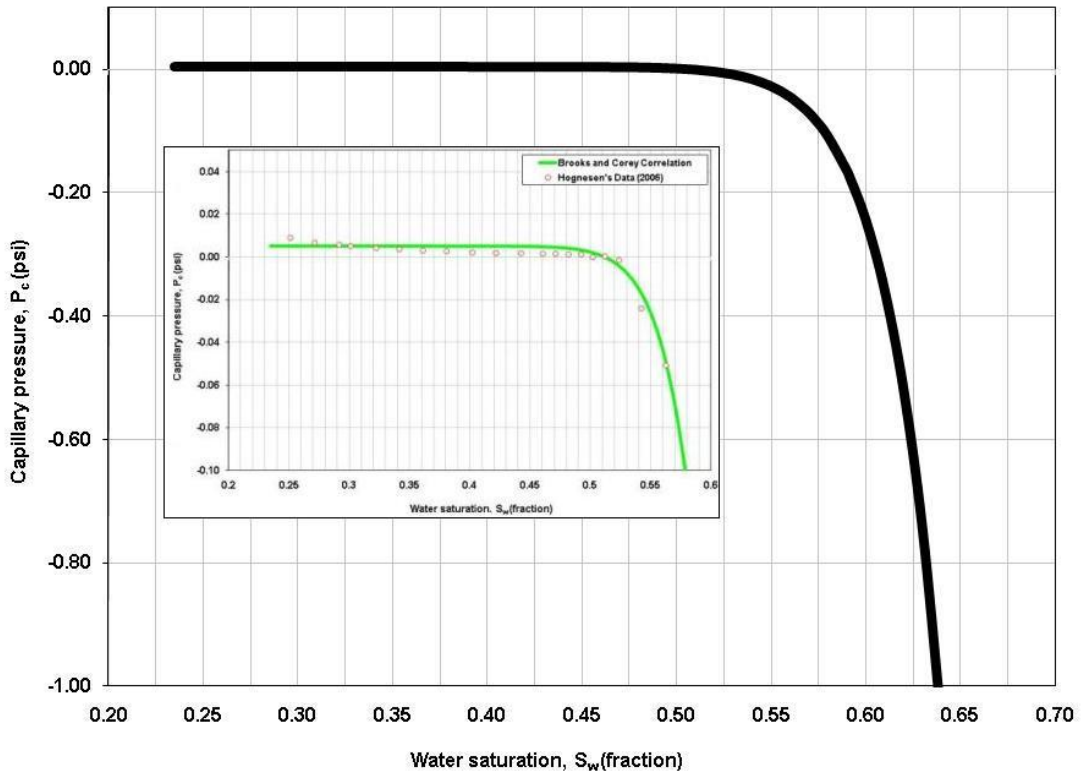

Figure 4-39: Capillary pressure-saturation relation

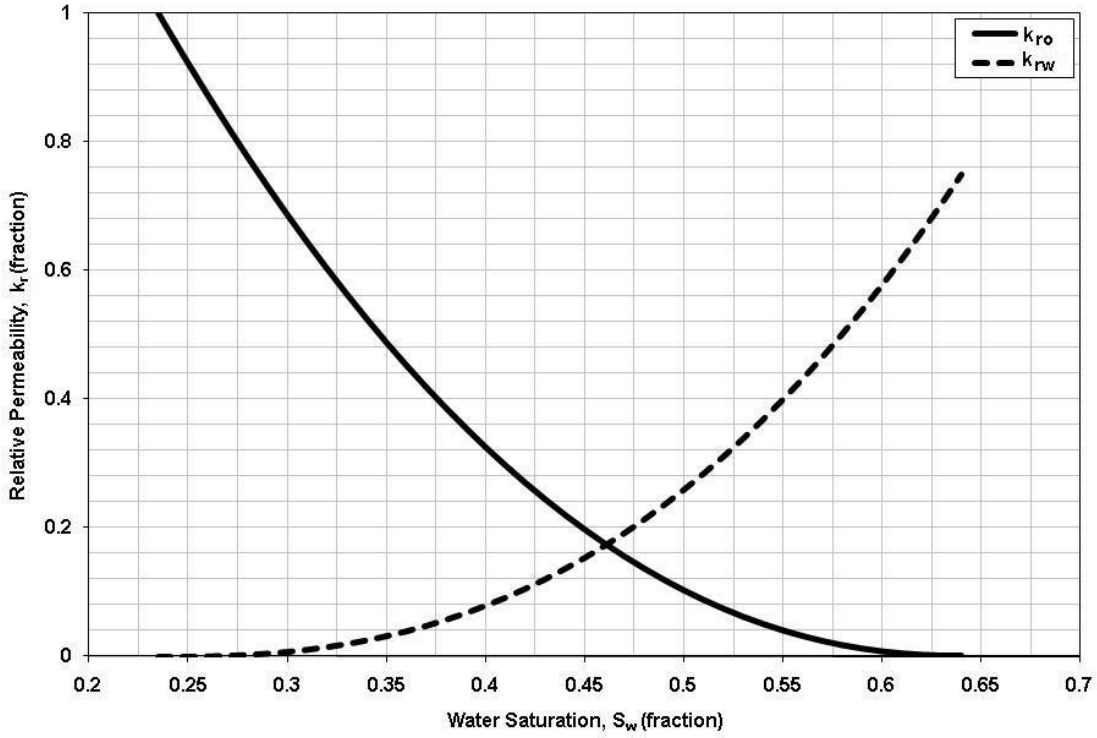

Figure 4-40: Relative permeability-saturation relations

The result of the experimental data along with outcome of the simulation is shown in Figure 4-41. A very close match of the experimental data was obtained by this simulation and gave promising results to use in the simulation of wettability alteration tests; i.e. test 33. This figure shows that the oil production reached a plateau after six days of the brine imbibition.

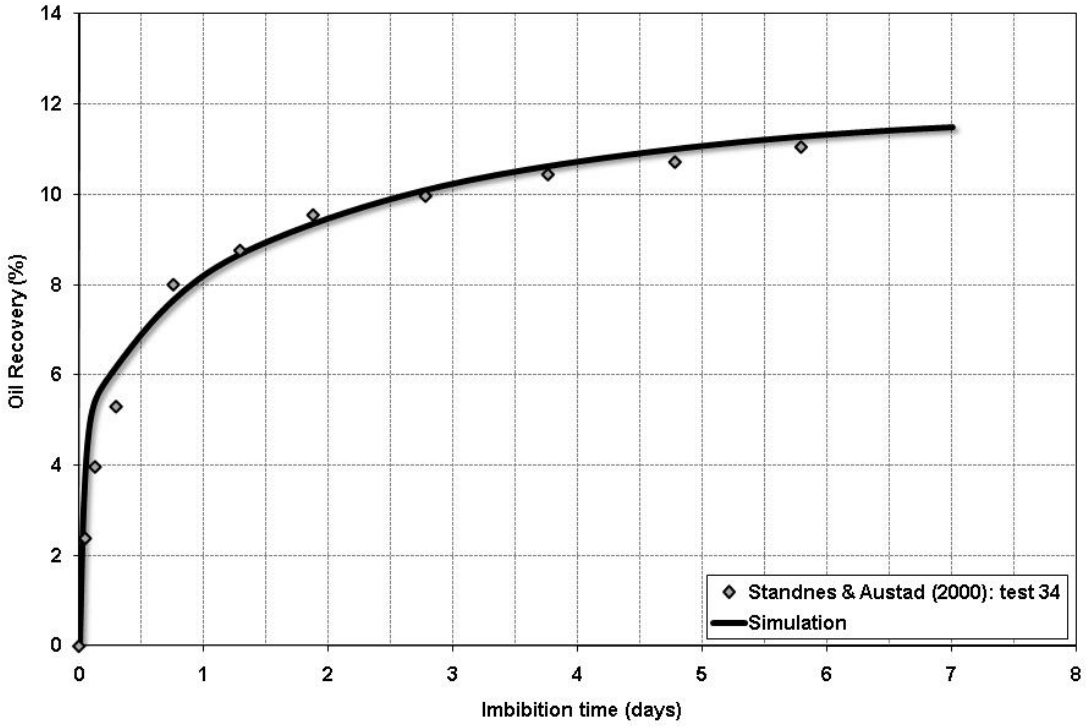

Figure 4-41: Oil production history matching with the test 34 of Standnes and Austad (2000b)

In the next stage, a 1 wt% cationic C_{12}TAB (dodecyltrimethylammonium bromide) surfactant solution was used in test 33 instead of pure water. For this test, rock and fluid properties are the same as those presented in Table 4-11, with the exception of length, porosity, and initial water saturation; which are 5.52 cm, 44.1%, and 26.9%, respectively.

The phase behavior studies showed that no middle phase was observed (Austad *et al.* 1998); therefore an assumption that two phases existed, oil and aqueous phase, is a valid assumption. Since surfactant is added to the system, it is necessary to define other parameters to model this test. For instance, parameters applied in interfacial tension reduction and the wettability alteration models are listed in Table 4-13.

Table 4-13: Parameters used in modeling the test 33

Parameter	Value
ε in Chun Huh Equation	0.9
η in Chun Huh Equation	0.22
Initial Contact Angle	70°
Final Contact Angle	12°
d in the Wettability Alteration Model	-2

The results from wettability alteration modeling of the experimental test 33 of Standnes and Austad (2000b) are presented in Figure 4-42, showing that the simulation of oil production rate is a very good match to the experimental data. This supports the validity of the wettability alteration model.

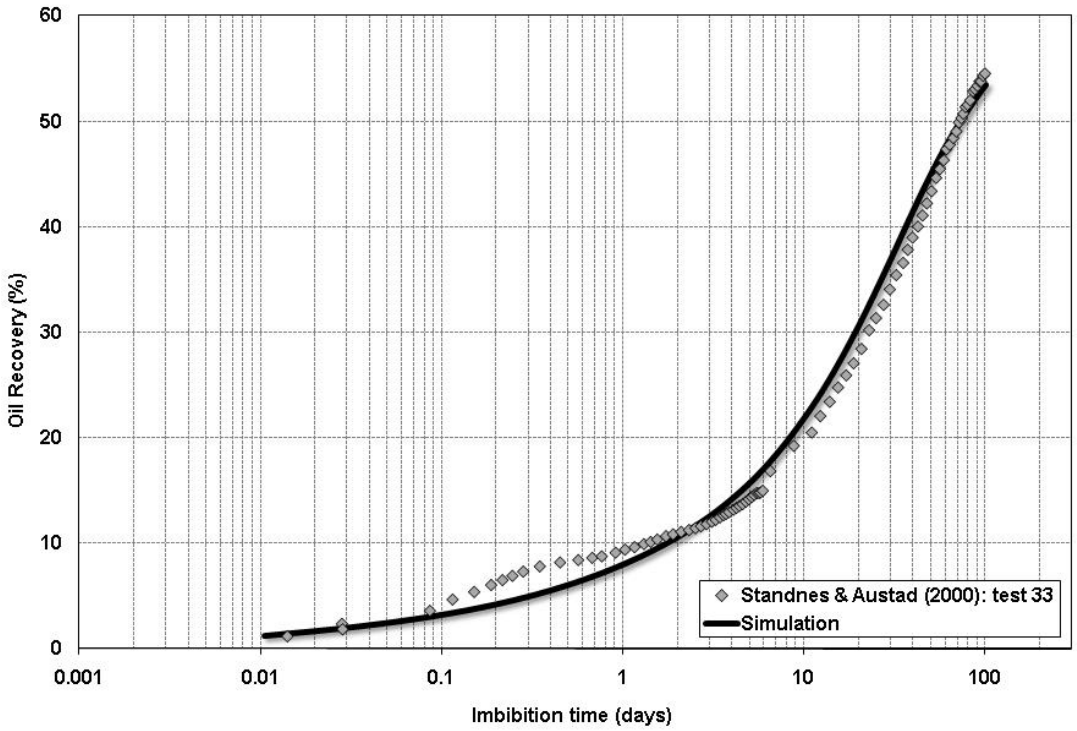

Figure 4-42: Simulation result of experimental data (Standnes and Austad 2000b: test 33) by using the proposed wettability alteration model

By comparing the oil saturation distributions between tests 33 and 34, it can be concluded that wettability alteration and interfacial tension reduction are effective in increasing oil production from oil-wet cores, as shown in Figure 4-43 (The distance from center of the core is the X-axis and the distance from bottom of the core is the Y-axis). The water saturation at top of the core in test 33 is higher than that in test 34 after 4 days of imbibition process. Water entered the core mostly from the lateral side and oil was mainly produced from top of the core in test 34; however, water was able to enter the core from top as well as lateral side in test 33. This shows that the counter-current flow drives the process in test 33, which explains the effectiveness of wettability alteration in this test.

At the beginning of the imbibition, interfacial tension reduction occurs, lowering the capillary pressure toward zero so that gravity force becomes dominant. As time lapses, however, wettability alteration happens and produces more oil from the core as shown in the last snap-shot of Figure 4-43. This clearly shows that oil was produced from both top and lateral side of the core.

For instance, after producing 10% of original oil in place (OOIP) in both test 33 and 34, calculations show that 50.1% of the produced oil was recovered from top of the core in test 34 and 49.9% was produced from the side. In test 33, the corresponding amount of oil produced from the top was 26.7% while 73.3% was recovered from the side. Total oil recovery is approximately 55% in test 33 and is around 11.5% in test 34. Therefore, wettability alteration was an effective mechanism in test 33 and counter-current fluid flow became more effective in this test.

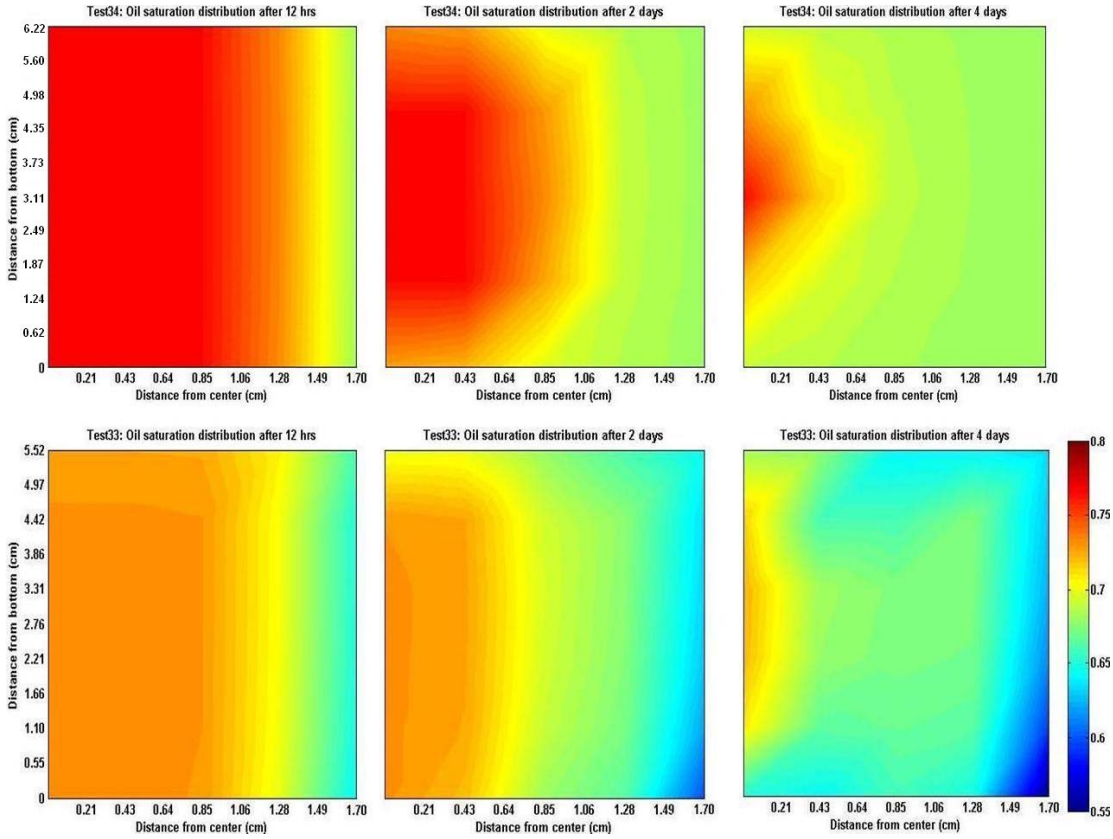

Figure 4-43: Oil saturation distribution comparison between tests 33 and 34 at various times

Capillary pressure distribution and surfactant concentration distribution for various times of surfactant solution imbibition in test 33 are shown in Figure 4-44. The distance from center of the core is the X-axis and the distance from bottom of the core is the Y-axis.

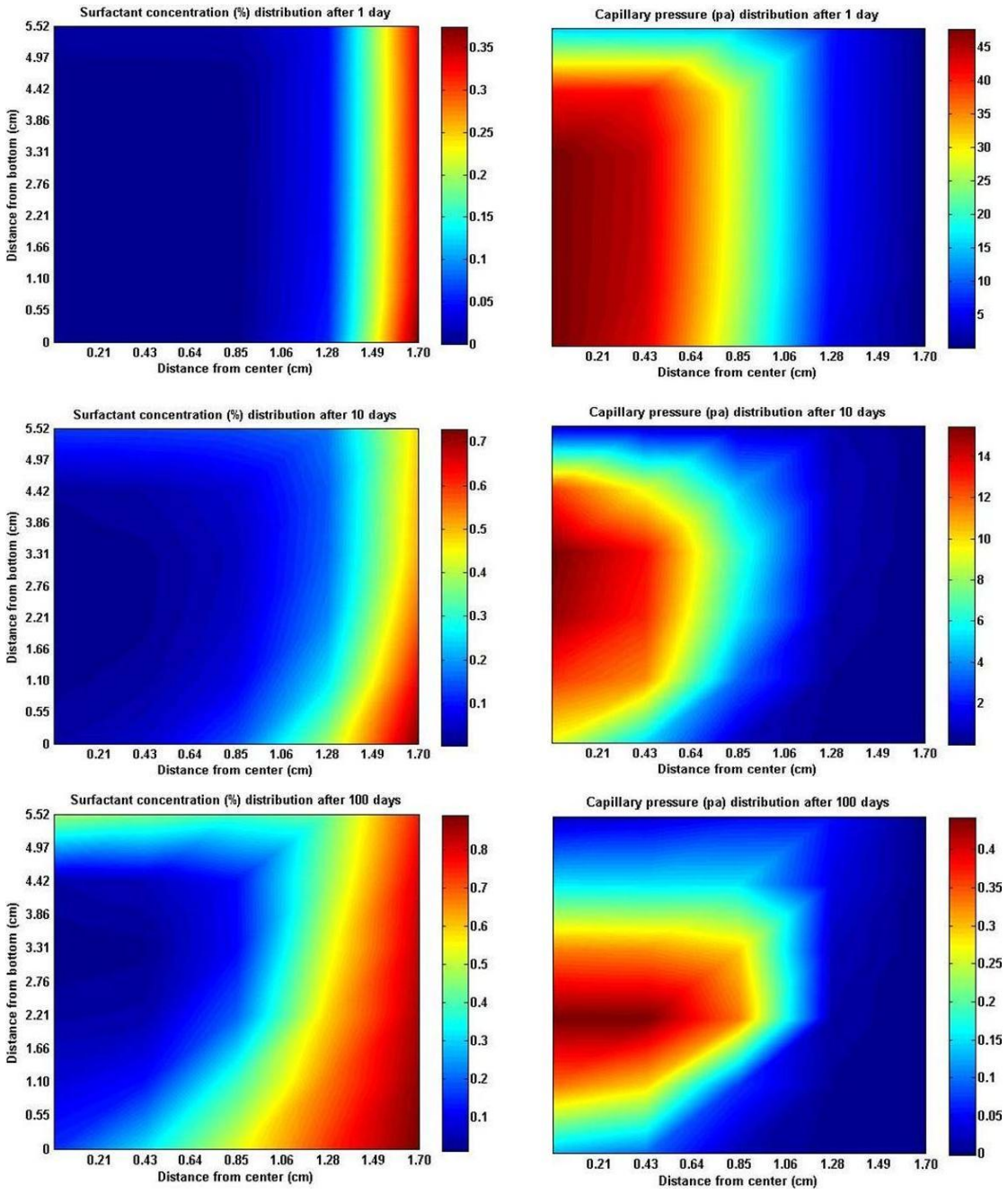

Figure 4-44: Results at different times of surfactant solution imbibition for test 33: left) surfactant concentration and right) capillary pressure

4.3.4 Case Study 8: Effect of Wettability Alteration on Imbibition: Standnes and Austad (2000b): Test 4

Standnes and Austad (2000b) also performed some imbibition experiments on cores without initial water saturation ($S_{oi} = 100\%$). The cores were placed in Hassler core holders, flooded with 1-2 pore volumes of the oil in each direction and aged for four days at 50°C in a closed container filled with oil. Referring to Standnes and Austad (2000b), test 4 was chosen for the current study with fluid and rock properties as listed in Table 4-14.

Table 4-14: Fluids and rock properties of test 4 (Standnes and Austad 2000b)

Property	Value
Length (cm)	5.85
Diameter (cm)	3.83
Porosity (%)	44.9
Permeability (md)	6
Oil Viscosity (cp)	2.6
Water Viscosity (cp)	0.8
Oil Density (lb/ft^3)	50.94
Water Density (lb/ft^3)	64.36
Initial Oil Saturation (%)	100
Initial Interfacial Tension (dynes/cm)	15.4

The experimental result of the brine imbibition for this test showed no oil production after 35 days. This clearly indicates that the initial wettability of the core tends to be more oil-wet than that of the core in tests 33 and 34. After this time, the brine was substituted by brine containing 1.0 wt% surfactant solution of C_{12}TAB. Figure 4-45 and Figure 4-46 were chosen to use as capillary pressure and relative permeability

curves, respectively, in this study. For the same reason, the initial contact angle was assumed to be 120°.

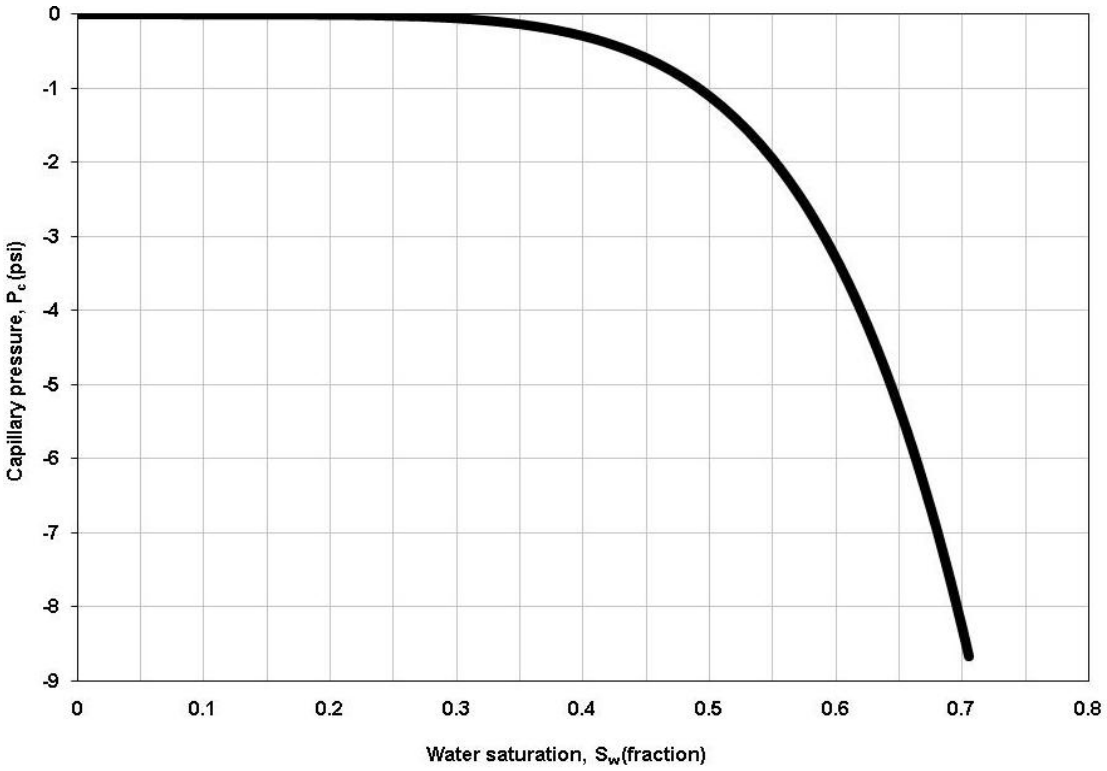

Figure 4-45: Capillary pressure-saturation relation

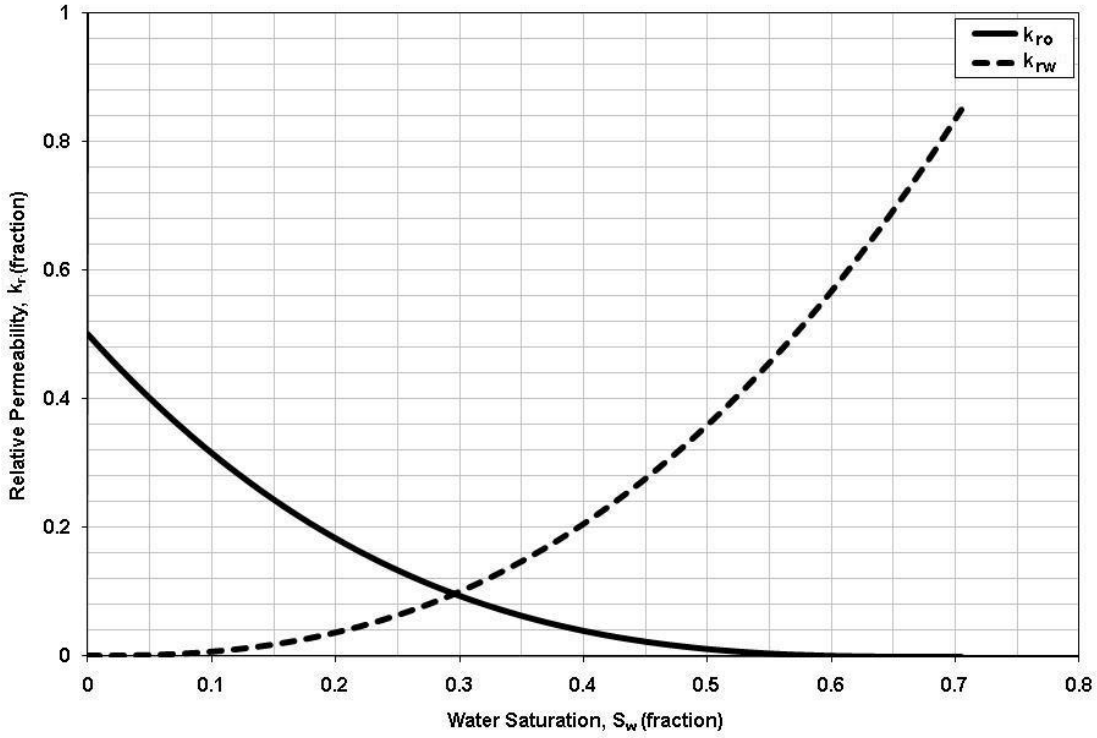

Figure 4-46: Relative permeability-saturation relations

Table 4-15 shows a summary of input data for simulation of their experimental data in test 4.

Table 4-15: Input parameters in the simulation of case study 8

Parameter	**Value**
Grid Block Sizes Δx, Δy, Δz (mm)	3.4, 3.4, 7.3
Number of Grid Blocks in X, Y, Z Direction	10, 10, 8
Time Interval (sec)	5
Number of Days Simulated (days)	45

The result of modeling the experimental data is presented in Figure 4-47. A good match between the experimental data and simulation result is seen.

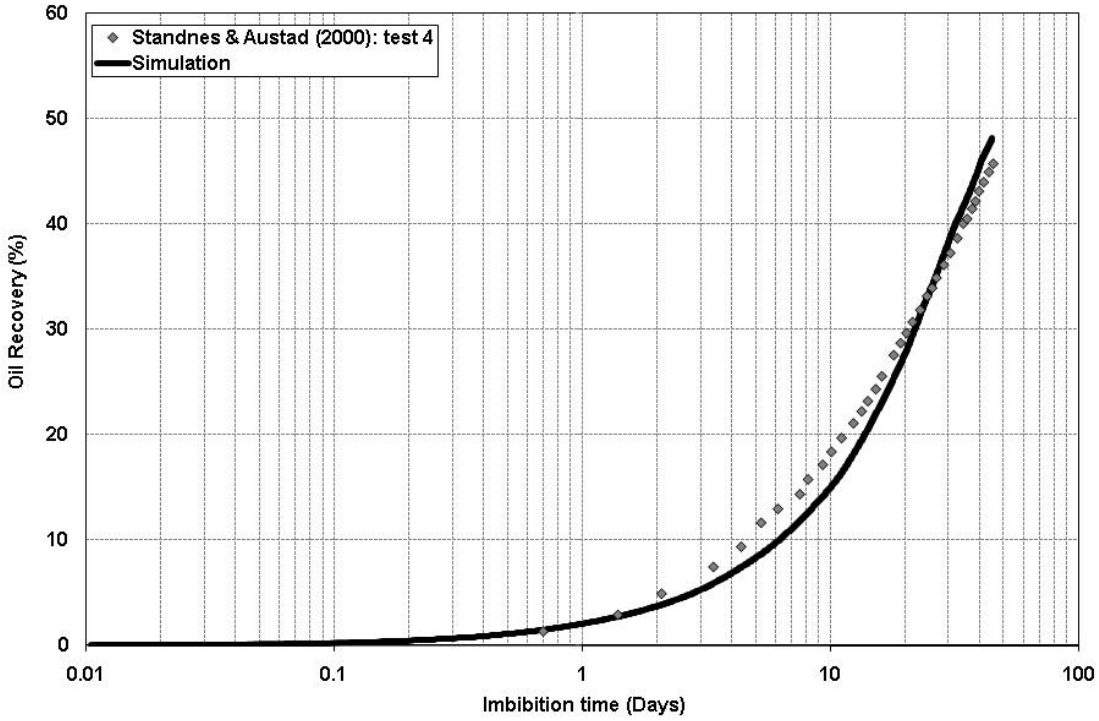

Figure 4-47: Simulation result of the experimental data (Standnes and Austad 2000b: test 4) by using the proposed wettability alteration model

Snap-shots of the oil saturation at various times of surfactant solution imbibition process are shown in Figure 4-48. At each time, the oil saturation is plotted. The distance from center of the core is the X-axis and the distance from bottom of the core is the Y-axis. This figure shows that surfactant solution invades the core according to the difference between the aqueous phase pressure inside and outside of the core at the early time of the imbibition.

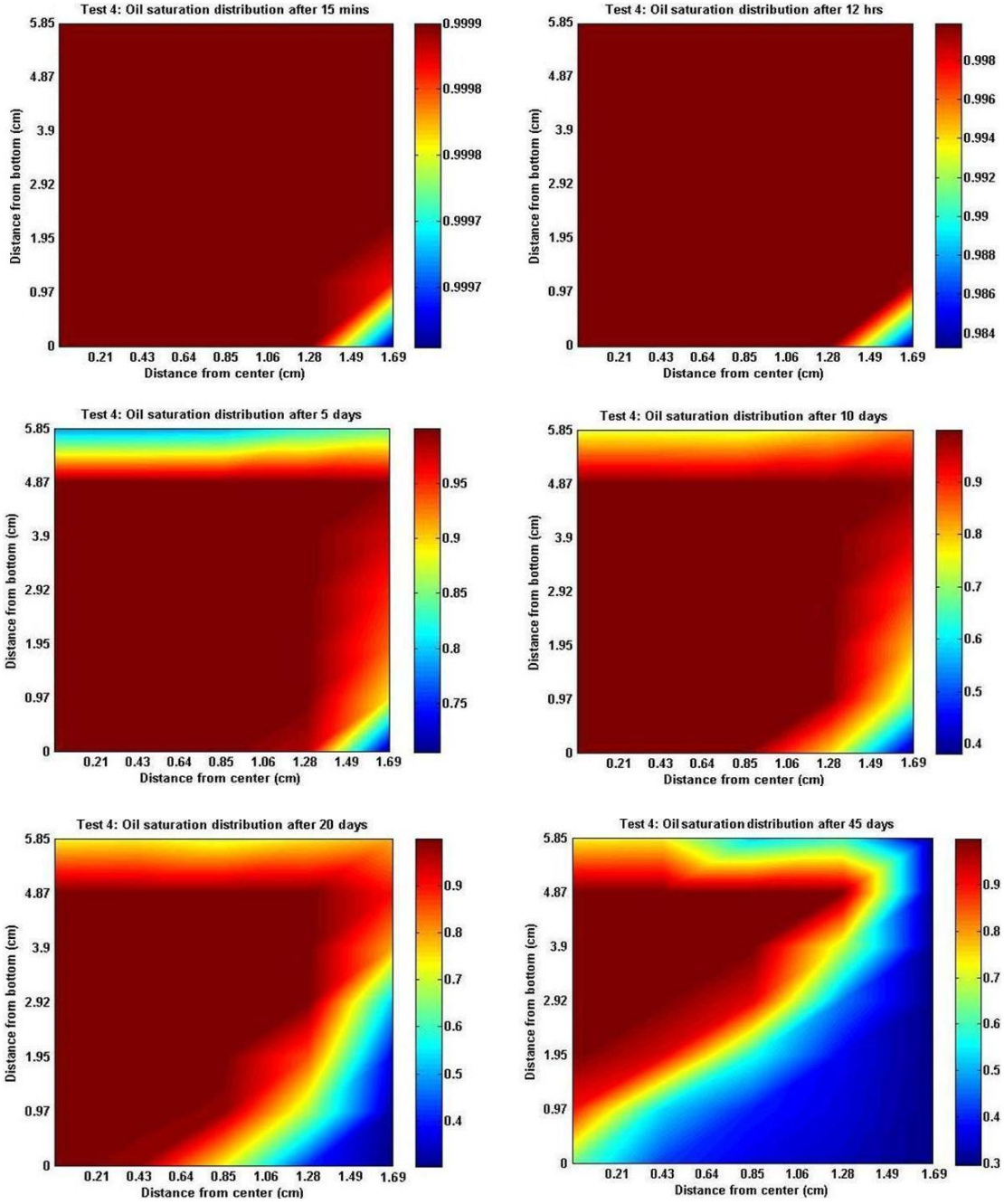

Figure 4-48: Longitudinal view of oil saturation distributions at various times for half core in test 4 (Standnes and Austad 2000b)

As shown in Figure 4-48, surfactant solution entered the core from the side and oil was produced from top of the core (co-current displacement). However, after wettability alteration became dominant, the solution enters from top of the core as well as the sides. It means that the imbibition process was being performed via counter-current flow (oil is produced from top and sides as well as aqueous solution enters the core from top and sides). This indicates that gravity is the dominative process at the early time.

In the second snap-shot (12 hours), water saturation has increased in relation to the early time while the swept area is almost the same. This means that wettability of the rock is altered towards water-wet and the flow is counter-current as surfactant concentration increases. The counter-current flow pattern can be clearly seen after 5 days in this figure. The water saturation increased on top of the core, explaining that water enters from the top as well as sides. For instance, surfactant solution has entered from all over the core at the end of the experiment (45 days); which confirms the wettability alteration effect on oil recovery.

Wettability alteration from oil-wet to less oil-wet and interfacial tension reduction both occur due to the increase in the amount of surfactant inside the core. As noted before, surfactant enters the core along with water as a surfactant solution due to the pressure difference between the aqueous phase in the fracture (or in the laboratory scale: the beaker) and water phase in the matrix. Some people believe that diffusion can be also responsible for surfactant entering into the core. Although diffusion has been included in the present study, it does not play a significant role in the laboratory

time scale as compared to the gravity force as an initial driving force. Surfactant concentration (as ppm in aqueous phase) distributions are plotted in Figure 4-49. The X-axis represents the distance from the center and Y-axis shows the elevation from bottom of the core.

There is an area that has not been invaded by surfactant where the rock wettability is still the same as initial wettability. This can be seen by plotting contact angle distribution for number of layers at 45 days; which is exhibited in Figure 4-50.

Along with wettability alteration, interfacial tension reduction is another mechanism involved in oil recovery. Decreasing interfacial tension causes negative capillary pressure to approach zero and the gravity force to become dominant. The distribution of interfacial tension in the core is presented in Figure 4-51.

Alteration in both contact angle and interfacial tension is greater in the bottom layer than in other layers due to the higher surfactant concentration. The driving force to push the surfactant solution into the core is higher at lower sides of the core. This has been experimentally confirmed in the literature (Standnes and Austad 2000b: Fig.4).

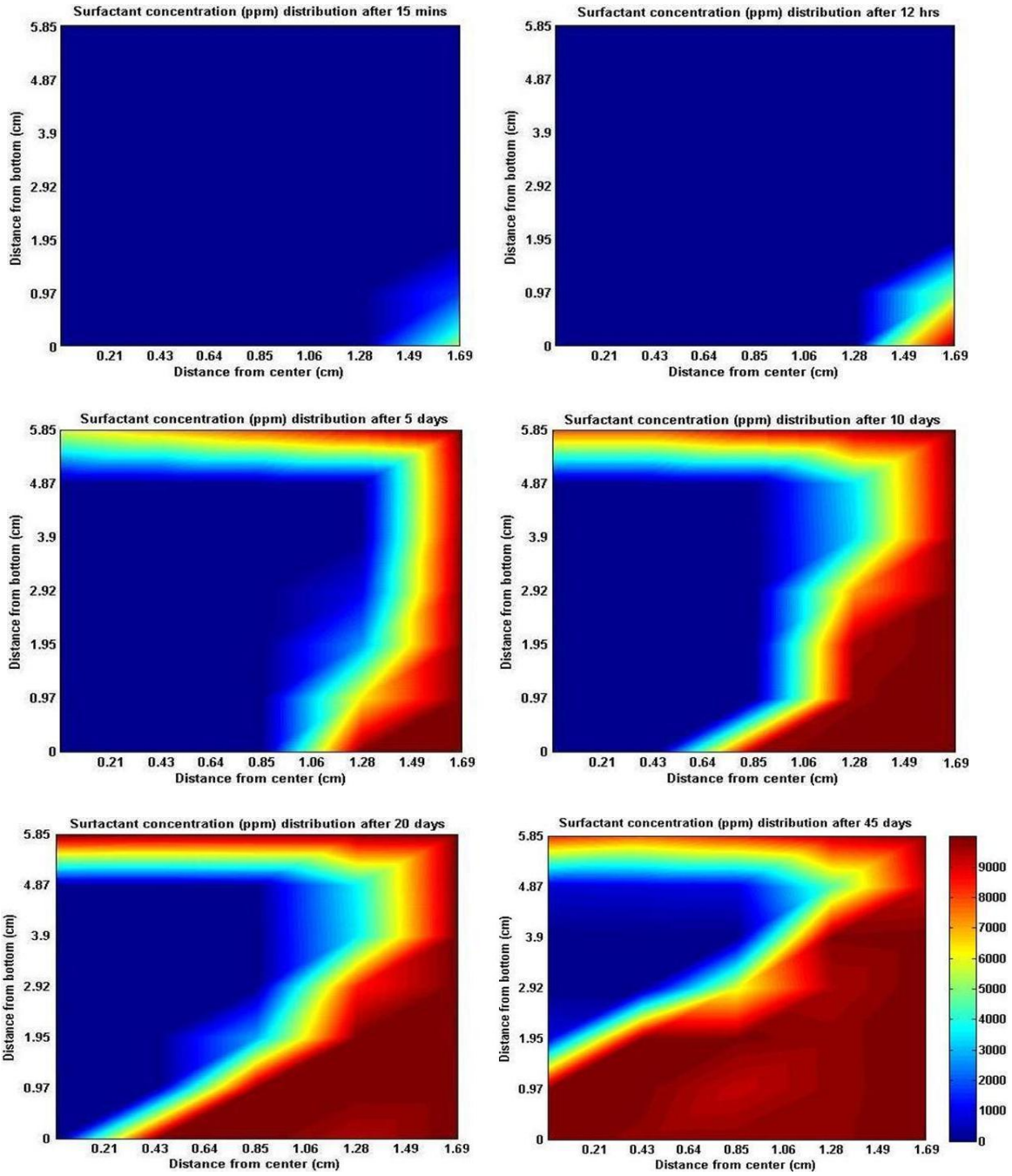

Figure 4-49: Longitudinal view of surfactant concentration distributions at various times for half core in test 4 of Standnes & Austad (2000b)

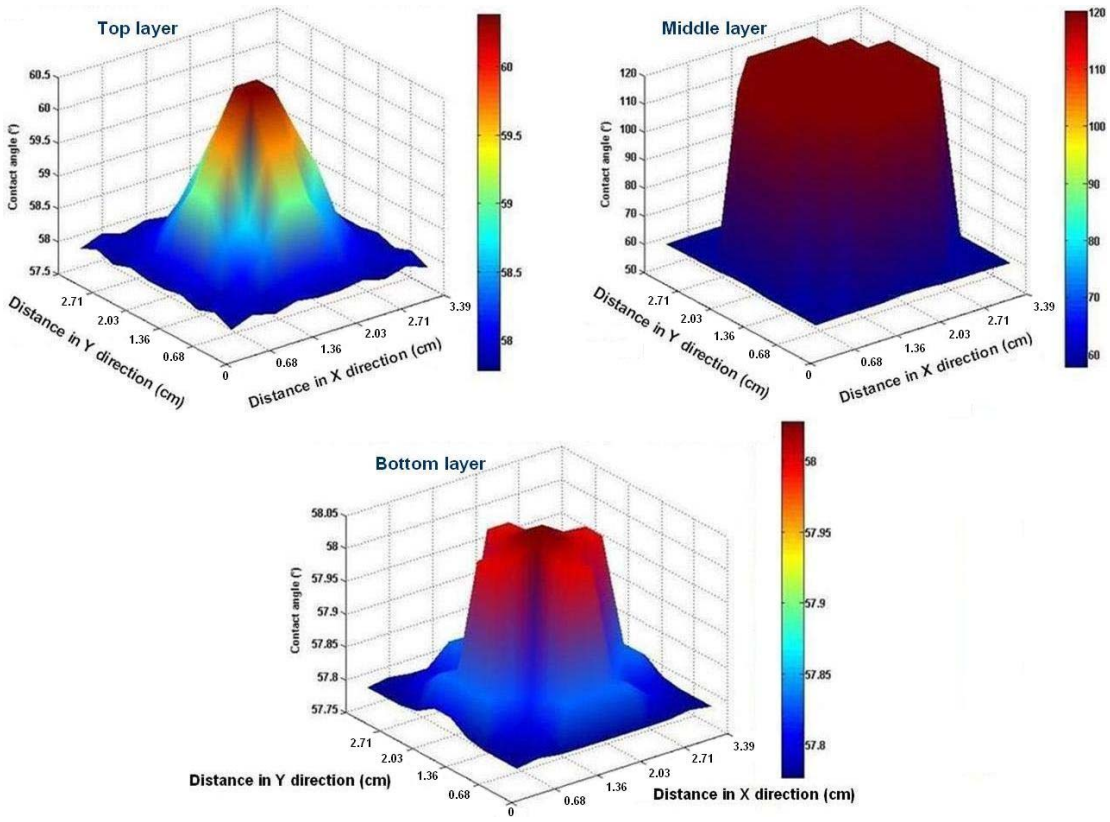

Figure 4-50: Contact angle distribution after 45 days of surfactant solution imbibition test (Standnes and Austad 2000b: test 4) at different layers

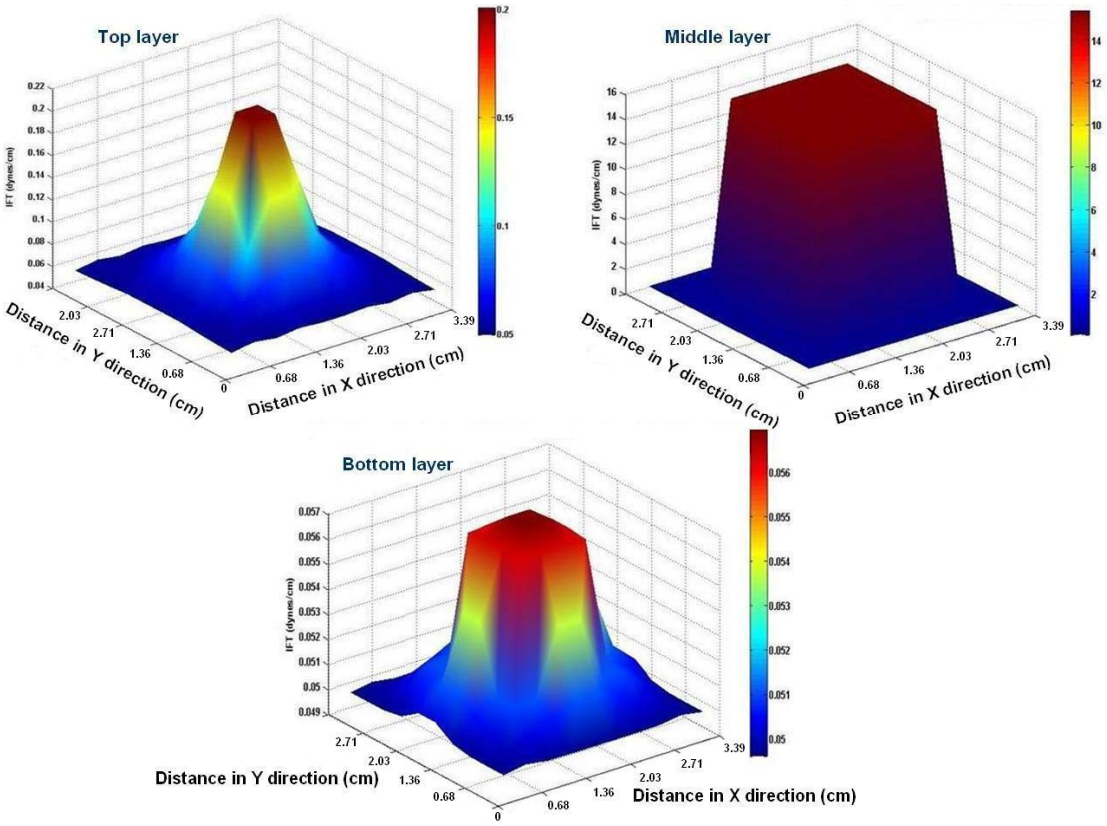

Figure 4-51: Interfacial tension distribution after 45 days of surfactant solution imbibition test (Standnes and Austad 2000b: test 4) at various layers

As described in Chapter 2 and 3, the water/oil relative permeabilities are functions of the rock wettability and fluid saturation. The oil relative permeability is not high when the core is oil-wet. However, wettability alteration towards less oil-wet increases the oil relative permeability. Here, the endpoint of oil relative permeability is shown in Figure 4-52 at the beginning and end of the imbibition process.

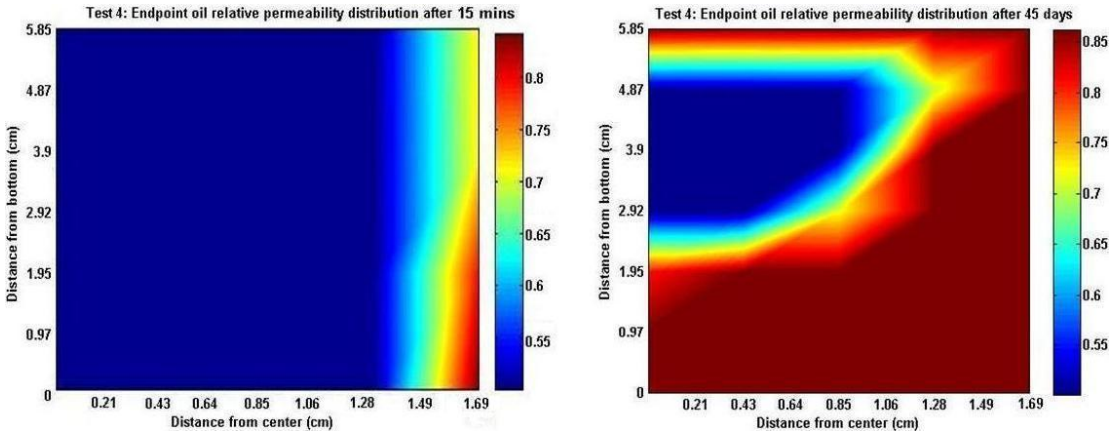

Figure 4-52: Endpoint oil relative permeability

4.3.5 Case Study 9: Effect of Wettability Alteration on Imbibition: Hirasaki et al. (2004)

A number of experimental tests in wettability alteration of laboratory oil-wet cores were performed at Rice University by Hirasaki (2003; 2004; 2005; 2006). One of the imbibition experiments was used in the current study to validate the wettability alteration model presented in this study. The carbonate core, called Core B, had a permeability of 122 md and was aged in crude oil at 80°C prior to the imbibition tests. The core taken from Yates field in West Texas was assumed to be homogeneous and isotropic. Oil recovery by spontaneous imbibition was measured by placing the oil-saturated cores in imbibition cells filled with either formation brine or surfactant solution. No oil was recovered from the core by placing the core in an imbibition cell filled with pure brine after one to two weeks. The lack of oil recovery was ascribed to the wettability of the reservoir cores.

Surfactant solution imbibition test was then performed by using a core from the same outcrop. The surfactant solution was a mixture of 0.025 wt% TDA-4PO-sulfate (C_{13}-4PO- sulfate) and 0.025 wt% CS-330 (C_{12}-3EOsulfate). To reduce the surfactant adsorption a 0.3 M sodium carbonate was also added to the aqueous solution. Therefore, the surfactant adsorption is assumed to be zero. It is also assumed that the surfactant forms a type II (-) microemulsion where two phases of oil and aqueous are in equilibrium during the simulation. This is a reasonable assumption based on the salinity of the surfactant solution and the phase behavior data used in the experiments (Hirasaki and Zhang 2003).

Rock and fluid properties listed in Table 4-16 were obtained from the literature (Hirasaki *et al.* 2004). The surfactant phase behavior parameters were adjusted to obtain a value of IFT (0.02 dynes/cm) that matched the laboratory results (Hirasaki *et al.* 2004).

Table 4-16: Fluids and rock properties of core B (Hirasaki *et al.* 2004)

Property	Value
Length (cm)	7.6
Diameter (cm)	3.83
Porosity (%)	24
Permeability (md)	122
Oil Viscosity (cp)	19.1
Water Viscosity (cp)	1.0
Oil Density (lb/ft^3)	55
Water Density (lb/ft^3)	62.35
Initial Water Saturation (%)	32
Interfacial Tension (dynes/cm)	19.95

The primary relative permeability curves used in the current study were based on the literature (Delshad *et al.* 2006). Since the core did not produce oil during the spontaneous imbibition of pure brine, the capillary pressure curve was set up to be oil-wet as shown in Figure 4-53. The oil/water relative permeability curves are exhibited in Figure 4-54.

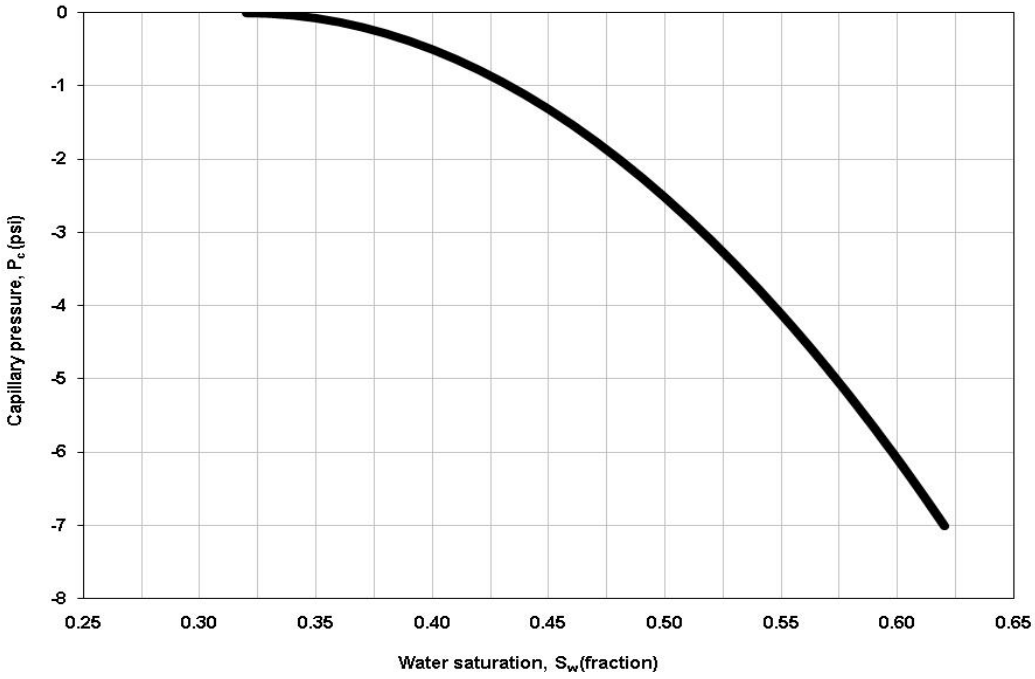

Figure 4-53: Capillary pressure-saturation relation

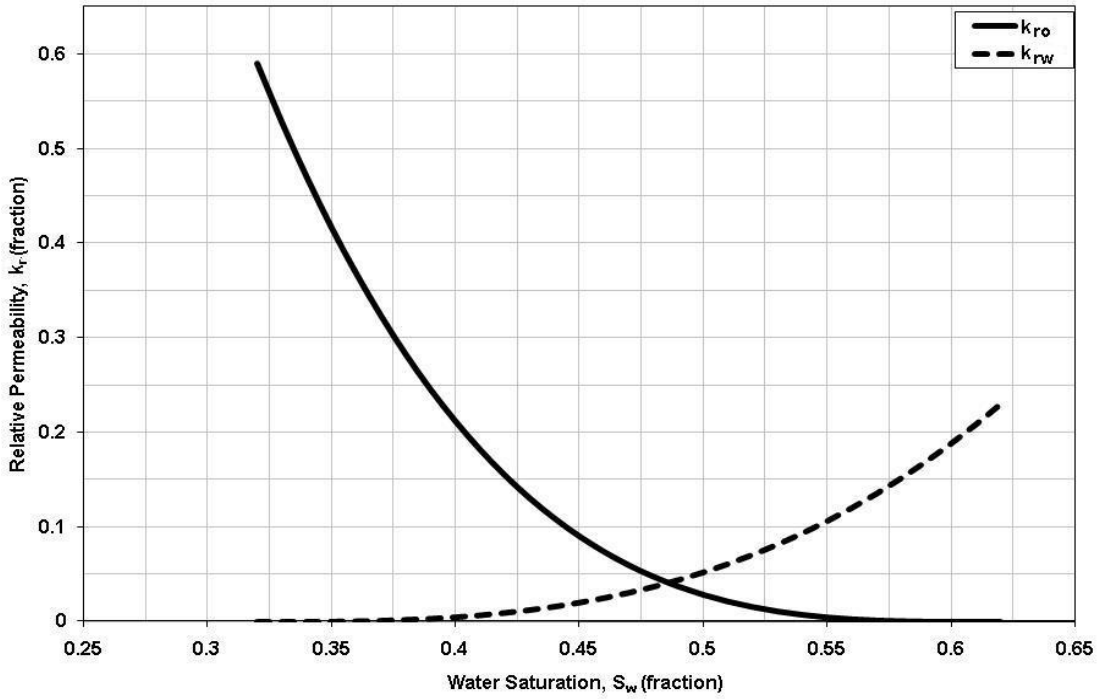

Figure 4-54: Relative permeability-saturation relations

Parameters used in the interfacial tension correlation and wettability alteration model are presented in Table 4-17.

Table 4-17: Parameters used in the current study for IFT and WA model

Parameter	Value
ε in Chun Huh Equation	0.9
η in Chun Huh Equation	0.22
Initial Contact Angle	120°
Final Contact Angle	55°
d in the Wettability Alteration Model	-3

Table 4-18 shows a summary of input data for simulation of their experimental data on Core B.

Table 4-18: Input parameters in the simulation of case study 9

Parameter	Value
Grid Block Sizes Δx, Δy, Δz (mm)	3.4, 3.4, 9.5
Number of Grid Blocks in X, Y, Z Direction	10, 10, 8
Time Interval (sec)	5
Number of Days Simulated (days)	140

They observed oil appearing at the top of core shortly after the beginning of the experiment. The test for this core, which was aged in crude oil, recovered 44% of the oil. Figure 4-55 shows the simulation results of modeling the experimental recovery data taken from Figure 2-38.

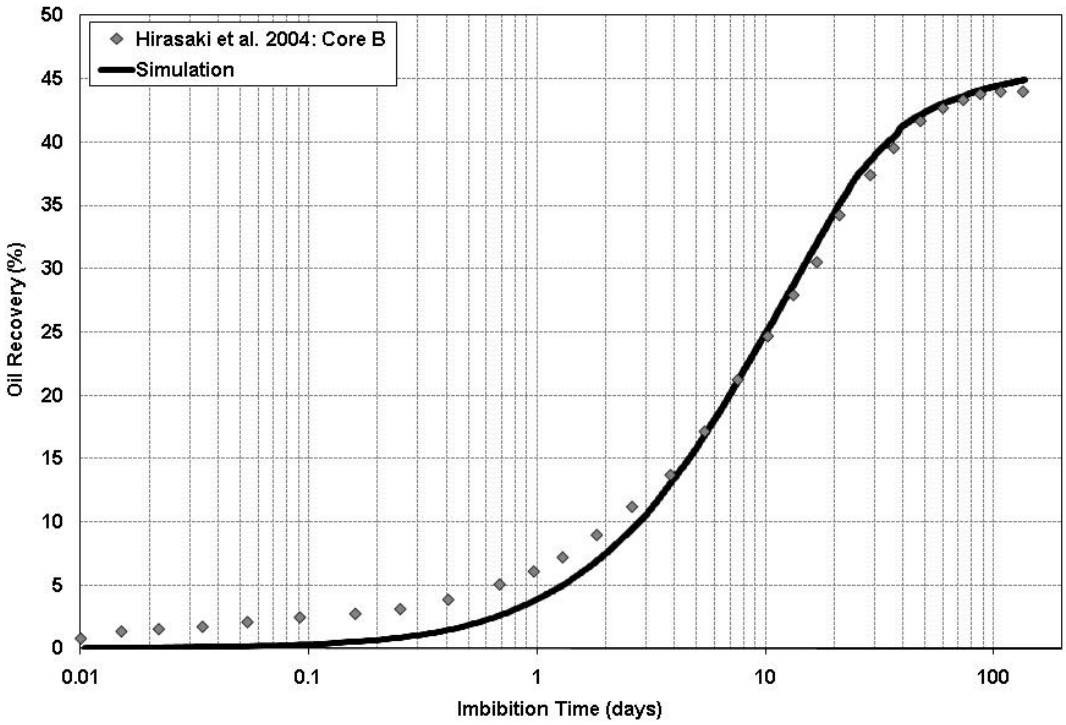

Figure 4-55: Simulation result of the experimental data (Hirasaki *et al.* 2004) by using the proposed wettability alteration model

As seen, a very good match of the Core B experimental data (Hirasaki *et al.* 2004) was obtained. This shows that surfactant solution may enhance oil mobilization by redistribution of fluid phases via wettability alteration as well as interfacial tension reduction.

Understanding the transport mechanism of the surfactant into the core and producing the oil is crucial in analyzing the results. For surfactant imbibition, gravity force can play a significant role depending on the magnitude of the interfacial tension reduction. A reduction in the oil/water interfacial tension can move the negative capillary pressure to values close to zero. This reduction in IFT allows for a decrease

in the inverse Bond number and buoyancy driven flow to take place. The simulation result shows that the inverse Bond number (N_B^{-1} in Equation 2.11) in the invaded places by the surfactant was lowered to values as low as 0.374. It was also observed that the oil was producing from the top of the core (Hirasaki *et al.* 2004). Therefore, the imbibition process was heavily gravity dominated.

The saturation plots for this system are shown in Figure 4-56 at different time intervals. This figure supports the conclusion that the process is mainly dominated by the gravity force at early times. This means that the surfactant solution enters from the sides and oil is only produced from top of the core. However, wettability alteration caused counter-current flow even on top of the core after a while (e.g. 10 days in Figure 4-56). Oil is produced from the top and sides and aqueous solution also enters the core from the top and sides. This can especially be seen in the late times of the process when the water saturation increases upward in the center of the core.

Wettability alteration of the core for two different time steps is shown in Figure 4-57. Reduction of the interfacial tension between oil and water due to the surfactant invasion produced a value as low as 0.02 dynes/cm on the edge area of the core bottom although there is still a region with high interfacial tension as shown in Figure 4-58. As the rock wettability shifts towards a water-wet state, the water phase becomes the wetting phase, hence its relative permeability decreases and/or oil relative permeability increases which causes oil production to increase. Therefore, it can be seen that, irrespective of interfacial tension reduction, decrease in contact angle moving towards a less oil-wet state increases the rate of oil recovery.

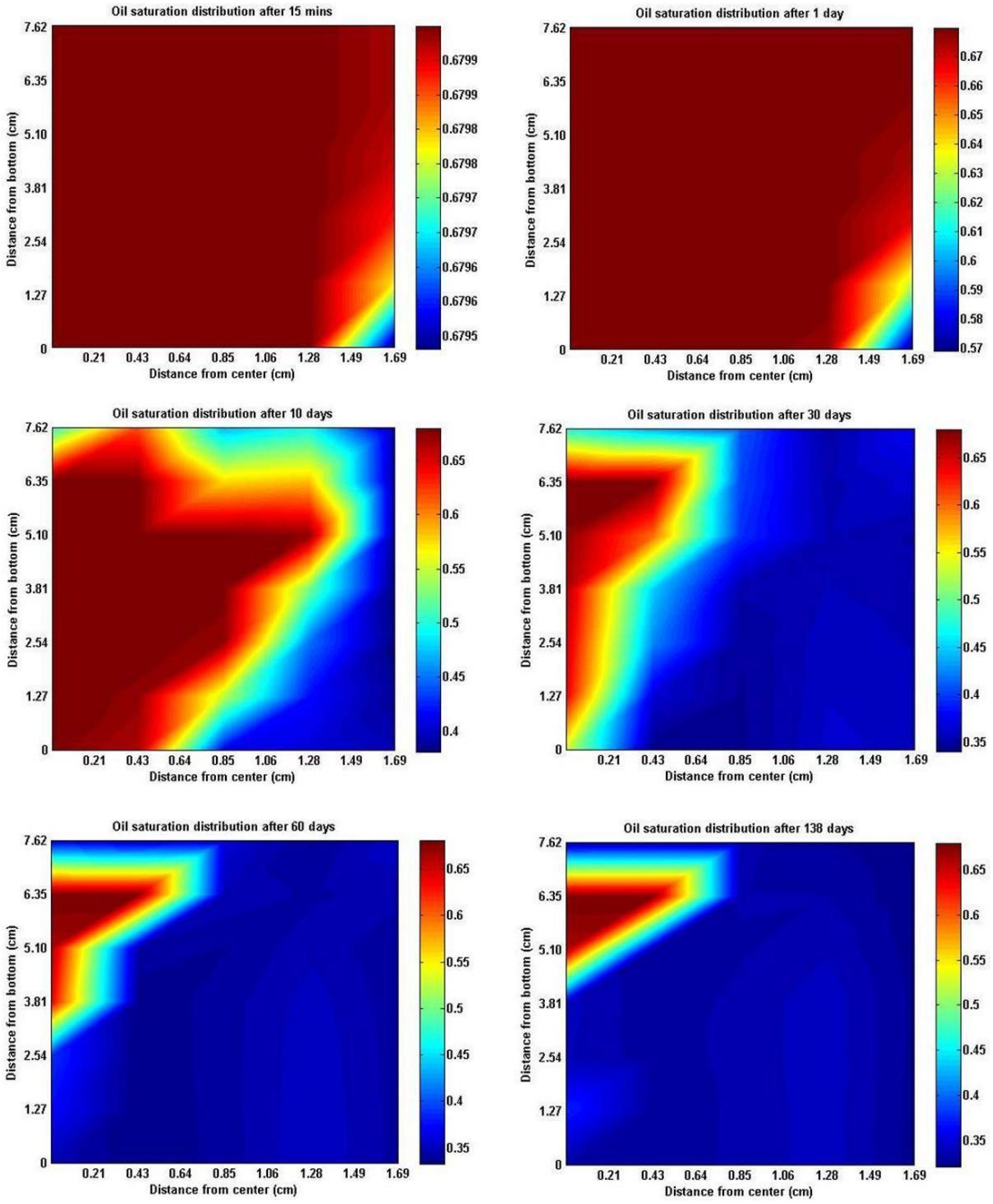

Figure 4-56: Lengthwise view of oil saturation distributions at various times for half core in Core B of Hirasaki *et al.* (2004)

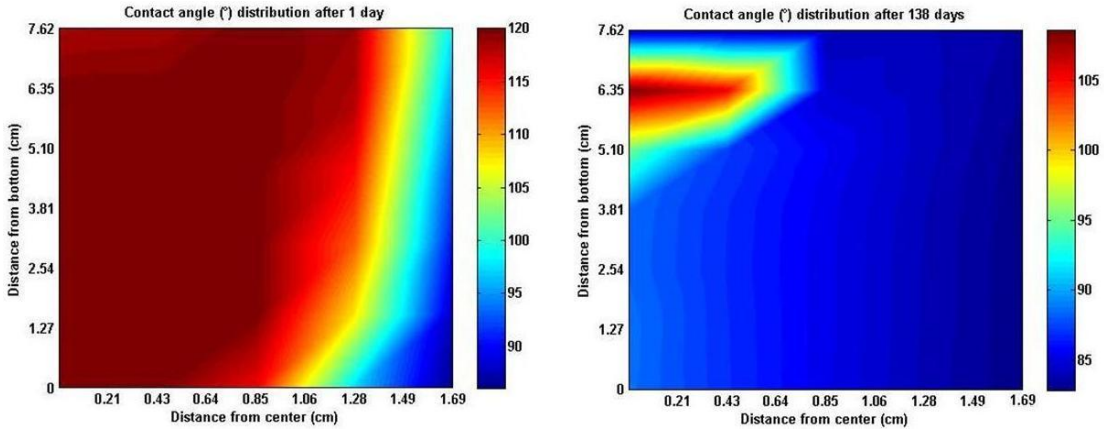

Figure 4-57: Contact angle distribution for early and late time of the surfactant solution imbibition process

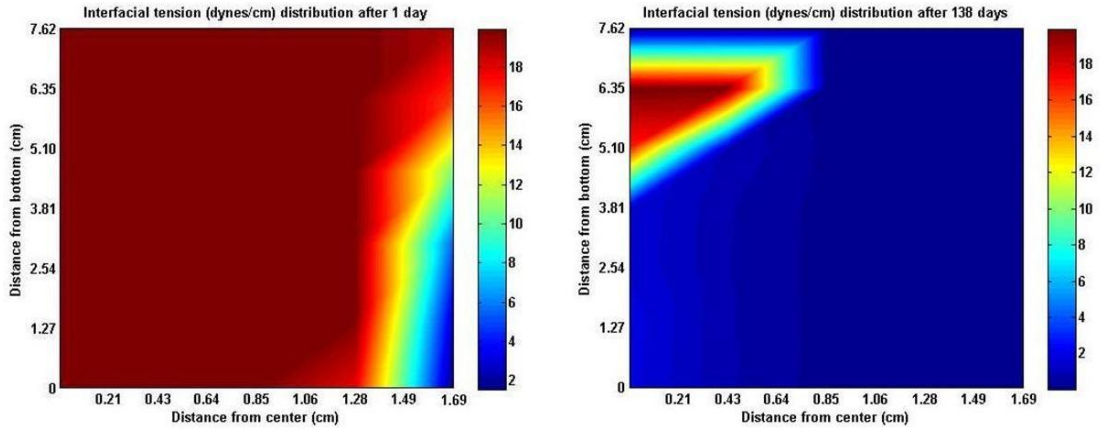

Figure 4-58: Interfacial tension distribution for early and late time of the surfactant solution imbibition process

4.3.6 Case Study 10: Effect of Wettability Alteration on Imbibition: Adibhatla & Mohanty (2005; 2007)

A research study to understand the process of using dilute anionic surfactants in oil recovery from fractured oil-wet carbonate reservoirs was conducted at the University of Houston by Mohanty (2005; 2007; 2008). This process was claimed to be surfactant-aided gravity drainage where surfactant invades the matrix and reduces oil/water interfacial tension and contact angle (Adibhatla and Mohanty 2007). Fourteen different surfactants were tested on the cores taken from the Yates field in West Texas. Oil and brine was from the same field; however, brine was reformulated due to elimination of divalent ions. Among the experiments, test 12 was chosen for the current study. The crude oil used had an API gravity of 30° and a viscosity of 19.1 cp. The core was first completely saturated with brine and then 5.0 pore volumes of crude oil were injected to drive the core to connate water. The core was then immersed in the crude oil and aged for 18 days at 80°C. The imbibition cell was filled with surfactant solution (0.05 %wt.), called Alf-38 (Propoxylated sulfates-8PO), and the aged core was placed in the cell to monitor the oil production by spontaneous imbibition. The surfactant solution contained sodium carbonate to suppress the surfactant adsorption. Rock and fluid properties are provided in Table 4-19.

Table 4-19: Rock and fluid properties of test 12 (Mohanty 2006)

Property	Value
Length (cm)	14.88
Diameter (cm)	3.81
Porosity (%)	22.5
Permeability (mD)	7
Oil Viscosity (cp)	19.1
Water Viscosity (cp)	1
Oil Density (lb/ft^3)	55
Water Density (lb/ft^3)	62.35
Initial Water Saturation (%)	27.5
Initial Interfacial Tension (dynes/cm)	30

Table 4-20 shows a summary of input data for simulation of their experimental data in this case study.

Table 4-20: Input parameters in the simulation of case study 10

Parameter	Value
Grid Block Sizes Δx, Δy, Δz (mm)	3.37, 3.37, 18.6
Number of Grid Blocks in X, Y, Z Direction	10, 10, 8
Time Interval (sec)	5
Number of Days Simulated (days)	40

Prior to the surfactant imbibition test, the core was placed in a beaker of water. Since the core barely produces oil during the spontaneous imbibition of brine, the capillary pressure curve was set up to be nearly oil-wet as shown in Figure 4-59. The original relative permeability curves used in the current study are presented in Figure 4-60 and are taken from the literature (Adibhatla *et al.* 2005).

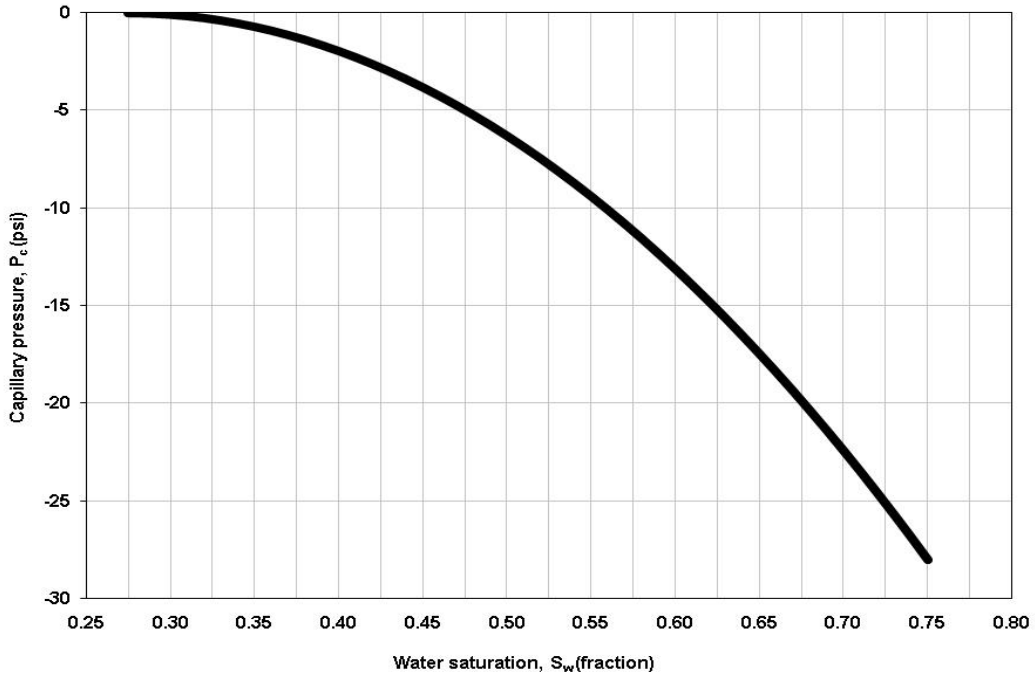

Figure 4-59: Capillary pressure-saturation relation

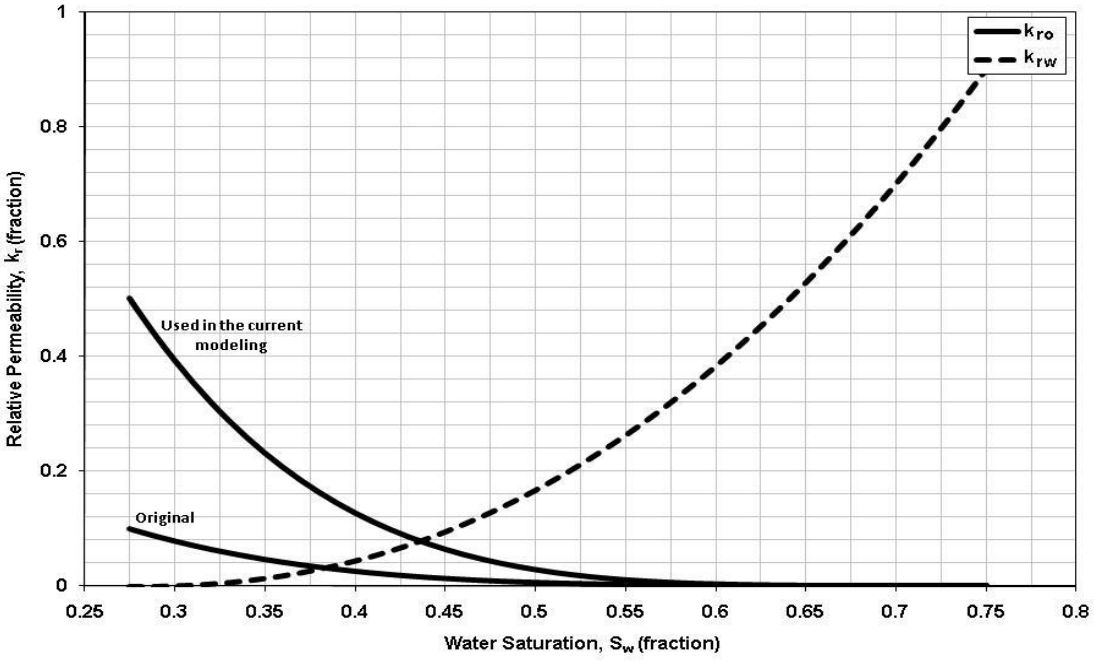

Figure 4-60: Relative permeability-saturation relations

Initial and final contact angle were also estimated around 160° and 65°, respectively (Mohanty 2006). In the wettability alteration model for this study, parameter "d" in Equation 3.7 was chosen as -0.8.

Interfacial tension between oil and water depends on the surfactant and salt concentration. As mentioned earlier, the present simulator incorporates oil/surfactant/brine phase behavior using Hand's rule which generates some parameters needed to calculate IFT reduction. In this study; however, data for interfacial tension reduction documented in the literature was used (Seethepalli *et al.* 2004; Adibhatla *et al.* 2005), as presented in Figure 4-61.

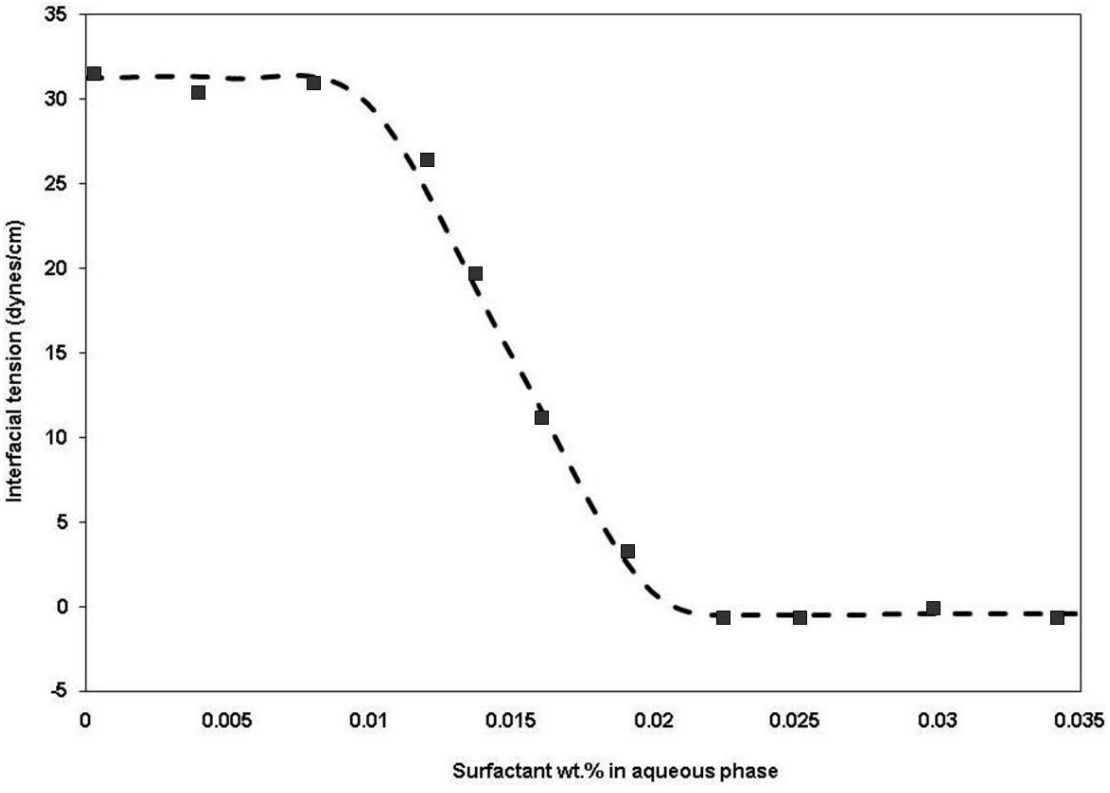

Figure 4-61: Interfacial tension experimental data (Adibhatla *et al.* 2005)

The simulation of oil recovery due to the surfactant solution imbibition matches the experimentally observed imbibition data of test 12, shown in Figure 4-62. The oil relative permeability in the numerical model was adjusted as shown in Figure 4-60 to get this match. This figure shows how accurate the current simulator is when compared to the reported model (Adibhatla and Mohanty 2007).

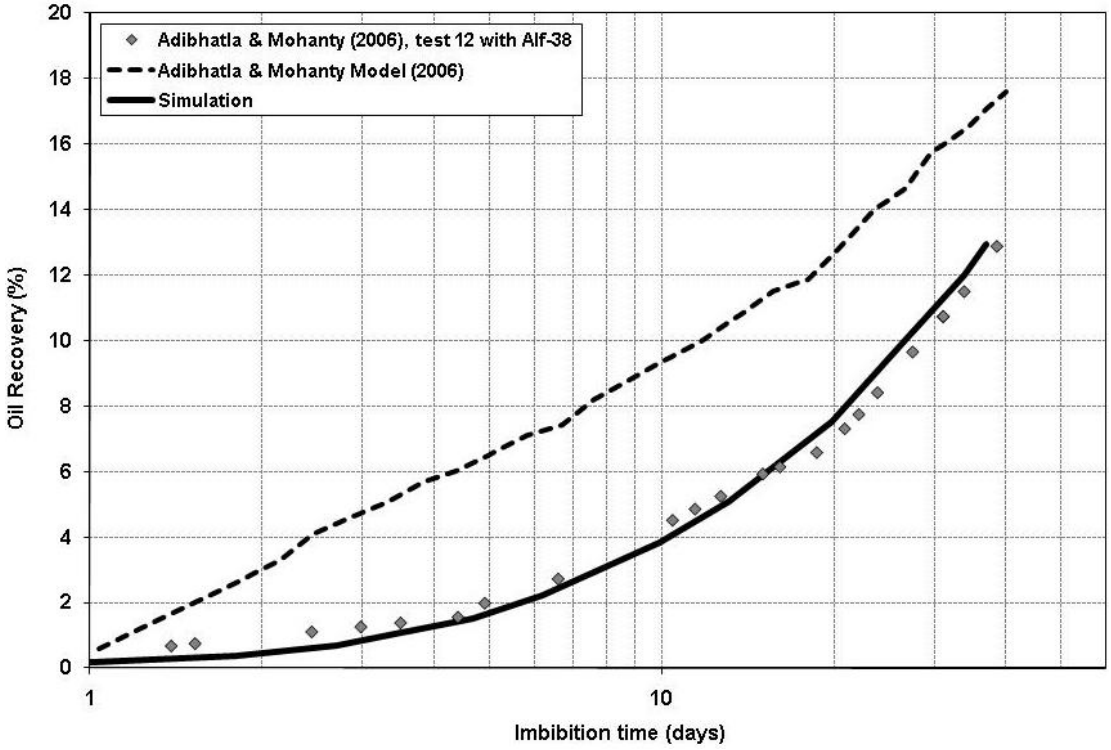

Figure 4-62: Simulation result of test 12 in Mohanty (2006)

Oil saturation distributions at various times of the surfactant solution imbibition are shown in Figure 4-63. In this figure, the X-axis represents the distance from center of the core and the Y-axis shows the distance (or elevation) from the bottom of the core.

Since the permeability of the rock was very low, surfactant solution invaded a small region of the core. At the early days, oil was produced from the top and water entered the core from side. As surfactant concentration was increased in the invaded area, wettability alteration became more effective and oil was produced from the bottom lateral part as well as top of the core. At the end of the imbibition, Figure 4-63 shows a clear gradient in the oil saturation, with water saturation being higher at the bottom of the core than the top.

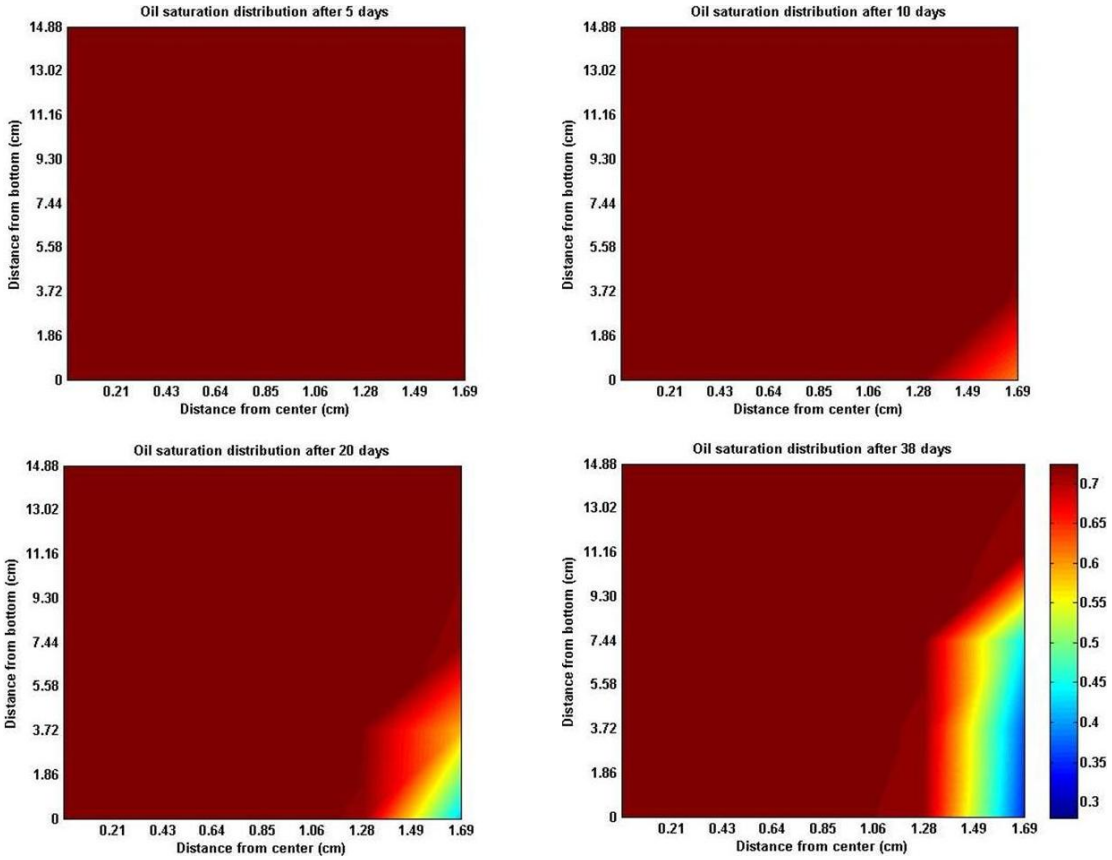

Figure 4-63: Lengthwise view of oil saturation distributions at various times for half core in test 12 of Mohanty (2006)

After 38 days of the surfactant solution imbibition, the maximum oil trapping number was around 1.0×10^{-6} which is not large enough to affect the residual oil saturation. The residual oil saturation of the core after 38 days of the imbibition shows almost no changes as compared to its initial value. This is shown in Figure 4-64.

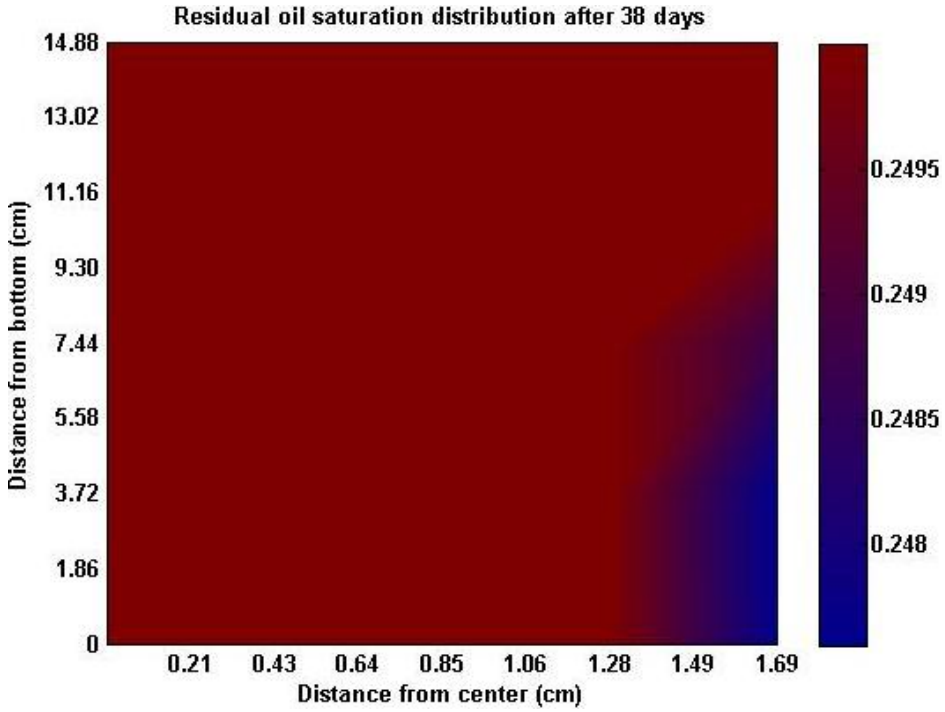

Figure 4-64: Residual oil saturation distribution at the end of the imbibition process

Contact angle distribution for the bottom layer at the end of the imbibition is shown in Figure 4-65. This figure demonstrates the effectiveness of the wettability alteration.

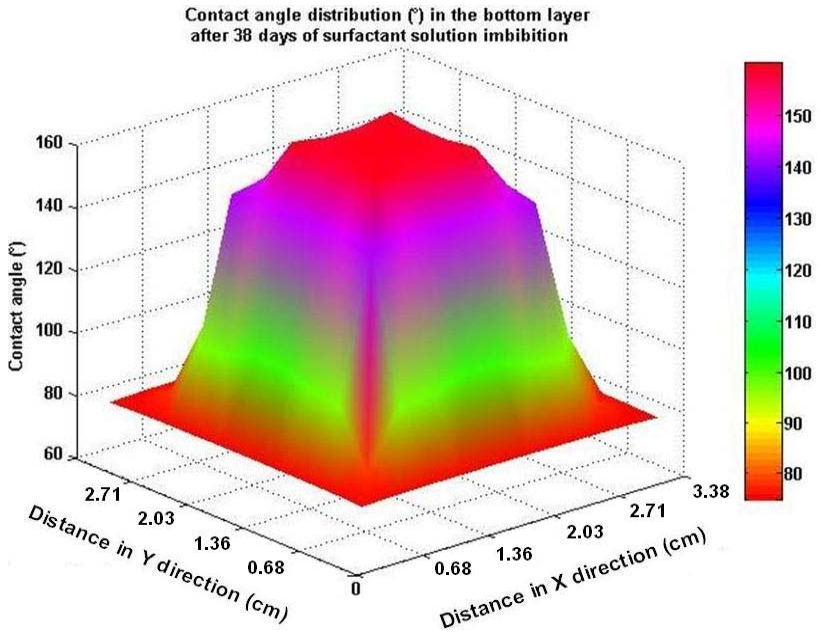

Figure 4-65: Contact angle distribution at the bottom layer of the core in test 12 of Mohanty (2006)

The edge area of the core was the only region where the core wettability has changed to the water-wet state, i.e. the rest of the core region is still oil-wet. This may be also understood by examining at the saturation profiles in Figure 4-63.

When the core is primarily immersed in the imbibition cell and surrounded by Alf-38 solution, the aqueous solution penetrates into the core. As the surfactant advances in the core, the interfacial tension and the rock wettability change. Interfacial tension reduction changes the negative capillary pressure towards zero. Therefore, gravity force becomes more effective than at the initial condition. Also, as the rock wettability is altered the capillary pressure moves towards positive values around the edge where surfactant concentration is high enough to alter the rock wettability as presented in Figure 4-66. However, this leads to little counter-current flow in the lateral side because the magnitude of capillary pressure is low. If the

change in wettability was sufficient, an increase in the capillary forces due to the core wettability alteration towards a less oil-wet must overcome the decrease in the capillary forces due to a decrease in the interfacial tension between oil and aqueous phases.

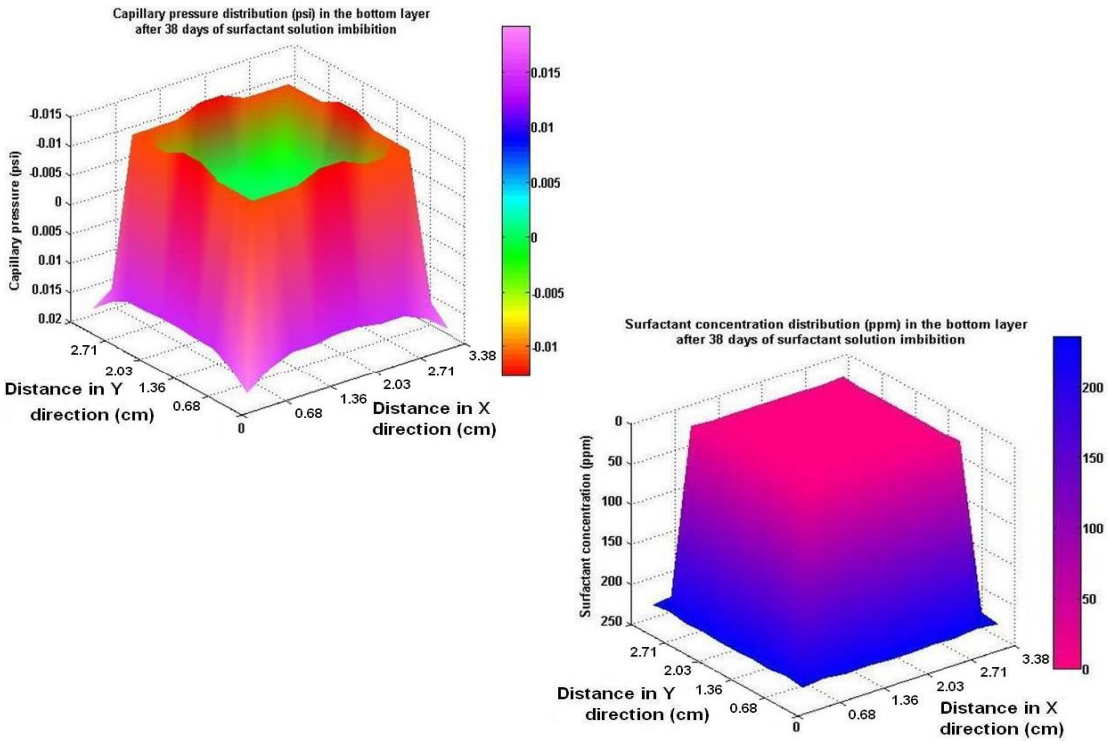

Figure 4-66: Distribution of: left) capillary pressure & right) surfactant concentration distribution after 38 days of surfactant solution imbibition at the bottom layer of the core

Therefore, capillary pressure in center region of the core, where the surfactant was not able to invade, kept its initial capillary pressure. If the core was left for more time in the imbibition cell or a core with higher permeability was used, the oil recovery could have been higher.

Chapter 5: Conclusions and Recommendations

5.1 Conclusion

- A numerical model was developed that simulates oil displacement when laboratory cores are immersed in an aqueous solution which reduces the interfacial tension and/or alters the wettability of the rock.
- A wettability alteration model was developed between the contact angle and surfactant concentration that enables simulation of wettability alteration of laboratory cores.
- The simulator was validated by matching ten sets of experimental data from the literature representing a wide range of conditions where interfacial tension and/or rock wettability were the principal mechanisms contributing to spontaneous oil displacement by gravity segregation.
- Simulations performed in water-wet and oil wet systems demonstrate that both capillary forces and, gravity force contribute to spontaneous displacement of oil.
- Oil displacement is independent of core orientations when capillary forces dominate the displacement.
- When gravity force is the primary displacement mechanism (low IFT) in a water-wet rock, ultimate oil recovery in both horizontal and vertical core orientations is the same although the oil rate histories are not the same. When

capillary force is negligible, fluids moves co-currently in spontaneous imbibition process.

- Gravity forces become important in the system with low interfacial tension, which causes more oil production due to suppression of entrapment mechanisms.
- The model is capable of simulating different boundary conditions including all faces open (AFO), two ends closed (TEC) and one end open (OEO).
- At the boundary condition of all faces open, changing the oil viscosity such that the water/oil viscosity ratio stays very close to unity does not change the ultimate oil recovery, but it changes the oil rate production.

5.2 Recommendations

- The proposed wettability alteration model was tested against the laboratory core data. It is recommended to use this model in a commercial simulator to predict the field data.
- Parameter "*d*" in this model is suspected to have a dependency to HLB of surfactant as well as rock type. Therefore, experimental procedure that can establish this relationship is noteworthy.
- Correlation of relative permeability versus rock wettability needs to be confirmed by experimental tests.

Nomenclatures:

a= Langmuir fitting parameter, dimensionless

b=Langmuir fitting parameter, P.V. ft^3 /ft^3 of surfactant

A= cross sectional area, cm^2 in Equation 2.5

B = FVF of a phase, ft^3/std ft^3

k= absolute permeability, md

K_p = partitioning coefficient of surfactant, fraction

k_r = relative permeability of a phase

S = saturation of a phase, fraction

S_{wf} = water saturation at the front, fraction

S_{wi} = initial water saturation, fraction

S_{wr} = residual water saturation, fraction

S_{or} = residual oil saturation, fraction

u_x = superficial velocity or flux of a phase in X direction, ft^3/ft^2.day

u_y = superficial velocity or flux of a phase in Y direction, ft^3/ft^2.day

u_z = superficial velocity or flux of a phase in Z direction, ft^3/ft^2.day

x= distance in the X direction, ft

y= distance in the Y direction, ft

z= distance in the Z direction, ft

P= phase pressure, psi

P^0= reference pressure, psi

P_c= capillary pressure, psi

q= darcy flow rate, cm^3/sec in Equation 2.5

L= core length, cm in Equation 2.5

C_s = concentration of surfactant in aqueous phase, $ft^3$of surfactant/P.V. ft^3

C_{sg} = Adsorbed surfactant concentration, $ft^3$of surfactant/ rock ft^3

c_ϕ = compressibility of rock, 1/psi

D= elevation with respect to datum (positive downward), ft

T= trapping value defined in Equation 3.18

N_T = trapping number defined in Equation 2.12

t= time, days

Δt= time step ($\Delta t=t^{n+1}-t^n$), days

Δx= difference along X direction ($\Delta x=x_{i+1}-x_i$), ft

Δy= difference along Y direction ($\Delta y=y_{j+1}-y_j$), ft

Δz= difference along Z direction ($\Delta z=z_{k+1}-z_k$), ft

θ= contact angle between fluids and solid surface, degree (°)

ρ_s = mass density of surfactant, lb_m/ft^3

β= coefficient in Equation 3.1 and 3.2

σ= interfacial tension between wetting and nonwetting phases, dynes/cm

μ = viscosity of a phase, cp

$\gamma = \frac{\rho}{144}\frac{g}{g_c}$ =fluid gravity gradient, psi/ft

ζ= interfacial free energy per unit area of interaction

ϕ= rock porosity, fraction

D^0 = diffusion coefficient of surfactant, ft^2/day

Subscript:

w= water (or wet) phase

nw= nonwetting phase

e= effective

o= oil phase

s= surfactant

x= X direction

y= Y direction

z= Z direction

Superscript:

n: step time

high: high trapping number

low: low trapping number

0: initial condition (usually time zero)

Appendix A: Derivation of Differential Equation Describing Oil and Water Flow

The material-balance equation for two phases of oil and water over the finite control volume of a porous medium, shown in figure (3.1), over a time interval Δt is:

$$m_{in} - m_{out} - m_{cons.} = m_{acc.} \tag{A.1}$$

For the water phase in Cartesian coordinates, for instance, the material-balance equation can be written as follows:

$$\left(m\big|_x + m\big|_y + m\big|_z\right)\Big|_{w-in} - \left(m\big|_x + m\big|_y + m\big|_z\right)\Big|_{w-out} = m_{w-acc.} + m_{w-cons.} \tag{A.2}$$

The terms in equation (A.2) may be expressed as:

$$m_{w-in/out}\big|_x = \alpha\rho_w u_{w-x}\big|_{in/out}\left(\Delta y\Delta z\Delta t\right) \tag{A.3}$$

$$m_{w-in/out}\big|_y = \alpha\rho_w u_{w-y}\big|_{in/out}\left(\Delta x\Delta z\Delta t\right) \tag{A.4}$$

$$m_{w-in/out}\big|_z = \alpha\rho_w u_{w-z}\big|_{in/out}\left(\Delta x\Delta y\Delta t\right) \tag{A.5}$$

$$m_{w-acc.} = \rho_w S_w \phi\left(\Delta x\Delta y\Delta z\right)\big|_{t+\Delta t} - \rho_w S_w \phi\left(\Delta x\Delta y\Delta z\right)\big|_t \tag{A.6}$$

where α is the volume conversion factor. By substituting equations (A.3) to (A.6) into the equation (A.2), the following mass-conservation equation is obtained:

$$\begin{aligned}&\left[\alpha\rho_w u_{w-x}\big|_x\left(\Delta y\Delta z\Delta t\right) + \alpha\rho_w u_{w-y}\big|_y\left(\Delta x\Delta z\Delta t\right) + \alpha\rho_w u_{w-z}\big|_z\left(\Delta x\Delta y\Delta t\right)\right]_{in} - \\ &\left[\alpha\rho_w u_{w-x}\big|_{x+\Delta x}\left(\Delta y\Delta z\Delta t\right) + \alpha\rho_w u_{w-y}\big|_{y+\Delta y}\left(\Delta x\Delta z\Delta t\right) + \alpha\rho_w u_{w-z}\big|_{z+\Delta z}\left(\Delta x\Delta y\Delta t\right)\right]_{out} = \\ &\rho_w S_w \phi\left(\Delta x\Delta y\Delta z\right)\big|_{t+\Delta t} - \rho_w S_w \phi\left(\Delta x\Delta y\Delta z\right)\big|_t\end{aligned} \tag{A.7}$$

The following equation is taken by dividing both sides of the above equation to $\Delta x\Delta y\Delta z$:

$$\left[\frac{\rho_w u_{w-x}\big|_{x+\Delta x}-\rho_w u_{w-x}\big|_x}{\Delta x}\right]+\left[\frac{\rho_w u_{w-y}\big|_{y+\Delta y}-\rho_w u_{w-y}\big|_y}{\Delta y}\right]+$$
$$\left[\frac{\rho_w u_{w-z}\big|_{z+\Delta z}-\rho_w u_{w-z}\big|_z}{\Delta z}\right]=-\frac{1}{\alpha}\left[\frac{\rho_w S_w\phi\big|_{t+\Delta t}-\rho_w S_w\phi\big|_t}{\Delta t}\right] \tag{A.8}$$

By taking the limit of terms enclosed in the brackets as Δx , Δy , Δz , and Δt approach zero and substituting the definition of the partial derivative, equation (A.8) becomes:

$$\frac{\partial}{\partial x}\left(\rho_w u_{w-x}\right)+\frac{\partial}{\partial y}\left(\rho_w u_{w-y}\right)+\frac{\partial}{\partial z}\left(\rho_w u_{w-z}\right)=-\frac{1}{\alpha}\frac{\partial}{\partial t}\left(\rho_w S_w\phi\right) \tag{A.9}$$

Now, by multiplying both sides to $\Delta x\Delta y\Delta z$ and assuming:

$$A_y=\Delta x\Delta z,\ A_z=\Delta x\Delta y,\ V_b=\Delta x\Delta y\Delta z \tag{A.10}$$

Equation (A.9) can be presented as:

$$\boxed{\frac{\partial}{\partial x}\left(A_x\rho_w u_{w-x}\right)\Delta x+\frac{\partial}{\partial y}\left(A_y\rho_w u_{w-y}\right)\Delta y+\frac{\partial}{\partial z}\left(A_z\rho_w u_{w-z}\right)\Delta z=-\frac{V_b}{\alpha}\frac{\partial}{\partial t}\left(\rho_w S_w\phi\right)} \tag{A.11}$$

The Darcy equation for phase "α" can be written as follows:

$$u_\alpha=-0.006328\frac{Kk_{r\alpha}}{\mu_\alpha}\nabla\psi_\alpha=-0.006328\frac{Kk_{r\alpha}}{\mu_\alpha}\left(\nabla P_\alpha-\frac{\rho_\alpha}{144}\nabla D\right) \tag{A.12}$$

where,

$$\nabla P=\left(\frac{\partial P}{\partial x},\frac{\partial P}{\partial y},\frac{\partial P}{\partial z}\right),\nabla D=\left(\frac{\partial D}{\partial x},\frac{\partial D}{\partial y},\frac{\partial D}{\partial z}\right) \tag{A.13}$$

If the following parameters are defined as follows:

$$\beta=0.006328,\ B_\alpha=\frac{\rho_{\alpha-sc}}{\rho_\alpha},\ \gamma_\alpha=\frac{\rho_\alpha}{144} \tag{A.14}$$

Then equation (A.11) can be written as:

$$\frac{\partial}{\partial x}\left(\beta A_x K_x \frac{k_{rw}}{\mu_w B_w}\left(\frac{\partial P_w}{\partial x}-\gamma_w \frac{\partial D}{\partial x}\right)\right)\Delta x+\frac{\partial}{\partial y}\left(\beta A_y K_y \frac{k_{rw}}{\mu_w B_w}\left(\frac{\partial P_w}{\partial y}-\gamma_w \frac{\partial D}{\partial y}\right)\right)\Delta y$$
$$+\frac{\partial}{\partial z}\left(\beta A_z K_z \frac{k_{rw}}{\mu_w B_w}\left(\frac{\partial P_w}{\partial z}-\gamma_w \frac{\partial D}{\partial z}\right)\right)\Delta z=\frac{V_b}{\alpha}\frac{\partial}{\partial t}\left(S_w \frac{\phi}{B_w}\right) \tag{A.15}$$

Similarly, the mass-conservation equation for the oil phase is:

$$\frac{\partial}{\partial x}\left(\beta A_x K_x \frac{k_{ro}}{\mu_o B_o}\left(\frac{\partial P_o}{\partial x}-\gamma_o \frac{\partial D}{\partial x}\right)\right)\Delta x+\frac{\partial}{\partial y}\left(\beta A_y K_y \frac{k_{ro}}{\mu_o B_o}\left(\frac{\partial P_o}{\partial y}-\gamma_o \frac{\partial D}{\partial y}\right)\right)\Delta y$$
$$+\frac{\partial}{\partial z}\left(\beta A_z K_z \frac{k_{ro}}{\mu_o B_o}\left(\frac{\partial P_o}{\partial z}-\gamma_o \frac{\partial D}{\partial z}\right)\right)\Delta z=\frac{V_b}{\alpha}\frac{\partial}{\partial t}\left(S_o \frac{\phi}{B_o}\right) \tag{A.16}$$

In the current model, B_w and B_o can be essentially constant, which is a reasonable assumption. Therefore, these two terms are canceled out from both sides of equations (A.15) and (A.16).

Also,

$$\phi=\phi^0\left[1+c_\phi\left(P-P^0\right)\right] \tag{A.17}$$

Therefore, the right side of equations (A.15), for example, can be simplified as follows (after omitting B_w):

$$\frac{\partial}{\partial t}\left(S_w\phi\right)=\phi\frac{\partial S_w}{\partial t}+S_w\frac{\partial}{\partial t}\left(\phi\right)=\phi\frac{\partial S_w}{\partial t}+S_w\phi^0 c_\phi\frac{\partial P}{\partial t} \tag{A.18}$$

So by considering equation (3.20) & (A.18) and adding the mass conservation equations of water and oil, the following equation results:

$$\frac{\partial}{\partial x}\left(\beta A_x K_x\left(\frac{k_{rw}}{\mu_w B_w}+\frac{k_{ro}}{\mu_o B_o}\right)\left(\frac{\partial P_o}{\partial x}\right)-\beta A_x K_x\left(\frac{k_{rw}}{\mu_w B_w}\gamma_w+\frac{k_{ro}}{\mu_o B_o}\gamma_o\right)\left(\frac{\partial D}{\partial x}\right)-\beta A_x K_x\left(\frac{k_{rw}}{\mu_w B_w}\right)\left(\frac{\partial P_c}{\partial x}\right)\right)\Delta x+$$
$$\frac{\partial}{\partial y}\left(\beta A_y K_y\left(\frac{k_{rw}}{\mu_w B_w}+\frac{k_{ro}}{\mu_o B_o}\right)\left(\frac{\partial P_o}{\partial y}\right)-\beta A_y K_y\left(\frac{k_{rw}}{\mu_w B_w}\gamma_w+\frac{k_{ro}}{\mu_o B_o}\gamma_o\right)\left(\frac{\partial D}{\partial y}\right)-\beta A_y K_y\left(\frac{k_{rw}}{\mu_w B_w}\right)\left(\frac{\partial P_c}{\partial y}\right)\right)\Delta y+$$
$$\frac{\partial}{\partial z}\left(\beta A_z K_z\left(\frac{k_{rw}}{\mu_w B_w}+\frac{k_{ro}}{\mu_o B_o}\right)\left(\frac{\partial P_o}{\partial z}\right)-\beta A_z K_z\left(\frac{k_{rw}}{\mu_w B_w}\gamma_w+\frac{k_{ro}}{\mu_o B_o}\gamma_o\right)\left(\frac{\partial D}{\partial z}\right)-\beta A_z K_z\left(\frac{k_{rw}}{\mu_w B_w}\right)\left(\frac{\partial P_c}{\partial z}\right)\right)\Delta z=$$
$$\frac{V_b}{\alpha}\left(\phi^0 c_\phi\right)\frac{\partial P_o}{\partial t} \tag{A.19}$$

or in a compact form (Moreno *et al.* 2004):

$$-\left(\phi^0 c_\phi\right)\frac{\partial P_o}{\partial t}=-\nabla.\vec{K}\lambda_t\nabla P_o+\nabla.\lambda_w\nabla p_c+\nabla.\left(\lambda_o\gamma_o+\lambda_w\gamma_w\right)\nabla\vec{D} \tag{A.20}$$

Discretization refers to the process of approximating a differential equation by a set of finite-difference equations. To discretize the above equation, it is necessary to use the central-difference approximation for the first derivatives. For example, the water part of the first term of equation (A.19) can be approximated as follows:

$$\frac{\partial}{\partial x}\left(\beta A_x K_x\frac{k_{rw}}{\mu_w B_w}\left(\frac{\partial P_o}{\partial x}\right)\right)_i\Delta x\approx$$
$$\frac{1}{\Delta x_i}\left\{\left(\beta A_x K_x\frac{k_{rw}}{\mu_w B_w}\frac{\partial P_o}{\partial x}\right)_{i+\frac{1}{2}}-\left(\beta A_x K_x\frac{k_{rw}}{\mu_w B_w}\frac{\partial P_o}{\partial x}\right)_{i-\frac{1}{2}}\right\}\times\Delta x= \tag{A.21}$$
$$\left(\beta A_x K_x\frac{k_{rw}}{\mu_w B_w}\right)_{i+\frac{1}{2}}\left(\frac{\partial P_o}{\partial x}\right)_{i+\frac{1}{2}}-\left(\beta A_x K_x\frac{k_{rw}}{\mu_w B_w}\right)_{i-\frac{1}{2}}\left(\frac{\partial P_o}{\partial x}\right)_{i-\frac{1}{2}}$$

Now, by using central differences, the pressure terms are approximated as:

$$\left(\frac{\partial P_o}{\partial x}\right)_{i+\frac{1}{2}}=\frac{P_{o\,i+1}-P_{oi}}{\Delta x_{i+\frac{1}{2}}} \tag{A.22}$$

$$\left(\frac{\partial P_o}{\partial x}\right)_{i-\frac{1}{2}} = \frac{P_{o\,i} - P_{oi-1}}{\Delta x_{i-\frac{1}{2}}} \tag{A.23}$$

Then, substituting equations (A.22) and (A.23) into equation (A.21) results in:

$$\frac{\partial}{\partial x}\left(\beta A_x K_x \frac{k_{rw}}{\mu_w B_w}\left(\frac{\partial P_o}{\partial x}\right)\right)_i \Delta x \approx$$
$$\left(\beta A_x K_x \frac{k_{rw}}{\mu_w B_w \Delta x}\right)_{i+\frac{1}{2}} \left(P_{oi+1} - P_{oi}\right) - \left(\beta A_x K_x \frac{k_{rw}}{\mu_w B_w \Delta x}\right)_{i-\frac{1}{2}} \left(P_{oi} - P_{oi-1}\right) = \tag{A.24}$$
$$T_{wx_{i+\frac{1}{2},j,k}} \left(P_{oi+1} - P_{oi}\right)_{j,k} - T_{wx_{i-\frac{1}{2},j,k}} \left(P_{oi} - P_{oi-1}\right)_{j,k}$$

The coefficients $T_{wx_{i+\frac{1}{2},j,k}}$ and $T_{wx_{i-\frac{1}{2},j,k}}$ refer to the water transmissibilities of the porous medium and are defined as:

$$T_{wx_{i+\frac{1}{2},j,k}} = \left(\beta A_x K_x \frac{k_{rw}}{\mu_w B_w \Delta x}\right)_{i+\frac{1}{2},j,k} \tag{A.25}$$

$$T_{wx_{i-\frac{1}{2},j,k}} = \left(\beta A_x K_x \frac{k_{rw}}{\mu_w B_w \Delta x}\right)_{i-\frac{1}{2},j,k} \tag{A.26}$$

Similarity, the equations for oil transmissibilities are as follows;

$$T_{ox_{i+\frac{1}{2},j,k}} = \left(\beta A_x K_x \frac{k_{ro}}{\mu_o B_o \Delta x}\right)_{i+\frac{1}{2},j,k} \tag{A.27}$$

$$T_{ox_{i-\frac{1}{2},j,k}} = \left(\beta A_x K_x \frac{k_{ro}}{\mu_o B_o \Delta x}\right)_{i-\frac{1}{2},j,k} \tag{A.28}$$

*T*he transmissibility of a porous medium is considered to be a property of the porous medium, the fluid flowing through the medium, the direction of flow, and the position in space. To discretize the right hand side of equations (A.25) to (A.28),

different averaging methods are considered. $\left(\beta\frac{A_x K_x}{\Delta x}\right)_{ave}$ is calculated with the weighted harmonic average method, while $\left(\frac{k_{ro}}{\mu_o B_o}\right)$ is found based on the single point upstream method.

Finally, the water-oil finite expansion of differential equation (A.19) can be approximated by:

$$\begin{Bmatrix}\left(T_w+T_o\right)_{i+\frac{1}{2},j,k}\left(P_{o_{i+1}}^{n+1}-P_{o_i}^{n+1}\right)_{j,k}+\left(T_w+T_o\right)_{i-\frac{1}{2},j,k}\left(P_{o_{i-1}}^{n+1}-P_{o_i}^{n+1}\right)_{j,k}+\\ \left(T_w+T_o\right)_{i,j+\frac{1}{2},k}\left(P_{o_{j+1}}^{n+1}-P_{o_j}^{n+1}\right)_{i,k}+\left(T_w+T_o\right)_{i,j-\frac{1}{2},k}\left(P_{o_{j-1}}^{n+1}-P_{o_j}^{n+1}\right)_{i,k}+\\ \left(T_w+T_o\right)_{i,j,k+\frac{1}{2}}\left(P_{o_{k+1}}^{n+1}-P_{o_k}^{n+1}\right)_{i,j}+\left(T_w+T_o\right)_{i,j,k-\frac{1}{2}}\left(P_{o_{k-1}}^{n+1}-P_{o_k}^{n+1}\right)_{i,j}+\end{Bmatrix}-$$
$$\begin{Bmatrix}\left(T_w\gamma_w+T_o\gamma_o\right)_{i+\frac{1}{2},j,k}\left(D_{i+1}-D_i\right)_{j,k}+\left(T_w\gamma_w+T_o\gamma_o\right)_{i-\frac{1}{2},j,k}\left(D_{i-1}-D_i\right)_{j,k}+\\ \left(T_w\gamma_w+T_o\gamma_o\right)_{i,j+\frac{1}{2},k}\left(D_{j+1}-D_j\right)_{i,k}+\left(T_w\gamma_w+T_o\gamma_o\right)_{i,j-\frac{1}{2},k}\left(D_{j-1}-D_j\right)_{i,k}+\\ \left(T_w\gamma_w+T_o\gamma_o\right)_{i,j,k+\frac{1}{2}}\left(D_{k+1}-D_k\right)_{i,j}+\left(T_w\gamma_w+T_o\gamma_o\right)_{i,j,k-\frac{1}{2}}\left(D_{k-1}-D_k\right)_{i,j}+\end{Bmatrix}-$$
$$\begin{Bmatrix}\left(T_w\right)_{i+\frac{1}{2},j,k}\left(P_{c_{i+1}}^{n}-P_{c_i}^{n}\right)_{j,k}+\left(T_w\right)_{i-\frac{1}{2},j,k}\left(P_{c_{i-1}}^{n}-P_{c_i}^{n}\right)_{j,k}+\\ \left(T_w\right)_{i,j+\frac{1}{2},k}\left(P_{c_{j+1}}^{n}-P_{c_j}^{n}\right)_{i,k}+\left(T_w\right)_{i,j-\frac{1}{2},k}\left(P_{c_{j-1}}^{n}-P_{c_j}^{n}\right)_{i,k}+\\ \left(T_w\right)_{i,j,k+\frac{1}{2}}\left(P_{c_{k+1}}^{n}-P_{c_k}^{n}\right)_{i,j}+\left(T_w\right)_{i,j,k-\frac{1}{2}}\left(P_{c_{k-1}}^{n}-P_{c_k}^{n}\right)_{i,j}+\end{Bmatrix}=\frac{V_{b_{i,j,k}}}{\alpha\Delta t}\left(\phi^0 c_\phi\right)_{i,j,k}\left(P_o^{n+1}-P_o^{n}\right)_{i,j,k}$$

(A.29)

All transmisibilities in the above equation is calculated at time step *n*. To reduce the round-off errors, equation (A.29) can be written by adding and subtracting the first braces in the time step n as follows:

$$
\begin{Bmatrix}
\left(T_w+T_o\right)_{i+\frac{1}{2},j,k}\left(\Delta P_{o_{i+1}}^{n+1}-\Delta P_{o_i}^{n+1}\right)_{j,k}+\left(T_w+T_o\right)_{i-\frac{1}{2},j,k}\left(\Delta P_{o_{i-1}}^{n+1}-\Delta P_{o_i}^{n+1}\right)_{j,k}+\\
\left(T_w+T_o\right)_{i,j+\frac{1}{2},k}\left(\Delta P_{o_{j+1}}^{n+1}-\Delta P_{o_j}^{n+1}\right)_{i,k}+\left(T_w+T_o\right)_{i,j-\frac{1}{2},k}\left(\Delta P_{o_{j-1}}^{n+1}-\Delta P_{o_j}^{n+1}\right)_{i,k}+\\
\left(T_w+T_o\right)_{i,j,k+\frac{1}{2}}\left(\Delta P_{o_{k+1}}^{n+1}-\Delta P_{o_k}^{n+1}\right)_{i,j}+\left(T_w+T_o\right)_{i,j,k-\frac{1}{2}}\left(\Delta P_{o_{k-1}}^{n+1}-\Delta P_{o_k}^{n+1}\right)_{i,j}+
\end{Bmatrix}+
$$

$$
\begin{Bmatrix}
\left(T_w+T_o\right)_{i+\frac{1}{2},j,k}\left(P_{o_{i+1}}^{n}-P_{o_i}^{n}\right)_{j,k}+\left(T_w+T_o\right)_{i-\frac{1}{2},j,k}\left(P_{o_{i-1}}^{n}-P_{o_i}^{n}\right)_{j,k}+\\
\left(T_w+T_o\right)_{i,j+\frac{1}{2},k}\left(P_{o_{j+1}}^{n}-P_{o_j}^{n}\right)_{i,k}+\left(T_w+T_o\right)_{i,j-\frac{1}{2},k}\left(P_{o_{j-1}}^{n}-P_{o_j}^{n}\right)_{i,k}+\\
\left(T_w+T_o\right)_{i,j,k+\frac{1}{2}}\left(P_{o_{k+1}}^{n}-P_{o_k}^{n}\right)_{i,j}+\left(T_w+T_o\right)_{i,j,k-\frac{1}{2}}\left(P_{o_{k-1}}^{n}-P_{o_k}^{n}\right)_{i,j}+
\end{Bmatrix}
$$

$$
\begin{Bmatrix}
\left(T_w\gamma_w+T_o\gamma_o\right)_{i+\frac{1}{2},j,k}\left(D_{i+1}-D_i\right)_{j,k}+\left(T_w\gamma_w+T_o\gamma_o\right)_{i-\frac{1}{2},j,k}\left(D_{i-1}-D_i\right)_{j,k}+\\
\left(T_w\gamma_w+T_o\gamma_o\right)_{i,j+\frac{1}{2},k}\left(D_{j+1}-D_j\right)_{i,k}+\left(T_w\gamma_w+T_o\gamma_o\right)_{i,j-\frac{1}{2},k}\left(D_{j-1}-D_j\right)_{i,k}+\\
\left(T_w\gamma_w+T_o\gamma_o\right)_{i,j,k+\frac{1}{2}}\left(D_{k+1}-D_k\right)_{i,j}+\left(T_w\gamma_w+T_o\gamma_o\right)_{i,j,k-\frac{1}{2}}\left(D_{k-1}-D_k\right)_{i,j}+
\end{Bmatrix}-
$$

$$
\begin{Bmatrix}
\left(T_w\right)_{i+\frac{1}{2},j,k}\left(P_{c_{i+1}}^{n}-P_{c_i}^{n}\right)_{j,k}+\left(T_w\right)_{i-\frac{1}{2},j,k}\left(P_{c_{i-1}}^{n}-P_{c_i}^{n}\right)_{j,k}+\\
\left(T_w\right)_{i,j+\frac{1}{2},k}\left(P_{c_{j+1}}^{n}-P_{c_j}^{n}\right)_{i,k}+\left(T_w\right)_{i,j-\frac{1}{2},k}\left(P_{c_{j-1}}^{n}-P_{c_j}^{n}\right)_{i,k}+\\
\left(T_w\right)_{i,j,k+\frac{1}{2}}\left(P_{c_{k+1}}^{n}-P_{c_k}^{n}\right)_{i,j}+\left(T_w\right)_{i,j,k-\frac{1}{2}}\left(P_{c_{k-1}}^{n}-P_{c_k}^{n}\right)_{i,j}+
\end{Bmatrix}=\frac{V_{b_{i,j,k}}}{\alpha\Delta t}\left(\phi^0 c_\phi\right)_{i,j,k}\left(\Delta P_o^{n+1}\right)_{i,j,k}
\tag{A.30}
$$

where $\Delta P_o^{n+1}=P_o^{n+1}-P_o^{n}$.

The left side of the equation (A.30) is the total velocity. So, the finite difference form of the water phase velocity is presented as an example in the following equation:

$$
u_{x\,i+\frac{1}{2},j,k}^{w}=-\left(K_x\frac{k_{rw}}{\mu_w\Delta x}\right)_{i+\frac{1}{2},j,k}\left[\left(P_{i+1,j,k}^{w}-P_{i,j,k}^{w}\right)-\gamma_w\left(D_{i+1,j,k}-D_{i,j,k}\right)\right]
\tag{A.31}
$$

Also, the flow rates of each phase can be determined at the interface between the matrix and fracture using the phase Darcy velocities. For instance, the following equation represents water flow:

$$q^w = A\left(u^w \Delta t\right) = -\left[T^w\left(\Delta P^w - \gamma_w \Delta D\right)\right]\Big|_{boundary} \Delta t \qquad \text{(A. 32)}$$

Appendix B: Derivation of Differential Equation Describing Surfactant Concentration

The material-balance equation of surfactant over the finite control volume of a porous medium, shown in figure (3.1), over time interval Δt is:

$$m_{in} - m_{out} - m_{cons.} = m_{acc.} \tag{B.1}$$

Surfactant can exist in both the water phase and oil phase, so in Cartesian coordinates; the material-balance equation for surfactant can be written as follows:

$$\left(m\big|_x + m\big|_y + m\big|_z\right)\Big|_{s-in} - \left(m\big|_x + m\big|_y + m\big|_z\right)\Big|_{s-out} = m_{acc.} + m_{cons.} \tag{B.2}$$

The left terms of the above equation may be expressed with both bulk flow and dispersive flux ($\vec{\vec{D}}'$) as:

$$m_{s-in/out}\big|_x = \alpha\left(\rho_w \omega_{sw} u_{w-x} - \vec{\vec{D}}'_{sw} + \rho_o \omega_{so} u_{o-x} - \vec{\vec{D}}'_{so}\right)_{in/out}\left(\Delta y \Delta z \Delta t\right) \tag{B.3}$$

$$m_{s-in/out}\big|_y = \alpha\left(\rho_w \omega_{sw} u_{w-y} - \vec{\vec{D}}'_{sw} + \rho_w \omega_{so} u_{o-y} - \vec{\vec{D}}'_{so}\right)_{in/out}\left(\Delta x \Delta z \Delta t\right) \tag{B.4}$$

$$m_{s-in/out}\big|_z = \alpha\left(\rho_w \omega_{sw} u_{w-z} - \vec{\vec{D}}'_{sw} + \rho_o \omega_{so} u_{o-z} - \vec{\vec{D}}'_{so}\right)_{in/out}\left(\Delta x \Delta y \Delta t\right) \tag{B.5}$$

Also,

$$\begin{aligned} m_{acc.} = &\left(\phi\rho_w S_w \omega_{sw} + \phi\rho_o S_o \omega_{so} + (1-\phi)\rho_{gr}\omega_{sg}\right)\left(\Delta x \Delta y \Delta z\right)\Big|_{t+\Delta t} \\ &- \left(\phi\rho_w S_w \omega_{sw} + \phi\rho_o S_o \omega_{so} + (1-\phi)\rho_{gr}\omega_{sg}\right)\left(\Delta x \Delta y \Delta z\right)\Big|_{t} \end{aligned} \tag{B.6}$$

Where α is the volume conversion factor, ρ_{gr} is grain density (lb_m/ft^3), ω_{sw} and ω_{so} are surfactant concentration in water and oil phase (mass fraction) respectively, and ω_{sg} is the adsorbed concentration of surfactant (mass fraction) (Green and Willhite

1998). It is assumed that the dispersive flux terms are presented in a Fickian form as follows:

$$\begin{aligned}\vec{\vec{D}}'_{sw} &= \rho_w \vec{\vec{D}}_{sw} = \rho_w \phi S_w D^0_{sw}\left(\frac{\partial \omega_{sw}}{\partial x}+\frac{\partial \omega_{sw}}{\partial y}+\frac{\partial \omega_{sw}}{\partial z}\right)\\ \vec{\vec{D}}'_{so} &= \rho_o \vec{\vec{D}}_{so} = \rho_o \phi S_o D^0_{so}\left(\frac{\partial \omega_{so}}{\partial x}+\frac{\partial \omega_{so}}{\partial y}+\frac{\partial \omega_{so}}{\partial z}\right)\end{aligned} \tag{B.7}$$

If the phase volume (phase β) does not change during a process, then the mass fraction and volume fraction of component α can be correlated as follows (Orr 2007):

$$\rho_\beta \omega_{\alpha\beta} = \rho_\alpha C_{\alpha\beta} \tag{B.8}$$

By considering equation (B.8) and substituting equations (B.3)-(B.6) into equation (B.2), the following mass-conservation equation is obtained assuming surfactant density is constant:

$$\begin{aligned}&\left[\begin{array}{l}\alpha\left(C_{sw}u_{w-x}-\vec{\vec{D}}_{sw}+C_{so}u_{o-x}-\vec{\vec{D}}_{so}\right)\left(\Delta y\Delta z\Delta t\right)+\\ \alpha\left(C_{sw}u_{w-y}-\vec{\vec{D}}_{sw}+C_{so}u_{o-y}-\vec{\vec{D}}_{so}\right)\left(\Delta x\Delta z\Delta t\right)+\\ \alpha\left(C_{sw}u_{w-z}-\vec{\vec{D}}_{sw}+C_{so}u_{o-z}-\vec{\vec{D}}_{so}\right)\left(\Delta x\Delta y\Delta t\right)\end{array}\right]_{in}-\left[\begin{array}{l}\alpha\left(C_{sw}u_{w-x}-\vec{\vec{D}}_{sw}+C_{so}u_{o-x}-\vec{\vec{D}}_{so}\right)\left(\Delta y\Delta z\Delta t\right)+\\ \alpha\left(C_{sw}u_{w-y}-\vec{\vec{D}}_{sw}+C_{so}u_{o-y}-\vec{\vec{D}}_{so}\right)\left(\Delta x\Delta z\Delta t\right)+\\ \alpha\left(C_{sw}u_{w-z}-\vec{\vec{D}}_{sw}+C_{so}u_{o-z}-\vec{\vec{D}}_{so}\right)\left(\Delta x\Delta y\Delta t\right)\end{array}\right]_{out}=\\ &\left(\phi S_w C_{sw}+\phi S_o C_{so}+(1-\phi)C_{sg}\right)\left(\Delta x\Delta y\Delta z\right)\Big|_{t+\Delta t}-\left(\phi S_w C_{sw}+\phi S_o C_{so}+(1-\phi)C_{sg}\right)\left(\Delta x\Delta y\Delta z\right)\Big|_{t}\end{aligned} \tag{B.9}$$

Assume that:

$$A_x = \Delta y\Delta z,\ A_y = \Delta x\Delta z,\ A_z = \Delta x\Delta y,\ V_b = \Delta x\Delta y\Delta z \tag{B.10}$$

By dividing equation (B.9) to $\Delta x\Delta y\Delta z\Delta t$ and taking the limit of terms enclosed in the brackets as Δx, Δy, Δz, and Δt all approach zero, based on the definition of the partial derivative, equation (B.9) becomes:

$$
\begin{aligned}
&-\frac{\partial}{\partial x}\left(\left(C_{sw}u_{w-x}-\vec{\vec{D}}_{sw}\right)+\left(C_{so}u_{o-x}-\vec{\vec{D}}_{so}\right)\right)\\
&-\frac{\partial}{\partial y}\left(\left(C_{sw}u_{w-y}-\vec{\vec{D}}_{sw}\right)+\left(C_{so}u_{o-y}-\vec{\vec{D}}_{so}\right)\right)\\
&-\frac{\partial}{\partial z}\left(\left(C_{sw}u_{w-z}-\vec{\vec{D}}_{sw}\right)+\left(C_{so}u_{o-z}-\vec{\vec{D}}_{so}\right)\right)\\
&=\frac{1}{\alpha}\frac{\partial}{\partial t}\left(\phi\left(S_wC_{sw}+S_oC_{so}\right)+\left(1-\phi\right)C_{sg}\right)
\end{aligned}
\qquad (B.11)
$$

This equation is the final mass balance differential equation for surfactant. Now, both sides of the above equation are multiplied by V_b, and then the above equation can be rewritten as:

$$
\begin{aligned}
&-\frac{\partial}{\partial x}\left(A_x\left[\left(C_{sw}u_{w-x}-\vec{\vec{D}}_{sw}\right)+\left(C_{so}u_{o-x}-\vec{\vec{D}}_{so}\right)\right]\right)\Delta x\\
&-\frac{\partial}{\partial y}\left(A_y\left[\left(C_{sw}u_{w-y}-\vec{\vec{D}}_{sw}\right)+\left(C_{so}u_{o-y}-\vec{\vec{D}}_{so}\right)\right]\right)\Delta y\\
&-\frac{\partial}{\partial z}\left(A_z\left[\left(C_{sw}u_{w-z}-\vec{\vec{D}}_{sw}\right)+\left(C_{so}u_{o-z}-\vec{\vec{D}}_{so}\right)\right]\right)\Delta z\\
&=\frac{V_b}{\alpha}\frac{\partial}{\partial t}\left(\phi\left(S_wC_{sw}+S_oC_{so}\right)+\left(1-\phi\right)C_{sg}\right)
\end{aligned}
\qquad (B.12)
$$

or;

$$
\begin{aligned}
&-\frac{\partial}{\partial x}\left(A_x\left[\left(C_{sw}u_{w-x}+C_{so}u_{o-x}\right)-\left(\vec{\vec{D}}_{sw}+\vec{\vec{D}}_{so}\right)\right]\right)\Delta x\\
&-\frac{\partial}{\partial y}\left(A_y\left[\left(C_{sw}u_{w-y}+C_{so}u_{o-y}\right)-\left(\vec{\vec{D}}_{sw}+\vec{\vec{D}}_{so}\right)\right]\right)\Delta y\\
&-\frac{\partial}{\partial z}\left(A_z\left[\left(C_{sw}u_{w-z}+C_{so}u_{o-z}\right)-\left(\vec{\vec{D}}_{sw}+\vec{\vec{D}}_{so}\right)\right]\right)\Delta z\\
&=\frac{V_b}{\alpha}\frac{\partial}{\partial t}\left(\phi\left(S_wC_{sw}+S_oC_{so}\right)+\left(1-\phi\right)C_{sg}\right)
\end{aligned}
\qquad (B.13)
$$

And finally,

$$
\begin{aligned}
&-\frac{\partial}{\partial x}\left(A_x\left(C_{sw}u_{w-x}+C_{sw}u_{o-x}\right)\right)\Delta x+\frac{\partial}{\partial x}\left(A_x\left(\bar{\bar{D}}_{sw}+\bar{\bar{D}}_{so}\right)\right)\Delta x\\
&-\frac{\partial}{\partial y}\left(A_y\left(C_{sw}u_{w-y}+C_{sw}u_{o-y}\right)\right)\Delta y+\frac{\partial}{\partial y}\left(A_y\left(\bar{\bar{D}}_{sw}+\bar{\bar{D}}_{so}\right)\right)\Delta y\\
&-\frac{\partial}{\partial z}\left(A_z\left(C_{sw}u_{w-z}+C_{sw}u_{o-z}\right)\right)\Delta z+\frac{\partial}{\partial z}\left(A_z\left(\bar{\bar{D}}_{sw}+\bar{\bar{D}}_{so}\right)\right)\Delta z\\
&=\frac{V_b}{\alpha}\frac{\partial}{\partial t}\left(\phi C_{sw}\left(S_w+K_pS_o\right)+\left(1-\phi\right)C_{sg}\right)
\end{aligned}
\qquad \text{(B.14)}
$$

If we assume that $K_p=\dfrac{C_{so}}{C_{sw}}$ (partitioning factor), then equation (B.14) can be written as follows:

$$
\begin{aligned}
&-\frac{\partial}{\partial x}\left(A_xC_{sw}\left(u_{w-x}+K_pu_{o-x}\right)\right)\Delta x+\frac{\partial}{\partial x}\left(A_x\left(\bar{\bar{D}}_{sw}+\bar{\bar{D}}_{so}\right)\right)\Delta x\\
&-\frac{\partial}{\partial y}\left(A_yC_{sw}\left(u_{w-y}+K_pu_{o-y}\right)\right)\Delta y+\frac{\partial}{\partial y}\left(A_y\left(\bar{\bar{D}}_{sw}+\bar{\bar{D}}_{so}\right)\right)\Delta y\\
&-\frac{\partial}{\partial z}\left(A_zC_{sw}\left(u_{w-z}+K_pu_{o-z}\right)\right)\Delta z+\frac{\partial}{\partial z}\left(A_z\left(\bar{\bar{D}}_{sw}+\bar{\bar{D}}_{so}\right)\right)\Delta z\\
&=\frac{V_b}{\alpha}\frac{\partial}{\partial t}\left(\phi C_{sw}\left(S_w+K_pS_o\right)+\left(1-\phi\right)C_{sg}\right)
\end{aligned}
\qquad \text{(B.15)}
$$

Hence, if surfactant does not exist in the oil phase, for example, the partitioning factor will be zero.

Each term of the above equation can be named as follows:

$$
\begin{aligned}
AA^x=&-\frac{\partial}{\partial x}\left(A_xC_{sw}\left(u_{w-x}+K_pu_{o-x}\right)\right)\Delta x=\\
&-\left[\frac{\partial}{\partial x}\left(A_x\left(u_{w-x}+K_pu_{o-x}\right)\right)\Delta x\right]\left(C_{sw}\right)\Big|_x-\left[A_x\left(u_{w-x}+K_pu_{o-x}\right)\right]\Big|_x\left(\frac{\partial C_{sw}}{\partial x}\Delta x\right)
\end{aligned}
\qquad \text{(B.16)}
$$

$$
\begin{aligned}
AA^y=&-\frac{\partial}{\partial y}\left(A_yC_{sw}\left(u_{w-y}+K_pu_{o-y}\right)\right)\Delta y=\\
&-\left[\frac{\partial}{\partial y}\left(A_y\left(u_{w-y}+K_pu_{o-y}\right)\right)\Delta y\right]\left(C_{sw}\right)\Big|_y-\left[A_y\left(u_{w-y}+K_pu_{o-y}\right)\right]\Big|_y\left(\frac{\partial C_{sw}}{\partial y}\Delta y\right)
\end{aligned}
\qquad \text{(B.17)}
$$

$$AA^z = -\frac{\partial}{\partial z}\left(A_z C_{sw}\left(u_{w-z} + K_p u_{o-z}\right)\right)\Delta z = -\left[\frac{\partial}{\partial z}\left(A_z\left(u_{w-z} + K_p u_{o-z}\right)\right)\Delta z\right]\left(C_{sw}\right)\Big|_z - \left[A_z\left(u_{w-z} + K_p u_{o-z}\right)\right]\Big|_z\left(\frac{\partial C_{sw}}{\partial z}\Delta z\right) \tag{B.18}$$

$$BB^x = \frac{\partial}{\partial x}\left(A_x\left(\bar{\bar{D}}_{sw} + \bar{\bar{D}}_{so}\right)\right)\Delta x \tag{B.19}$$

$$BB^y = \frac{\partial}{\partial y}\left(A_y\left(\bar{\bar{D}}_{sw} + \bar{\bar{D}}_{so}\right)\right)\Delta y \tag{B.20}$$

$$BB^z = \frac{\partial}{\partial z}\left(A_z\left(\bar{\bar{D}}_{sw} + \bar{\bar{D}}_{so}\right)\right)\Delta z \tag{B.21}$$

$$CC = \frac{V_b}{\alpha}\frac{\partial}{\partial t}\left(\phi C_{sw}\left(S_w + K_p S_o\right) + \left(1-\phi\right)C_{sg}\right) \tag{B.22}$$

Discretization of equation (B.16) is as follows:

$$AA^x = -\frac{\partial}{\partial x}\left(A_x C_{sw}\left(u_{w-x} + K_p u_{o-x}\right)\right)\Delta x = \underbrace{-\left[\frac{\partial}{\partial x}\left(A_x\left(u_{w-x} + K_p u_{o-x}\right)\right)\Delta x\right]}_{\mathrm{AA}_1^x}\left(C_{sw}\right)\Big|_x \underbrace{-\left[A_x\left(u_{w-x} + K_p u_{o-x}\right)\right]\Big|_x}_{AA_2^x}\underbrace{\left(\frac{\partial C_{sw}}{\partial x}\Delta x\right)}_{AA_3^x} \tag{B.23}$$

$$AA_1^x = -\frac{\partial}{\partial x}\left(A_x\left(u_{w-x} + K_p u_{o-x}\right)\right)\Delta x \tag{B.24}$$

$$AA_2^x = -\left(A_x\left(u_{w-x} + K_p u_{o-x}\right)\right)\Big|_x \tag{B.25}$$

$$AA_3^x = \frac{\partial C_{sw}}{\partial x}\Delta x \tag{B.26}$$

Darcy equation for phase "η" can be written as following:

$$u_\eta = -0.006328\frac{k_\eta}{\mu_\eta}\nabla\psi_\eta = -0.006328\frac{Kk_{r\eta}}{\mu_\eta}\left(\nabla P_\eta - \frac{\rho_\eta}{144}\nabla D\right) \tag{B.27}$$

where,

$$\nabla P = \left(\frac{\partial P}{\partial x}, \frac{\partial P}{\partial y}, \frac{\partial P}{\partial z} \right), \nabla D = \left(\frac{\partial D}{\partial x}, \frac{\partial D}{\partial y}, \frac{\partial D}{\partial z} \right) \tag{B.28}$$

If the following values are defined as follows:

$$\beta = 0.006328, B_\eta = \frac{\rho_{\eta-sc}}{\rho_\eta}, \gamma_\eta = \frac{\rho_\eta}{144} \tag{B.29}$$

then by applying equations (B.27) to (B.29) in equation (B.24), the latter equation can be written as follows:

$$\begin{aligned} AA_1^x &= -\frac{\partial}{\partial x}\left(A_x\left(u_{w-x} + K_p u_{o-x}\right)\right)\Delta x = \\ &\frac{\partial}{\partial x}\left(\beta A_x K_x \frac{k_{rw}}{\mu_w}\left(\frac{\partial P_w}{\partial x} - \gamma_w \frac{\partial D}{\partial x}\right) + K_p \beta A_x K_x \frac{k_{ro}}{\mu_o}\left(\frac{\partial P_o}{\partial x} - \gamma_o \frac{\partial D}{\partial x}\right)\right)\Delta x \end{aligned} \tag{B.30}$$

By considering equation 3.3 (the capillary pressure equation), equation (B.30) is rearranged as follows:

$$\begin{aligned} AA_1^x &= \frac{\partial}{\partial x}\left(\beta A_x K_x \frac{k_{rw}}{\mu_w}\left(\frac{\partial P_o}{\partial x} - \frac{\partial P_c}{\partial x} - \gamma_w \frac{\partial D}{\partial x}\right) + K_p \beta A_x K_x \frac{k_{ro}}{\mu_o}\left(\frac{\partial P_o}{\partial x} - \gamma_o \frac{\partial D}{\partial x}\right)\right)\Delta x = \\ &\frac{\partial}{\partial x}\left(\beta A_x K_x \left(\frac{k_{rw}}{\mu_w} + K_p \frac{k_{ro}}{\mu_o}\right)\left(\frac{\partial P_o}{\partial x}\right)\right)\Delta x - \frac{\partial}{\partial x}\left(\beta A_x K_x \left(\gamma_w \frac{k_{rw}}{\mu_w} + K_p \gamma_o \frac{k_{ro}}{\mu_o}\right)\left(\frac{\partial D}{\partial x}\right)\right)\Delta x \\ &- \frac{\partial}{\partial x}\left(\beta A_x K_x \frac{k_{rw}}{\mu_w}\left(\frac{\partial P_c}{\partial x}\right)\right)\Delta x \end{aligned} \tag{B. 31}$$

To discretize the above equation, it is necessary to use the central-difference approximation for the first derivatives. For example, the water part of the first term of equation (B.31) can be approximated as follows:

$$\frac{\partial}{\partial x}\left(\beta A_x K_x \frac{k_{rw}}{\mu_w B_w}\left(\frac{\partial P_o}{\partial x}\right)\right)_i \Delta x \approx$$

$$\frac{1}{\Delta x_i}\left\{\left(\beta A_x K_x \frac{k_{rw}}{\mu_w B_w}\frac{\partial P_o}{\partial x}\right)_{i+\frac{1}{2}} - \left(\beta A_x K_x \frac{k_{rw}}{\mu_w B_w}\frac{\partial P_o}{\partial x}\right)_{i-\frac{1}{2}}\right\} \times \Delta x = \tag{B.32}$$

$$\left(\beta A_x K_x \frac{k_{rw}}{\mu_w B_w}\right)_{i+\frac{1}{2}}\left(\frac{\partial P_o}{\partial x}\right)_{i+\frac{1}{2}} - \left(\beta A_x K_x \frac{k_{rw}}{\mu_w B_w}\right)_{i-\frac{1}{2}}\left(\frac{\partial P_o}{\partial x}\right)_{i-\frac{1}{2}}$$

Now, by using central differences, the pressure terms are approximated as follows:

$$\left(\frac{\partial P_o}{\partial x}\right)_{i+\frac{1}{2}} = \frac{P_{o\,i+1} - P_{oi}}{\Delta x_{i+\frac{1}{2}}} \tag{B.33}$$

$$\left(\frac{\partial P_o}{\partial x}\right)_{i-\frac{1}{2}} = \frac{P_{o\,i} - P_{oi-1}}{\Delta x_{i-\frac{1}{2}}} \tag{B.34}$$

Then, substituting equations (B.33) and (B.34) into equation (B.32) results in:

$$\frac{\partial}{\partial x}\left(\beta A_x K_x \frac{k_{rw}}{\mu_w B_w}\left(\frac{\partial P_o}{\partial x}\right)\right)_i \Delta x \approx$$

$$\left(\beta A_x K_x \frac{k_{rw}}{\mu_w B_w \Delta x}\right)_{i+\frac{1}{2}}\left(P_{oi+1} - P_{oi}\right) - \left(\beta A_x K_x \frac{k_{rw}}{\mu_w B_w \Delta x}\right)_{i-\frac{1}{2}}\left(P_{oi} - P_{oi-1}\right) = \tag{B.35}$$

$$T_{wx_{i+\frac{1}{2},j,k}}\left(P_{oi+1} - P_{oi}\right)_{j,k} - T_{wx_{i-\frac{1}{2},j,k}}\left(P_{oi} - P_{oi-1}\right)_{j,k}$$

The above transmissibilities can be defined as:

$$T_{wx_{i+\frac{1}{2},j,k}} = \beta\left(\frac{K_x A_x}{\Delta x}\right)_{i+\frac{1}{2},j,k}\left(\frac{k_{rw}}{\mu_w}\right)_{i+\frac{1}{2},j,k} \tag{B.36}$$

$$T_{wx_{i-\frac{1}{2},j,k}} = \beta\left(\frac{K_x A_x}{\Delta x}\right)_{i-\frac{1}{2},j,k}\left(\frac{k_{rw}}{\mu_w}\right)_{i-\frac{1}{2},j,k} \tag{B.37}$$

Similarity,

$$T_{ox_{i+\frac{1}{2},j,k}} = \beta\left(\frac{K_x A_x}{\Delta x}\right)_{i+\frac{1}{2},j,k}\left(\frac{k_{ro}}{\mu_o}\right)_{i+\frac{1}{2},j,k} \tag{B.38}$$

$$T_{ox_{i-\frac{1}{2},j,k}} = \beta\left(\frac{K_x A_x}{\Delta x}\right)_{i-\frac{1}{2},j,k}\left(\frac{k_{ro}}{\mu_o}\right)_{i-\frac{1}{2},j,k} \tag{B.39}$$

So, by applying the above transmissibility equations, equation (B.31) can be summarized as the equation below:

$$\begin{aligned} AA_1^x = &\left(T_w + K_p T_o\right)_{i+\frac{1}{2},j,k}\left(P_{oi+1,j,k} - P_{oi,j,k}\right) - \left(\gamma_w T_w + K_p \gamma_o T_o\right)_{i+\frac{1}{2},j,k}\left(D_{i+1,j,k} - D_{i,j,k}\right) - T_{w_{i+\frac{1}{2},j,k}}\left(P_{c_{i+1,j,k}} - P_{c_{i,j,k}}\right) + \\ &\left(T_w + K_p T_o\right)_{i-\frac{1}{2},j,k}\left(P_{oi-1,j,k} - P_{oi,j,k}\right) - \left(\gamma_w T_w + K_p \gamma_o T_o\right)_{i-\frac{1}{2},j,k}\left(D_{i-1,j,k} - D_{i,j,k}\right) - T_{w_{i-\frac{1}{2},j,k}}\left(P_{c_{i-1,j,k}} - P_{c_{i,j,k}}\right) \end{aligned} \tag{B.40}$$

Now, it is necessary to discretize equations of (B.25) and (B.26) as well:

$$\begin{aligned} AA_2^x &= -\left(A_x\left(u_{w-x} + K_p u_{o-x}\right)\right)\Big|_x = -\left(A_x u_{w-x} + K_p A_x u_{o-x}\right)\Big|_x \\ &= -\left(A_x u_{w-x} + K_p A_x u_{o-x}\right)\Big|_{i,j,k} \end{aligned} \tag{B.41}$$

Where,

$$\left(A_x u_{w-x}\right)_{i,j,k} = \text{Resultant}\left\{\left(A_x u_{w-x}\right)_{i+\frac{1}{2},j,k}, \left(A_x u_{w-x}\right)_{i-\frac{1}{2},j,k}\right\} \tag{B.42}$$

$$\left(A_x u_{o-x}\right)_{i,j,k} = \text{Resultant}\left\{\left(A_x u_{o-x}\right)_{i+\frac{1}{2},j,k}, \left(A_x u_{o-x}\right)_{i-\frac{1}{2},j,k}\right\} \tag{B.43}$$

Also;

$$\begin{aligned} AA_3^x &= \frac{\partial C_{sw}}{\partial x}\Delta x = \frac{C_{sw_{i+\frac{1}{2},j,k}} - C_{sw_{i-\frac{1}{2},j,k}}}{\Delta x}\Delta x = \left[\frac{C_{sw_{i+1,j,k}} + C_{sw_{i,j,k}}}{2} - \frac{C_{sw_{i,j,k}} + C_{sw_{i-1,j,k}}}{2}\right] \\ &= \frac{C_{sw_{i+1,j,k}} - C_{sw_{i-1,j,k}}}{2} \end{aligned} \tag{B.44}$$

So, equation (B.16) can be summarized as follows:

$$AA^x = \left(AA_1^x\right)C_{sw}\big|_x + \left(AA_2^x\right)\left(AA_3^x\right) =$$
$$\left\{\begin{array}{l}\left(T_w + K_pT_o\right)_{i+\frac{1}{2},j,k}\left(P_{oi+1,j,k} - P_{oi,j,k}\right) - \left(\gamma_wT_w + K_p\gamma_oT_o\right)_{i+\frac{1}{2},j,k}\left(D_{i+1,j,k} - D_{i,j,k}\right) - T_{w_{i+\frac{1}{2},j,k}}\left(P_{c_{i+1,j,k}} - P_{c_{i,j,k}}\right) + \\ \left(T_w + K_pT_o\right)_{i-\frac{1}{2},j,k}\left(P_{oi-1,j,k} - P_{oi,j,k}\right) - \left(\gamma_wT_w + K_p\gamma_oT_o\right)_{i-\frac{1}{2},j,k}\left(D_{i-1,j,k} - D_{i,j,k}\right) - T_{w_{i-\frac{1}{2},j,k}}\left(P_{c_{i-1,j,k}} - P_{c_{i,j,k}}\right)\end{array}\right\}C_{sw_{i,j,k}}$$
$$-\left(A_xu_{w-x} + K_pA_xu_{o-x}\right)\Big|_{i,j,k}\left(\frac{C_{sw_{i+1,j,k}} - C_{sw_{i-1,j,k}}}{2}\right) \tag{B.45}$$

By applying the same procedure, then:

$$AA^y = \left(AA_1^y\right)C_{sw}\big|_y + \left(AA_2^y\right)\left(AA_3^y\right) =$$
$$\left\{\begin{array}{l}\left(T_w + K_pT_o\right)_{i,j+\frac{1}{2},k}\left(P_{oi,j+1,k} - P_{oi,j,k}\right) - \left(\gamma_wT_w + K_p\gamma_oT_o\right)_{i,j+\frac{1}{2},k}\left(D_{i,j+1,k} - D_{i,j,k}\right) - T_{w_{i,j+\frac{1}{2},k}}\left(P_{c_{i,j+1,k}} - P_{c_{i,j,k}}\right) + \\ \left(T_w + K_pT_o\right)_{i,j-\frac{1}{2},k}\left(P_{oi,j-1,k} - P_{oi,j,k}\right) - \left(\gamma_wT_w + K_p\gamma_oT_o\right)_{i,j-\frac{1}{2},k}\left(D_{i,j-1,k} - D_{i,j,k}\right) - T_{w_{i,j-\frac{1}{2},k}}\left(P_{c_{i,j-1,k}} - P_{c_{i,j,k}}\right)\end{array}\right\}C_{sw_{i,j,k}}$$
$$-\left(A_yu_{w-y} + K_pA_yu_{o-y}\right)\Big|_{i,j,k}\left(\frac{C_{sw_{i,j+1,k}} - C_{sw_{i,j-1,k}}}{2}\right) \tag{B.46}$$

$$AA^z = \left(AA_1^z\right)C_{sw}\big|_z + \left(AA_2^z\right)\left(AA_3^z\right) =$$
$$\left\{\begin{array}{l}\left(T_w + K_pT_o\right)_{i,j,k+\frac{1}{2}}\left(P_{oi,j,k+1} - P_{oi,j,k}\right) - \left(\gamma_wT_w + K_p\gamma_oT_o\right)_{i,j,k+\frac{1}{2}}\left(D_{i,j,k+1} - D_{i,j,k}\right) - T_{w_{i,j,k+\frac{1}{2}}}\left(P_{c_{i,j,k+1}} - P_{c_{i,j,k}}\right) + \\ \left(T_w + K_pT_o\right)_{i,j,k-\frac{1}{2}}\left(P_{oi,j,k-1} - P_{oi,j,k}\right) - \left(\gamma_wT_w + K_p\gamma_oT_o\right)_{i,j,k-\frac{1}{2}}\left(D_{i,j,k-1} - D_{i,j,k}\right) - T_{w_{i,j,k-\frac{1}{2}}}\left(P_{c_{i,j,k-1}} - P_{c_{i,j,k}}\right)\end{array}\right\}C_{sw_{i,j,k}}$$
$$-\left(A_zu_{w-z} + K_pA_zu_{o-z}\right)\Big|_{i,j,k}\left(\frac{C_{sw_{i,j,k+1}} - C_{sw_{i,j,k-1}}}{2}\right) \tag{B.47}$$

Now, the molecular diffusion terms needs to be discretized as follows:

$$BB^x = \frac{\partial}{\partial x}\left(A_x\left(\tilde{\tilde{D}}_{sw} + \tilde{\tilde{D}}_{so}\right)\right)\Delta x \tag{B.48}$$

The molecular dispersion can be expanded as:

$$\tilde{\tilde{D}}_{sw} = \phi S_w D_{sw}^0 \left(\frac{\partial C_{sw}}{\partial x} + \frac{\partial C_{sw}}{\partial y} + \frac{\partial C_{sw}}{\partial z} \right) \tag{B.49}$$

By applying partitioning factor for surfactant diffusion in oil phase, then:

$$\tilde{\tilde{D}}_{so} = \phi S_o D_{so}^0 \left(\frac{\partial C_{so}}{\partial x} + \frac{\partial C_{so}}{\partial y} + \frac{\partial C_{so}}{\partial z} \right) = \phi S_o D_{so}^0 K_p \left(\frac{\partial C_{sw}}{\partial x} + \frac{\partial C_{sw}}{\partial y} + \frac{\partial C_{sw}}{\partial z} \right) \tag{B.50}$$

So, equation (B.48) can be written as the following equation:

$$\begin{aligned} BB^x &= \frac{\partial}{\partial x} \left(A_x \left(\tilde{\tilde{D}}_{sw} + \tilde{\tilde{D}}_{so} \right) \right) \Delta x = \frac{\partial}{\partial x} \left(A_x \left(\phi S_w D_{sw}^0 + \phi S_o D_{so}^0 K_p \right) \left(\frac{\partial C_{sw}}{\partial x} + \frac{\partial C_{sw}}{\partial y} + \frac{\partial C_{sw}}{\partial z} \right) \right) \Delta x \\ &\cong \frac{\partial}{\partial x} \left(A_x \left(\phi S_w D_{sw}^0 + \phi S_o D_{so}^0 K_p \right) \left(\frac{\partial C_{sw}}{\partial x} \right) \right) \Delta x \end{aligned} \tag{B.51}$$

Now, the applied procedure through equations (B.32) to (B.35) is used here, so, transmissibilities of the above equation should be defined as follows:

$$T'_{x_{i+\frac{1}{2},j,k}} = \left[\frac{A_x}{\Delta x} \left(\phi S_w D_{sw}^0 + \phi S_o D_{so}^0 K_p \right) \right]_{i+\frac{1}{2},j,k} \tag{B.52}$$

$$T'_{x_{i-\frac{1}{2},j,k}} = \left[\frac{A_x}{\Delta x} \left(\phi S_w D_{sw}^0 + \phi S_o D_{so}^0 K_p \right) \right]_{i-\frac{1}{2},j,k} \tag{B.53}$$

So,

$$BB^x = T'_{x\,i+\frac{1}{2},j,k} \left(C_{sw_{i+1,j,k}} - C_{sw_{i,j,k}} \right) + T'_{x\,i-\frac{1}{2},j,k} \left(C_{sw_{i-1,j,k}} - C_{sw_{i,j,k}} \right) \tag{B.54}$$

Similarity,

$$BB^y = T'_{y\,i,j+\frac{1}{2},k} \left(C_{sw_{i,j+1,k}} - C_{sw_{i,j,k}} \right) + T'_{y\,i,j-\frac{1}{2},k} \left(C_{sw_{i,j-1,k}} - C_{sw_{i,j,k}} \right) \tag{B.55}$$

$$BB^z = T'_{z\,i,j,k+\frac{1}{2}} \left(C_{sw_{i,j,k+1}} - C_{sw_{i,j,k}} \right) + T'_{z\,i,j,k-\frac{1}{2}} \left(C_{sw_{i,j,k-1}} - C_{sw_{i,j,k}} \right) \tag{B.56}$$

Now, the right side of equation (B.15) is discretized as follows:

$$CC = \frac{V_b}{\alpha}\frac{\partial}{\partial t}\left(\phi C_{sw}\left(S_w + K_p S_o\right) + \left(1-\phi\right)C_{sg}\right) \tag{B.57}$$

Mathematically speaking, (Ertekin *et al.* 2001):

$$\Delta_t\left(UVX\right) = X^{n+1}V^n\Delta_t U + X^n U^n \Delta_t V + V^{n+1}U^n\Delta_t X \tag{B.58}$$

So,

$$\begin{aligned}\frac{\partial}{\partial t}\left(C_{sw}\phi\left(S_w + K_p S_o\right)\right) = \phi^n\left(S_w + K_P S_o\right)^{n+1}\frac{\partial C_{sw}}{\partial t} + \left[C_{sw}\left(S_w + K_P S_o\right)\right]^n\frac{\partial \phi}{\partial t} \\ + \phi^{n+1}C_{sw}^n\left(1-K_P\right)\frac{\partial S_w}{\partial t}\end{aligned} \tag{B.59}$$

$$\frac{\partial}{\partial t}\left(\left(1-\phi\right)C_{sg}\right) = \left(1-\phi\right)^{n+1}\frac{\partial C_{sg}}{\partial t} + C_{sg}^n\frac{\partial \phi}{\partial t} = \left(1-\phi\right)^{n+1}\frac{\partial C_{sg}}{\partial C_{sw}}\times\frac{\partial C_{sw}}{\partial t} - C_{sg}^n\frac{\partial \phi}{\partial t} \tag{B.60}$$

C_{sg} can be found by using the Langmuir-Type isotherm equation (equation 3.17 or B.64). So, equation (B.57) can be summarized as the following equation by considering equation $\phi = \phi^0\left[1 + c_\phi\left(P - P^0\right)\right]$:

$$\begin{aligned}CC &= \frac{V_b}{\alpha}\frac{\partial}{\partial t}\left(\phi C_{sw}\left(S_w + K_p S_o\right) + \left(1-\phi\right)C_{sg}\right) \\ &= \frac{V_b}{\alpha}\left\{\begin{array}{l}\left[\phi^n\left(S_w + K_p S_o\right)^{n+1} + \left(1-\phi\right)^{n+1}\dfrac{\partial C_{sg}}{\partial C_{sw}}\right]\dfrac{\partial C_{sw}}{\partial t} + \\ \left[C_{sw}\left(S_w + K_p S_o\right) - C_{sg}\right]^n \phi_0 c_\phi \dfrac{dP_o}{dt} + \phi^{n+1}C_{sw}^n\left(1-K_p\right)\dfrac{\partial S_w}{\partial t}\end{array}\right\}\end{aligned} \tag{B.61}$$

Equation (B.61) can be approximately written as follows:

$$
\begin{aligned}
CC &\cong \frac{V_b}{\alpha}\left\{\begin{array}{l}\left[\phi^n\left(S_w+K_pS_o\right)^{n+1}+\left(1-\phi\right)^{n+1}\frac{\partial C_{sg}}{\partial C_{sw}}\right]\frac{\Delta C_{sw}}{\Delta t}+\\ \left[C_{sw}\left(S_w+K_pS_o\right)-C_{sg}\right]^n\phi_0 c_\phi\frac{\Delta P_o}{\Delta t}+\phi^{n+1}C_{sw}^n\left(1-K_p\right)\frac{\partial S_w}{\partial t}\end{array}\right\}\\
&= \frac{V_b}{\alpha\Delta t}\left\{\begin{array}{l}\left[\phi^n\left(S_w+K_pS_o\right)^{n+1}+\left(1-\phi\right)^{n+1}\frac{\partial C_{sg}}{\partial C_{sw}}\right]\Delta C_{sw}+\\ \left[C_{sw}\left(S_w+K_pS_o\right)-C_{sg}\right]^n\phi_0 c_\phi\Delta P_o+\phi^{n+1}C_{sw}^n\left(1-K_p\right)\Delta S_w\end{array}\right\}\\
&= \underbrace{\frac{V_b}{\alpha\Delta t}\left[\left(C_{sw}\left(S_w+K_pS_o\right)-C_{sg}\right)^n\phi_0 c_\phi\Delta P_o+\phi^{n+1}C_{sw}^n\left(1-K_p\right)\Delta S_w\right]}_{HHH}\\
&+\underbrace{\frac{V_b}{\alpha\Delta t}\left[\phi^n\left(S_w+K_pS_o\right)^{n+1}+\left(1-\phi\right)^{n+1}\frac{\partial C_{sg}}{\partial C_{sw}}\right]}_{JJJ}\Delta C_{sw}
\end{aligned}
\tag{B.62}
$$

where,

$$
\begin{aligned}
\Delta P_o &= P_o^{n+1}-P_o^n\\
\Delta S_w &= S_w^{n+1}-S_w^n\\
\Delta C_{sw} &= C_{sw}^{n+1}-C_{sw}^n
\end{aligned}
\tag{B.63}
$$

$$
C_{sg}=\frac{aC_{sw}}{1+bC_{sw}} \text{ and } \frac{\partial C_{sg}}{\partial C_{sw}}=\frac{a}{\left(1+bC_{sw}\right)^2}
\tag{B.64}
$$

Because pressure and saturation values are known in time *n+1*, all parameters in *HHH* and *JJJ* are known. Finally, the surfactant concentration equation can be summarized as:

$$\left(AA_1^x+AA_1^y+AA_1^z-\left(T'_{x\,i+\frac{1}{2},j,k}+T'_{x\,i-\frac{1}{2},j,k}+T'_{y\,i,j+\frac{1}{2},k}+T'_{y\,i,j-\frac{1}{2},k}+T'_{z\,i,j,k+\frac{1}{2}}+T'_{z\,i,j,k-\frac{1}{2}}\right)\right)C^{n+1}_{sw\;i,j,k}+$$
$$\left(\frac{AA_2^x}{2}+T'_{x\,i+\frac{1}{2},j,k}\right)C^{n+1}_{sw_{i+1,j,k}}+\left(-\frac{AA_2^x}{2}+T'_{x\,i-\frac{1}{2},j,k}\right)C^{n+1}_{sw_{i-1,j,k}}+$$
$$\left(\frac{AA_2^y}{2}+T'_{y\,i,j+\frac{1}{2},k}\right)C^{n+1}_{sw_{i,j+1,k}}+\left(-\frac{AA_2^y}{2}+T'_{y\,i,j-\frac{1}{2},k}\right)C^{n+1}_{sw_{i,j-1,k}}+$$
$$\left(\frac{AA_2^z}{2}+T'_{z\,i,j,k+\frac{1}{2}}\right)C^{n+1}_{sw_{i,j,k+1}}+\left(-\frac{AA_2^z}{2}+T'_{z\,i,j,k-\frac{1}{2}}\right)C^{n+1}_{sw_{i,j,k-1}}=HHH+JJJ\left(C^{n+1}_{sw}-C^{n}_{sw}\right)_{i,j,k}$$

(B.65)

To reduce round-off errors, equation (B.65) can be written by adding and subtracting the left hand side of the above equation in the time step n as follows:

$$\left(AA_1^x+AA_1^y+AA_1^z-\left(T'_{x\,i+\frac{1}{2},j,k}+T'_{x\,i-\frac{1}{2},j,k}+T'_{y\,i,j+\frac{1}{2},k}+T'_{y\,i,j-\frac{1}{2},k}+T'_{z\,i,j,k+\frac{1}{2}}+T'_{z\,i,j,k-\frac{1}{2}}+JJJ\right)\right)\Delta C^{n+1}_{sw\;i,j,k}+$$
$$\left(\frac{AA_2^x}{2}+T'_{x\,i+\frac{1}{2},j,k}\right)\Delta C^{n+1}_{sw_{i+1,j,k}}+\left(-\frac{AA_2^x}{2}+T'_{x\,i-\frac{1}{2},j,k}\right)\Delta C^{n+1}_{sw_{i-1,j,k}}+$$
$$\left(\frac{AA_2^y}{2}+T'_{y\,i,j+\frac{1}{2},k}\right)\Delta C^{n+1}_{sw_{i,j+1,k}}+\left(-\frac{AA_2^y}{2}+T'_{y\,i,j-\frac{1}{2},k}\right)\Delta C^{n+1}_{sw_{i,j-1,k}}+$$
$$\left(\frac{AA_2^z}{2}+TT_D\right)\Delta C^{n+1}_{sw_{i,j,k+1}}+\left(-\frac{AA_2^z}{2}+TT_U\right)\Delta C^{n+1}_{sw_{i,j,k-1}}=HHH-$$
$$\left[\begin{array}{l}\left(AA_1^x+AA_1^y+AA_1^z-\left(T'_{x\,i+\frac{1}{2},j,k}+T'_{x\,i-\frac{1}{2},j,k}+T'_{y\,i,j+\frac{1}{2},k}+T'_{y\,i,j-\frac{1}{2},k}+T'_{z\,i,j,k+\frac{1}{2}}+T'_{z\,i,j,k-\frac{1}{2}}\right)\right)C^{n}_{swi,j,k}+\\ \left(\frac{AA_2^x}{2}+T'_{x\,i+\frac{1}{2},j,k}\right)C^{n}_{sw_{i+1,j,k}}+\left(-\frac{AA_2^x}{2}+T'_{x\,i-\frac{1}{2},j,k}\right)C^{n}_{sw_{i-1,j,k}}+\\ \left(\frac{AA_2^y}{2}+T'_{y\,i,j+\frac{1}{2},k}\right)C^{n}_{sw_{i,j+1,k}}+\left(-\frac{AA_2^y}{2}+T'_{y\,i,j-\frac{1}{2},k}\right)C^{n}_{sw_{i,j-1,k}}+\\ \left(\frac{AA_2^z}{2}+T'_{z\,i,j,k+\frac{1}{2}}\right)C^{n}_{sw_{i,j,k+1}}+\left(-\frac{AA_2^z}{2}+T'_{z\,i,j,k-\frac{1}{2}}\right)C^{n}_{sw_{i,j,k-1}}\end{array}\right]$$

(B.66)

Appendix C:

Property	Values for case study:									
	1	2	3	4	5	6	7	8	9	10
Oil relative permeability endpoint	0.75	0.75	0.9	0.85	0.981	0.981	1.00	0.501	0.59	0.501
Water relative permeability endpoint	0.6	0.6	0.65	0.381	0.702	0.702	0.751	0.851	0.23	0.9
Oil relative permeability exponent	1.5	1.5	1.5	1.3	3.0	3.0	2.0	3.0	3.3	4.5
Water relative permeability exponent	3.8	3.8	1.8	1.5	1.81	1.81	2.5	2.51	2.9	2.25
Capillary pressure endpoint	15	0.01	0.017	0.097	-5.01	-5.01	-0.11	-1.01	-5.0	-5.01
Capillary pressure exponent	3.0	3.0	2.0	1.2	2.1	2.1	13.0	6.0	2.0	2.0
Residual oil Saturation	0.15	0.15	0.56	0.475	0.5	0.5	0.362	0.295	0.38	0.25
Residual water saturation	0.092	0.092	0	0	0.3	0.3	0.235	0	0.32	0.275
Initial interfacial tension	38.1	0.026	38.1	36.8	50	50	15.4	15.4	19.95	30
ε in interfacial tension model	-	-	-	-	-	10	9	9	9	-
η in interfacial tension model	-	-	-	-	-	0.3	0.22	0.22	0.22	-
Initial contact angle	-	-	-	-	-	-	70	120	120	160
Final contact angle	-	-	-	-	-	-	12	70	55	65
Critical micelle concentration	-	-	-	-	-	0.0008	0.0012	0.0012	0.00005	0.00005
d in wettability alteration model	-	-	-	-	-	-	-2.0	-3.0	-3.0	-0.8
Water trapping value	-	-	-	-	-	-	20000	20000	59000	59000
Oil trapping value	-	-	-	-	-	-	10000	1000	2000	2000
Initial trapping number	-	-	-	-	-	-	3.3E-10	3.3E-10	6.3E-10	1.0E-10
a in Equation 3.17	-	-	-	-	-	-	12	12	-	-
b in Equation 3.17	-	-	-	-	-	-	1000	1000	-	-

References:

Adams, W.T. and Schievelbein, V.H. (1987) "Surfactant flooding carbonate reservoirs" *SPE Reservoir Engineering*, **2** (4): 619-626.

Adamson, W. and Gast, A.P. (1997) "Physical Chemistry of Surfaces", 6th edition, Wiley: New York. p. 784.

Adibhatla, B. and Mohanty, K.K. (2007) "SPE 106161: Simulation of Surfactant-Aided Gravity Drainage in Fractured Carbonates" in *SPE Reservoir Simulation Symposium*. Houston, TX: Society of Petroleum Engineers.

Adibhatla, B. and Mohanty, K.K. (2008) "SPE 99773: Oil Recovery from Fractured Carbonates by Surfactant-aided Gravity Drainage: Laboratory Experiments and Mechanistic Simulations" *SPE Reservoir Evaluation & Engineering*, **11** (1): 119-130.

Adibhatla, B., Sun, X., and Mohanty, K.K. (2005) "SPE 97678: Numerical Studies of Oil Production from Initially Oil-wet Fracture Blocks by Surfactant Brine Imbibition" in *Improved Oil Recovery Conference in Asia Pacific*. Kuala Lumpur, Malaysia: Society of Petroleum Engineers.

Ahmed, T. (2001) "Reservoir Engineering Handbook", 2nd edition, Gulf Professional Publishing: Houston, TX. p. 1186.

Amott, E. (1959) "Observations Relating to the Wettability of Porous Rock" *Petroleum Transactions, AIME*, **216**: 156–162.

Anderson, G.A. (2006), "Simulation of Chemical Flood Enhanced Oil Recovery Processes Including the Effects of Reservoir Wettability." *Petroleum &*

Geosystems Engineering Department at University of Taxes at Austin: Austin, TX. p. 252.

Anderson, W.G. (1986a) "SPE 13932: Wettability Literature Survey-part 1: Rock/Oil/Brine Interactions and the Effects of Core Handling on Wettability" *Journal of Petroleum Technology*, **38** (10): 1125-1144.

Anderson, W.G. (1986b) "SPE 13933: Wettability Literature Survey-part 2: Wettability Measurement" *Journal of Petroleum Technology*, **38** (11): 1246-1262.

Austad, T., Matre, B., Milter, J., Sævareid, A., and Øyno, L. (1998) "Chemical Flooding of Oil Reservoirs 8. Spontaneous Oil Expulsion from Oil-and Water-wet Low Permeable Chalk Material by Imbibition of Aqueous Surfactant Solutions" *Colloids and Surfaces A: Physicochemical and Engineering Aspects*, **137** (1-3): 117-129.

Austad, T. and Milter, J. (1997) "SPE 37236: Spontaneous Imbibition of Water into Low Permeable Chalk at Different Wettabilities Using Surfactants" in *International Symposium on Oilfield Chemistry*. Houston, TX: Society of Petroleum Engineers.

Austad, T. and Standnes, D.C. (2003) "Spontaneous Imbibition of Water into Oil-wet Carbonates" *Journal of Petroleum Science and Engineering*, **39** (3): 363-376.

Austad, T., Strand, S., Madland, M.V., Puntervold, T., and Korsnes, R.I. (2008) "SPE 118431: Seawater in Chalk: An EOR and Compaction Fluid" *SPE Reservoir Evaluation & Engineering*, **11** (4): 648-654.

Babadagli, T. (2003) "SPE 84866: Analysis of Oil Recovery by Spontaneous Imbibition of Surfactant Solution " in *SPE International Improved Oil Recovery Conference in Asia Pacific*. Kuala Lumpur, Malaysia: Society of Petroleum Engineers

Bardon, C. and Longeron, D.G. (1980) "SPE 7609: Influence of Very Low Interfacial Tensions on Relative Permeability" *SPE Journal*, **20** (5): 391-401.

Behrenbruch, P. and Goda, H.M. (2006) "SPE 101150: Two-Phase Relative Permeability Prediction: A Comparison of the Modified Brooks-Corey Methodology with a New Carman-Kozeny-Based Flow Formulation" in *SPE Asia Pacific Oil & Gas Conference and Exhibition*. Adelaide, Australia: Society of Petroleum Engineers.

Blair, P.M. (1964) "SPE 873: Calculation of Oil Displacement by Countercurrent Water Imbibition" *Journal of Society of Petroleum Engineers*, **4** (3): 195-202.

Bourbiaux, B.J. and Kalaydjian, F.J. (1990) "SPE 18283: Experimental Study of Cocurrent and Countercurrent Flows in Natural Porous Media" *SPE Reservoir Engineering*, **5** (3): 361-368.

Brooks, R.H. and Corey, A.T. (1965) "Properties of Porous Media Affecting Fluid Flow", Colorado Agricultural Experiment Station. p.

Brown, R.J.S., Fatt, I., and Habra, L. (1956) "SPE 743-G: Measurements of Fractional Wettability of Oil Fields' Rocks by The Nuclear Magnetic Relaxation Method" in *31st Annual Fall Meeting of the Petroleum Branch of*

the American Institute of Mining, Metallurgical, and Petroleum Engineers. Los Angeles: Petroleum Branch, AIME.

Burdine, N.T. (1953) "Relative Permeability Calculations from Pore-size Distribution Data" *Transactions of the American Institute of Mining, Metallurgical and Petroleum Engineers*, **198**: 71-78.

Carman, P.C. (1937) "Fluid Flow through Granular Beds" *Chemical Engineering Research and Design*, **15** (a): 150-166.

Chen, H.L., Lucas, L.R., Nogaret, L.A.D., Yang, H.D., and Kenyon, D.E. (2001) "SPE 69197: Laboratory Monitoring of Surfactant Imbibition With Computerized Tomography" *SPE Reservoir Evaluation and Engineering*, **4** (1): 16-25.

Chilingar, G.V. and Yen, T.F. (1993) "Some Notes on Wettability and Relative Permeabilities of Carbonate Reservoir Rocks, II" *Energy Sources, Part A: Recovery, Utilization, and Environmental Effects*, **7** (1): 67-75.

Cinar, Y., Marquez, S., and Orr, F.M. (2007) "SPE 90572: Effect of IFT Variation and Wettability on Three-Phase Relative Permeability" *SPE Reservoir Evaluation & Engineering*, **10** (3): 10.

Coats, K.H. (1980) "SPE 8284: An Equation of State Compositional Model" *SPE Journal*, **20** (5): 363-376.

Coats, K.H. (1982) "SPE 10020: Reservoir Simulation: State of the Art" *Journal of Petroleum Technology*, **34** (8): 1633-1642.

Cole, F.W. (1969) "Reservoir Engineering Manual", 2nd edition, Gulf Publishing Company: Houston. p.

Corey, A.T. (1954) "The Interrelation between Gas and Oil Relative Permeabilities" *Transactions of the American Institute of Mining, Metallurgical and Petroleum Engineers*, **19** (1): 38-41.

Corey, A.T., Rathjens, C.H., Henderson, J.H., and Wyllie, M.R.J. (1956) "Three-phase Relative Permeability" *Transactions of the American Institute of Mining, Metallurgical and Petroleum Engineers*, **207**: 349-351.

Craig, F.F. (1971) "The Reservoir Engineering Aspects of Waterflooding", SPE: Dallas, TX. p. 134.

Cuiec, L.E., Evaluation of Reservoir Wettability and Its Effect on Oil Recovery in Interfacial Phenomena in Petroleum Recovery, N.R. Morrow ed., Marcel Dekker Inc.: New York (1991), 319-373.

Cuiec, L.E., Bourbiaux, B., and Kalaydjian, F. (1994) "SPE 20259: Oil Recovery by Imbibition in Low-Permeability Chalk " *SPE Formation Evaluation*, **9** (3): 200-208.

Dandekar, A.Y. (2006) "Petroleum Reservoir Rock and Fluid Properties", Taylor & Francis: Boca Raton. p. 460.

Darcy, H. (1856) "Les Fontaines Publiques De La Ville De Dyon", Victor Dalmont. p.

Delshad, M., Najafabadi, N.F., Anderson, G., Pope, G.A., and Sepehrnoori, K. (2006) "SPE 100081: Modeling Wettability Alteration in Naturally Fractured

Reservoirs" in *Improved Oil Recovery Symposium*. Tulsa, OK: Society of Petroleum Engineers.

Delshad, M., Najafabadi, N.F., and Sepehrnoori, K. (2009) "SPE 118915: Scale Up Methodology for Wettability Modification in Fractured Carbonates" in *SPE Reservoir Simulation Symposium*. The Woodlands, TX: Society of Petroleum Engineers.

Delshad, M., Pope, G.A., and Sepehrnoori, K. (1996) "A Compositional Simulator for Modeling Surfactant Enhanced Aquifer Remediation, 1 Formulation" *Journal of Contaminant Hydrology*, **23** (4): 303-327.

Demond, A.H. and Roberts, P.V. (1987) "An Experimental of Relative Permeability Relations for Two-phase Flow in Porous Media" *Water Resources Bulletin*, **23** (4): 12.

Dicarlo, D.A., Sahni, A., and Blunt, M.J. (2000) "The Effect of Wettability on Three-phase Relative Permeability" *Transport in Porous Media*, **39**: 347-366.

Donaldson, E.C., Thomas, R.D., and Lorenz, P.B. (1969) "SPE 2338: Wettability Determination and Its Effect on Recovery Efficiency" *SPE Journal*, **9** (1): 13-20.

Doust, A.R., T.P.Puntervold, S.Strand, and Austad, T. (2009) "EAGE B12: Smart Water as Wettability Modifier in Carbonate and Sandstone" in *15th European Symposium on Improved Oil Recovery*. Paris, France: European Association of Geoscientists and Engineers.

Downs, H.H. and Hoover, P.D. (1989) "Oil Field Chemistry: Enhanced Recovery and Production Stimulation", American Chemical Society: Washington, DC. p.

Ehrlich, R., Hasiba, H.H., and Raimondi, P. (1974) "SPE 4905: Alkaline Waterflooding for Wettability Alteration-Evaluating a Potential Field Application" *Journal of Petroleum Technology*, **26** (12): 1335-1343.

Ertekin, T., Abou-Kassem, J.H., and King, G.R. (2001) "Basic Applied Reservoir Simulation", SPE: Richardson, TX. p. 406.

Firoozabadi, A. and Aziz, K. (1986) "SPE 15059: Relative Permeability from Centrifuge Data" in *SPE California Regional Meeting*. Oakland, CA: Society of Petroleum Engineers.

Fischer, H. and Morrow, N.R. (2005) "SPE 96812: Spontaneous Imbibition with Matched Liquid Viscosities" in *SPE Annual Technical Conference and Exhibition*. Dallas, TX: Society of Petroleum Engineers.

Fletcher, P.D.I. and Nicholls, R.J. (2000) "Contact Angles of Surfactant Solutions in Oil Solvents on Low Energy Solid Surfaces" *Physics and Chemistry*, **2**: 4.

Genuchten, M.T.V. and Nielsen, D.R. (1985) "On Describing and Predicting the Hydraulic Properties of Unsaturated Soils" *Annuls Geophysical*, **3** (5): 13.

Green, D.W. and Willhite, P.G. (1998) "Enhanced Oil Recovery", Society of Petroleum Engineers: Richardson, TX. p.

Gupta, R., Adibhatla, B., and Mohanty, K.K. (2008) "SPE 116485: Parametric Study to Enhance Oil Recovery Rate From Fractured Oil-Wet Carbonate Reservoirs"

in *SPE Annual Technical Conference and Exhibition*. Denver, CO: Society of Petroleum Engineers.

Gupta, R. and Mohanty, K.K. (2008) "SPE 113407: Wettability Alteration of Fractured Carbonate Reservoirs" in *Improved Oil Recovery Symposium*. Tulsa, OK: Society of Petroleum Engineers.

Gupta, S.P. and Trushenski, S.P. (1979) "SPE 7063: Micellar Flooding - Compositional Effects on Oil Displacement " *SPE Journal*, **19** (2): 116-128.

Hamon, G. and Vidal, J. (1986) "SPE 15852: Scaling-Up the Capillary Imbibition Process From Laboratory Experiments on Homogeneous and Heterogeneous Samples" in *SPE European Petroleum Conference*. London, United Kingdom: Society of Petroleum Engineers.

Han, C., Delshad, M., Sepehrnoori, K., and Pope, G.A. (2007) "SPE 97217: A Fully Implicit, Parallel, Compositional Chemical Flooding Simulator" *SPE Journal*, **12** (3): 322-338.

Hidajat, I., Mohanty, K.K., Flaum, M., and Hirasaki, G. (2004) "SPE 88995: Study of Vuggy Carbonates Using NMR and X-Ray CT Scanning" *SPE Reservoir Evaluation & Engineering*, **7** (5): 365-378.

Hirasaki, G.J. (1981) "SPE 8373: Application of the Theory of Multi-component, Multiphase Displacement to Three-Component, Two-Phase Surfactant Flooding " *SPE Journal*, **21** (2): 191-204.

Hirasaki, G.J., Miller, C.A., and Pope, G.A., "Surfactant Based Enhanced Oil Recovery and Foam Mobility Control."(2004) 1st Annual Technical Report, DE-FC26-03NT15406.

Hirasaki, G.J., Miller, C.A., and Pope, G.A., "Surfactant Based Enhanced Oil Recovery and Foam Mobility Control."(2005) 2nd Annual Technical Report, DE-FC26-03NT15406.

Hirasaki, G.J., Miller, C.A., and Pope, G.A., "Surfactant Based Enhanced Oil Recovery and Foam Mobility Control."(2006) 3rd Annual Technical Report, DE-FC26-03NT15406.

Hirasaki, G.J., Miller, C.A., and Puerto, M. (2008) "SPE 115386: Recent Advances in Surfactant EOR" in *SPE Annual Technical Conference and Exhibition*. Denver, CO: Society of Petroleum Engineers.

Hirasaki, G.J., Rohan, J.A., and Dudley, J.W. (1992) "SPE 25290: Modification of Centrifuge and Software for Determination of Relative Permeability Curves" *SPE Unsolicited Paper*.

Hirasaki, G.J., Rohan, J.A., and Dudley, J.W. (1995) "SPE 24879: Interpretation of Oil/Water Relative Permeabilities From Centrifuge Displacement" *SPE Advanced Technology Series*, **3** (1): 66-75.

Hirasaki, G.J. and Zhang, D.L. (2003) "SPE 80988: Surface Chemistry of Oil Recovery from Fractured, Oil-wet, Carbonate Formation" in *International Symposium in Oilfield Chemistry*. Houston, TX: Society of Petroleum Engineers

Hirasaki, G.J. and Zhang, D.L. (2004) "SPE 88365: Surface Chemistry of Oil Recovery from Fractured, Oil-wet, Carbonate Formations" *Journal of Petroleum Science and Engineering*, **9**: 151-162.

Høgnesen, E.J., Olsen, M., and Austad, T. (2006a) "Capillary and Gravity Dominated Flow Regimes in Displacement of Oil from an Oil-Wet Chalk Using Cationic Surfactant" *Energy & Fuels*, **20**: 1118-1122.

Hognesen, E.J., Standnes, D.C., and Austad, T. (2004) "Scaling Spontaneous Imbibition of Aqueous Surfactant Solution into Preferential Oil-wet Carbonates" *Energy & Fuels*, **18** (6): 1665-1675.

Hognesen, E.J., Standnes, D.C., and Austad, T. (2006) "Experimental and Numerical Investigation of High Temperature Imbibition into Preferential Oil-wet Chalk" *Journal of Petroleum Science and Engineering*, **53**: 100-112.

Høgnesen, E.J., Standnes, D.C., and Austad, T. (2004) "Scaling Spontaneous Imbibition of Aqueous Surfactant Solution into Preferential Oil-wet Carbonates" *Energy & Fuels*, **18** (6): 1665-1675.

Høgnesen, E.J., Standnes, D.C., and Austad, T. (2006b) "Experimental and Numerical Investigation of High Temperature Imbibition into Preferential Oil-wet Chalk" *Journal of Petroleum Science and Engineering*, **53**: 100-112.

Høgnesen, E.J., Strand, S., and Austad, T. (2005) "SPE 94166: Waterflooding of Preferential Oil-wet Carbonates: Oil Recovery Related to Reservoir Temperature and Brine Composition" in *Europec/EAGE Annual Conference*. Madrid, Spain: Society of Petroleum Engineers.

Honarpour, M., Koederitz, L., and Harvey, A.H. (1986) "Relative Permeability of Petroleum Reservoirs", C.R.C. Press Inc: Boca Raton, FL. p. 208.

Honarpour, M.M., Cromwell, V., Hatton, D., and Satchwell, R. (1985) "SPE 14272: Reservoir Rock Descriptions Using Computed Tomography (CT) " in *SPE Annual Technical Conference and Exhibition*. Las Vegas, NE: Society of Petroleum Engineering.

Jerauld, G.R. and Rathmell, J.J. (1997) "SPE 28576: Wettability and Relative Permeability of Prudhoe Bay: A Case Study in Mixed-Wet Reservoirs " *SPE Reservoir Engineering*, **12** (1): 58-65.

Jia, F., Zhou, K., Yangtze, U., and Li, K. (2006) "SPE 99893: Determination of Capillary Pressure and Relative Permeability From Spontaneous- Imbibition Data in Gas/Liquid/Rock " in *SPE Europec/EAGE Annual Conference and Exhibition*. Vienna, Austria: Society of Petroleum Engineers.

Johnson, S.J., Salehi, M., Eisert, K.E., Liang, J.-T., Bala, G., and Fox, S.L. (2007) "SPE 106078: Biosurfactants Produced From Agriculture Process Waste Streams To Improve Oil Recovery in Fractured Carbonate Reservoirs" in *International Symposium on Oilfield Chemistry*. Houston, TX: Society of Petroleum Engineering.

Kamath, J., deZabala, E.F., and R.E. Boyer (1995) "SPE 26092: Water/Oil Relative Permeability Endpoints of Intermediate-Wet, Low-Permeability Rocks " *SPE Formation Evaluation*, **10** (1): 4-10.

Kazemi, H. and Merrill, L.S. (1979) "SPE 6895: Numerical Simulation of Water Imbibition in Fractured Cores " *SPE Journal*, **19** (3): 175-182.

Killins, C.R., Nielsen, R.F., and Calhoun, J.C. (1953) "Capillary Desaturation and Imbibition in Porous Rocks" *Producers Monthly*, **18** (2): 30-39.

Knaebel, K.S., Adsorbent Selection. (2006). Adsorption Research, Inc.: Dublin, Ohio.

Kozeny, J. (1927) "Ueber kapillare Leitung des Wassers im Boden, Sitzungsberichte" *Sitzungsber. Akad. Wiss. Wien*, **136**: 271-306.

Kyte, J.R. (1970) "SPE 2729: A Centrifuge Method To Predict Matrix-Block Recovery in Fractured Reservoirs" *SPE Journal*, **10** (2): 164-170.

Kyte, J.R., Rapoport, L.A., and Tlhsa, O. (1958) "Linear Waterflood Behavior and End Effects in Water-wet Porous Media" *Transactions of the American Institute of Mining, Metallurgical and Petroleum Engineers*, **213**: 423-426.

Lake, L.W. (1989) "Enhanced Oil Recovery", Prentice Hall: New Jersey. p.

Li, K. and Horne, R.N. (2002) "SPE 77544: A General Scaling Method for Spontaneous Imbibition" in *SPE Annual Technical Conference and Exhibition*. SanAntonio, TX: Society of Petroleum Engineers.

Li, K. and Horne, R.N. (2006) "Generalized Scaling Approach for Spontaneous Imbibition: An Analytical Model" *SPE Reservoir Evaluation & Engineering*, **9** (3): 251-258.

Li, K., Peking, U., Chow, K., and Horne, R.N. (2006) "Influence of Initial Water Saturation on Recovery by Spontaneous Imbibition in Gas/Water/Rock

Systems and the Calculation of Relative Permeability" *SPE Reservoir Evaluation & Engineering*, **24** (10): 295-301.

Li, K., Yangtze, U., and Horne, R.N. (2005) "Computation of Capillary Pressure and Global Mobility from Spontaneous Water Imbibition into Oil-saturated Rock" *SPE Journal*, **10** (4): 458-465.

Ma, S., Morrow, N.R., and Zhang, X. (1995) "Paper 95138: Generalized Scaling of Spontaneous Imbibition Data for Strongly Water-wet Systems" in *6th Petroleum Conference of the South Saskatchewan Section*. Regina, Saskatchewan, Canada: The Petroleum Society of CIM.

Mattax, C.C. and Kyte, J.R. (1962) "SPE 187: Imbibition Oil Recovery from Fractured, Water-Drive Reservoir " *SPE Journal*, **2** (2): 177-184.

McCaffery, F.G. and Bennion, D.W. (1974) "The Effect of Wettability on Two-phase Relative Permeabilities" *Journal of Canadian Petroleum Technology*, **13**: 12.

McDougall, S.R., Salino, P.A., and Sorbie, K.S. (1997) "SPE 38920: The Effect of Interfacial Tension Upon Gas-Oil Relative Permeability Measurements: Interpretation Using Pore-Scale Models " in *SPE Annual Technical Conference and Exhibition*. San Antonio, TX: SPE.

Melrose, J.C. (1982) "SPE 10971: Interpretation of Mixed Wettability States in Reservoir Rocks" in *SPE Annual Technical Conference and Exhibition*. New Orleans, Louisiana: Society of Petroleum Engineers of AIME.

Milter, J. and Austad, T. (1996a) "Chemical Flooding of Oil Reservoirs 6. Evaluation of the Mechanism for Oil Expulsion by Spontaneous Imbibition of Brine with

and without Surfactant in Water-wet, Low Permeability Chalk Material" *Colloids and Surfaces A: Physicochemical and Engineering Aspects* **113**: 269-278.

Milter, J. and Austad, T. (1996b) "Chemical Flooding of Oil Reservoirs 7. Oil Expulsion by Spontaneous Imbibition of Brine with and without Surfactant in Mixed-wet, Low Permeability Chalk Material" *Colloids and Surfaces A: Physicochemical and Engineering Aspects*, **117** (1-2): 109-115.

Mohanty, K.K., "Dilute Surfactant Methods for Carbonate Formations."(2006) DE-FC26-02NT 15322.

Moreno, J., Kazemi, H., and Gilman, J.R. (2004) "SPE 89880: Streamline Simulation of Countercurrent Water-oil and Gas-Oil Flow in Naturally Fractured Dual-porosity Reservoirs " in *SPE Annual Technical Conference and Exhibition*. Houston, TX: Society of Petroleum Engineers.

Morrow, N.R. (1976) "Capillary Pressure Correlations for Uniformly Wetted Porous Media" *Journal of Canadian Petroleum Technology*, **15** (4): 49–69.

Morrow, N.R. (1990) "Wettability and Its Effect on Oil Recovery" *Journal of Petroleum Technology*, **42** (12): 9.

Morrow, N.R. and Mason, G. (2001) "Recovery of Oil by Spontaneous Imbibition" *Current Opinion in Colloid and Interface Science*, **6**: 321-337.

Morrow, N.R. and Songkran, B., Effect of Viscous and Buoyancy Forces on Nonwetting Phase Trapping in Porous Media in Surface Phenomena in

Enhanced Oil Recovery, D.O. Shah ed., Plenum Press: New York (1981), 387-411.

Najafabadi, N.F., Delshad, M., Kamy Sepehrnoori, Nguyen, Q.P., and Zhang, J. (2008) "SPE 113369: Chemical Flooding of Fractured Carbonates Using Wettability Modifiers" in *Improved Oil Recovery Symposium*. Tulsa, OK: Society of Petroleum Engineers.

Orr, F.M. (2007) "Theory of Gas Injection Processes", Tie-Line Publications: Denmark. p.

Osoba, J.S., Richardson, J.G., Kerver, J.K., Hafford, J.A., and Blair, P.M. (1951) "Laboratory Measurements of Relative Permeability" *Petroleum Transactions, AIME*, **192**: 10.

Parker, J.C., Lenhard, R.J., and Kuppusamy, T. (1987) "A Parametric Model for Constitutive Properties Governing Multiphase Flow in Porous Media" *Water Resources Research*, **23** (4): 7.

Perkins, F.M.J. (1957) "An Investigation of the Role of Capillary Forces in Laboratory Waterfloods" *Transactions of the American Institute of Mining, Metallurgical and Petroleum Engineers*, **210**: 409-411.

Pope, G.A. and Nelson, R.C. (1977) "Chemical Flooding Compositional Simulator" *Soc. Pet. Eng. AIME*, **6725** (52).

Pope, G.A., Wu, W., Narayanaswamy, G., Delshad, M., Sharma, M.M., and Wang, P. (2000) "Modeling Relative Permeability Effects in Gas-Condensate

Reservoirs With a New Trapping Model" *SPE Reservoir Evaluation & Engineering*, **3** (2): 8.

Purcell, W.R. (1949) "Capillary Pressures—Their Measurement Using Mercury and the Calculation of Permeability Therefrom" *Petroleum Transactions of AIME*, **186**: 39-48.

Pursley, S.A., Healy, R.N., and Sandvik, E.I. (1973) "Field test of surfactant flooding, Loudon, Illinois" *Journal of Petroleum Technology*, **25** (7): 793-802.

Resitsma, S. and Kueper, B.H. (1994) "Laboratory Measurement of Capillary Pressure-saturation Relationships in a Rock Fracture" *Water Resources Research*, **30** (4): 14.

Rosen, M.J. (1963) "Surfactants and Interfacial Phenomena", Wiley: New York. p.

Rosen, M.J. (1989) "Surfactants and Interfacial Phenomena", 2nd edition, John Wiley & Sons: New York. p. 431.

Salathiel, R.A. (1973) "SPE 4104: Oil Recovery by Surface Film Drainage In Mixed-wettability Rocks " *Journal of Petroleum Technology*, **25** (10): 1216-1224.

Salehi, M. (2009), "Enhancing Spontaneous Imbibition Process in Naturally Fractures Reservoirs through Wettability Alteration Using Surfactants: Mechanistic Study and Feasibility of Using Biosurfactants Produced from Agriculture Waste Streams." *Chemical and Petroleum Department* at University of Kansas: Lawrence, KS. p. 214.

Salehi, M., Johnson, S.J., and Liang, J.-T. (2008) "Mechanistic Study of Wettability Alteration Using Surfactants with Applications in Naturally Fractured Reservoirs" *Langmuir*, **24** (24): 14099-14107.

Schechter, D.S., Zhou, D., and Jr., F.M.O. (1991) "SPE 22594: Capillary Imbibition and Gravity Segregation in Low IFT Systems" in *SPE Annual Technical Conference and Exhibition*. Dallas, TX: Society of Petroleum Engineers.

Schechter, D.S., Zhou, D., and Jr., F.M.O. (1994) "Low IFT Drainage and Imbibition" *Journal of Petroleum Science and Engineering*, **11**: 283-300.

Schembre, J.M. and Kovscek, A.R. (2003) "A Technique for Measuring Two-phase Relative Permeability in Porous Media via X-ray CT Measurements" *Journal of Petroleum Science and Engineering*, **39**: 17.

Schneider, F.N. (1976) "SPE 5554: Relative Permeability Studies of Gas-Water Flow Following Solvent Injection in Carbonate Rocks" *SPE Journal*, **16** (1): 23-30.

Seethepalli, A., Adibhatla, B., and Mohanty, K.K. (2004) "SPE 89423: Wettability Alteration During Surfactant Flooding of Carbonate Reservoirs" in *Improved Oil Recovery Symposium*. Tulsa, OK: Society of Petroleum Engineers.

Shah, B.N. (1978), "An Experimental Study of Inaccessible Pore Volume, as a Function of Polymer Concentration, During Flow through Porous Media." *Chemical and Petroleum Engineering Department* at University of Kansas: Lawrence, KS. p.

Shen, P., Zhu, B., Li, X.-B., and Wu, Y.-S. (2006) "SPE 95405: The Influence of Interfacial Tension on Water/Oil Two-Phase Relative Permeability" in

SPE/DOE Symposium on Improved Oil Recovery. Tulsa, Oklahoma: Society of Petroleum Engineers.

Standnes, D.C. and Austad, T. (2000a) "Wettability Alteration in Chalk 1. Preparation of Core Material and Oil Properties" *Journal of Petroleum Science and Engineering*, **28** (3): 111-121.

Standnes, D.C. and Austad, T. (2000b) "Wettability Alteration in Chalk 2. Mechanism for Wettability Alteration from Oil-wet to Water-wet Using Surfactants" *Journal of Petroleum Science and Engineering*, **28** (3): 123-143.

Standnes, D.C. and Austad, T. (2003) "Wettability Alteration in Carbonates Interaction between Cationic Surfactant and Carboxylates as a Key Factor in Wettability Alteration from Oil-wet to Water-wet Conditions" *Colloids and Surfaces A: Physicochemical and Engineering Aspects*, **216** (1-3): 243-259.

Standnes, D.C., Nogaret, L.A.D., Chen, H.-L., and Austad, T. (2002) "An Evaluation of Spontaneous Imbibition of Water into Oil-wet Carbonate Reservoir Cores Using a Nanionic and a Cationic Surfactant" *Energy & Fuels*, **16**: 1557-1564.

Strand, S., Standnes, D.C., and Austad, T. (2006) "New Wettability Test for Chalk Based on Chromatographic Separation of SCN^- and SO_4^{2-}" *Journal of Petroleum Science and Engineering*, **52** (1-4): 187-197.

Szymczyk, K., Zdziennicka, A., Janczuk, B., and Wojcik, W. (2006) "The Wettability of Polytetrafluoroethylene and Polymethylmethacrylate by Aqueous Solution of Two Cationic Surfactants Mixture" *Journal of Colloid and Interface Science*, **293**: 9.

Torabzadey, S.J. (1984) "SPE 12689: The Effect of Temperature and Interfacial Tension on Water/Oil Relative Permeabilities of Consolidated Sands" in *SPE Enhanced Oil Recovery Symposium*. Tulsa, OK: Society of Petroleum Engineers.

Treiber, L.E. and Owens, W.W. (1972) "SPE 3526: A Laboratory Evaluation of the Wettability of Fifty Oil-Producing Reservoirs" *SPE Journal*, **12** (6): 531-540.

Tweheyo, M.T., Zhang, P., and Austad, T. (2006) "SPE 99438: The Effect of Temperature and Potential Determining Ions Present in Seawater on Oil Recovery from Fractured Carbonates" in *Improved Oil Recovery Symposium*. Tulsa, OK: Society of Petroleum Engineers.

Washburn, E.W. (1921) "The Dynamics of Capillary Flow" *Physical Review*, **17** (3): 273-283.

Webb, K.J., Black, J.J., and Tjetland, G. (2005) "IPTC 10506: A Laboratory Study Investigating Methods for Improving Oil Recovery in Carbonates" in *International Petroleum Technology Conference*. Doha, Qatar: Society of Petroleum Engineers.

Willhite, G.P. (1986) "Waterflooding", Society of Petroleum Engineers: Richardson, TX. p. 326.

Zhang, P. and Austad, T. (2005a) "SPE 92999: The Relative Effects of Acid Number and Temperature on Chalk Wettability" in *International Symposium on Oilfield Chemistry*. Houston, TX: Society of Petroleum Engineers.

Zhang, P. and Austad, T. (2005b) "SPE 94209: Waterflooding in Chalk: Relationship between Oil Recovery, New Wettability Index, Brine Composition and Cationic Wettability Modifier" in *Europec/EAGE Annual Conference*. Madrid, Spain: Society of Petroleum Engineers.

Zhang, P., Tweheyo, M.T., and Austad, T. (2007) "Wettability Alteration and Improved Oil Recovery by Spontaneous Imbibition of Seawater into Chalk: Impact of the Potential Determining Ions Ca^{2+}, Mg^{2+}, and SO_4^{2-}" *Colloids and Surfaces A: Physicochemical and Engineering Aspects*, **301** (1-3): 199-208.

Zhou, X., Morrow, N.R., and Ma, S. (2000) "SPE 62507: Interrelationship of Wettability, Initial Water Saturation, Aging Time, and Oil Recovery by Spontaneous Imbibition and Waterflooding" *SPE Journal*, **5** (2): 199-207.